Multidisciplinary investigations for the hydrogeological parametrization of fractured carbonate aquifers : the case study of the Daruvar hydrothermal system

Kosović, Ivan

Doctoral thesis / Disertacija

2024

Degree Grantor / Ustanova koja je dodijelila akademski / stručni stupanj: **University of Zagreb, Faculty of Mining, Geology and Petroleum Engineering / Sveučilište u Zagrebu, Rudarsko-geološko-naftni fakultet**

Permanent link / Trajna poveznica: https://urn.nsk.hr/urn:nbn:hr:169:189658

University of Zagreb

Faculty of Mining, Geology and Petroleum Engineering

Ivan Kosović

MULTIDISCIPLINARY INVESTIGATIONS FOR THE HYDROGEOLOGICAL PARAMETRIZATION OF FRACTURED CARBONATE AQUIFERS: THE CASE STUDY OF THE DARUVAR HYDROTHERMAL SYSTEM

DOCTORAL DISSERTATION

Supervisors:
Assoc. Prof. Bojan Matoš, PhD
Marco Pola, PhD

Zagreb, 2024

Sveučilište u Zagrebu

Rudarsko-geološko-naftni fakultet

Ivan Kosović

PRIMJENA MULTIDISCIPLINARNIH ISTRAŽIVANJA S CILJEM HIDROGEOLOŠKE PARAMETRIZACIJE RASPUCANIH KARBONATNIH VODONOSNIKA: PRIMJER DARUVARSKOG HIDROTERMALNOG SUSTAVA

DOKTORSKI RAD

Mentori:
Dr.sc. Bojan Matoš, izv. profesor
Dr.sc. Marco Pola, znanstveni savjetnik u trajnom izboru

Zagreb, 2024

Supervisors:

Assoc. Prof. Bojan Matoš, PhD
University of Zagreb
Faculty of Mining, Geology and Petroleum Engineering
Department of Geology and Geological Engineering

and

Marco Pola, PhD, Scientific Advisor in Permanent Vocation
Croatian Geological Survey
Department of Hydrogeology and Engineering Geology

ACKNOWLEDGMENTS

This doctoral thesis is part of the HyTheC project (Multidisciplinary Approach to Conceptual Modelling of Hydrothermal Systems in Croatia), financed by the Croatian Science Foundation (HRZZ) grant number UIP-2019-04-1218.

I would first like to thank my research supervisors Marco Pola and Bojan Matoš for their support, scientific discussions, fieldwork, and guidance throughout this work.

I would like to thank the members of the dissertation committee, Assist. Prof. Ivica Pavičić, Prof. Željko Duić, and PhD. Staša Borović, on the review of this dissertation and valuable comments and suggestions.

Many thanks to colleagues from the Department of Hydrogeology and Engineering Geology of the Croatian Geological Survey for support.

I wish to express my gratitude to the co-authors of scientific papers for their input, diligence and successful collaboration.

...many thanks to my friends...

ABSTRACT

Geothermal resources are important among groundwater resources in fractured aquifers because they are potential renewable energy sources. Their development and hydrothermal characteristics mostly depend on the regional and local geological and hydrogeological settings. Reconstructing the geometrical characteristics of the regional and local fracture network systems and the stress field deforming the rock mass can be useful in determining the preferential flow paths of the thermal waters fostering the conceptual model of the system. The integration with the hydrogeological parametrization of the reservoir is crucial for the quantification of the renewable component of the system and the development of site-specific management plans for the sustainable utilization of the resource. Highly fractured Mesozoic carbonate rocks form the main reservoir for many geothermal resources in central and northern Croatia. One of the most significant thermal manifestations in this region is the thermal springs area in Daruvar with water temperatures ranging from 38 to 50°C. These springs are part of the Daruvar hydrothermal system (DHS), an intermediate scale, tectonically controlled, system hosted within a Mesozoic carbonate rock complex. In this research, a multidisciplinary and multiscale methodological approach was used for the geological reconstruction of the study area, the proposal of a new hydrogeological conceptual model of the DHS, and the hydrogeological parametrization of the fractured carbonate reservoir. This approach combined structural, geophysical, and hydrogeological investigations conducted at regional and local scales. Results display a complex polyphase structural pattern with an E-W and N-S striking system of fractures cogenetic with regional NNE-SSW striking folds that enhance the fluid flow on a regional and local scale. Hydrogeological parameters of the aquifer were calculated by analytical and numerical modeling. The obtained results highlighted the high porosity and permeability of the thermal aquifer connected to the intense fracturing of the bedrock in the Daruvar subsurface. The results of this research improved the conceptual hydrogeological model of the DHS emphasizing the impact of regional and local structures on the circulation of thermal waters and the development of the Daruvar geothermal resource. The multidisciplinary approach used for this research represents a step forward in the investigation of hydrothermal systems and their hydrogeological characterization. Furthermore, it can be applied in the research of similar fractured carbonate aquifers characterized by a complex geological structure.

Keywords: structural reconstruction, 3D geological modeling, DFN modeling, geophysical investigations, well testing, thermal water, Pannonian Basin System, northern Croatia

PROŠIRENI SAŽETAK

U području Panonskog bazenskog sustava (PBS) nerijetko na površini izdanjuju stijene predneogenske podloge u vidu otočnih gora koje su često građene od mezozojskog karbonatnog kompleksa. U većini slučajeva predstavljeni su dolomitima, relativno niske primarne, no značajne sekundarne poroznosti. Ovisno o njihovom strukturnom položaju i mehaničkim obilježjima, karbonati predstavljaju idealne rezervoarske stijene, odnosno mogu biti kolektori ugljikovodika ili vodonosnici geotermalne ili pitke vode. Poznato je da područje PBS-a ima povoljne geotermalne karakteristike, a prirodni izvori termalne vode temperatura do 65°C pojavljuju se na dvadesetak lokacija diljem panonske Hrvatske. U ovom radu područje istraživanja je prirodno izvorište termalne vode u Daruvaru, ali i šira okolica koja obuhvaća JI dijelove Lonjsko-ilovske zavale te zapadne obronke Papuka koji su dominantno građeni od mezozojskog karbonatnog kompleksa. Daruvarski hidrotermalni sustav (DHS) jedan je od najbolje istraženih hidrotermalnih sustava u Hrvatskoj. Sustavna geološka, hidrogeološka i geofizička istraživanja na području Daruvara provode se od sedamdesetih godina prošlog stoljeća. Daruvarsko izvorište obuhvaća nekoliko termalnih izvora (Ivanovo vrelo, Antunovo vrelo i Marijina vrela) s temperaturama od 38 do 50 °C. Unatoč prethodno provedenim geološkim i geofizičkim istraživanja na području Daruvara, detaljne geološke i strukturne rekonstrukcije DHS-a pokazale su se nepotpunima te nepouzdanima. U okviru doktorske disertacije i provedenih istraživanja, primarni je cilj bio primijeniti multidisciplinarni metodološki pristup za provedbu detaljne strukturno - hidrogeološke karakterizacije DHS-a. Ovaj pristup je objedinio rezultate detaljnih terenskih i kabinetskih strukturnih, geofizičkih i hidrogeoloških istraživanja provedenih na regionalnoj i lokalnoj razini s postojećim geološkim, geofizičkim, hidrogeološkim i hidrokemijskim podacima. Multidisciplinarni pristup primijenjen je sa ciljem detaljne strukturno - geološke i hidrogeološke rekonstrukcije te hidrauličke parametrizacije raspucanog karbonatnog vodonosnika DHS-a.

Sukladno tome, glavni ciljevi provedenog istraživanja bili su: (i) odrediti regionalne i lokalne strukturno-geološke značajke koje su omogućile postanak DHS-a; (ii) identificirati sustave pukotina koji dominantno sudjeluju u toku fluida u DHS-u; (iii) izraditi 3D model DHS-a; (iv) geofizičkim istraživanjima dokazati postojanje i povezanost širokih oštećenih zona rasjeda u izvorišnom području DHS-a; (v) usporediti hidrogeološke parametre karbonatnog vodonosnika procijenjene na temelju analize pukotinskih sustava te izračunate iz rezultata pokusnog crpljenja.

Rekonstrukcija geoloških značajki šireg područja omogućila je detaljan opis geometrije termalnog vodonosnika i pukotinskih sustava. Uloga rasjednih sustava i bora na regionalnoj i lokalnoj razini u razvoju DHS-a detaljno je razrađena na temelju terenskih istraživanja i prikupljenih strukturnih podataka. Rezultati su pokazali prisutnost sustava bora s generalnim pružanjem osi bora S-J i I-Z te kogenetskih povezanih sustava pukotina s orijentacijama paralelnim osima bora koje omogućavaju protok fluida na regionalnoj i lokalnoj razini. Također, utvrđena je polifazna tektonska evolucija istraživanog područja koja ukazuje na strukturnu reaktivaciju Daruvarske antiklinale kroz razdoblje kenozoika. Strukturni razvoj Daruvarske antiklinale započeo je krajem krede, odnosno početkom paleogena, pri čemu je prevladavalo kompresijsko polje naprezanja orijentirano I-Z. Rezultat kredno-paleogenske kompresije je postanak regionalnih reversnih rasjeda pružanja SZ-JI te formiranja en-échelon tipa bora s orijentiranim osima bora SZ-JI. Tektonska evolucija Daruvarskog područja dodatno se zakomplicirala tijekom neogena u kojem je na naslijeđene strukture utjecalo neogensko ekstenzijsko polje naprezanja orijentirano I-Z. Rezultat neogenske ekstenzije je lokalna rotacija, strukturna reaktivacija i tektonska inverzija struktura. U završnoj fazi razvoja DHS-a, tijekom pliokvartara, Daruvarsko područje konačno je zahvaćeno tektonskom inverzijom postojećih struktura uslijed regionalnih S-J kompresijskih/transpresijskih naprezanja. Nadalje, rezultati sugeriraju da se termalne vode izdižu prema površini u rasjednoj zoni Daruvarskog rasjeda koji se generalno pruža ISI-ZJZ i kogenetskih sustava pukotina koje nastaju kao posljedica krte deformacije Daruvarske antiklinale. Subvertikalni Topličkи rasjed, pružanja SI-JZ, koji je tijekom pliokvartara strukturno reaktiviran i tektonski invertiran, predstavlja naslijeđeni sustav tenzijskih pukotina koji danas predstavljaju preferencijalni put za brzi protok termalnih voda iz dubljeg dijela vodonosnika prema površini, odnosno termalnom izvorištu u Daruvaru. U okviru hidrogeološkog modeliranja DHS-a, hidrogeološki parametri vodonosnika su izračunati analitičkim i numeričkim modeliranjem. Uspoređujući podatke terenskih mjerenja s kvantitativnom strukturnom analizom napravljenom na temelju digitalnog modela kamenoloma, identificirana su dva subvertikalna sustava diskontinuiteta koji imaju smjer nagiba prema SZ odnosno ZJZ. U isto vrijeme, procjena hidrogeoloških značajki vodonosnika provedena je na temelju numeričkog modeliranja diskretne mreže pukotina (engl. DFN), pokusnog crpljenja i bušotinske karotaže. Glavne geometrijske značajke sustava diskontinuiteta i njihove statističke raspodijele korištene su za izradu DFN modela u mjerilu izdanka (100 x 100 x 30 m) i mjerilu vodonosnika (700 x 700 x 150 m). Na području Daruvara provedena su i hidrogeološka istraživanja pokusnim crpljenjem i analizom rezultata bušotinske karotaže sa ciljem procjene transmisivnosti (T) vodonosnika. Dobivene vrijednosti T koristile

su se za izračun propusnosti (k), čije se vrijednosti kreću u rasponu 7,4 – 122,8 D, uzimajući u obzir različite debljine vodonosnika dobivene iz bušotine Dar 1. Izračun poroznosti (Φ) također je napravljen iz rezultata karotaže bušotine Dar 1 u kojoj je izdvojen najreprezentativniji dio stjenki bušotine (dubina 100-130 m) na temelju kojeg su dobivene realistične vrijednosti poroznosti vodonosnika u rasponu 0,03 – 9,1 % (prosječni Φ za ovu dionicu bio je 2,7 %). Rezultati DFN modela u mjerilu vodonosnika, koji je reprezentativniji u odnosu na model izdanka za procijenu hidrogeoloških značajki, sugeriraju da vrijednosti Φ (0,2%) i k (60,5 D) pokazuju dobru korelaciju s rezultatima dobivenim na temelju terenskih hidrogeoloških istraživanja.

Iz svega navedenog, na temelju provedenih istraživanja, u ovom radu predložen je novi strukturno-geološki i hidrogeološki model Daruvarskog hidrotermalnog sustava. Definiran je strukturni sklop hidrotemalnog sustava, izdvojeni su glavni smjerovi toka fluida u regionalnom i lokalnom mjerilu te su analitičkim i numeričkim modeliranjem proračunati hidrogeološki parametri vodonosnika. Dobiveni rezultati predstavljaju značajno poboljšanje postojećeg konceptualnog hidrogeološkog modela Daruvarskog hidrotermalnog sustava. Korištena metodologija predstavlja iskorak u istraživanjima hidrotermalnih sustava i njihovoj hidrogeološkoj parametrizaciji te se korišteni multidisciplinarni pristup može primijeniti u istraživanjima sličnih raspucanih karbonatnih vodonosnika koji se odlikuju kompleksnom strukturnom građom.

Ključne riječi: strukturna rekonstrukcija, 3D geološko modeliranje, DFN modeliranje, geofizička istraživanja, pokusno crpljenje, termalne vode, Panonski bazenski sustav, sjeverna Hrvatska

TABLE OF CONTENTS

LIST OF FIGURES

LIST OF TABLES

1. INTRODUCTION

Groundwater represents a strategic resource (UNITED NATIONS, 2022) since it provides approximately half of the volume of water for domestic use and approximately one-fourth of the water for irrigation (MARGAT & DER GUN, 2013). The global volume of groundwater resources in rock aquifers is not well constrained, but hard rocks cover approximately half of the Earth's land surface and they can host valuable local aquifers (OFTERDINGER et al., 2019; SINGHAL & GUPTA, 2010). Approximately 15 % of the land surface is characterized by the near-surface exposure of carbonate rocks being potential aquifers (GOLDSCHEIDER et al., 2020), and approximately 10 % of the world population relies on freshwater from carbonate aquifers (STEVANOVIĆ, 2019). Karst groundwater-dependent ecosystems are particularly important in the Mediterranean region where they are extensively used facing serious environmental threats (SIEGEL et al., 2023). Due to this strategic role, the preservation of groundwater resources is crucial (GWD2006/118/EC) and site-specific, regional to local, plans are required for appropriate management. In order to achieve these goals, it is important to: i) assess the principal flow paths avoiding interactions with potential pollution sources, and ii) quantify the hydraulic properties of the aquifer (i.e., permeability, porosity, storativity) determining the optimal exploitation with an acceptable drawdown.

Since undeformed rock has low porosity and permeability, the groundwater flow commonly occurs in water-bearing discontinuities (i.e., bedding, schistosity, joints, shear fractures, veins, stylolites, and other dissolution features, deformation and compaction bands, etc.; hereafter generally referred to as fractures) that control the bulk hydraulic properties of the aquifer (SINGHAL & GUPTA, 2010). Due to their importance for fluid migration, the structural architecture of fault zones and the impact of fracture networks on the permeability field have been extensively investigated. BENSE et al., (2013) reviewed these topics with a particular focus on the structural and hydrogeological approaches.

Among groundwater resources in fractured aquifers, geothermal resources are particularly important in the current global economy because they are potential renewable sources of energy and raw materials (FINSTER et al., 2015; SZANYI et al., 2023). In addition, they are profitably used for heating, industrial applications, balneological and recreational purposes (LUND & TOTH, 2021). Northern Croatia is rich in thermal springs that are mostly used for recreational and health tourism (BOROVIĆ & MARKOVIĆ, 2015). These geothermal resources have great potential since they share the favorable thermal features of the Pannonian basin area (HORVÁTH et al., 2015). One of the most relevant thermal manifestations in northern Croatia

is the thermal spring area in Daruvar city. The occurrence of thermal waters in Daruvar has been known since the Roman age, and it has been extensively investigated since the 1970s (BABIĆ et al., 1971; MRAZ, 1983; LARVA & MRAZ, 2008; BOROVIĆ, 2015; BOROVIĆ et al., 2019; KOSOVIĆ et al., 2023; URUMOVIĆ et al., 2023). The thermal springs with water temperatures ranging from 38 to 50 °C are part of an intermediate scale hydrothermal system (i.e., Daruvar hydrothermal system; DHS) hosted in a fractured carbonate aquifer (BOROVIĆ et al., 2019).

Geothermal aquifers can be classified based on their geological, hydrogeological, and thermal settings (MOECK, 2014). Several investigation approaches at different scales can be applied depending on the goal of the research and target depth. Geological and geophysical investigations can be used to reconstruct the surficial and deep geological settings detailing the architecture of the aquifer and the systems of faults. Hydrogeological and hydrochemical investigations can be used to determine the hydrogeological setting of the thermal aquifer and the physico-chemical characteristics of the thermal waters. The integration of these investigations allows the construction of the conceptual model of the geothermal system that is crucial for assessing the impact of geological processes on hydraulic characteristics of the geothermal system, and on the quantitative and qualitative status of the resource. These data allow quantifying the renewable component of the geothermal system and developing management plans for the long-term sustainable exploitation of the associated resource (RYBACH & MONGILLO, 2006; AXELSSON, 2010; TORRESAN et al., 2020).

In this research, a multidisciplinary and multiscale methodological approach was used for the hydrogeological characterization of the DHS. This approach combined structural, geophysical, and hydrogeological investigations conducted at regional and local scales with available geological, geophysical, hydrogeological, and hydrochemical data. The multidisciplinary dataset allowed assessing the impact of regional and local geological structures and fracture networks on the thermal water flow and the hydrogeological properties of the thermal aquifer.

2. GEOLOGICAL AND HYDROGEOLOGICAL SETTINGS OF THE STUDY AREA

The study area is presented in Figure 1 and includes both the thermal spring area of DHS (Daruvar), the western slopes of Mount Papuk (Petrov vrh), and the SE part of the Lonja-Ilova subdepression. Papuk is a mountain located in the eastern part of Croatia and belongs to the Slavonian Mountains. It is bounded by the Bilogora and Drava River valleys in the north, the Požega basin in the south, the Lonja-Ilova valley in the west, and Krndija Mountain in the east.

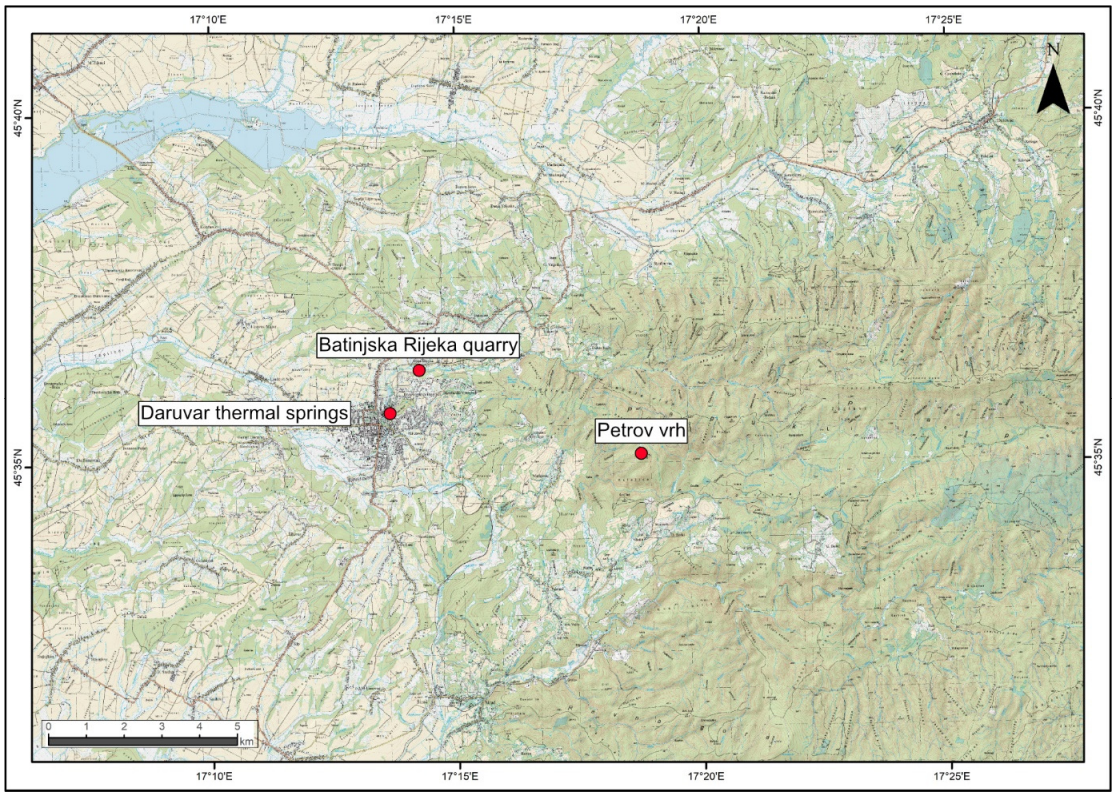

Figure 1. Geographical overview of the study area (https://dgu.gov.hr/sluzbene-drzavne-karte-i-ostale-karte/167).

2.1. Tectonostratigraphic settings

The study area is located in the western part of the Slavonian mountains and SW margin of the Pannonian Basin System (PBS; Figure 2). Slavonian mountains are the best exposures of the Tisza continental Mega-Unit, i.e., a lithospheric fragment of the European foreland that formed beside the Adria microplate during the Middle Jurassic (SCHMID et al., 2008). This area experienced a complex tectono-metamorphic evolution that started with the Variscan and continued through the Alpine-Dinarides-Carpathian orogeny. As a part of the Alpine-Dinarides-

Carpathian orogenic system, the study area is positioned in the vicinity of the Sava Zone, i.e., the Cretaceous-Paleogene suture zone between the Tisza Mega-Unit in the NE and the Adria plate in the SW. The Sava Zone is composed of a complex assemblage of ophiolitic, magmatic-metamorphic, and deep-water sedimentary rocks formed in the Neotethys and the Sava Ocean (SCHMID et al., 2008). These rock complexes are often displaced by regional fault zones (i.e., Mid-Hungarian fault line, Periadriatic lineament), which are characterized by a polyphase tectonic evolution (SCHMID et al., 2008). Regional faults played important roles as tectonic boundaries accommodating the clockwise rotation of the Tisza Mega-Unit, the counterclockwise rotation of the Adria plate, and the eastward lateral extrusion, at a scale of several hundreds of km (SCHMID et al., 2020).

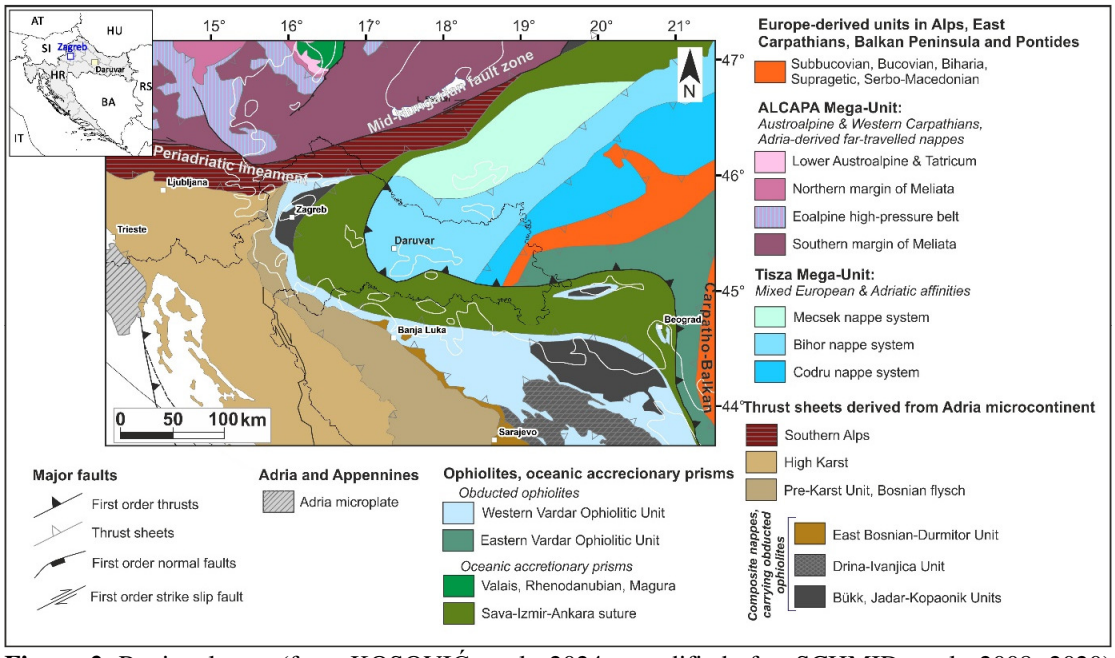

Figure 2. Regional map (from KOSOVIĆ et al., 2024a; modified after SCHMID et al., 2008, 2020) showing: i) the main tectonic units, ii) the regional fault structures, and iii) the borderline of the Pannonian basin (white line). The study area is located in the Tisza Mega Unit at the contact with the Sava Suture Zone and is a part of the Pannonian basin. A schematic geographic map is reported in the upper left corner showing Daruvar, Zagreb, Croatia, and the neighboring states (acronyms: AT – Austria, BA – Bosnia and Herzegovina, HR – Croatia, HU – Hungary, IT – Italy, Sl – Slovenia, RS – Serbia).

After the Cretaceous-Palaeogene tectonism, the area between the Carpathians and the Dinarides was affected by polyphase opening of the Pannonian Basin System (PBS) and its secondary local tectonic deformations. The Croatian part of the PBS (PRELOGOVIĆ et al., 1998; LUČIĆ et al., 2001; TOMLJENOVIĆ & CONTOS, 2001; SAFTIĆ et al., 2003) was affected by an Early–Middle Miocene E-W extensional tectonic phase that formed systems of

grabens and half-grabens, i.e., regional depressions (e.g., Drava and Sava depressions; see PRELOGOVIĆ et al., 1998). The initial extension was followed by a Middle Miocene local scale compression and a Middle-Late Miocene deepening of the basin system due to crustal thermal subsidence. Tectonic inversion and structural reactivation commenced during the Pliocene–Quaternary, which enabled the regional compression/transpression of existing structures as a result of the continuous Adria–Europe plates collision and the general N-S compression (HANDY et al., 2015). The present-day structural setting of the Papuk area is mostly affected by the last Pliocene–Quaternary deformational phase characterized by compression/transpression (JAMIČIĆ, 1995). The N-S compression caused the reactivation of two regional dextral faults, producing a conjugated fault set composed of NW-SE dextral and NE-SW sinistral faults in their interaction zone. Progressive regional transpression was accommodated by folding and uplifting of the structures along the sinistral strike-slip faults (JAMIČIĆ, 1995).

The geological setting of the Daruvar area was described in the Basic Geological Map of SFRY 1:100,000 and Explanatory Notes for Sheet Daruvar (Figure 3; JAMIČIĆ et al., 1989). The complex lithostratigraphic sequence of the study area from the structural bottom to the top can be simplied as follows (KOSOVIĆ et al., 2024a):

- pre-Permian crystalline rocks representing the oldest rocks in the study area. They cover the largest area in western Papuk and are composed of migmatites, granitoids, pegmatites, gneisses, and chlorite schists;
- Permian sedimentary units transgressively cover the crystalline basement. They are composed of well-layered conglomerates and quartz sandstones. The conglomerates contain clasts with a variable lithological composition depending on the underlying basement. The thickness of the Permian unit is approximately 400 m;
- Triassic carbonate rock complex was continuously sedimented over the Permian deposits. The formation of clastic deposits prevailed during the Lower Triassic, while shallow-water carbonate sedimentation with occasional clastic sediment deposition occurred in the Middle and Upper Triassic (ŠIKIĆ, 1981; JAMIČIĆ et al., 1989). The result is a Triassic sedimentary complex composed of: i) Lower Triassic sandstones, siltstones, and laminated shales, ii) Middle Triassic dolomites, limestones, and crinoid limestones with chert, and c) Upper Triassic dolomites and limestones. The total thickness of the Triassic unit is approximately 500 m;

- Jurassic deposits are represented by platy limestones with cherts with a thickness of approximately 100 m. Within the Slavonian Mountains, these deposits are only found in the area of western Papuk (JAMIČIĆ et al., 1989);
- Miocene sedimentary and magmatic rocks are found transgressively over the Mesozoic carbonates or the crystalline basement. Sedimentary units are mostly composed of conglomerates, sandstones, marls, marly and bioclastic limestones, and loose clayey-sandy sediments. Furthermore, pyroclastic and effusive rocks can be found, with andesites occurring in the western part of the study area. The thickness of the Miocene succession is in the range of 600-650 m;
- Pliocene clastic sediments follow the Miocene deposits and are composed of sandstones and marls in different proportions, as well as sands and gravels. The total thickness is between 700 and 900 m;
- Pleistocene sediments are the youngest unconsolidated Quaternary sediments. They can often be found as a "transgressive" cover of the older units and consist of sandy gravels, quartz sands, silty sands, and sandy clays;
- Holocene is represented mostly by alluvial and colluvial unconsolidated sediments.

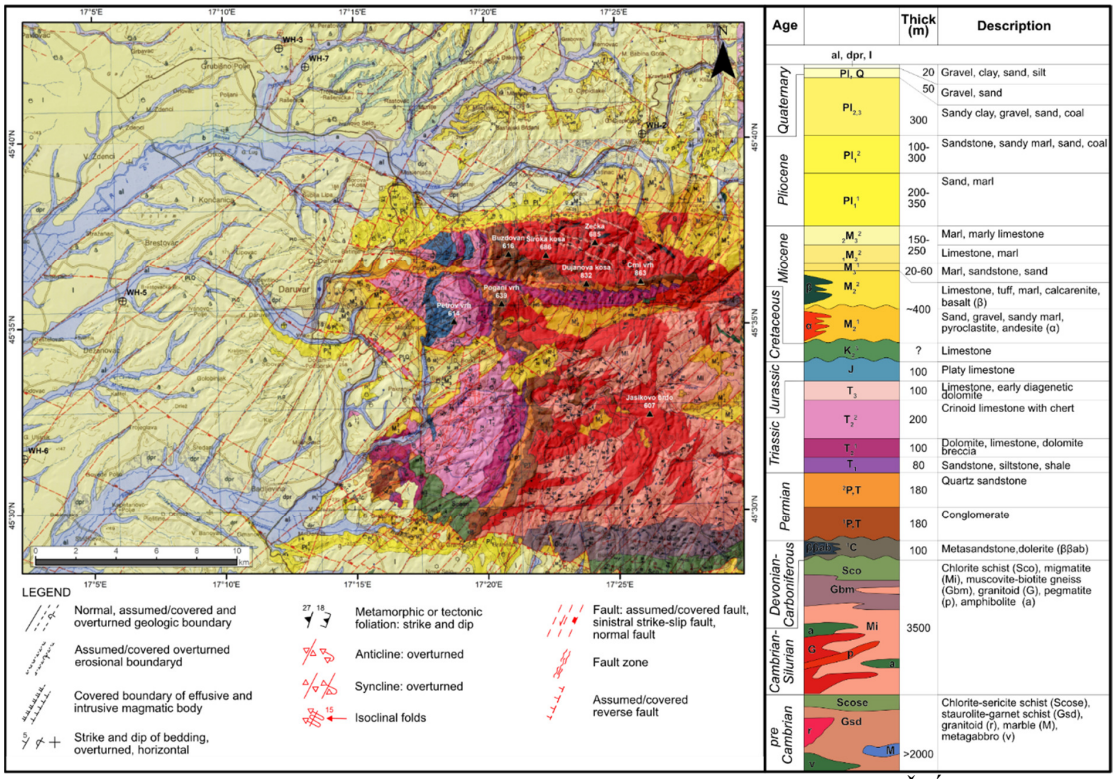

Figure 3. Geological map of the study area and detailed lithological column (JAMIČIĆ et al., 1989).

2.2. Hydrogeological setting

The Daruvar spring area consists of a few thermal springs (Antunovo vrelo, Blatna kupelj, Ivanovo vrelo, and Marijina vrela springs; Figures 4A and 4C) with temperatures ranging from 38 to 50 °C located in the left bank of the Toplica river (BOROVIĆ et al., 2019). In the wider spring area, 109 boreholes had been drilled from 1971 to 2009. The most important wells are D 1, Dar 1, DS 1, and HZ 1 (8.5, 190, 119, and 2.5 m deep, respectively; Figure 4A) with temperatures from 22.7 to 43.5 °C. Furthermore, the PD 2 exploration well (60 m deep; Figure 4A) was drilled to the west of the spring area on the right bank of the Toplica river. Among these objects, the D 1 well and the Antunovo vrelo and Ivanovo vrelo springs are exploited for supplying the Daruvar spa and pool complexes providing approximately 10 l/s of thermal waters. The Dar 1 well (Figure 4B) shows the most comprehensive stratigraphic sequence in the spring area. It is composed of: i) Quaternary unconsolidated sediments mostly made of clays, sands, and gravels, ii) a Miocene sedimentary complex, which is constituted by marls, Lithotamnium limestones, and compact breccias locally marking the unconformity at the base of Badenian, and iii) a Triassic carbonate complex with dolomites, limestones, and dolomitic breccias. The Neogene–Quaternary tectonic activity in the Daruvar area was proven by the occurrence of highly fractured intervals at depths of approximately 90, 135, 180, and 190 m. In the spring area (i.e., D 1 and DS 1 wells), the Triassic carbonate complex is in direct contact with the alluvial deposits. The thermal waters are hosted in the fractured horizons of the Triassic carbonates. Secondary, cooler thermal aquifers are located within the shallower sandy layers of the alluvial cover and the Miocene biocalcarenite (BOROVIĆ et al., 2019). The transmissivity of the Triassic carbonate aquifer, determined through pumping and well tests, ranges from 0.015 to 0.03 m²/s (BOROVIĆ et al., 2019; URUMOVIĆ et al., 2023). Hydrochemical and isotope analyses of the thermal waters (BOROVIĆ, 2015) evidenced: i) temperature from 18.2 to 49.8°C; ii) nearly-neutral pH ranging from 6.7 to 7.5; iii) electrical conductivity of 550 - 700 µS/cm; iv) a calcium-bicarbonate hydrochemical facies, and v) a reservoir equilibrium temperature of 80°C calculated using SiO_2 geothermometers. The hydrochemical facies and the Mg^{2+}/Ca^{2+} versus Mg^{2+} ratio close to 0.5 suggest an interaction of the thermal waters with both limestones and dolomites. Furthermore, O and H stable isotope ratios suggest a meteoric origin of the Daruvar waters, while ^{14}C activity points to a mean residence time between 11 and 15 ka.

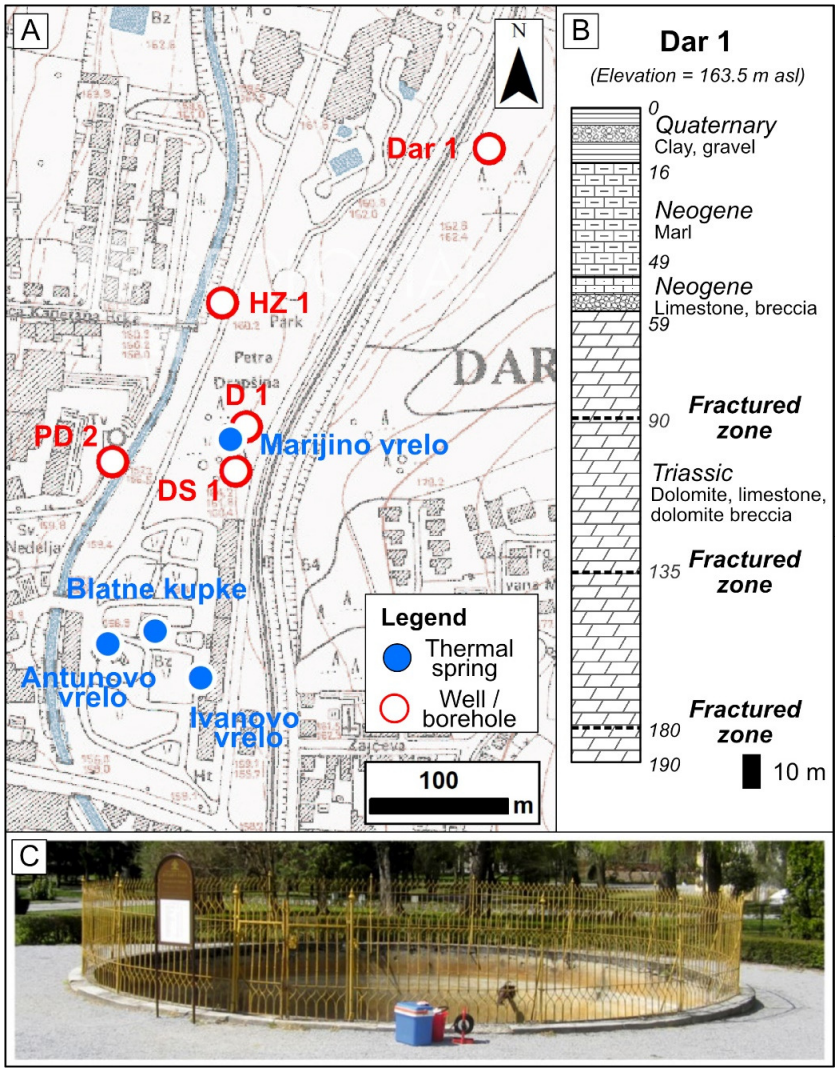

Figure 4. (A) Map of the Daruvar thermal field area showing the thermal springs (blue dots) and the main wells and exploration boreholes (red circle). (B) Stratigraphic log of the Dar 1 well showing the deepest and most comprehensive stratigraphic sequence in Daruvar. (C) Ivanovo vrelo spring in Daruvar.

BOROVIĆ et al. (2019) proposed a conceptual model of the DHS (Figure 5). The recharge area of the system is located in the highest part of the western slopes of Mount Papuk (Figure 5). Same authors suggested that e thermal aquifer's high permeability Triassic carbonate formations extensively crop out due to a regional overturned syncline. The dip of the layers, the karstification, and the fracturing enable deep infiltration of the meteoric water. Low permeable Permian sedimentary units and pre-Permian crystalline rocks at the base of the carbonates prevent further downward circulation of waters. A part of the infiltrated water forms local systems where shallow cold waters and deep warm waters mix, developing hypothermal and subthermal springs. The remaining portion continues its flow in the deep carbonate reservoir

reaching a maximum depth of approximately_1 km below the ground surface. The regional Daruvar fault and the multiphase regional tectonic evolution intensively deformed the bedrock in Daruvar, locally increasing its permeability. In addition, the fault juxtaposes the aquifer with middle to low permeable Neogene deposits, forming a barrier for the regional fluid flow toward W. The resulting permeability contrast favors the upwelling of the thermal waters outflowing in natural thermal springs with temperatures from 38 to 50 °C within the city of Daruvar.

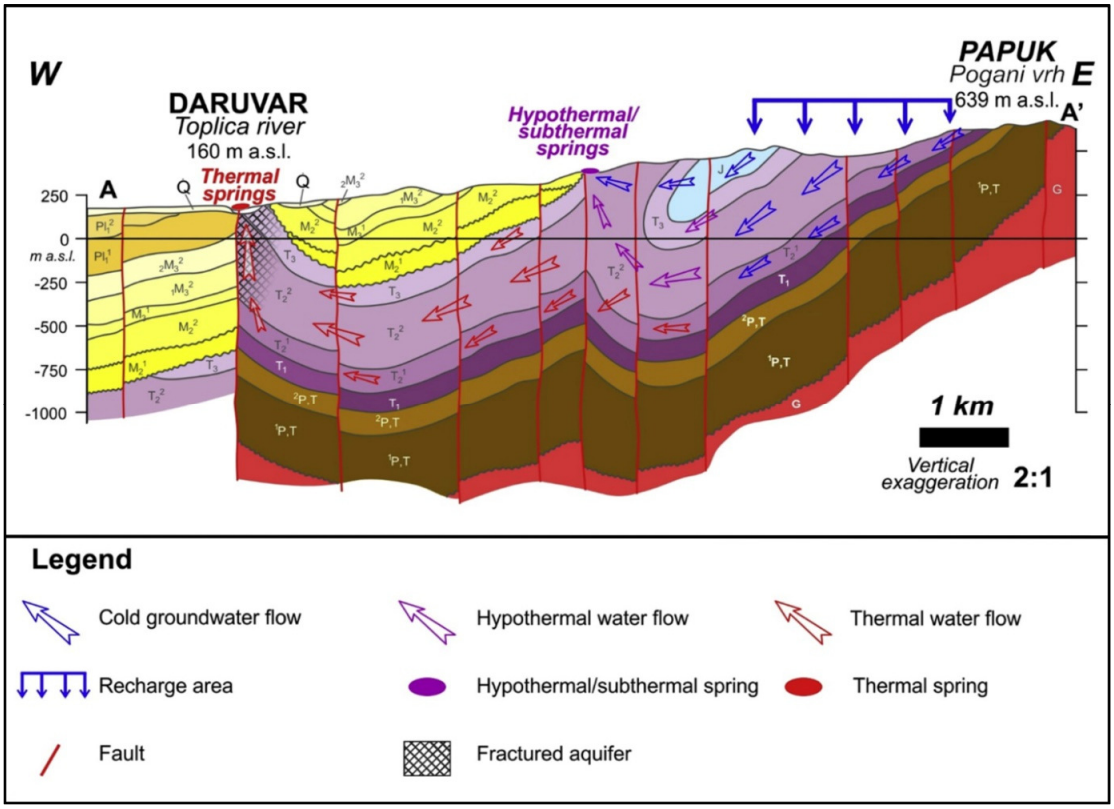

Figure 5. Schematic geological profile and simplified conceptual model of the Daruvar hydrothermal system (BOROVIĆ et al., 2019).

3. MULTIDISCIPLINARY APPROACH

The multidisciplinary methodology used in this research for the multiscale geological and hydrogeological reconstruction of the DHS consisted of: i) structural investigations, which were used to reconstruct the regional geological settings, the surficial distribution of the lithostratigraphic units, and the geometry of regional and local scale faults, folds, and fracture systems, ii) geophysical investigations, where different geophysical approaches were combined to assess the distribution of the lithostratigraphic units in the subsurface and to reconstruct the geometry of faults and their damage zones at both local and regional scale, and iii) hydrogeological investigations, which integrated well testing and logging and discrete fracture network (DFN) numerical modeling to detail the hydraulic properties of the thermal aquifer (Figure 6).

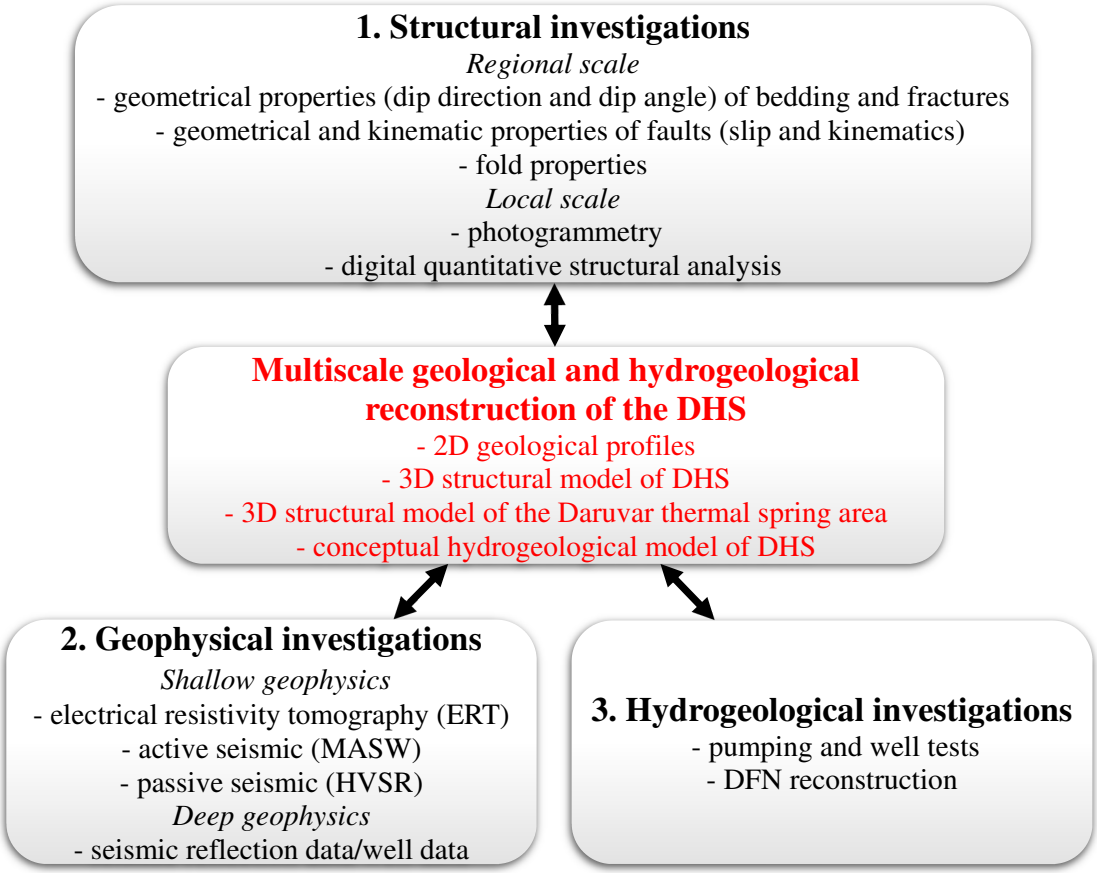

Figure 6. Schematic flow chart used in the multiscale geological and hydrogeological reconstruction of the DHS.

i. Structural investigations

Structural investigations were focused on the implementation of field structural-geological research and measurements both at regional and local scales. The results were integrated with geological and geophysical data to develop 2D composite geological profiles and a 3D geological model of the wider DHS area. Structural investigations included:

- *Regional scale* investigations that were used to determine the geometrical properties of strata bedding and fractures/joints (i.e., dip direction and dip angle) and the fault kinematics. For the reconstruction of fault kinematics, data of dip direction and dip angle of fault planes and kinematic indicators, i.e., the orientation of slickensides defined by azimuth and plunge and their sense of movement (DOBLAS, 1998) were used. Based on kinematic criteria, the shear fracture data were analyzed and separated into compatible fault groups where synthetic focal mechanisms were calculated for each group using the Right Dihedra Method (ANGELIER & MECHLER, 1977). Where local scale folds were visible, the fold axes were determined. Field investigations were carried out from 2021 to 2024 by collecting structural data at the 305 field points. The resulting dataset comprised 134, 659, and 91 measurements of bedding, fractures, and faults, respectively. The regional scale investigations enabled the reconstruction of the geological assemblage that influences the regional DHS fluid flow and water-rock interaction.
- *Local scale* investigation that included structural measurement and the photogrammetric imagining in the area of the Batinjska Rijeka quarry (BRQ), east of Daruvar, where the Mesozoic carbonate rock complex is exposed. This approach was used for the development of a digital outcrop model (DOM), which permits to collect large datasets of discontinuities for a solid statistical analysis of their geometrical properties (HYMAN et al., 2015; THIELE et al., 2017; BENEDETTI et al., 2024). The imaging of BRQ was performed in April 2023 using DJI Matrice 300 RTK unmanned aerial vehicle. 702 images were acquired with an image overlap up to of 90% resulting in a DOM (surface of 222,135 m^2) with sub-centimeter resolution (0.29-0.56 px/cm). Results of the virtual structural analysis in the BRQ were constrained by field measurement and were used to stochastically reconstruct the fracture network using the DFN approach. Local scale investigations were employed to detail the architecture of the fracture networks in the BRQ outcrop analog of the thermal aquifer.

ii. Geophysical investigations

Geophysical investigations were used to measure the spatial variations of the physical properties of the subsurface obtaining a quantitative model that completes the geological reconstruction. They included:

- *Deep measurements*: reflection seismic profiles and well data were employed to reconstruct the geological features of the Lonja-Ilova depression on a regional scale. These seismic profiles and well data were collected as part of investigation projects conducted by INA - Industrija nafte d.d. in the Lonja-Ilova depression between Daruvar and Kutina in the timeframe from 1980s to 1990s.
- *Shallow measurements:* an integrated geophysical approach based on electrical resistivity tomography (ERT) and both active and passive seismic (MASW and HVSR) methods was used for the 3D reconstruction of the geological setting of the subsurface in the Daruvar city thermal spring area. ERT is a widely used geophysical method for reconstructing the geometry of lithologies and subsurface structures (LOKE et al., 2013). This technique has proven highly effective in hydrogeological and structural investigations, particularly in geothermal systems (i.e., LÉVY et al., 2019; PAVIĆ et al., 2023). Eight profiles with a maximum investigating depth of approximately 115 m were acquired in 2021 and 2022. Furthermore, a combined approach using the passive horizontal-to-vertical spectral ratio (HVSR) and active multichannel analysis of surface waves (MASW) methods was applied to map the thickness of the Quaternary cover. Similar methods have been employed in thermal areas where recent sediments conceal bedrock geometry (CHENG et al., 2021). In this study, MASW investigations were conducted using six seismic profiles composed of 24 geophones, with HVSR measurement conducted in the center of each seismic profile.

iii. Hydrogeological investigations

In this study, both classical hydrogeological investigations and DFN modeling were conducted for the hydraulic parametrization of the Daruvar carbonate thermal aquifer.

- *Pumping test* of the thermal aquifer was performed on February 27th, 2022. The water was pumped from well Dar 1 at different flow rates and the variations of the water level were measured in many observation points in the spring area. The results were interpreted using the *Theis-Hantush* analytical solution (THEIS, 1935; HANTUSH, 1961a) for pumping tests since the thermal aquifer is highly fractured and it can be considered as a quasi-homogenous porous medium at the investigated scale. This

approach allowed to estimate the hydrogeological parameters of the aquifer (i.e., transmissivity, storativity, hydraulic conductivity anisotropy ratio, and saturated thickness). Besides the pumping test analysis, the data collected in Dar 1 were further investigated as a step-drawdown well test (KRUSEMAN et al., 2000). The collected data were used to determine the theoretical drawdown vs. flow rate curve of the well, the well efficiency, and its specific capacity and to assess the transmissivity of the aquifer through empirical relations.

- *DFN modeling* was used to reconstruct the network system of discontinuities for quantifying the hydraulic parameters (i.e., porosity and permeability) of the aquifer (FAYBISHENKO et al., 2000; BUNDSCHUH & SUÁREZ, 2010; MEDICI et al., 2023). The results obtained from the virtual structural analysis of BRQ's DOM were used to build DFN models at the scales of the outcrop (100×100×30 m) and the aquifer volume investigated by the pumping test (700×700×150 m). The results of DFN models were calibrated and tested using data collected from several well tests and logs conducted in the Daruvar thermal field.

4. OBJECTIVES AND HYPOTHESES OF RESEARCH

The presented multidisciplinary approach was applied for the geological and hydrogeological reconstruction and the hydraulic parameterization of the Daruvar hydrothermal system fractured carbonate aquifer. Accordingly, the main objectives of this research were:

i. definition of the regional and local structural-geological features that enable the development of the DHS;
ii. identification of the fracture systems that represent preferential flow paths in the DHS;
iii. construction of a 3D model of DHS;
iv. reconstruction of fault damage zones in the spring area of the DHS using geophysical investigations;
v. comparison of the hydrogeological parameters of the dolomite aquifer estimated based on the fracture system analysis and results of pumping tests.

These objectives are based on the following hypotheses:

1. Regional and local geological and structural-geological influence on the development of DHS.
2. Fracture networks are preferential flow paths in the DHS.
3. Extensive tectonized fault zones in the Daruvar area allow the rising of thermal waters.
4. Hydrogeological parameters in dolomite aquifers can be determined through numerical modeling of fracture systems.

5. ORIGINAL SCIENTIFIC PAPERS

5.1. # Paper 1: Geological modeling of a tectonically controlled hydrothermal system in the southwestern part of the Pannonian basin (Croatia)

By

Ivan Kosović, Bojan Matoš, Ivica Pavičić, Marco Pola, Morena Mileusnić, Mirja Pavić and Staša Borović

frontiers | Frontiers in Earth Science

TYPE Original Research
PUBLISHED 07 June 2024
DOI 10.3389/feart.2024.1401935

OPEN ACCESS

EDITED BY
Guillermo Booth-Rea,
University of Granada, Spain

REVIEWED BY
Nimesh Chettri,
Royal University of Bhutan, Bhutan
Bayu Rudiyanto,
State Polytechnic of Jember, Indonesia

*CORRESPONDENCE
Bojan Matoš,
bojan.matos@rgn.unizg.hr

RECEIVED 16 March 2024
ACCEPTED 09 May 2024
PUBLISHED 07 June 2024

CITATION
Kosović I, Matoš B, Pavičić I, Pola M, Mileusnić M, Pavić M and Borović S (2024), Geological modeling of a tectonically controlled hydrothermal system in the southwestern part of the Pannonian basin (Croatia).
Front. Earth Sci. 12:1401935.
doi: 10.3389/feart.2024.1401935

Geological modeling of a tectonically controlled hydrothermal system in the southwestern part of the Pannonian basin (Croatia)

Ivan Kosović[1], Bojan Matoš[2]*, Ivica Pavičić[2], Marco Pola[1], Morena Mileusnić[3], Mirja Pavić[1] and Staša Borović[1]

[1]Croatian Geological Survey, Zagreb, Croatia, [2]Faculty of Mining, Geology and Petroleum Engineering, Department of Geology and Geological Engineering, University of Zagreb, Zagreb, Croatia, [3]State Geodetic Administration, Zagreb, Croatia

Geothermal energy is an important resource in the green economy transition. For the preservation of a geothermal resource it is crucial to assess its renewability and the sustainability of the exploitation. These aspects are influenced by the interaction among the physical, chemical, geological, and hydrogeological processes. The reconstruction of the geological assemblage allows the detailing of the geometries of the reservoir and fracture systems that influence the fluid flow and the water/rock interaction. The control of regional/local scale fault and fold systems on the development of the Daruvar hydrothermal system (DHS), located in Croatian part of the Pannonian basin, is detailed in this work. Field investigations were conducted to collect structural data on strata orientation and fault/fracture systems. The dataset was integrated with geological and geophysical data to develop composite geological profiles and a 3D geological model. Results display a pattern of generally N-S and E-W striking folds and cogenetic fracture systems with orientations parallel to the fold axes. The geological reconstruction was integrated with geophysical, hydrogeological, and geochemical data to propose a conceptual model of the DHS. The DHS is a topographically driven system hosted in a Mesozoic carbonate reservoir where E-W striking fracture systems are regional flow paths that enable infiltration of meteoric water to 1 km depth and its reheating in its reservoir area. In Daruvar, an anticline and fault/fracture systems accommodate the uplift of reservoir to shallow depths, promoting the bedrock fracturing and increase of the permeability field. These conditions favor the localized upwelling of thermal water resulting in four thermal springs (38°C and 50°C) in Daruvar city area. This work highlights the importance of employing a multidisciplinary approach to detail the complex interaction among the processes driving the geothermal resource.

KEYWORDS

Daruvar hydrothermal system, 3D structural modeling, polyphase evolution, fault damage zone, Mesozoic carbonate aquifer, thermal water

1 Introduction

The sustainable management of natural resources is one of the most important challenges in the 21st century (ECE, 2021). Natural resources developed by geological processes are very important since they support many industrial activities. Geothermal resources have a pivotal role in the current global economy since they are potential renewable sources of both raw materials and energy (e.g., Finster et al., 2015; Szanyi et al., 2023). The sustainable utilization of geothermal resources is crucial since their development and renewability depend on a delicate balance between physical and chemical processes (e.g., Rybach and Mongillo, 2006; Axelsson, 2010; Rman, 2014; Shortall et al., 2015; Fabbri et al., 2017).

The most relevant processes affecting the characteristics of a geothermal resource are the conduction of heat and the convection of fluids (Moeck, 2014). The magnitude of these processes mostly depends on the geological and hydrogeological settings of the geothermal system associated with the resource (Kühn and Gessner, 2009; Bundschuh and César Suárez A., 2010; Pasquale et al., 2014). The conductive component of the heat transfer is mostly related to the regional subsurface geological setting that affects: i) the distribution of lithologies and their thermal properties, and ii) the occurrence of deep structures favoring an increased heat flow from the deeper part of the Earth's crust. Convection encompasses the transfer of mass and heat occurring by bulk fluid motion and depends on the subsurface permeability field (Ataie-Ashtiani et al., 2018). In bedrock aquifers, the original permeability can be enhanced by the fracturing with fault damage zones being preferential paths for the fluid flow (e.g., Faulkner et al., 2010; Bense et al., 2013). In particular, thermal springs are generally associated with systems of faults that enable or enhance the outflow of thermal waters (e.g., Curewitz and Karson, 1997; Nelson et al., 2009; Pola et al., 2014; Keegan-Treloar et al., 2022; Pavić et al., 2023). Therefore, a detailed reconstruction of the geological, tectonic, and hydrogeological settings is crucial to determine the processes favoring the circulation of thermal waters and influencing the renewability of the geothermal resource and its exploitation sustainability (Magri et al., 2010; Faulds et al., 2013; Scheck-Wenderoth et al., 2014; Brehme et al., 2016; Pola et al., 2020; Torresan et al., 2021).

The reconstruction of the geo-tectonic settings of a certain area is generally conducted by integration of field investigations and geophysical data, at regional and local scales. While field investigations enable the reconstruction of the surficial geometry of geological formations and fractures and the assessment of the kinematics of the principal faults, geophysical data can add crucial subsurface information to the geological reconstruction. Geological and geophysical datasets can be integrated to construct a 3D geological model of the subsurface (Pavičić et al., 2018; Olierook, 2020; Jia et al., 2021; Panzera et al., 2022). 3D modeling, as a backbone in geological and hydrogeological applications, provides a useful tool for the interpretation and visualization of geological structures, especially when their geometrical complexity cannot be fully represented through 2D sections (Caumon et al., 2009; Pavičić et al., 2018; Wellmann and Caumon, 2018; Pan et al., 2020; Lyu et al., 2021). Assessing the tectonic setting and the stress regimes can improve the geological reconstruction. It permits understanding the kinematics of the local fracture networks that influence the permeability field in the reservoir (Wang et al., 2014; Santilano et al., 2016; Xie et al., 2017; Li Y. et al., 2018; Price et al., 2018; Pan et al., 2020). Furthermore, it is crucial to quantify the hydrogeological properties of the thermal aquifer that can be used to forecast the quantity of exploitable waters. These reconstructions are fundamental for a detailed hydrogeological modeling, which explains the processes driving the formation of a thermal resource (Moeck et al., 2010; Calcagno et al., 2014; Fulignati et al., 2014; Mroczek et al., 2016; Montanari et al., 2017; Torresan et al., 2020).

According to Borović and Marković (2015), Northern Croatia is rich in geothermal resources sharing the favorable thermal properties of the Pannonian basin area (Horváth et al., 2015). Most of the thermal springs in Croatia are used for balneotherapy and tourism, however, they also have a great potential for additional utilization (e.g., district heating, industrial processes). One of the most investigated thermal regions in Croatia is the Daruvar city area (Figure 1), with thermal springs documented since the Roman era. Systematic geological, hydrogeological, and geophysical investigations in the Daruvar area have been conducted since the 1970s (e.g., Babić et al., 1971; Mraz, 1983; Larva and Mraz, 2008; Borović, 2015; Borović et al., 2019; Kosović et al., 2023; Urumović et al., 2023). The thermal spring area is the outflow area of an intermediate scale, tectonically-controlled, topographically driven, geothermal system hosted in a Mesozoic carbonate rock complex. The thermal waters are exploited from a thermal well and two springs that provide approximately 10 l/s.

Despite several multidisciplinary investigations in Daruvar, the detailed quantitative geological and structural reconstructions of the recharge area and flow-through parts of the Daruvar hydrothermal system (DHS) are still unreliable and outdated. This study aims to present results of field investigations conducted in the hinterland area of Daruvar to detail its geological setting, structural framework, and tectonic evolution. Geological and structural data were combined with available seismic reflection data and stratigraphic logs of deep wells to perform a 3D geological model. Results were furthermore used to refine the hydrogeological conceptual model of the DHS focusing on the correlation of the geological and tectonic models with the preferential flow paths in the system.

2 Geological and hydrogeological settings

2.1 Regional tectonics evolution

The DHS area is located in the western part of the Slavonian mountains (Mount Papuk), which are one of the best exposures of the Tisza-Dacia Mega-Unit, a lithospheric fragment formed between the European and Adria plates during the Middle Jurassic (Figure 1; e.g.; Balen et al., 2006; Schmid et al., 2008 with references). This area experienced a complex tectono-metamorphic evolution that started with the Variscan and continued through the Alpine-Dinarides-Carpathian orogeny. The Variscan events were characterized by structural stacking of the Mecsek, Bihor, and Codru nappe systems (Figure 1), with various metamorphic overprints of the preexisting crystalline basement, intruded by granitoids and migmatites (Balen et al., 2006 with references).

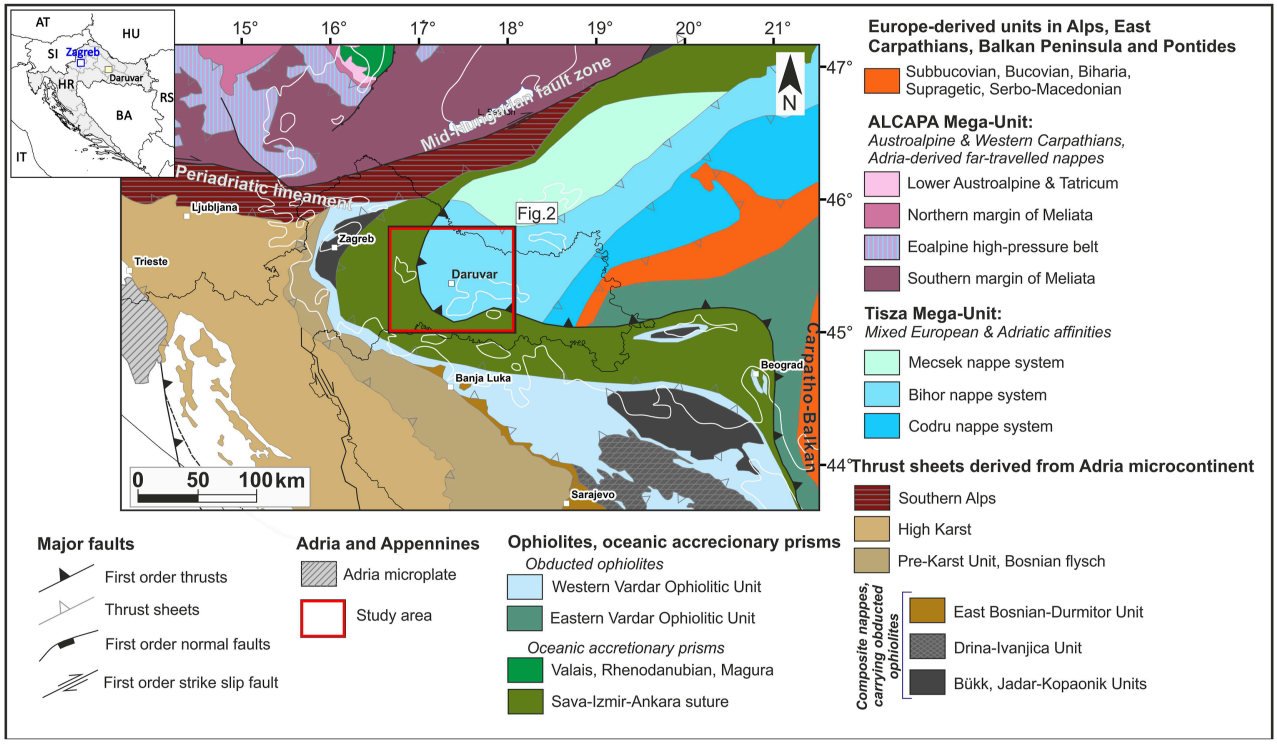

FIGURE 1
Regional map (modified after Schmid et al., 2008; 2020) showing: i) the main tectonic units, ii) the regional fault structures, and iii) the border line of the Pannonian basin (white line). The study area is located in the Tisza-Dacia Mega Unit at the contact with the Sava Suture Zone and is a part of the Pannonian basin. The red rectangle marks the extent of the structural map in Figure 2. A schematic geographic map is reported in the upper left corner showing Daruvar, Zagreb (the capital city of Croatia), Croatia, and the neighboring states (acronyms: AT–Austria, BA–Bosnia and Herzegovina, HR–Croatia, HU–Hungary, IT–Italy, SI–Slovenia, RS–Serbia).

According to Schmid et al. (2008, 2020), Bihor nappe system exposures can be found in southern Hungary and the Slavonian mountains. Balen et al. (2006) suggested that metamorphic and plutonic basement rocks of the Slavonian mountains were locally covered by a Paleozoic-Mesozoic carbonate/clastic succession deposited at the passive margin of the Adria plate. Neogene-Quaternary deposits further concealed the older rock sequence after the intensive Cretaceous-Paleogene tectonism (Balen et al., 2006 with references). As a part of the Alpine-Dinarides-Carpathian orogenic system, the study area is positioned in the vicinity of the Sava Zone, i.e., the Cretaceous-Paleogene suture zone between the Tisza-Dacia Mega-Unit in the NE and the Adria plate in the SW. The Sava Zone is composed of complex assemblage of ophiolitic, magmatic-metamorphic, and deep-water sedimentary rocks formed in the Neotethys and the Sava Ocean (Schmid et al., 2008 with references). These rock complexes are often displaced by regional fault zones (i.e., Mid-Hungarian fault line), which are characterized by a polyphase tectonic evolution (Figure 1; Figure 2; Schmid et al., 2008).

The Neogene-Quaternary tectonic evolution of the Pannonian Basin System (PBS), which is characterized by repeated extension, compression, and tectonic inversion, further affected the structural assemblage of the study area. In particular, it was conditioned by the Adria-Europe collision, the eastward lateral-extrusion of the continental blocks between these plates, and the clockwise rotation of the Tisza-Dacia Mega-Unit (Prelogović et al., 1998; Tari et al., 1999; Csontos and Vörös, 2004; Schmid et al., 2008).

PBS was formed by Early to Late Miocene (c. 26–11.5 Ma) NNE-SSW directed "back-arc type" lithospheric extension along the NNW-striking listric normal faults (Figure 2; Fodor et al., 2005; Horváth et al., 2006; Schmid et al., 2008; Brückl et al., 2010). Rift and wrench-related troughs were filled with large amounts of syn-rift deposits (Tari and Pamić, 1998; Horváth and Tari, 1999; Steininger and Wessely, 2000; Ustaszewski et al., 2010). In the Croatian part of the PBS, deposition commenced along the listric faults forming the basins and subbasins (Pavelić et al., 2001; Ćorić et al., 2009). Though local structural tectonic inversion occurred at the end of the Middle Miocene (c. 13.0–11.6 Ma), Croatian part of PBS was characterized by continuous deepening and rapid thermal subsidence along the existing faults until the Late Miocene - Early Pliocene (c. 11.5–5.3 Ma; Csontos et al., 1992; Horváth and Tari, 1999; Tomljenović and Csontos, 2001; Fodor et al., 2005; Malvić and Velić, 2011). A significant change in the stress field, with N-S trending compressional and/or transpressional P-axes, occurred during the Pliocene. Translation and counterclockwise rotation of the Adria plate in combination with consumption of the subducted European plate lithosphere led to regional tectonic inversion (Horváth and Tari, 1999; Grenerczy et al., 2005; Dolton, 2006; Jarosiński et al., 2006; Bada et al., 2007; Jarosinski et al., 2011; Ustaszewski et al., 2014). The Pliocene-Quaternary tectonic inversion accommodated

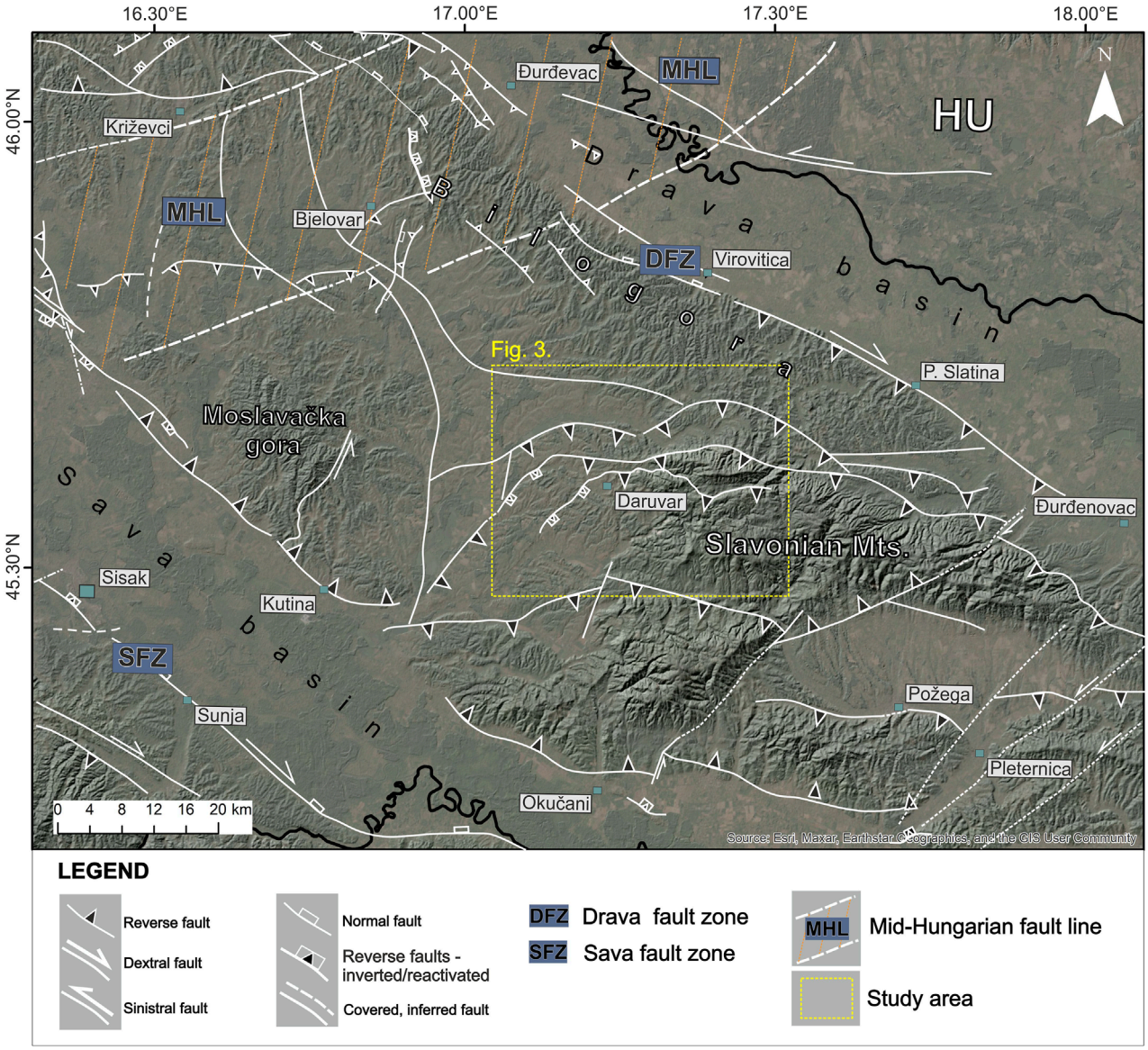

FIGURE 2
Simplified structural map of the regional tectonic framework with regional fault systems within northern Croatia. The yellow rectangle corresponds to the extent of the geological map in Figure 3. Fault systems are compiled after: Jamičić, 1995; Prelogović et al., 1998; Tomljenović and Csontos, 2001; Schmid et al., 2008; Šolaja, 2010; Matoš et al., 2016; Wacha et al., 2018; Baize et al., 2022; Herak and Herak, 2023.

large-scale lithospheric folding, vertical/horizontal motions along the existing regional faults, and horizontal/vertical displacement along the co-genetic reverse and strike-slip faults (e.g., Periadriatic fault, Mid-Hungarian fault line, Sava and Drava fault zones; Figure 2; Horváth and Cloetingh, 1996; Prelogović et al., 1998; Horváth and Tari, 1999; Fodor et al., 2005; Dolton, 2006; Bada et al., 2007; Jarosinski et al., 2011). In the Croatian part of the PBS, the tectonic uplift yielded final uplift of pre-Neogene basement highs (e.g., Slavonian mountains), which caused tectonic overprint of basement structures, block rotations, and formation of the positive flower structures with kilometer-scale folds along the reactivated and newly formed strike-slip faults (Figure 2; Jamičić, 1995; Prelogović et al., 1998; Tomljenović and Csontos, 2001; Balen et al., 2006).

2.2 Geological setting

The geological setting of the Daruvar area was extensively investigated by Jamičić et al. (1989). Since the scope of this work is the geological reconstruction of the DHS for a detailed hydrogeological conceptual modeling, the original geological map (Supplementary Figure S1) was simplified considering the hydrogeological properties of the lithological units together with their age (Figure 3). The units (Supplementary Figure S2) were reorganized as follows: i) pre-Permian crystalline rocks, ii) Permian sedimentary units, iii) Triassic carbonate rock complex, iv) Jurassic limestones, v) Miocene sedimentary and magmatic rock complex, vi) Pliocene clastic sediments, vii) Pleistocene unconsolidated sediments, and viii) Holocene alluvial and colluvial unconsolidated sediments.

The oldest rocks in the study area are the pre-Permian crystalline rocks. They cover the largest area in western Papuk and are composed of migmatites, granitoids, pegmatites, gneisses, and chlorite schists. Granitoids are the most common lithology and they are S-type granites concordant with migmatite bodies (Jamičić et al., 1989; Pamić et al., 2003). The crystalline rocks are generally in transgressive contact with Permian or Miocene units. Permian rocks are composed of well-layered conglomerates and quartz sandstones. The conglomerates contain clasts with a variable lithological composition depending on the underlying basement. Locally, these sediments can show a low-grade metamorphism. The thickness of the Permian unit is approximately 400 m. The Triassic sedimentary rock complex was continuously sedimented over the Permian deposits. The formation of clastic deposits prevailed during the Lower Triassic, while shallow-water carbonate sedimentation with occasional clastic sediment deposition occurred in the Middle and Upper Triassic (Šikić, 1981; Jamičić et al., 1989). The result is a sedimentary complex composed of: i) Lower Triassic sandstones, siltstones, and laminated shales, ii) Middle Triassic dolomites, limestones, and crinoid limestones with chert, and iii) Upper Triassic dolomites and limestones. The total thickness of the Triassic unit is approximately 500 m. During the Jurassic, western Papuk as the contact zone of the Adria plate and the Tisza block was characterized by deep-sea basin sedimentation. Jurassic deposits are preserved exclusively in western Papuk (Jamičić, 2009). They are represented by platy limestones with cherts (Jamičić et al., 1989), with thickness approximately 100 m. From the Lower Cretaceous, western Papuk experienced tectonic uplift and emersion. It was characterized by coastal environments with frequent sea-level oscillations and alternations of marine, brackish, and freshwater sedimentation. The sedimentation was partly restored in the Middle Miocene due to the PBS E-W extension and regional transgression. Sea level oscillations and alternations in the Neogene-Quaternary deposition environments resulted in marine, brackish, and freshwater sedimentation in the structural lows of the previously formed structures. Miocene sediments are mostly composed of conglomerates, sandstones, marls, marly and bioclastic limestones, and loose clayey-sandy sediments. Furthermore, pyroclastic and effusive rocks can be found, with andesites occurring in the western part of the study area. The thickness of the Miocene succession is in the range of 600–650 m. The clastic sedimentation continued in the Pliocene with sandstones and marls in different proportions, as well as sands and gravels, with a total thickness between 700 and 900 m. The youngest unconsolidated Quaternary sediments can often be found as a "transgressive" cover of the older units. Quaternary sediments consist of sandy gravels, quartz sands, silty sands, and sandy clays (Jamičić et al., 1989). Pleistocene deposits are characterized by alluvial and loess-like deposits, while alluvial and slope sediments occur during the Holocene. The Pleistocene and Holocene units are up to 25 and 5 m thick, respectively.

The youngest Plio-Quaternary tectonic phase significantly affected the structural assemblage of the study area. This tectonic activity is associated with the proximal compressional/transpressional stresses accommodated along the Drava and Sava fault zones (Figure 2) which led to both the formation of folds, new faults, and the structural reactivation with local inversion of inherited structures (Figure 3; Jamičić, 1995). The principal mapped faults in the study area are mostly E-W, NE-SW, and NW-SE striking faults with cogenetic N-S, NW-SE, and NE-SW striking fold axes (Jamičić et al., 1989; Jamičić, 1995; Šolaja, 2010).

2.3 Hydrogeological setting

Four thermal springs with temperatures between 38°C and 50°C occur in Daruvar. Furthermore, approximately 100 shallow boreholes and a few deep wells have been drilled since the 1970s. The lithostratigraphic sequence was detailed through two wells deeper than 100 m (Kosović et al., 2023). It consists of: i) Quaternary alluvial deposits with a thickness of up to 20 m, ii) Miocene or Pliocene marls up to 30 m thick, iii) Miocene bioclastic limestone with a thickness of 10 m, and iv) Triassic dolomites and limestones with thickness of 130 m. Where the thermal springs occur, the stratigraphic logs show that the Triassic carbonates are in direct contact with the Quaternary cover. The Triassic carbonates are moderately to highly fractured. This formation represents the primary thermal aquifer, while secondary, colder, thermal aquifers are found in the sandy layers of the alluvial cover and the Miocene biocalcarenite (Borović et al., 2019). The transmissivity of the Triassic carbonate aquifer was assessed through pumping and well tests ranging from 0.015 to 0.03 m^2/s (Borović et al., 2019; Urumović et al., 2023). The main physico-chemical characteristics of thermal waters in springs and wells (Borović, 2015) are: i) temperature from 18.2°C to 49.8°C, ii) nearly neutral pH with values between 6.7 and 7.8, iii) EC between 550 and 700 µS/cm, and iv) calcium-bicarbonate hydrochemical facies. O and H stable isotope ratios suggest a meteoric origin of the Daruvar waters, while ^{14}C activity points to a mean residence time between 11 and 15 ka (Borović, 2015).

These data were used to propose an initial conceptual model of the DHS (Borović et al., 2019). The recharge area of the system is located in the topographically highest part of the eastern hinterland of Daruvar (i.e., western Papuk and Petrov vrh area) where the Triassic carbonates are uplifted by a regional fault system (Figure 3). The deep infiltration of the meteoric waters is favored by the dip of the layers, the karstification, and the fracturing of the rock mass. The low permeable Permian and pre-Permian units at the base act as a barrier for further downward circulation. Locally, shallow cold and deep warm waters mix developing hypothermal and subthermal springs in the Daruvar hinterland. In the Daruvar area, existing regional thrust and strike-slip faults (Figure 3) and their polyphase tectonic history enhanced the deformation of the aquifer and its permeability field. Furthermore, faults juxtapose the aquifer with low permeable Miocene-Pliocene deposits forming a barrier for the fluid flow toward W.

3 Materials and methods

3.1 Structural-geological investigation and analysis

Structural-geological field investigation was carried out from 2021 to 2024. Data were collected at 305 field points, digitized, and spatially georeferenced using GIS software. The structural investigation included measurements of the geometrical properties

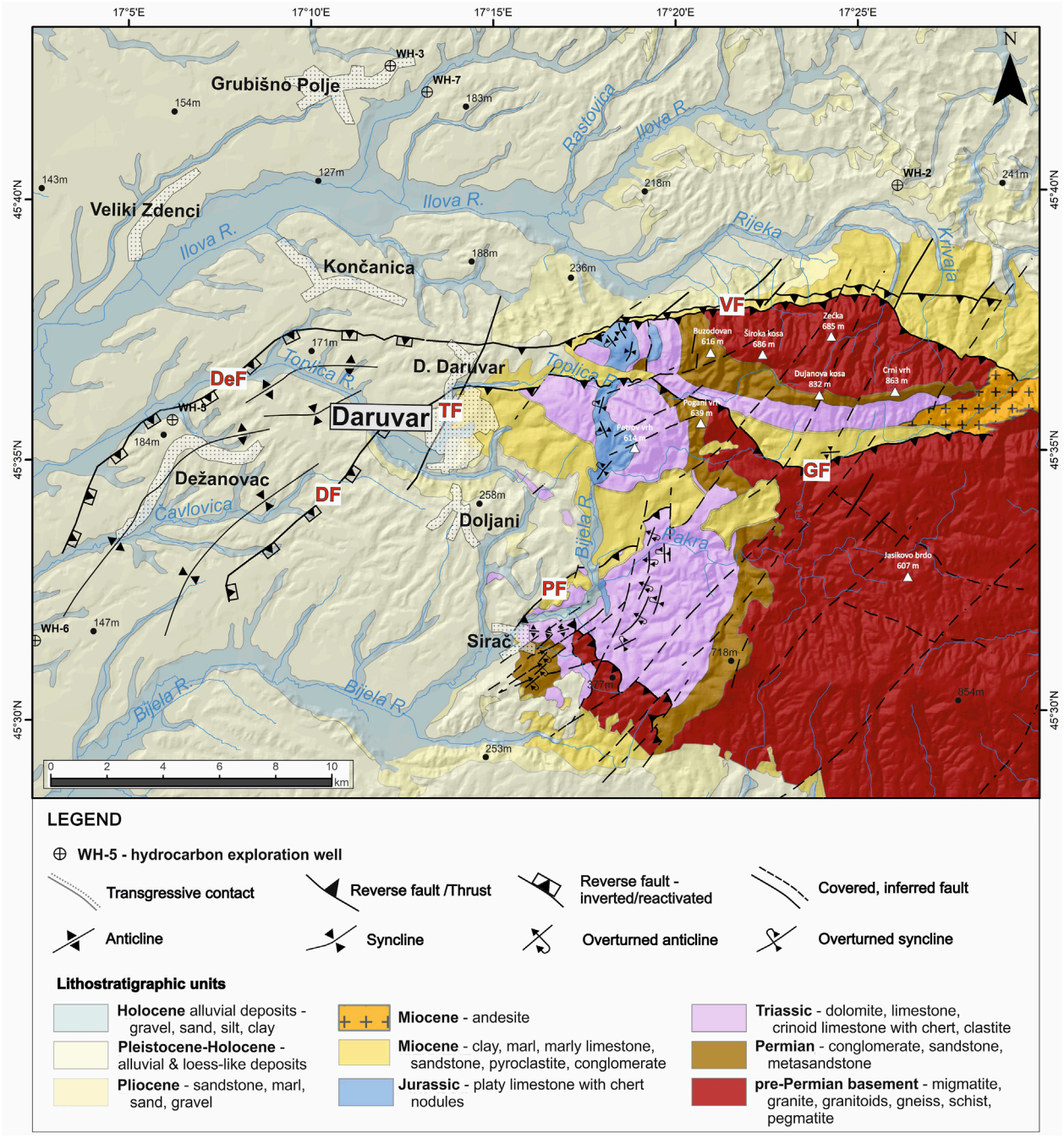

FIGURE 3
Simplified geological map of the Daruvar area (modified from Jamičić et al., 1989; Šolaja, 2010). Fault acronyms: DF, Daruvar fault; DeF, Dežanovac fault; GF, Gradina fault; PF, Pakrac fault; TF, Toplica fault; VF, Voćin fault. Topographic peaks are denoted by white triangles. White polygons indicate larger settlements and towns.

of strata bedding and fractures/joints (i.e., dip direction and dip angle). Furthermore, outcrop-scale structural data on fault geometrical properties, fault slip, and kinematics were also collected. The resulting dataset comprised 134, 659, and 91 measurements of bedding, fractures, and faults, respectively. Where local scale folds were visible, the fold axis was determined. Following the principal structural units, the Daruvar structural framework (Figure 4) was divided into three structural domains separated by regional E-W or NE-SW striking reverse faults: i) Dujanova kosa (DK), ii) Petrov vrh (PV), and iii) Sirač (SI). Structural observations in these domains were subdivided into eastern, central, and western sections obtaining a detailed analysis of the structural style within each block composing the structural fabric of the Daruvar hinterland.

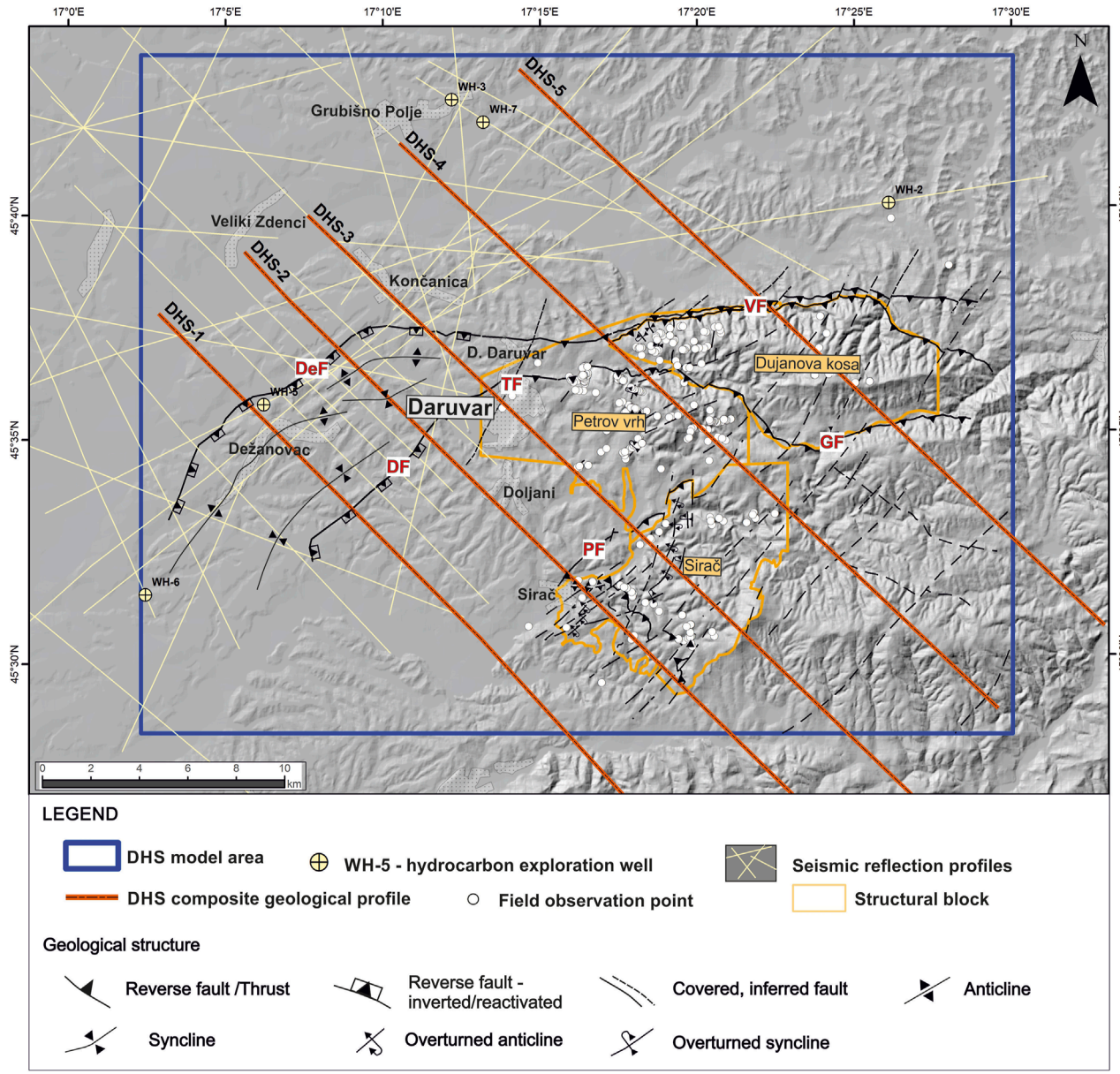

FIGURE 4
Distribution of the field measurement points (white dots), and traces of constructed composite geological profiles (red line) in the Daruvar area. Measured data, coupled with seismic reflection profiles (light yellow lines) and stratigraphic logs of deep wells, were used to construct the 3D model (blue rectangle). The structural domains (Dujanova kosa, Petrov vrh, and Sirač; orange polygons), the main geological structures, and towns (light grey polygons) are also shown. The acronyms of the main faults are reported in Figure 3.

In this study, data were plotted by the Stereonet v.11 software (Allmendinger et al., 2011; Cardozo and Allmendinger, 2013). A representative bedding was calculated for every measurement point. The results were plotted to graphically determine the most common orientations within each domain. Poles of fracture planes were used to construct contour plots of the poles distribution using the 1% area contour method (Allmendinger et al., 2011; Cardozo and Allmendinger, 2013). The plots were used to determine the most representative sets of fractures in each domain. For the determination of fault kinematics, we used data of dip direction and dip angle of fault planes and kinematic indicators, i.e., orientation of slickensides defined by azimuth and plunge, and, their sense of movement (Doblas, 1998). Based on kinematic criteria, the shear fracture data were analyzed by Win-Tensor v. 5.9.2 software (Delvaux and Sperner, 2003). The obtained data was separated into compatible fault groups and processed by TectonicsFP v. 1.7.9 software (Ortner et al., 2002). Theoretical maximum (σ1), mean (σ2) and minimum stress axes (σ3) were calculated using the P–T axis method (Turner, 1953; Marrett and Allmendinger, 1990). For the analyzed fault groups, synthetic focal mechanisms were calculated using the Right Dihedra Method (Angelier and Mechler, 1977).

3.2 Composite geological profiles and 3D geological modeling

Composite geological profiles are key components in the interpretation of the 2D/3D subsurface relations and structures. The composite geological profiles were constructed using: i) field data collected within this study, ii) existing geological data (i.e., geological maps, explanatory notes, published geological data), iii) seismic reflection profiles collected for hydrocarbon exploration, and iv) stratigraphic logs of deep wells drilled during the hydrocarbon exploration campaign and geophysical well-logging data. Here, five NW-SE composite geological profiles were constructed (DHS-1 to DHS-5; Figure 4), representing surface/subsurface 2D models of the Lonjsko-Ilovska depression and the western part of Mount Papuk.

Constructed composite geological profiles combined with field dataset were further integrated to develop the 3D geological model of the DHS area (blue rectangle in Figure 4). Petroleum Experts Move 2019.1 (https://www.petex.com/products/move-suite/move/) software package was used to build the subsurface model. The workflow for the model construction is shown in Figure 5. Since the geological setting of the study area is very complex (i.e., fault with variable architecture, regional folds, disconformities, angular unconformities, nonconformities), 15 additional geological sections mostly perpendicular and longitudinal to the geological structures were constructed. Furthermore, 20 smaller auxiliary (temporary) sections were made to obtain a more detailed reconstruction at the local scale. Fault surfaces were obtained by extending fault traces from geological profiles and maps into the subsurface using detailed measurements from the fieldwork and fitting the geological sections. Horizon surfaces were constructed by the ordinary kriging interpolation algorithm with "*Use Meshed Alpha Shape as Input Points*" option. This option allows a better interpolation of the complex surfaces based on sparse and irregular data. A construction mesh with vertices exactly at the XY location of irregularly spaced data points was performed (Petroleum Expert, 2019). The algorithm then used a convex hull to create a surface. Grid geometry provided an option (i.e., Honour Points) to create an interpolated surface with Z elevations at the XY locations of existing data points and is geomathematically predicted at other vertex locations of the construction mesh (Petroleum Expert, 2019). Surface Sampling controls the triangle size of the mesh, and it was fitted based on the density of input data.

4 Results

4.1 Analysis of bedding and fracture system

4.1.1 Dujanova kosa (DK)

The structural domain of Dujanova kosa (DK) encompasses the northern segment of the study area (Figure 4). It is positioned between two E-W striking low-angle thrust faults (Voćin and Gradina faults; VF and GF, respectively, in Figure 3; Figure 4). Structural measurements were conducted on 68 geological stations (Figure 4) with collected data about 48 strata orientations and 158 fracture planes.

Field observations of the ***basement*** section evidenced that the granitoids are heavily weathered. They are structurally missing geometrical properties, i.e., foliations/bedding orientations, but they are deformed by two systems of fractures (Table 1; Figure 8). The system Fs_1 is characterized by steeply dipping (dip angle 80°) NNW-SSE striking fractures, whereas Fs_2 is composed of discontinuities that dip towards SSE at a dip angle of 52°.

The ***eastern section*** of the DK encompasses the Permian clastic and the Triassic carbonate succession. It is mostly characterized by folded structures with fold axes gently dipping towards SW or NW (dip angle of 12° and 5°, respectively; Figure 6). In the first fold set beds are gently dipping SE and WNW at average angles of respectively 48° and 37°, or towards ENE and WSW at 28° and 52° for the second fold set. These observations indicate a polyphase tectonic evolution of the Permian-Triassic succession that enabled the formation of at least two generations of folds. Four fracture systems were further evidenced (Table 1; Figure 8). The Fs_1 fracture system is characterized by discontinuities steeply dipping towards N with a dip angle of 71°. The system Fs_2 includes predominantly N-S striking fractures that are gently dipping towards E at 36°. Fracture system Fs_3 shows a strike parallel to Fs_2, but these discontinuities are dipping towards W at the angle of 58°. The Fs_4 system is characterized by subvertical NE-SW striking fractures that are dipping at the angle of 76° towards SE.

The structural measurements in the ***central section*** of the DK were mainly conducted in Upper Triassic and Jurassic carbonates (Figure 3; Figure 4). Beds are dipping either towards NE or W at the average angle of 43° and 64°, respectively, resulting in folded structures with fold axes gently dipping towards NNW at the angle of 15° (Figure 6). Fracture data suggest the existence of three fracture systems (Table 1; Figure 8). The system Fs_1 is characterized by fractures steeply dipping towards WSW with an average dip angle of 63°. The Fs_2 set is composed of NE-SW striking discontinuities that are steeply dipping towards SE at the angle of 73°. Fs_3 has a strike similar to Fs_1, but these discontinuities are dipping towards NE at 61°. All these fracture systems are characterized by subvertical geometry implying their structural position with respect to the fold hinge zones.

The ***western section*** of the DK includes field investigations that were conducted in Triassic carbonates and its Neogene sedimentary cover. Bedding measurements show similar structural pattern to the central section of the DK. NW-SE striking beds dipping towards NE and SW (dip angle of 81° and 63°, respectively) compose isoclinal folded structures with axes gently dipping towards NW, at the angle of 19° (Figure 6). Measured fracture discontinuities suggest the presence of two systems (Table 1; Figure 8). The Fs_1 fracture system is characterized by E-W striking discontinuities dipping towards N with a dip angle of 53°. The Fs_2 fracture system includes NNE-SSW striking discontinuities dipping towards ESE at the angle of 59°.

4.1.2 Petrov vrh (PV)

The PV structural domain includes the central segment of the study area (Figure 4). It is bounded by the E-W striking Gradina fault (GF) and the NW-SE striking Pakrac fault (PF). Here, the rock complex has been intensively folded by a series of kilometer-scale displaced anticlines and synclines. Structural measurements were conducted on 184 geological stations (Figure 4) with collected data about 57 strata orientations and 332 fracture planes.

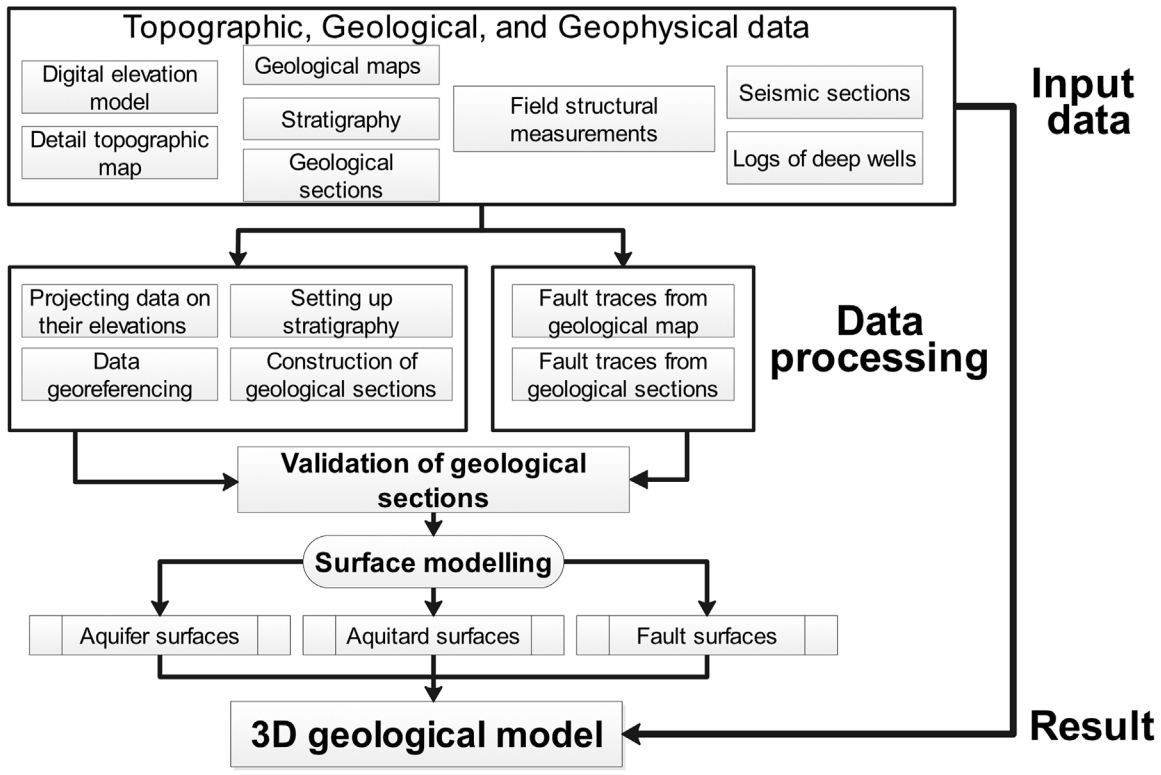

FIGURE 5
Schematic flow chart used in the construction of the 3D geological model of the DHS area.

As observed in DK, the pre-Permian granitoids of the ***basement*** are structurally missing recognizable foliation/bedding orientations. However, three systems of fractures (Table 1; Figure 8) were observed. Fracture system Fs_1 is characterized by discontinuities that dip towards NE at an average dip angle of 45°. The system Fs_2 is composed of discontinuities that dip towards W at a dip angle of 68°. The group Fs_3 is a WNW-ESE striking system of fractures that are steeply dipping (dip angle 87°) towards SSW.

The ***eastern section*** of the PV, which includes the Permian clastic and Triassic carbonate successions, is mostly characterized by folded structures with fold axes gently dipping towards S at an angle of 4° (Figure 6). Field measurements in these folded clastic and carbonate layers indicate that beds are dipping either E or W at the average angle of 48° and 31°, respectively. Three fracture systems were determined (Table 1; Figure 8). The first fracture system (Fs_1) is characterized by discontinuities steeply dipping towards N (dip angle of 88°). The Fs_2 system includes predominantly NNE-SSW striking discontinuities that are dipping towards ESE at the angle of 50°. The fracture system Fs_3 has a NNW-SSE strike and these discontinuities are dipping towards ENE at 61°.

The structural measurements in the ***central section*** of the PV, similarly to the central section of DK, were mainly conducted in fractured Upper Triassic-Jurassic carbonates (Figure 7A). Folded structures are characterized by fold axes gently dipping either towards SSE or SW (dip angle of 21° and 25°, respectively; Figure 6). Beds of the first group of folds are steeply dipping towards E and WSW at the average angle of 66° and 80°. For the second fold series, beds are gently dipping towards W and S at the angle of 33° and 32°, respectively. These observations indicate a polyphase tectonic evolution in the domain that enabled the formation of at least two generations of folds. At the same time, two main fracture systems can be delineated (Table 1; Figure 8). The system Fs_1 is characterized with fractures steeply dipping towards ESE at a dip angle of 82°. The second fracture system Fs_2 is characterized by WNW-ESE striking discontinuities that are steeply dipping towards SSW at the angle of 87°.

The ***western section*** of the PV encompasses the Triassic carbonates and their transgressive Neogene sedimentary cover (Figure 3; Figure 4). Similarly, to the central section, bedding measurements indicate a polyphase tectonics, with at least two generations of folds. Folded structures are characterized by fold axes gently dipping towards SSW or ENE (dip angle of 23° and 14°, respectively; Figure 6). Beds in the first fold group are dipping either ESE or W at the angle of 60° and 65°, respectively. For the second generation of folds, they are dipping towards SE and NNW at the angle of 26° and 53°, respectively. The analyses of the measured fracture discontinuities (Table 1; Figure 8) suggested the presence of three fracture systems. The Fs_1 fracture system includes NNE-SSW striking discontinuities that are dipping towards ESE with a dip angle of 52°. The Fs_2 system is dipping steeply towards N (average dip angle of 84°), while fracture system Fs_3 has a strike parallel to the strike of Fs_1, but these discontinuities are steeply dipping towards WNW at the angle of 82°.

TABLE 1 Average orientations of the main fracture systems in the structural domains of the study area and number of data constituting the sets.

Section	Fracture system	Dujanova kosa				Petrov vrh				Sirač			
		Data	Dip direction (°)	Dip angle (°)	Strike	Data	Dip direction (°)	Dip angle (°)	Strike	Data	Dip direction (°)	Dip angle (°)	Strike
Basement	Fs_1	6	252	80	162–342	16	34	45	124–304	8	239	44	149–329
	Fs_2	4	168	52	78–258	4	263	68	173–353	3	20	13	110–290
	Fs_3	–	–	–	–	4	199	87	109–289	–	–	–	–
East	Fs_1	25	357	71	87–267	29	11	88	101–281	18	180	72	90–270
	Fs_2	15	99	36	9–189	27	119	50	29–209	16	251	49	161–341
	Fs_3	8	257	58	167–347	26	57	61	147–327	10	149	30	59–239
	Fs_4	6	130	76	40–220	–	–	–	–	–	–	–	–
Central	Fs_1	18	251	63	161–341	55	117	82	27–207	59	76	84	166–346
	Fs_2	15	138	73	48–228	42	208	87	118–298	41	129	61	39–219
	Fs_3	10	35	61	125–305	–	–	–	–	35	205	60	115–295
West	Fs_1	19	354	53	84–264	28	118	52	28–208	20	205	68	115–295
	Fs_2	10	109	59	19–199	25	8	84	98–278	19	127	65	37–217
	Fs_3	–	–	–	–	24	299	82	29–209	14	95	77	5–185

4.1.3 Sirač (SI)

The SI structural domain encompasses the southern part of the study area and is mostly composed of Mesozoic carbonate succession (Figure 3). Its northern boundary follows the NW-SE striking low-angle Pakrac thrust (PF; Figure 3). Field investigations at the 58 geological stations resulted in measurements of 29 strata orientations and 243 fracture planes.

The ***basement section*** of the SI refers to a small area located in the farthest NE part. The structural fabric of the pre-Permian granitoids is similar to the DK and PV domains being deformed by two fracture systems (Table 1; Figure 8). Fs_1 is an NNW-SSE striking fracture system dipping towards WSW (dip angle of 44°), whereas the second fracture system, Fs_2, includes discontinuities that gently dip towards NNE at a dip angle of 13°.

The ***eastern section*** of the SI encompasses the Permian sedimentary units (Figure 7B) and the Triassic carbonate succession that are intensively fractured and folded. Folded structures are characterized by fold axes gently dipping towards S or W (dip angle of 10° and 4°, respectively; Figure 6). Beds of the first fold generation are dipping either E or W at the angle of 69° and 32°, or towards N or S (dip angle of 62°and 53°, respectively) for the second group of folds. As observed in other domains, it suggests a polyphase tectonic evolution that enabled at least two deformation events, i.e., fold generations. Measured fracture discontinuities pinpoint the existence of at least three fracture systems (Table 1; Figure 8). The first fracture system Fs_1 is characterized by discontinuities steeply dipping towards S with a dip angle of 72°. The second set Fs_2 includes predominantly NNW-SSE striking discontinuities that are dipping towards WSW (dip angle of 49°). Fs_3 fracture system is characterized by ENE-WSW striking discontinuities that are dipping at the angle of 30° towards SSE.

The structural measurements in the ***central section*** of the SI were mainly conducted in Upper Triassic dolomites (Figure 3). NNW-SSE striking beds (Figure 6) point to folded structures with fold axes gently dipping towards SSE at the angle of 2°. Beds in this structures are dipping towards either NE or SW at the angle of 40°, and 60°, respectively. Another set of measurements indicates a homocline where beds are gently dipping towards NNW at the angle of 33°. Three fracture systems were delineated (Table 1; Figure 8). The first fracture system Fs_1 is characterized by fractures steeply dipping towards ENE with a dip angle of 84°. The second set Fs_2 encompasses NE-SW striking discontinuities that are steeply dipping towards SE at the angle of 61°. Fs_3 group has a WNW-ESE strike and dips towards SSW at the angle of 60°. These fracture systems are characterized by subvertical geometry that implies their structural position with respect to the fold hinge zones.

The ***western section*** of the SI included field investigations that were mainly conducted in Triassic carbonates (Figure 3). NE-SW striking beds compose folded structures with axes gently dipping towards SW at the angle of 2° (Figure 6). Measured fracture discontinuities (Table 1; Figure 8) suggested the presence of three fracture systems. The system Fs_1 is characterized by ESE-WNW striking discontinuities that are dipping towards SSW with a dip angle of 68°. The Fs_2 fracture system includes

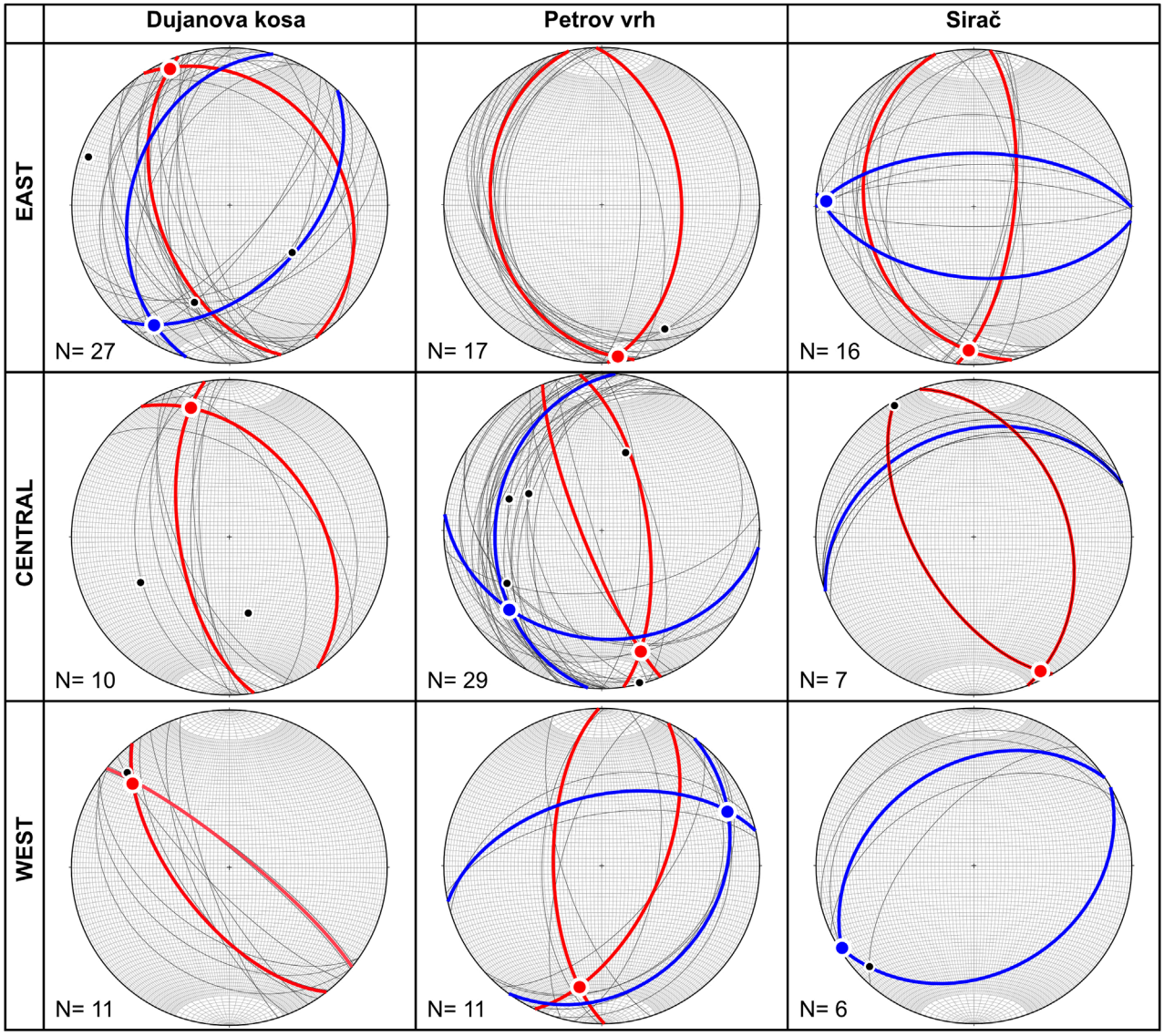

FIGURE 6
Stereonets of the bedding orientations (thin black circles) in the different domains of the study area. Their interpretation highlights the polyphase tectonic evolution of the study area with processes of refolding and occurrence of two generations of folds (thick blue and red circles) characterized by different fold axes (blue and red points). N indicates the number of measurements available in each structural domain.

NE-SW striking discontinuities dipping towards SE at the angle of 65°. Fs_3 is characterized by subvertical N-S striking discontinuities that are steeply dipping at the angle of 77° towards E.

4.2 Fault system and shear fracture analysis

Structural investigations focused also on the identification of the principal faults/fault zones that built the structural assemblage of the study area. Approximately 90 shear fractures/fault plane data at 47 geological stations were collected. Considering the stress field and kinematic criteria, three principal fault categories were delineated and further subdivided into compatible fault groups and subsets (Table 2; Figure 9).

4.2.1 Reverse faults

Reverse fault planes (17 measurements) were separated into RF/1 and RF/2 fault groups (Table 2; Figure 9). Measured dominantly in the Mesozoic carbonate succession, the RF/1 group is characterized by two fault subsets: RF1/a shows an average ENE dip direction (dip angle of 35°, Figure 9), whereas RF1/b steeply dips towards NW at a dip angle of 74°. The RF/2 reverse fault group is composed of two subsets striking both N-S and WNW-ESE. The RF2/a subset is characterized by an average E dipping direction (dip angle of 67°), whereas the RF2/b subset includes planes dipping towards SW (dip angle of 44°). Structural analysis of the representative paleostress field mechanisms indicate that the paleostress compressional field for the RF1 fault group is associated with a P-axis generally trending NW-SE (Table 2; Figure 9). The

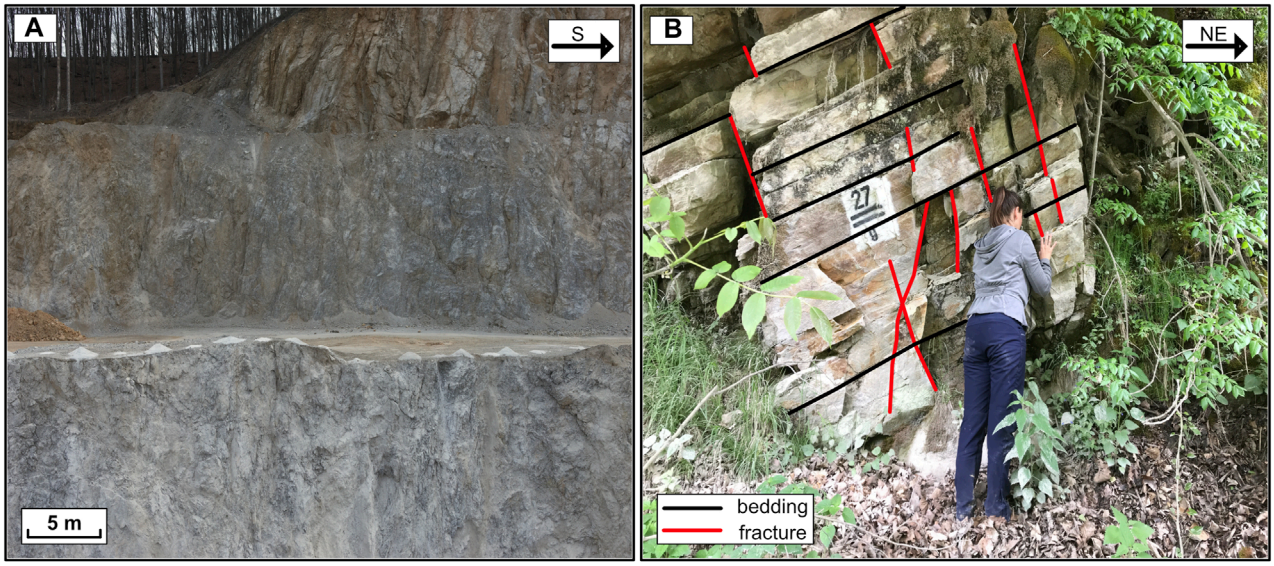

FIGURE 7
(A) Heavily fractured Triassic dolomites intercalated with dolomitized limestones and shales at the quarry of Batinjska rijeka steeply dipping toward WNW (central part of PV structural domain, NE of Daruvar; 45°36′20.76″N, 17°16′19.77″E). **(B)** Permian layered sandstones (eastern section of the SI domain; 45°33′14.52″N, 17°21′38.74″E) with bedding orientation of 237/32 (dip direction/dip angle) deformed by two sets of N-S and E-W striking subvertical fractures system (average dip direction/dip angle of 123/64 and 354/70, respectively).

computations for the RF2 fault group show a compressional paleostress field that is associated with a P-axis trending NE–SW (Table 2; Figure 9). These compressional paleostress fields resulted in the formation of the cogenetic fault-related structures (Figure 10A) that exhibit tectonic transport dominantly to NW/SE or NE/SW respectively.

4.2.2 Normal faults

Besides reverse fault planes, 31 normal fault planes were measured (Figure 10B,C). Normal faults were separated into NF1, NF2, and NF3 groups (Table 2; Figure 9). Group NF1 is characterized by NE-SW striking fault planes with fault subsets that are dipping towards either NNW or SE (dip angle of 46° and 43°, respectively). Kinematic analysis shows that these normal fault planes were formed within a paleostress field characterized by a subvertical P-axis steeply dipping towards the SSW (P-axis orientation is 206/86; Table 2) and subhorizontal T-axis trending NW–SE resulting NW–SE extension. The group NF2 encompasses ESE–WNW striking fault planes with fault subsets that are dipping towards N and S (dip angle of 64° and 28°, respectively). Kinematic and paleostress field analyses show that measured normal fault planes were formed within the paleostress field characterized by a subvertical P-axis steeply dipping towards the SSW and subhorizontal T-axis trending N–S (Table 2) that resulted in NNE–SSW directed extension. The third normal fault group NF3 encompasses N–S striking fault planes with fault subsets that were dipping towards ESE and WNW (dip angle of 44° and 47°, respectively; Table 2; Figure 9). Paleostress field analyses for this group show that fault planes were formed within the ESE–WNW directed extension that was influenced by the subvertical P-axis steeply dipping towards N (P-axis orientation is 11/86; Table 2), whereas the subhorizontal T-axis is generally trending E–W.

4.2.3 Strike-slip faults

Strike-slip fault planes (43 measurements) were separated according to their geometric properties and kinematic compatibility into two principal fault groups (SSF1 and SSF2; Table 2; Figure 9). The SSF1 group includes dextral/sinistral faults (dip angle between 79° and 89°) that are dominantly striking either NE–SW or NW–SE, while the SSF2 group resembles steeply dipping conjugate fault pairs with ESE–WNW and NNE–SSW strike (dip angle between 61° and 89°). Mapped strike-slip fault planes were often observed with structural reactivation features that encompassed slickenside overgrowths. Both dextral and sinistral movement indicators were visible (Figure 10D). This reactivation indicates the interchange and re-orientation of the principal stress axes σ1 and σ3 within the same stress field. Kinematic analysis also points to faults' structural reactivation indicating that the mapped fault planes were formed within two slightly different paleostress fields (Table 2): i) paleostress field associated with the NE–SW trending P-axis (T-axis trending NW–SE), and ii) paleostress field associated with general N-S trending P-axis that bends towards NNW or NNE (T-axis trending NE-SW or NW-SE; Figure 9). In addition, field observations of cross-cutting relationships between the mapped reverse/normal faults and strike-slip faults indicate that the strike-slip fault planes usually cut across and offset the reverse/normal faults. Structural reactivation indicators further evidence that some reverse/normal fault planes were also reactivated as dextral/sinistral faults.

4.3 Composite geological profiles and subsurface geological model of DHS

Composite geological profiles DHS-1 to DHS-5 (Figure 4; Figure 11; Supplementary Figure S3) represent the proposed

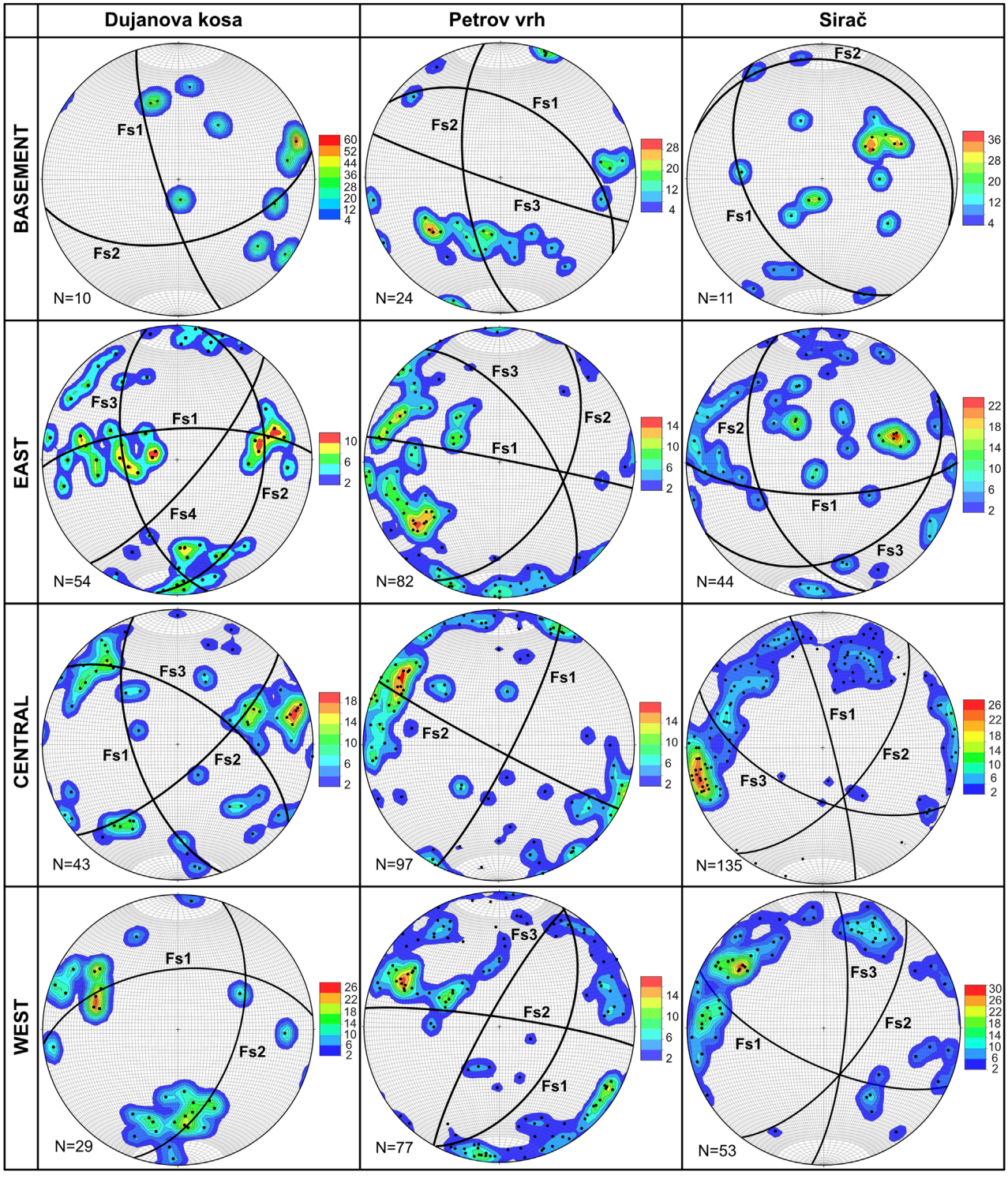

FIGURE 8
Structural diagrams of the main fracture systems (black circles) in the structural domains of the study area. The orientations of the representative fractures (F_S) in the systems are reported in Table 1. They are obtained from the distribution of the measured discontinuities represented here as poles (black points). The distribution is shown as a contour plot using a rainbow color ramp with values depending on the number of available data (N).

geological relationships in the surface and subsurface of the study area reaching approximately an investigation depth of 2.5 km. The model (Figure 12) extends on an area of approximately 1,000 km^2 (36 and 28 km in E-W and N-S directions, respectively) including the Lonja-Ilova subdepression and the western margin of Mount Papuk. It consists of eight fault plane surfaces representing

TABLE 2 Mean geometrical properties of the observed fault planes with calculated kinematic indicators and parameters. Fault planes were grouped following their geometrical and kinematic properties (Figure 9). Fault types: RF—reverse faults; NF—normal faults; SSF—strike-slip faults. Orientations of the P- and T-axes are based on constructed synthetic structural beach-ball diagrams.

Group	Subset	Data	Dip direction (°)	Dip angle (°)	Pitch (°)	Strike (°)	Fault type	Striation		P-axis		T-axis	
								Trend (°)	Plunge (°)	Trend (°)	Plunge (°)	Trend (°)	Plunge (°)
RF1	RF1/a	4	69	35	61	–	R	142	54	318	11	153	7
	RF1/b	5	321	74	72	–	R	302	64				
RF2	RF2/a	6	87	67	64	–	R	63	52	65	17	317	63
	RF2/b	2	206	44	62	–	R	205	48				
NF1	NF1/a	9	337	46	71	–	N	250	55	206	86	328	1
	NF1/b	6	146	43	77	–	N	159	61				
NF2	NF2/a	6	17	64	69	–	N	229	62	204	64	11	15
	NF2/b	2	179	28	50	–	N	208	32				
NF3	NF3/a	5	281	47	66	–	N	338	61	11	86	280	1
	NF3/b	3	121	44	72	–	N	108	61				
SSF 1	SSF 1/a1	7	–	–	15	34–214	S-S	217	22	248	2	352	1
	SSF 1/a2	4	–	–	6	124–304	S-S	160	5				
	SSF 1/b1	2	–	–	13	67–246	S-S	65	11	209	5	287	5
	SSF 1/b2	4	–	–	34	157–337	S-S	156	33				
	SSF 1/c1	3	–	–	17	11–291	S-S	80	17	69	21	334	13
	SSF 1/c2	4	–	–	18	21–201	S-S	200	15				
SSF 2	SSF 2/a1	4	–	–	12	19–199	S-S	174	10	325	3	238	14
	SSF 2/a2	3	–	–	35	101–281	S-S	273	34				
	SSF 2/b1	3	–	–	31	24–204	S-S	242	30	345	22	81	6
	SSF 2/b2	3	–	–	42	124–304	S-S	37	45				
	SSF 2/c1	4	–	–	41	20–200	S-S	285	41	19	35	264	18
	SSF 2/c2	2	–	–	3	116–296	S-S	104	3				

the principal regional faults and 42 horizon surface segments representing the base of the six main mapped units. In particular, the Quaternary deposits were modeled together with the Pliocene unit due to their limited thickness, while the Miocene andesites were merged with the coeval sedimentary unit.

Structurally, the constructed profiles could be subdivided into two domains. Here, the DHS-3 geological profile is used as an example (see Supplementary Figure S3 for other profiles) to describe the tectonic styles, geological units, and structures since it is located in the central part of the study area (Figure 11).

The NW domain of the geological profile covers the area of the Lonja-Ilova subdepression. This subdepression, a part of the Bjelovar depression, is filled with Neogene-Quaternary sediments that are up to 1.5 km thick, while the pre-Neogene basement is composed of Permian-Triassic sedimentary units and pre-Permian crystalline rocks (Malvić and Velić, 2011). The Permian-Triassic sedimentary complex is generally following the pre-Permian basement paleorelief. Going from NW towards SE, the Permian-Triassic complex is shallowing reaching the surface in the vicinity of Daruvar (Figure 3). Several NE-striking normal faults (e.g., Munija one and Munija 2; DHS-5 in Supplementary Figure S3) pinpoint the Neogene extension in the PBS and the opening of accommodation space. Furthermore, differential thicknesses of the Neogene deposits in the fault's hangingwall/footwall are

10.3389/feart.2024.1401935

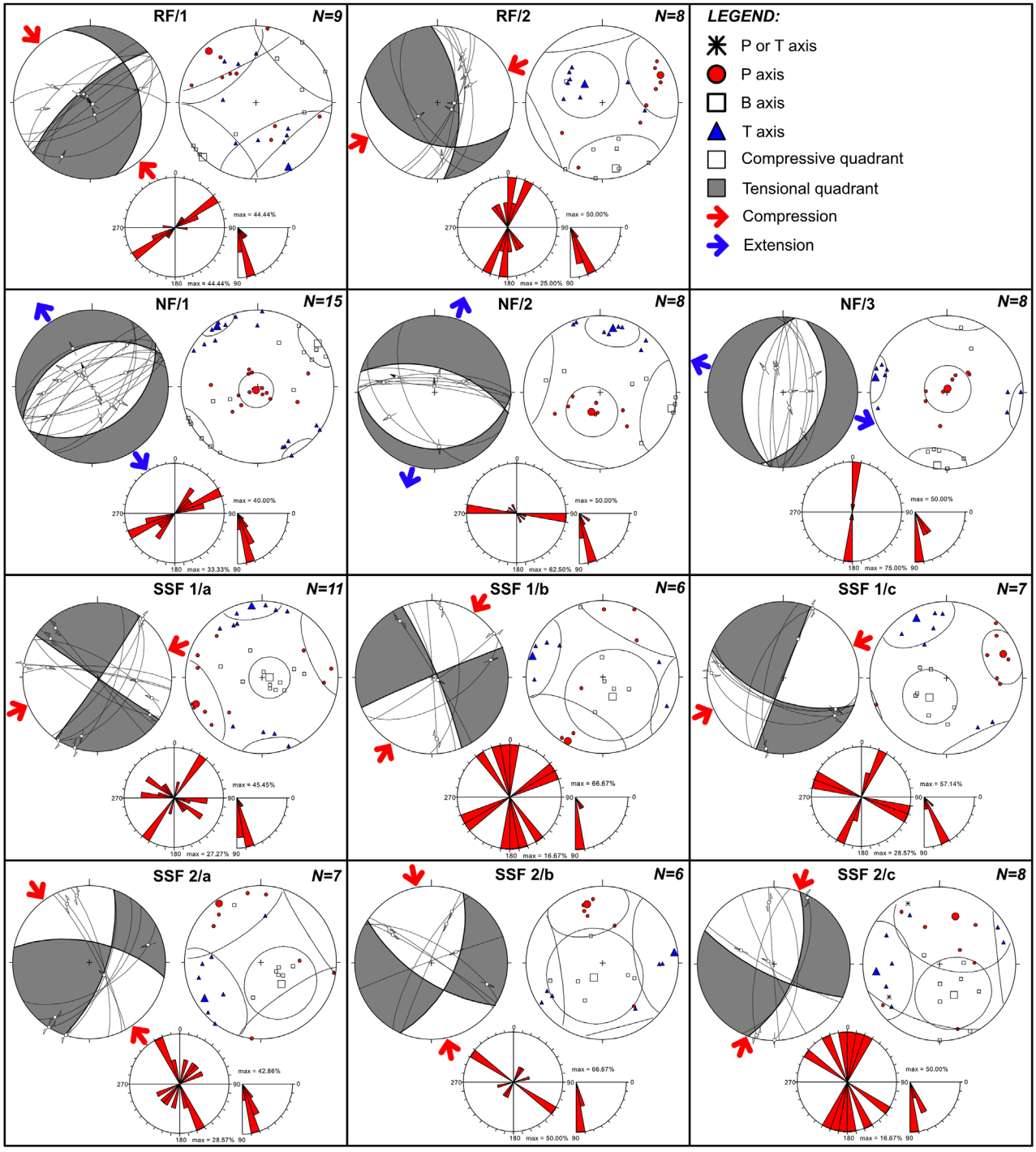

FIGURE 9
Structural diagrams for the interpreted fault systems in DHS area. RF1 and RF2 represent reverse fault groups. NF1, NF2, and NF3 represent normal fault groups, whereas SSF1(a,b,c) and SSF2 (a,b,c) represent strike-slip fault groups. The red points, white rectangles, and blue triangles indicate σ1, σ2, and σ3 stress axes, respectively.

observed in a few locations (e.g., Dežanovac fault in DHS-4; Supplementary Figure S3) suggesting structural reactivation and tectonic inversion. This implies that some of the interpreted faults are polyphase structures, accommodating extension through the Neogene, and tectonic inversion during the Pliocene-Quaternary. In the central part of the study area, the pre-Neogene complex of the Lonja-Ilova subdepression crops out forming the western slopes of Mount Papuk (Figure 3; Figure 11; Figure 12). Here, the contact between the Neogene-Quaternary sediments and the pre-Neogene rock complex is mainly transgressive, but dozens of mapped tectonic contacts indicate NW-SE contraction with cogenetic reverse faults. Low angle reverse faults are usually

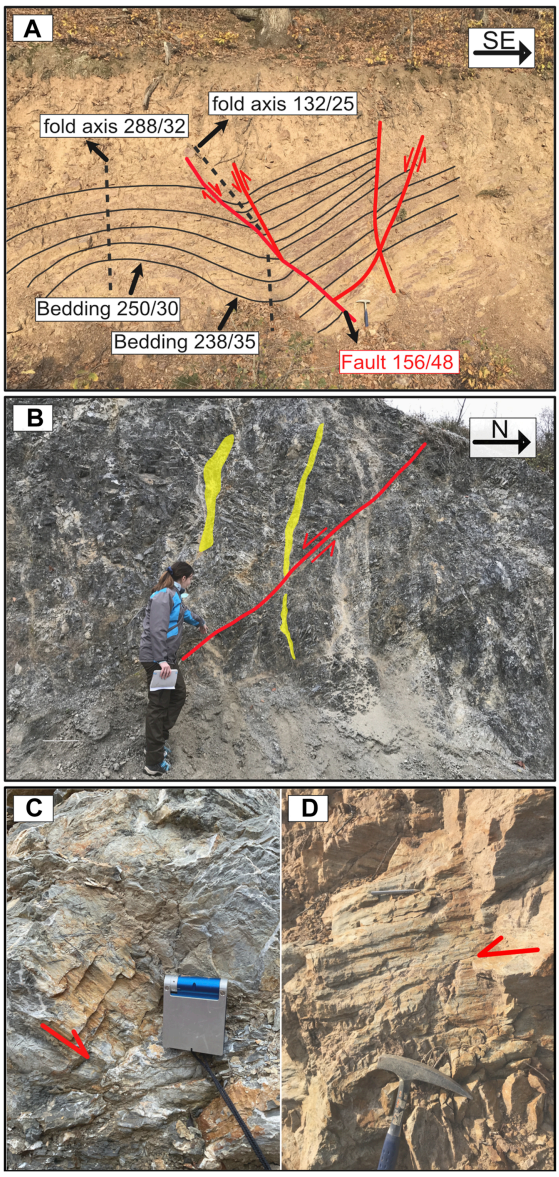

FIGURE 10
(A) Conjugate reverse and normal fault pairs with cogenetic fold axes. Reverse faults and asymmetric folds indicate tectonic transport top to the NW, whereas normal faults show post-folding extensional relaxation. Structures are observed within Permian sandstone (E of Daruvar in the PV structural domain; 45°35′17.24″N, 17°20′17.25″E). **(B)** Normal fault (F-2/37) measured within Triassic dolomites. Besides striations and slickensides fault kinematics are characterized by systematic tensional fractures filled with syntaxial minerals (E from Daruvar, in the PV structural domain; 45°35′31.55″N, 17°17′37.28″E). **(C)** Normal fault (F-293/88) measured within Jurassic limestone. Striations and slickensides indicate normal displacement with sinistral oblique movement (E of Daruvar in the PV structural domain; 45°35′34.87″N, 17°17′57.78″E). **(D)** Subvertical fault plane (F-340/88) measured within Permian sandstone. Striations and slickensides indicate sinistral/dextral movements (E of Daruvar in the PV structural domain; 45°35′16.61″N, 17°20′20.96″E).

either: i) blind faults forming cogenetic asymmetric anticlines (e.g., Dežanovac and Daruvar faults; DeF and DF, respectively, in Figure 11; Figure 12), or ii) thrust faults with ramps and flats (e.g., Pakrac fault; PF in Figure 11) forming fault-bend fold systems in the immediate hanging wall (Fossen, 2016; Nabavi and Fossen, 2021). The cogenetic asymmetric folds generally show gently inclined NW limbs, while SE limbs are steeper and shorter. This peculiar geometry suggests structure tectonic transport towards N-NW. Daruvar anticline is an example of a gentle asymmetric anticline (Figure 11 and DHS-2 and DHS-4 in Supplementary Figure S3) associated with the Daruvar fault (DF). It generally resembles a remobilized pre-Permian structural high that was transgressively covered by Permian-Triassic sediments and faulted afterward. In this context, the subvertical Toplica fault (TF in Figure 11) could be interpreted as a tensional fracture system developed in the hinge zone of the Daruvar anticline that was probably later reactivated as a dextral strike-slip fault zone (Kosović et al., 2023). Furthermore, NE-striking subvertical backthrust faults associated to the regional reverse faults were observed (e.g., Barica and Borki faults; Supplementary Figure S3). Mapped regional reverse faults are characterized by average dip angles of 45° and 55° in their steepest segments, while flat fault segments are characterized by dip angles ≤20°. Their maximum relative displacements are in a range between 0.5–1 km (Supplementary Figure S3). The Daruvar fault shows a maximum displacement of approximately 0.3 km (profile DHS-1 in Supplementary Figure S3).

The SE parts of the constructed profiles reflect the structural architecture of the western margin of the Slavonian mountains. Here, the tectonic uplift of the crystalline basement resulted in overall exposure of pre-Permian basement due to the erosion of the Permian-Mesozoic cover, while at the local scale, we could find patches of transgressively deposited Neogene sediments (Figure 11). Structural architecture of this area is cogenetic with two principal reverse low-angle faults, i.e., NNE-striking Voćin and Gradina faults (Figure 12; Supplementary Figure S3) which accommodated regional N-S compression. Relative displacements along the Voćin and Gradina reverse faults are in a range of a few hundred meters (Supplementary Figure S3).

5 Discussion

5.1 Tectonic emplacement and structural evolution of the study area

The Daruvar area, located in the immediate vicinity of the collision zone (i.e., Sava Suture Zone) between the Internal Dinarides and the Slavonian mountains resembles a complex litho-tectonic terrain that experienced a polyphase tectonic evolution (e.g., Jamičić, 1995; Balen et al., 2006). The different tectonic phases affected the structural relations in the subsurface, often showing tectonic overprints, without straightforward indication of distinctive deformation phases and associated geological features. Tectonic embayment of the study area started with the Variscan and afterward the Alpine-Dinarides-Carpathian orogeny which due to Cretaceous-Paleogene collision conveyed formation of the Slavonian mountains, a integral part of the regional nappe system (Schmid et al., 2008). The Cretaceous-Paleogene regional E-W (or NE-SW) compression promoted the formation of regional NW-SE striking reverse

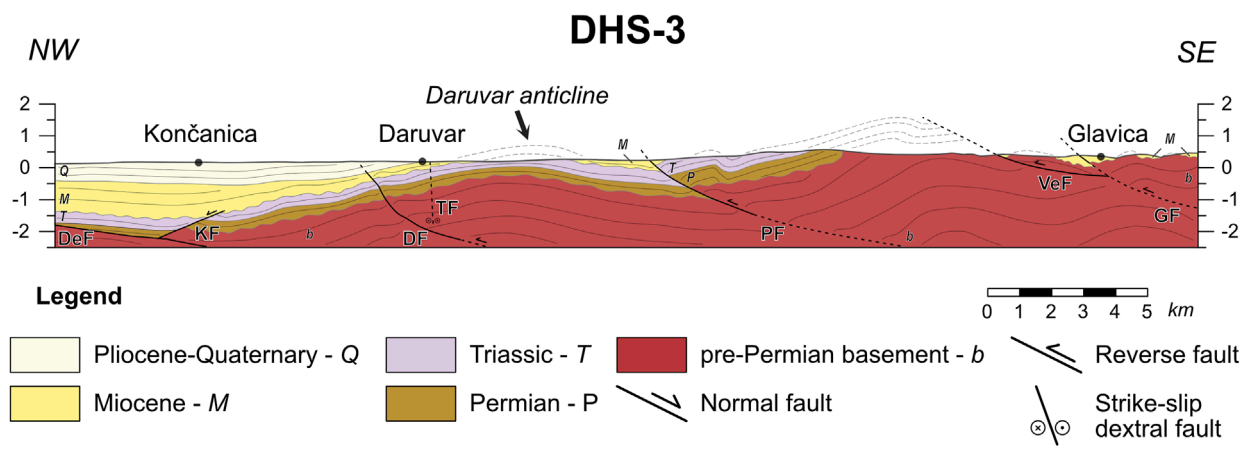

FIGURE 11
Composite NW-SE striking geological profile DHS-3 (trace in Figure 4) investigating the central part of the study area. It shows the Daruvar anticline deforming the subsurface in the vicinity of Daruvar. The main regional faults in the profile are: Dežanovac fault (DeF), Končanica fault (KF), Daruvar fault (DF), Toplica fault (TF), Pakrac fault (PF), Velika fault (VeF), Glavica fault (GF). A detailed lithological description of the units is in Figure 3 and Supplementary Figure S2. Horizontal and vertical scale is 1:1.

fault systems, and en-échelon folds characterized by NW-SE oriented fold axes. These structures were afterwards rotated counterclockwise of approximately 40° towards NE during the Paleogene (Tomljenović and Csontos, 2001; Ustaszewski et al., 2008). The post Cretaceous-Paleogene tectonic evolution of Daruvar area was further complicated by the Neogene-Quaternary evolution of the Pannonian Basin System (PBS). Inherited structures were affected by the Neogene E-W extension in the PBS, which locally caused additional rotation, structural reactivation, and tectonic inversion (Prelogović et al., 1998; Tari et al., 1999; Tomljenović and Csontos, 2001; Csontos and Vörös, 2004; Schmid et al., 2008; Ustaszewski et al., 2008). As a part of PBS, the Daruvar area during Pliocene-Quaternary was finally affected by the tectonic inversion of the existing structures due to regional N-S compression/transpression stresses (Ustaszewski et al., 2008; Schmid et al., 2020). Rejuvenated regional contraction enhanced the N-S shortening and continuous folding/re-folding processes of the existing structures synchronously with the lateral displacement processes along the strike-slip faults (Jamičić, 1995; Ustaszewski et al., 2008).

Structural data analysis of strata orientation, fracture systems, and fault systems presented in this study undoubtedly supports and confirms the complexity of the tectonic evolution in the Daruvar area. Analyses of strata orientations evidenced a polyphase folding in the area. Observed folds with fold axes that are gently dipping towards N or NW and S or SE (red folds in Figure 6) correspond to the Cretaceous-Paleogene E-W (NE-SW) contraction phase that culminated with the counterclockwise rotation of structures during the Paleogene (e.g., Tomljenović and Csontos, 2001; Ustaszewski et al., 2008). At the same time, E-W (or NE-SW) striking folded structures (blue folds in Figure 6) developed by the Pliocene-Quaternary N-S contraction were also observed in this study (Jamičić, 1995; Tomljenović and Csontos, 2001).

Cogenetically with the formation of these folded and refolded systems, the Paleozoic-Mesozoic sedimentary complex experienced extensive brittle deformation and the formation of fracture systems with preferred orientations (Figure 8). Measured fractures resembled N-S (locally NNE-SW, NNW-SSE) and subordinately E-W striking subvertical tensional fractures that were subparallel with the observed fold hinge zones (Figure 8). Locally, especially in the Mesozoic carbonate complex, N-S striking fracture systems show shear reactivation features (e.g., slickenside overgrowths) characterized by dextral/sinistral motions. This reactivation is connected to the Pliocene-Quaternary N-S oriented P-axis (Herak et al., 2009), and in general widens the damage zone of the N-S striking folded structures increasing the fracturing of the bedrock. On the other hand, E-W striking discontinuities are less frequent and generally without indications of structural reactivation suggesting that E-W striking folded structures are less affected by ongoing tectonic deformation due to their structural position in respect to the low strain rates (<1–2 mm/y; Grenerczy et al., 2005) of the N-S oriented P-axis (Herak et al., 2009).

Field observations of shear fractures/fault planes with associated kinematics and cross-cutting relationships support the results of bedding and fracture system analyses. Correlative to the Cretaceous-Paleogene (E-W contraction and counterclockwise structural rotation) and the Pliocene-Quaternary (N-S contraction) tectonics, formed fold systems and analyzed reverse fault group subsets suggested paleostress field with P-axes generally trending either NW-SE (RF1) or NE-SW (RF2) (Table 2; Figure 9). Synthetic structural focal mechanisms and field data suggested that orientations of average fault subsets are in correspondence with fault systems that accommodated the Cretaceous-Paleogene E-W contraction in the study area (today NW-SE orientated P-axis that rotated 40° counterclockwise) as well as Pliocene-Quaternary N-S contraction (i.e., Voćin fault, Gradina fault, Dežanovac fault and Daruvar fault; see Figure 3). At the same time, the RF2 reverse fault planes and the computed structural focal mechanisms

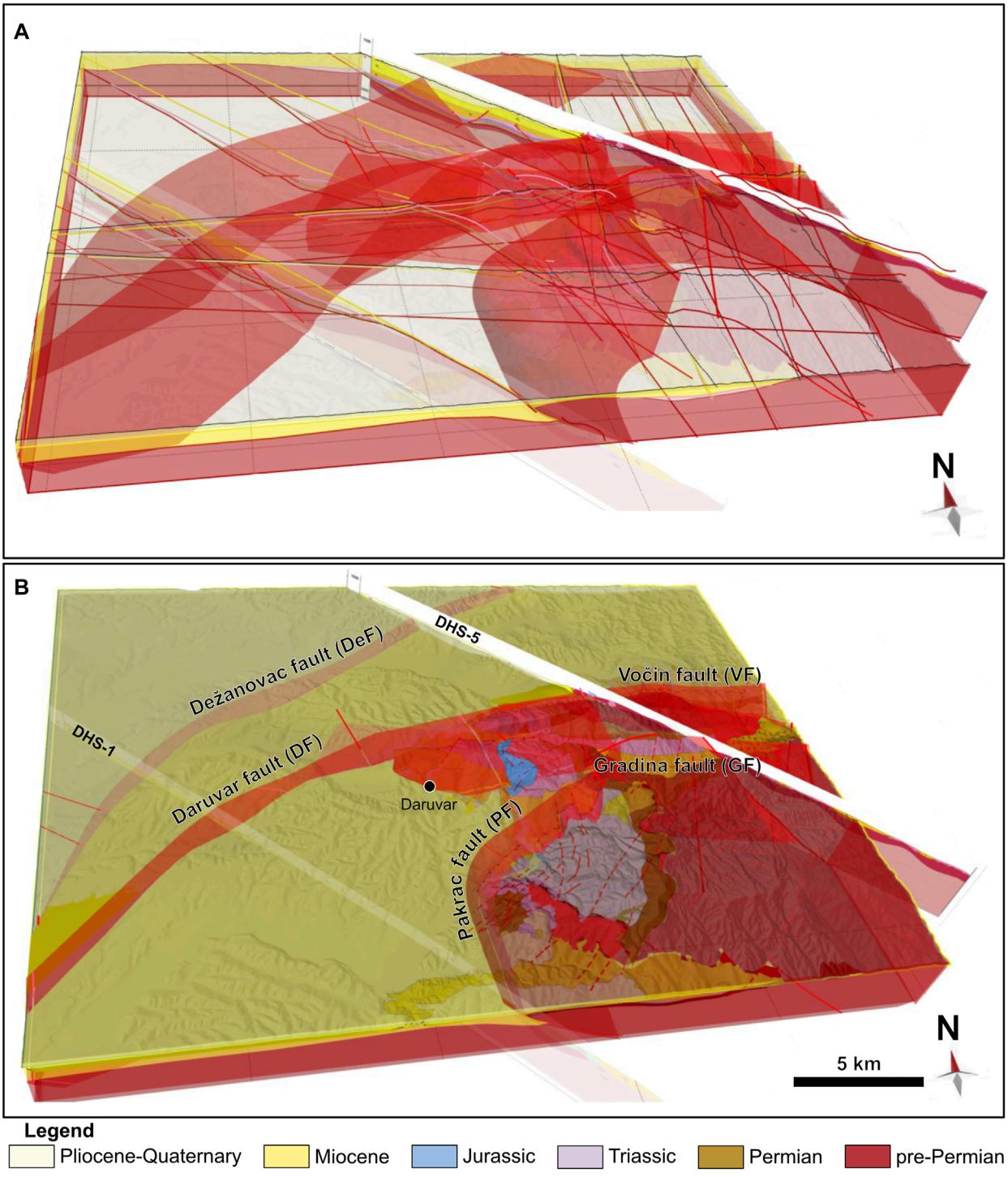

FIGURE 12
(A) Set of composite geological profiles and geological data used to construct the 3D geological model. **(B)** Finalized 3D model. It conveyed the stratigraphic surfaces and the regional faults that delineate the structural framework of the wider DHS area.

suggested also a NE–SW oriented contraction. Our structural results for this fault subset are slightly different in relation to the regional N-S contraction suggesting that local structural differences and inherited structures may contribute to a local reorientation of the P-axis. Focal mechanisms of normal faults generally suggest NW–SE, NNE–SSW, and ESE–WNW extension with subvertical P-axes (Table 2; Figure 9). This extension may be related to the final stages of the thrusting and folding in the area during the Late Cretaceous-Paleogene as a result of gravitational sliding of existing structures (e.g., Tavani et al., 2012)

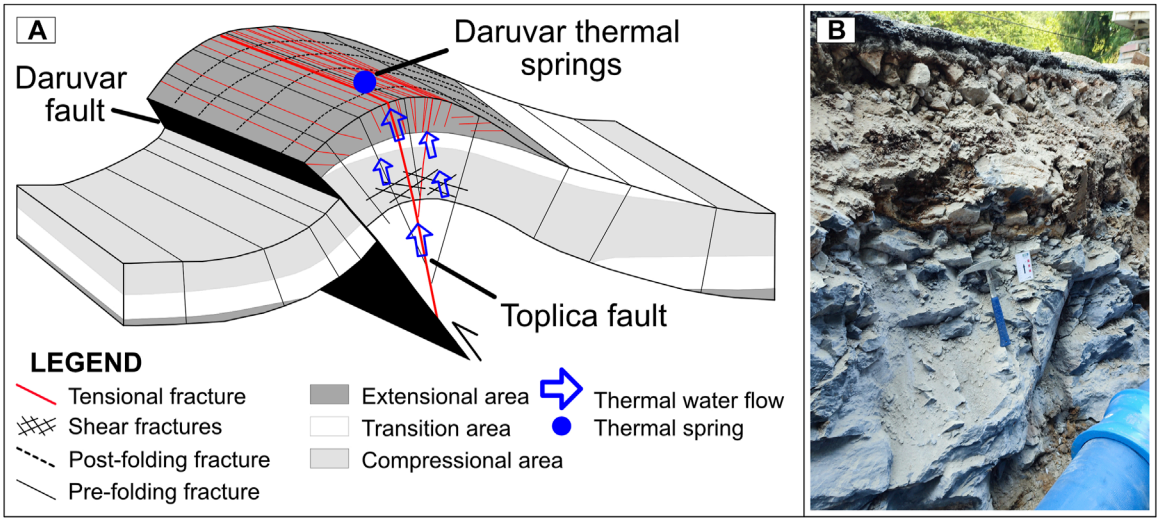

FIGURE 13
(A) Schematic conceptual model of the structural assemblage in the subsurface of the Daruvar area (modified from Frehner, 2011; Li Y. et al., 2018) affecting the upwelling of theDaruvar thermal waters. The NNE-SSW striking Daruvar anticline structurally forms in the hangingwall of the Daruvar reverse fault (see Figure 3 for location). In the hinge zone, cogenetic tensional fractures were structurally reactivated during the Pliocene-Quaternary and tectonically inverted as strike-slip fault zone (i.e., Toplica fault). The localized extensional regime in the topmost part of the hinge zone and its polyphase deformation increase the fracturing of the bedrock and the permeability field favouring the outflow of the thermal waters in the Daruvar spring area. **(B)** Heavily tectonized Triassic dolomites in the Daruvar thermal spring area (45°35′41.74″N, 17°13′38.43″E).

or by structural hanging wall collapse due to Late Oligocene-Miocene extension of the PBS. The most preserved slickensides, striations, and other kinematic indicators were observed along the strike-slip fault planes (SSF1 and SSF2; Table 2; Figure 9). Paleostress analysis and structural focal mechanisms indicate generally N-S oriented transpression which locally deflects to NW-SE and NE-SW (Figure 9). With their subvertical geometry mapped strike-slip faults may be associated with the Pliocene-Quaternary structural reactivation of faults originated during the Neogene extension of the PBS (Jamičić, 1995) or with the partly-tectonic reactivation of inherited fracture systems deforming the fold system hinge zones.

5.2 Hydrogeological conceptual model of the Daruvar hydrothermal system

The structural setting of the Daruvar hinterland and its tectonic evolution are integrated with available geochemical, hydrogeological, and geophysical data (Borović, 2015; Borović et al., 2019; Kosović et al., 2023; Urumović et al., 2023) on the Daruvar thermal field and the thermal waters accounting for: i) the correlation between fault and thermal systems (e.g., Curewitz and Karson, 1997; Faulds et al., 2013; Moeck, 2014), and ii) the increase of the permeability field due to fracture zones acting as preferential flow paths (e.g., Faulkner et al., 2010; Bense et al., 2013).

Geochemical and isotope data of the Daruvar thermal waters (Borović, 2015) show that: i) the waters are relatively young (10–15 ka) and originate from the precipitation in the nearby mountainous hinterland, which provides the hydraulic potential for the fluid flow, and ii) they circulate and most likely infiltrate into the Mesozoic carbonate complex constituting the geological assemblage of the western Papuk due to their calcium-bicarbonate hydrochemical facies. As a matter of fact, Mesozoic carbonates are an important reservoir for thermal waters in the PBS (Horváth et al., 2015; Rman et al., 2020) hosting approximately 20 geothermal installations just in its Croatian part (mostly thermal spas and balneological therapy centers; Borović and Marković, 2015).

The potential DHS recharge area could span over the outcrops of Mesozoic carbonates in the structural domains of Dujanova kosa, Petrov vrh, and Sirač (Figure 3). Since these areas are comprised in different tectonic blocks separated by reverse faults, they can be considered separate hydrogeological compartments. The Sirač structural domain is in the hanging wall of the Pakrac reverse fault (Figure 11). The Mesozoic units are here mostly in contact with Miocene formations in the footwall reducing the northward continuity of the Mesozoic carbonate aquifer (Figure 3). Furthermore, subthermal springs occur in the vicinity of Sirač and an artesian aquifer in a quarry nearby is reported (personal communication). Due to their geographical positions, they likely drain the recharge in the Sirač domain diminishing the potential recharge to the Daruvar thermal area. The Dujanova kosa structural domain has two outcrops of Mesozoic carbonates that could act as recharge areas of the DHS. The carbonates in the southeastern part of the domain (i.e., south of the Dujanova kosa and Crni vrh peaks; Figure 3) are included in a syncline structure bounded by the low permeable pre-Permian basement both to the N and the S (section DHS-5 in Supplementary Figure S3). Therefore, they can be considered hydrogeologically isolated. The carbonates in the western part of the block are at the footwall of the Daruvar/Gradina reverse fault being deeper than the same formations in both the Petrov vrh domain and the Daruvar area (sections

DHS-5 and DHS-3, respectively, in Supplementary Figure S3). Therefore, they could eventually drain the nearby blocks and it is unlikely that they could host waters with pressure high enough to flow into shallower aquifers. This fact is enforced by the low elevations of the Mesozoic outcrops in the study area, thus providing a similar hydraulic potential in all blocks.

The Mesozoic carbonate complex in the Petrov vrh structural domain is the most probable recharge area for the DHS due to its geographical and geological settings. The Mesozoic complex extends for approximately 15 km^2 eastward of Daruvar being approximately 4–8 km from the spring area. The elevation of the recharge area in Petrov vrh is generally the highest with an average elevation of 400 m a.s.l. And up to 613 m a.s.l. (average elevation of 397 and 349 m a.s.l. In Dujanova kosa and Sirač, respectively; maximum elevation of 570 and 552 m a.s.l. In Dujanova kosa and Sirač, respectively). The geological framework of Petrov vrh is characterized by a regional N-S striking overturned syncline (Figure 3) formed in the hanging wall of the Daruvar/Gradina fault (sections DHS-5 and DHS-3 in Supplementary Figure S3). The structural analysis conducted in the PV domain (Figure 8) revealed two sets of steeply dipping fractures that generally strike E-W (NE-SW) and N-S (NW-SE). Both sets are deformed by the last Pliocene-Quaternary N-S compression (Herak et al., 2009) and they can be considered tectonically active. The constant deformation of fractures is crucial since they maintains their aperture preventing the sealing by precipitation of minerals and preserving the permeability field of the bedrock. Due to its favorable structural position in respect to recent N-S oriented stress field, the N-S discontinuities could have a wider and highly deformed damage zone connected to their reactivation. The E-W discontinuities are less frequent, but they may result from a local transtensional regime in the hinge zone of the currently deformed E-W oriented folds. These conditions are favorable for the high permeability of the bedrock resulting in a high effective infiltration in the recharge zone.

The meteoric waters infiltrate due to the intense fracturing of the bedrock and flow westward favored by: i) the general westward dipping of the strata, ii) the pre-Permian and Permian units acting as the aquitard below the Mesozoic reservoir, and iii) the E-W tensional open fractures. The set of beds dipping W is the most frequent in both the eastern and central sectors of the PV domain (Figure 6). The pre-Permian crystalline rocks and the Permian sedimentary units have moderate to low permeability due to their lithologies (e.g., Domenico and Schwartz, 1998). Conversely, dissolution processes in the Mesozoic carbonates could add to the fracturing enhancing their permeability field (e.g., Goldscheider et al., 2010). This contrast prevents a deep infiltration of the meteoric waters that are more prone to flow in the carbonate reservoir. In addition, the dipping of the aquitard units toward W channels the fluid flow favoring the westward circulation of the infiltrated waters. Finally, the E-W fractures could act as preferential flow paths. The transtensional regime favors the opening of the fractures and increases the permeability that depends on the square of the fracture hydraulic aperture (e.g., Domenico and Schwartz, 1998).

The infiltrated waters are warmed by the heat flow of 80–100 mW/m^2 in this part of the PBS resulting in a local geothermal gradient of 35°C–40°C/km (Horváth et al., 2015; Borović et al., 2019). The reservoir equilibrium temperature of the thermal waters calculated using SiO_2 geothermometers is approximately 80°C (Borović, 2015). Considering an infiltration temperature of approximately 10°C and a purely conductive heat flow, the waters should reach a depth of approximately 2 km to approach the reservoir equilibrium temperature. However, the fracturing of the bedrock favors the occurrence of convective processes that increase the circulation and the temperature in the aquifer. As a matter of fact, a gradient of approximately 70°C/km is measured in the thermal wells of Daruvar (Borović et al., 2019) corroborating the impact of local convection on the temperature distribution. At the scale of the recharge and flow-through area of the DHS, it is reasonable to expect a gradient slightly higher than the regional value, which could permit to approach the reservoir equilibrium temperature at the maximum aquifer depth of the aquifer being 800–900 m below the ground level in the central part of Petrov vrh. The high geothermal gradient in the Daruvar area could add to the water temperature in the flow-through part of the system reaching the reservoir equilibrium temperature.

The thermal waters flow in the Mesozoic reservoir and reach the Daruvar city area located in the immediate vicinity of the Daruvar anticline (Figure 11; Figure 13). This NNE-SSW striking structure is an asymmetric fold (tectonic transport top to the W) cogenetic to the SE dipping Daruvar reverse fault. The polyphase tectonic evolution affecting the study area suggests structural reactivation of the Daruvar anticline favoring the continuous fracturing of the bedrock. A localized extensional regime is expected in the topmost section of the fold hinge zone increasing the fracture aperture and the permeability field (e.g., Frehner, 2011; Li N. et al., 2018). Field observations (Figure 13B) and core samples from the thermal wells showed that the Mesozoic reservoir is moderately fractured with localized zones of intense fracturing. The thermal waters rise to shallow depths in the damage zone of the Daruvar fault and cogenetic fractures that are deforming the hinge of the Daruvar anticline. In this context, the subvertical NE-striking dextral Toplica fault, which is a structurally reactivated and tectonically inverted tensional fracture system, could act as a preferential flow path for the quick rise of the thermal waters with a minor loss of temperature from the deeper part of the reservoir. The Toplica fault could be the fault F5 in the local scale model of the Daruvar spring area obtained through shallow geophysical investigations (Kosović et al., 2023). This fault borders Daruvar thermal field westwardly, and together with an E-W striking fault to the S (F1 in Kosović et al., 2023) accommodates the uplift of the Mesozoic thermal reservoir to shallower depths. The geophysical investigations highlighted that the thermal springs occur within the interaction zone of local scale faults/fractures. Interaction zones are preferential locations for thermal springs because they favor the kinematic transfer between faults increasing the rock fracturing and the permeability field (e.g., Curewitz and Karson, 1997; Faulds et al., 2013). This structure further localizes the flow of the Daruvar thermal waters resulting in four thermal springs with temperature between 38°C and 50°C.

6 Conclusion

This research focused on the reconstruction of the geological framework and the tectonic evolution of western Papuk to detail the impact of regional and local scale fold and fault/fracture systems on the development of the Daruvar hydrothermal system (DHS) and its geothermal resource. The reconstruction was conducted by integrating surficial field investigations and available surface and subsurface geological and geophysical data, both at regional and local scales. The structural data analysis evidences a complex pattern of folds deformed by faults and fracture systems in a manner compatible with the polyphase tectonic evolution of the Slavonian mountains and the SW part of the Pannonian Basin System. The construction of 2D composite geological profiles that were integrated into a 3D geological model favored the visualization of the geological assemblage detailing the structural relations among the different blocks in the study area. The geological and tectonic reconstructions were integrated with geochemical data on the Daruvar waters and local scale geological and geophysical data on the thermal field to propose a conceptual model of the DHS. The conceptual model highlighted the importance of regional and local structures (i.e., folds, faults, networks of fractures) that are causative factor for the regional to local flow of the Daruvar thermal waters.

The geological structure of the thermal system is characterized by a regional NNE-SSW striking asymmetric fold (tectonic transport top to the W) formed in the hangingwall of SE dipping Daruvar reverse fault, a western prolongation of the E-W striking Gradina thrust fault. This structure favors both the extensive outcropping of the Mesozoic carbonate rock complex (i.e., the reservoir of the system) in the recharge area and the fracturing of the bedrock. Deformed by the current Pliocene-Quaternary N-S compressional regime, cogenetic steeply dipping E-W and N-S striking fracture systems are potential paths for the infiltration, flow, and rise of the thermal waters. The E-W discontinuities could represent the principal regional flow paths, while N-S fractures (as the Toplica fault imaged in Daruvar through local scale geophysical investigations) could enable the local quick rise of the thermal water from the deeper part of the reservoir due to their structural position in the anticline hinge zone and the local extensional regime increasing the fractures aperture and the permeability field of the bedrock.

Insights gained through the application of these research methodologies can be utilized as an example for the 3D subsurface reconstruction of areas affected by the deep circulation of waters resulting in the development of a geothermal resource. Such kind of multidisciplinary reconstruction could foster the estimation of the potential of a geothermal resource aiding the assessment of the reservoir volumes and the development of hydrogeological numerical modeling of fluid flow and heat transport.

Data availability statement

The original contributions presented in the study are included in the article/Supplementary Material, further inquiries can be directed to the corresponding author.

Author contributions

IK: Conceptualization, Data curation, Formal Analysis, Investigation, Writing–original draft, Writing–review and editing. BM: Conceptualization, Formal Analysis, Investigation, Methodology, Writing–original draft, Writing–review and editing. IP: Investigation, Software, Validation, Visualization, Writing–review and editing. MP: Conceptualization, Investigation, Visualization, Writing–original draft, Writing–review and editing, Data curation. MM: Data curation, Formal Analysis, Writing–review and editing, Investigation. MiP: Investigation, Project administration, Writing–review and editing. SB: Conceptualization, Funding acquisition, Investigation, Project administration, Supervision, Writing–review and editing, Resources.

Funding

The author(s) declare that financial support was received for the research, authorship, and/or publication of this article. The research was funded by the HyTheC project of the Croatian Science Foundation (HRZZ), grant number UIP-2019-04-1218, and the publication fee was paid by the GeoTwinn project (H2020-WIDESPREAD-05-2017-Twinning project), grant number 809943.

Acknowledgments

The authors would like to thank the Daruvarske toplice–Special Hospital for Medical Rehabilitation for logistic help on-site and sharing of existing materials as well as to the Croatian Hydrocarbon Agency for granting access to the legacy hydrocarbon research data (seismic reflection profiles and deep exploration wells).

Conflict of interest

The authors declare that the research was conducted in the absence of any commercial or financial relationships that could be construed as a potential conflict of interest.

Publisher's note

Supplementary material

The Supplementary Material for this article can be found online at: https://www.frontiersin.org/articles/10.3389/feart.2024.1401935/full#supplementary-material

References

Allmendinger, R. W., Cardozo, N., and Fisher, D. M. (2011). *Structural geology algorithms: vectors and tensors*. doi:10.1017/CBO9780511920202

Angelier, J., and Mechler, P. (1977). Sur une methode graphique de recherche des contraintes principales egalement utilisables en tectonique et en seismologie: la methode des diedres droits. *Bull. Société Géologique Fr.* S7-XIX, 1309–1318. doi:10.2113/gssgfbull.S7-XIX.6.1309

Ataie-Ashtiani, B., Simmons, C. T., and Irvine, D. J. (2018). Confusion about "convection". *Groundwater* 56, 683–687. doi:10.1111/gwat.12790

Axelsson, G. (2010). Sustainable geothermal utilization - case histories; definitions; research issues and modelling. *Geothermics* 39, 283–291. doi:10.1016/j.geothermics.2010.08.001

Babić, Ž., Šikić, V., and Mraz, V. (1971). *Hidrogeološka istraživanja termomineralnih vrela kupališnog lječilišta daruvar (hydrogeological research of thermomineral springs at daruvar spa). Zagreb*.

Bada, G., Horváth, F., Dövényi, P., Szafián, P., Windhoffer, G., and Cloetingh, S. (2007). Present-day stress field and tectonic inversion in the Pannonian basin. *Glob. Planet. Change* 58, 165–180. doi:10.1016/j.gloplacha.2007.01.007

Baize, S., Amoroso, S., Belić, N., Benedetti, L., Boncio, P., Budić, M., et al. (2022). Environmental effects and seismogenic source characterization of the December 2020 earthquake sequence near Petrinja, Croatia. *Geophys. J. Int.* 230, 1394–1418. doi:10.1093/gji/ggac123

Balen, D., Horváth, P., Tomljenović, B., Finger, F., Humer, B., Pamić, J., et al. (2006). A record of pre-Variscan Barrovian regional metamorphism in the eastern part of the Slavonian Mountains (NE Croatia). *Mineralogy Petrology* 87, 143–162. doi:10.1007/s00710-006-0120-1

Bense, V. F., Gleeson, T., Loveless, S. E., Bour, O., and Scibek, J. (2013). Fault zone hydrogeology. *Earth-Science Rev.* 127, 171–192. doi:10.1016/j.earscirev.2013.09.008

Borović, S. (2015). Integrirani hidrogeološko—hidrogeokemijski model Daruvarskog geotermalnog vodonosnika (Integrated hydrogeological-hydrogeochemical model of Daruvar geothermal aquifer). Ph.D. Thesis. Zagreb, Croatia: University of Zagreb, Faculty of Mining, Geology and Petroleum Engineering.

Borović, S., and Marković, I. (2015). Utilization and tourism valorisation of geothermal waters in Croatia. *Renew. Sustain. Energy Rev.* 44, 52–63. doi:10.1016/j.rser.2014.12.022

Borović, S., Pola, M., Bačani, A., and Urumović, K. (2019). Constraining the recharge area of a hydrothermal system in fractured carbonates by numerical modelling. *Geothermics* 82, 128–149. doi:10.1016/j.geothermics.2019.05.017

Brehme, M., Blöcher, G., Cacace, M., Kamah, Y., Sauter, M., and Zimmermann, G. (2016). Permeability distribution in the Lahendong geothermal field: a blind fault captured by thermal–hydraulic simulation. *Environ. Earth Sci.* 75, 1088. doi:10.1007/s12665-016-5878-9

Brückl, E., Behm, M., Decker, K., Grad, M., Guterch, A., Keller, G. R., et al. (2010). Crustal structure and active tectonics in the Eastern Alps. *Tectonics* 29, n/a-n–a. doi:10.1029/2009TC002491

Bundschuh, J., and César Suárez, A. M. (2010). *Introduction to the numerical modeling of groundwater and geothermal systems*. London: CRC Press. doi:10.1201/b10499

Calcagno, P., Baujard, C., Guillou-Frottier, L., Dagallier, A., and Genter, A. (2014). Estimation of the deep geothermal potential within the Tertiary Limagne basin (French Massif Central): an integrated 3D geological and thermal approach. *Geothermics* 51, 496–508. doi:10.1016/j.geothermics.2014.02.002

Cardozo, N., and Allmendinger, R. W. (2013). Spherical projections with OSXStereonet. *Comput. Geosciences* 51, 193–205. doi:10.1016/j.cageo.2012.07.021

Caumon, G., Collon-Drouaillet, P., Le Carlier De Veslud, C., Viseur, S., and Sausse, J. (2009). Surface-based 3D modeling of geological structures. *Math. Geosci.* 41, 927–945. doi:10.1007/s11004-009-9244-2

Ćorić, S., Pavelić, D., Rögl, F., Mandić, O., Vrabac, S., Avanić, R., et al. (2009). Revised Middle Miocene datum for initial marine flooding of north Croatian basins (Pannonian Basin system, central Paratethys)The Pannonian Basin system (PBS) originated during the early Miocene as a result of extensional processes between the alpine-carp. *Geol. Croat.* 62, 31–43. doi:10.4154/GC.2009.03

Csontos, L., Nagymarosy, A., Horváth, F., and Kovác, M. (1992). Tertiary evolution of the Intra-Carpathian area: a model. *Tectonophysics* 208, 221–241. doi:10.1016/0040-1951(92)90346-8

Csontos, L., and Vörös, A. (2004). Mesozoic plate tectonic reconstruction of the Carpathian region. *Palaeogeogr. Palaeoclimatol. Palaeoecol.* 210, 1–56. doi:10.1016/j.palaeo.2004.02.033

Curewitz, D., and Karson, J. A. (1997). Structural settings of hydrothermal outflow: fracture permeability maintained by fault propagation and interaction. *J. Volcanol. Geotherm. Res.* 79, 149–168. doi:10.1016/S0377-0273(97)00027-9

Delvaux, D., and Sperner, B. (2003). New aspects of tectonic stress inversion with reference to the TENSOR program. *Geol. Soc.* 212, 75–100. London, Special Publications. doi:10.1144/GSL.SP.2003.212.01.06

Doblas, M. (1998). Slickenside kinematic indicators. *Tectonophysics* 295, 187–197. doi:10.1016/S0040-1951(98)00120-6

Dolton, G. L. (2006). Pannonian Basin province, central europe (province 4808) - petroleum Geology. *Total Petroleum Syst. Petroleum Resour. Assess*. doi:10.3133/b2204B

Domenico, P. A., and Schwartz, F. W. (1998). *Physical and chemical hydrogeology*. New York: Wiley.

Ece, U. N. (2021). *United nations resource management system: an overview of concepts, objectives and requirements*.

Fabbri, P., Pola, M., Piccinini, L., Zampieri, D., Roghel, A., and Dalla Libera, N. (2017). Monitoring, utilization and sustainable development of a low-temperature geothermal resource: a case study of the Euganean Geothermal Field (NE, Italy). *Geothermics* 70, 281–294. doi:10.1016/j.geothermics.2017.07.002

Faulds, J. E., Hinz, N. H., Dering, G. M., and Siler, D. L. (2013). The hybrid model — the most accommodating structural setting for geothermal power generation in the great basin, western USA. *Geotherm. Resour. Counc. Trans.* 37, 4–10.

Faulkner, D. R., Jackson, C. A. L., Lunn, R. J., Schlische, R. W., Shipton, Z. K., Wibberley, C. A. J., et al. (2010). A review of recent developments concerning the structure, mechanics and fluid flow properties of fault zones. *J. Struct. Geol.* 32, 1557–1575. doi:10.1016/j.jsg.2010.06.009

Finster, M., Clark, C., Schroeder, J., and Martino, L. (2015). Geothermal produced fluids: characteristics, treatment technologies, and management options. *Renew. Sustain. Energy Rev.* 50, 952–966. doi:10.1016/j.rser.2015.05.059

Fodor, L., Bada, G., Csillag, G., Horváth, E., Ruszkiczay-Rüdiger, Z., Palotás, K., et al. (2005). An outline of neotectonic structures and morphotectonics of the western and central Pannonian Basin. *Tectonophysics* 410, 15–41. doi:10.1016/j.tecto.2005.06.008

Fossen, H. (2016). *Structural geology*. Cambridge University Press.

Frehner, M. (2011). The neutral lines in buckle folds. *J. Struct. Geol.* 33, 1501–1508. doi:10.1016/j.jsg.2011.07.005

Fulignati, P., Marianelli, P., Sbrana, A., and Ciani, V. (2014). 3D geothermal modelling of the Mount Amiata hydrothermal system in Italy. *Energies* 7, 7434–7453. doi:10.3390/en7117434

Goldscheider, N., Mádl-Szőnyi, J., Erőss, A., and Schill, E. (2010). Revisión: Recursos de aguas termales en acuíferos de rocas carbonáticas. *Hydrogeology J.* 18, 1303–1318. doi:10.1007/s10040-010-0611-3

Grenerczy, G., Sella, G., Stein, S., and Kenyeres, A. (2005). Tectonic implications of the GPS velocity field in the northern Adriatic region. *Geophys. Res. Lett.* 32, 1–4. doi:10.1029/2005GL022947

Herak, D., Herak, M., and Tomljenović, B. (2009). Seismicity and earthquake focal mechanisms in North-Western Croatia. *Tectonophysics* 465, 212–220. doi:10.1016/j.tecto.2008.12.005

Herak, M., and Herak, D. (2023). Properties of the Petrinja (Croatia) earthquake sequence of 2020–2021 – results of seismological research for the first six months of activity. *Tectonophysics* 858, 229885. doi:10.1016/j.tecto.2023.229885

Horváth, F., Bada, G., Szafián, P., Tari, G., Ádám, A., and Cloetingh, S. (2006). Formation and deformation of the Pannonian Basin: constraints from observational data. *Geol. Soc. Mem.* 32, 191–206. doi:10.1144/GSL.MEM.2006.032.01.11

Horváth, F., and Cloetingh, S. (1996). Stress-induced late-stage subsidence anomalies in the Pannonian basin. *Tectonophysics* 266, 287–300. doi:10.1016/S0040-1951(96)00194-1

Horváth, F., Musitz, B., Balázs, A., Végh, A., Uhrin, A., Nádor, A., et al. (2015). Evolution of the Pannonian basin and its geothermal resources. *Geothermics* 53, 328–352. doi:10.1016/j.geothermics.2014.07.009

Horváth, F., and Tari, G. (1999). *IBS Pannonian Basin project: a review of the main results and their bearings on hydrocarbon exploration 156*. London, Special Publications: Geological Society, 195–213. doi:10.1144/GSL.SP.1999.156.01.11

Jamičić, D. (1995). The role of sinistral strike-slip faults in the formation of the structural fabric of the Slavonian Mts. (eastern Croatia). *Geol. Croat.* 48, 155–160. doi:10.4154/GC.1995.12

Jamičić, D. (2009). "Paleozoik (paleozoic)," in *Tumač geološke karte republike hrvatske 1:300.000 (explanatory notes of the geological map of the Croatian republic 1:300.00)*. Editors I. Velić, and I. Vlahović (Zagreb: Hrvatski geološki institut), 13–27.

Jamičić, D., Vragović, M., and Matičec, D. (1989). *Osnovna geološka karta SFRJ 1:100 000. Tumač za list Daruvar (Basic geological map of SFRJ 1:100 000. Explanatory notes for sheet Daruvar)*. Beograd: Geol. zavod, Zagreb, Sav. geol. zavod Beograd.

Jarosiński, M., Beekman, F., Bada, G., and Cloetingh, S. (2006). Redistribution of recent collision push and ridge push in Central Europe: insights from FEM modelling. *Geophys. J. Int.* 167, 860–880. doi:10.1111/j.1365-246X.2006.02979.x

Jarosinski, M., Beekman, F., Matenco, L., and Cloetingh, S. (2011). Mechanics of basin inversion: finite element modelling of the Pannonian Basin system. *Tectonophysics* 502, 121–145. doi:10.1016/j.tecto.2009.09.015

Jia, R., Lv, Y., Wang, G., Carranza, E., Chen, Y., Wei, C., et al. (2021). A stacking methodology of machine learning for 3D geological modeling with geological-geophysical datasets, Laochang Sn camp, Gejiu (China). *Comput. Geosciences* 151, 104754. doi:10.1016/j.cageo.2021.104754

Keegan-Treloar, R., Irvine, D. J., Solórzano-Rivas, S. C., Werner, A. D., Banks, E. W., and Currell, M. J. (2022). Fault-controlled springs: a review. *Earth-Science Rev.* 230, 104058. doi:10.1016/j.earscirev.2022.104058

Kosović, I., Briški, M., Pavić, M., Padovan, B., Pavičić, I., Matoš, B., et al. (2023). Reconstruction of fault architecture in the natural thermal spring area of daruvar hydrothermal system using surface geophysical investigations (Croatia). *Sustainability* 15, 12134. doi:10.3390/su151612134

Kühn, M., and Gessner, K. (2009). Coupled process models of fluid flow and heat transfer in hydrothermal systems in three dimensions. *Surv. Geophys.* 30, 193–210. doi:10.1007/s10712-009-9060-8

Larva, O., and Mraz, V. (2008). *Daruvarske toplice - elaborat utvrđivanja eksploatacijske izdašnosti Ivanovog vrela i objekta Š-3 (Daruvar thermal field – determination of the exploitation yield of the Ivano vrelo spring and the Š-3 well). Zagreb*.

Li, N., Song, X., Xiao, K., Li, S., Li, C., and Wang, K. (2018b). Part II: a demonstration of integrating multiple-scale 3D modelling into GIS-based prospectivity analysis: a case study of the Huayuan-Malichang district. China. *Ore Geol. Rev.* 95, 292–305. doi:10.1016/j.oregeorev.2018.02.034

Li, Y., Hou, G., Hari, K. R., Neng, Y., Lei, G., Tang, Y., et al. (2018a). The model of fracture development in the faulted folds: the role of folding and faulting. *Mar. Petroleum Geol.* 89, 243–251. doi:10.1016/j.marpetgeo.2017.05.025

Lyu, M., Ren, B., Wu, B., Tong, D., Ge, S., and Han, S. (2021). A parametric 3D geological modeling method considering stratigraphic interface topology optimization and coding expert knowledge. *Eng. Geol.* 293, 106300. doi:10.1016/j.enggeo.2021.106300

Magri, F., Akar, T., Gemici, U., and Pekdeger, A. (2010). Deep geothermal groundwater flow in the Seferihisar-Balçova area, Turkey: results from transient numerical simulations of coupled fluid flow and heat transport processes. *Geofluids* 10, 388–405. doi:10.1111/j.1468-8123.2009.00267.x

Malvić, T., and Velić, J. (2011). "Neogene tectonics in Croatian part of the Pannonian Basin and reflectance in hydrocarbon accumulations," in *New Frontiers in tectonic research - at the midst of plate convergence*. Editor U. Schattner (London, United Kingdom: InTech), 366 215–238. doi:10.5772/21270

Marrett, R., and Allmendinger, R. W. (1990). Kinematic analysis of fault-slip data. *J. Struct. Geol.* 12, 973–986. doi:10.1016/0191-8141(90)90093-E

Matoš, B., Pérez-Peña, J. V., and Tomljenović, B. (2016). Landscape response to recent tectonic deformation in the SW Pannonian Basin: evidence from DEM-based morphometric analysis of the Bilogora Mt. area, NE Croatia. *Geomorphology* 263, 132–155. doi:10.1016/j.geomorph.2016.03.020

Moeck, I. S. (2014). Catalog of geothermal play types based on geologic controls. *Renew. Sustain. Energy Rev.* 37, 867–882. doi:10.1016/j.rser.2014.05.032

Moeck, I. S., Hinz, N., Faulds, J., Bell, J., Kell-Hills, A., and Louie, J. (2010). 3D geological mapping as a new method in geothermal exploration: a case study from central Nevada. *Geotherm. Resour. Counc. Trans.* 34, 807–811.

Montanari, D., Minissale, A., Doveri, M., Gola, G., Trumpy, E., Santilano, A., et al. (2017). Geothermal resources within carbonate reservoirs in western Sicily (Italy): a review. *Earth-Science Rev.* 169, 180–201. doi:10.1016/j.earscirev.2017.04.016

Mraz, V. (1983). *Izvještaj o hidrogeološkim istražnim radovima na području Daruvarskih toplica II. faza (Report on conducted hydrogeological research in Daruvar thermal field - phase II). Zagreb*.

Mroczek, E. K., Milicich, S. D., Bixley, P. F., Sepulveda, F., Bertrand, E. A., Soengkono, S., et al. (2016). Ohaaki geothermal system: refinement of a conceptual reservoir model. *Geothermics* 59, 311–324. doi:10.1016/j.geothermics.2015.09.002

Nabavi, S. T., and Fossen, H. (2021). Fold geometry and folding – a review. *Earth-Science Rev.* 222, 103812. doi:10.1016/j.earscirev.2021.103812

Nelson, S. T., Mayo, A. L., Gilfillan, S., Dutson, S. J., Harris, R. A., Shipton, Z. K., et al. (2009). Enhanced fracture permeability and accompanying fluid flow in the footwall of a normal fault: the Hurricane fault at Pah Tempe hot springs, Washington County, Utah. *Bull. Geol. Soc. Am.* 121, 1–246. doi:10.1130/B26285.1

Olierook, H. K., Scalzo, R., Kohn, D., Chandra, R., Farahbakhsh, E., Clark, C., et al. (2020). Bayesian geological and geophysical data fusion for the construction and uncertainty quantification of 3D geological models. *Geosci. Front.* 12 (1), 479–493. doi:10.1016/j.gsf.2020.04.015

Ortner, H., Reiter, F., and Acs, P. (2002). Easy handling of tectonic data: the programs TectonicVB for mac and TectonicsFP for Windows™. *Comput. Geosciences* 28, 1193–1200. doi:10.1016/S0098-3004(02)00038-9

Pamić, J., Radonić, G., and Pavić, G. (2003). Geološki vodič kroz Park prirode Papuk (Geological guide through the Papuk nature park) Požega. Available at: https://www.pp-papuk.hr/download/geoloski-vodic-1-dio/.

Pan, D., Xu, Z., Lu, X., Zhou, L., and Li, H. (2020). 3D scene and geological modeling using integrated multi-source spatial data: methodology, challenges, and suggestions. *Tunn. Undergr. Space Technol.* 100, 103393. doi:10.1016/j.tust.2020.103393

Panzera, F., Alber, J., Imperatori, W., Bergamo, P., and Fäh, D. (2022). Reconstructing a 3D model from geophysical data for local amplification modelling: the study case of the upper Rhone valley, Switzerland. *Soil Dyn. Earthq. Eng.* 155, 107163. doi:10.1016/j.soildyn.2022.107163

Pasquale, V., Verdoya, M., and Chiozzi, P. (2014). *Geothermics*. Cham: Springer International Publishing. doi:10.1007/978-3-319-02511-7

Pavelić, D., Avanić, R., Bakrač, K., and Vrsaljko, D. (2001). Early Miocene braided river and lacustrine sedimentation in the kalnik mountain area (Pannonian Basin system, NW Croatia). *Geol. Carpathica* 52, 375–386.

Pavić, M., Kosović, I., Pola, M., Urumović, K., Briški, M., and Borović, S. (2023). Multidisciplinary research of thermal springs area in topusko (Croatia). *Sustainability* 15, 5498. doi:10.3390/su15065498

Pavičić, I., Dragičević, I., and Ivkić, I. (2018). High-resolution 3D geological model of the bauxite-bearing area Crvene Stijene (Jajce, Bosnia and Herzegovina) and its application in ongoing research and mining. *Geol. Q.* 62 (1), 100–120. doi:10.7306/gq.1396

Pola, M., Cacace, M., Fabbri, P., Piccinini, L., Zampieri, D., and Torresan, F. (2020). Fault control on a thermal anomaly: conceptual and numerical modeling of a low-temperature geothermal system in the southern alps foreland basin (NE Italy). *J. Geophys. Res. Solid Earth* 125, e2019JB017. doi:10.1029/2019jb017394

Pola, M., Gandin, A., Tuccimei, P., Soligo, M., Deiana, R., Fabbri, P., et al. (2014). A multidisciplinary approach to understanding carbonate deposition under tectonically controlled hydrothermal circulation: a case study from a recent travertine mound in the Euganean hydrothermal system, northern Italy. *Sedimentology* 61, 172–199. doi:10.1111/sed.12069

Prelogović, E., Saftić, B., Kuk, V., Velić, J., Dragaš, M., and Lučić, D. (1998). Tectonic activity in the Croatian part of the Pannonian basin. *Tectonophysics* 297, 283–293. doi:10.1016/S0040-1951(98)00173-5

Price, S. J., Terrington, R. L., Busby, J., Bricker, S., and Berry, T. (2018). 3D ground-use optimisation for sustainable urban development planning: a case-study from Earls Court, London. UK. *Tunn. Undergr. Sp. Technol.* 81, 144–164. doi:10.1016/j.tust.2018.06.025

Rman, N. (2014). Analysis of long-term thermal water abstraction and its impact on low-temperature intergranular geothermal aquifers in the Mura-Zala basin, NE Slovenia. *Geothermics* 51, 214–227. doi:10.1016/j.geothermics.2014.01.011

Rman, N., Bălan, L. L., Bobovečki, I., Gál, N., Jolović, B., Lapanje, A., et al. (2020). Geothermal sources and utilization practice in six countries along the southern part of the Pannonian basin. *Environ. Earth Sci.* 79, 1–12. doi:10.1007/s12665-019-8746-6

Rybach, L., and Mongillo, M. (2006). Geothermal sustainability-A review with identified research needs. *GRC Trans.* 30, 1083–1090.

Santilano, A., Donato, A., Galgaro, A., Montanari, D., Menghini, A., Viezzoli, A., et al. (2016). An integrated 3D approach to assess the geothermal heat-exchange potential: the case study of western Sicily (southern Italy). *Renew. Energy* 97, 611–624. doi:10.1016/j.renene.2016.05.072

Scheck-Wenderoth, M., Cacace, M., Maystrenko, Y. P., Cherubini, Y., Noack, V., Kaiser, B. O., et al. (2014). Models of heat transport in the Central European Basin System: effective mechanisms at different scales. *Mar. Petroleum Geol.* 55, 315–331. doi:10.1016/j.marpetgeo.2014.03.009

Schmid, S. M., Bernoulli, D., Fügenschuh, B., Matenco, L., Schefer, S., Schuster, R., et al. (2008). The Alpine-Carpathian-Dinaridic orogenic system: correlation and evolution of tectonic units. *Swiss J. Geosciences* 101, 139–183. doi:10.1007/s00015-008-1247-3

Schmid, S. M., Fügenschuh, B., Kounov, A., Matenco, L., Nievergelt, P., Oberhänsli, R., et al. (2020). Tectonic units of the Alpine collision zone between Eastern Alps and western Turkey. *Gondwana Res.* 78, 308–374. doi:10.1016/j.gr.2019.07.005

Shortall, R., Davidsdottir, B., and Axelsson, G. (2015). Geothermal energy for sustainable development: a review of sustainability impacts and assessment frameworks. *Renew. Sustain. Energy Rev.* 44, 391–406. doi:10.1016/j.rser.2014.12.020

Šikić, K. (1981). Facijesi mezozoika papuckog gorja (facies of the mesozoic of Mount Papuk). M.Sc. Thesis. Zagreb, Croatia: University of Zagreb, Faculty of Science.

Šolaja, D. (2010). Strukturna analiza recentne i neotektonske aktivnosti na području Lonjsko-Ilovske zavale između Daruvara i Kutine (Structural analysis of the recent and neotectonic activity in the area of the Lonja-Ilova depression between Daruvar and Kutina). M.Sc. Thesis. Zagreb, Croatia: University of Zagreb, Faculty of Science.

Steininger, F. F., and Wessely, G. (2000). From the tethyan ocean to the paratethys sea: Oligocene to Neogene stratigraphy, paleogeography and paleobiogeography of the circum-mediterranean region and the Oligocene to Neogene basin evolution in Austria. *Mitt. Österr. Geol. Ges.* 92, 95–116.

Szanyi, J., Rybach, L., and Abdulhaq, H. A. (2023). Geothermal energy and its potential for critical metal extraction—a review. *Energies* 16 (7168), 1–28. doi:10.3390/en16207168

Tari, G., Dövényi, P., Dunkl, I., Horváth, F., Lenkey, L., Stefanescu, M., et al. (1999). Lithospheric structure of the Pannonian basin derived from seismic, gravity and geothermal data. *Geol. Soc.* 156, 215–250. London, Special Publications. doi:10.1144/GSL.SP.1999.156.01.12

Tari, V., and Pamić, J. (1998). Geodynamic evolution of the northern Dinarides and the southern part of the Pannonian Basin. *Tectonophysics* 297, 269–281. doi:10.1016/S0040-1951(98)00172-3

Tavani, S., Storti, F., Bausà, J., and Muñoz, J. A. (2012). Late thrusting extensional collapse at the mountain front of the northern Apennines (Italy). *Tectonics* 31. doi:10.1029/2011TC003059

Tomljenović, B., and Csontos, L. (2001). Neogene–quaternary structures in the border zone between alps, Dinarides and Pannonian Basin (hrvatsko zagorje and karlovac basins, Croatia). *Int. J. Earth Sci.* 90, 560–578. doi:10.1007/s005310000176

Torresan, F., Piccinini, L., Cacace, M., Pola, M., Zampieri, D., and Fabbri, P. (2021). Numerical modeling as a tool for evaluating the renewability of geothermal resources: the case study of the Euganean Geothermal System (NE Italy). *Environ. Geochem. Health* 4, 2135–2162. doi:10.1007/s10653-021-01028-4

Torresan, F., Piccinini, L., Pola, M., Zampieri, D., and Fabbri, P. (2020). 3D hydrogeological reconstruction of the fault-controlled Euganean Geothermal System (NE Italy). *Eng. Geol.* 274, 105740. doi:10.1016/j.enggeo.2020.105740

Turner, F. J. (1953). Nature and dynamic interpretation of deformation lamellae in calcite of three marbles. *Am. J. Sci.* 251, 276–298. doi:10.2475/ajs.251.4.276

Urumović, K., Terzić, J., Kopić, J., and Kosović, I. (2023). Identification of aquifer and pumped well parameters using the data hidden in non-linear losses. *Sustain. Switz.* 15, 11170. doi:10.3390/su151411170

Ustaszewski, K., Herak, M., Tomljenović, B., Herak, D., and Matej, S. (2014). Neotectonics of the Dinarides-Pannonian Basin transition and possible earthquake sources in the Banja Luka epicentral area. *J. Geodyn.* 82, 52–68. doi:10.1016/j.jog.2014.04.006

Ustaszewski, K., Kounov, A., Schmid, S. M., Schaltegger, U., Krenn, E., Frank, W., et al. (2010). Evolution of the Adria-Europe plate boundary in the northern Dinarides: from continent-continent collision to back-arc extension. *Tectonics* 29. doi:10.1029/2010TC002668

Ustaszewski, K., Schmid, S. M., Fügenschuh, B., Tischler, M., Kissling, E., and Spakman, W. (2008). A map-view restoration of the Alpine-Carpathian-Dinaridic system for the Early Miocene. *Swiss J. Geosciences* 101, 273–294. doi:10.1007/s00015-008-1288-7

Wacha, L., Matoš, B., Kunz, A., Lužar-Oberiter, B., Tomljenović, B., and Banak, A. (2018). First post-IR IRSL dating results of Quaternary deposits from Bilogora (NE Croatia): implications for the Pleistocene relative uplift and incision rates in the area. *Quat. Int.* 494, 193–210. doi:10.1016/j.quaint.2017.08.049

Wang, W., Zhao, W., Huang, L., Vimarlund, V., and Wang, Z. (2014). Applications of terrestrial laser scanning for tunnels: a review. *J. Traffic Transp. Eng. Engl. Ed.* 1, 325–337. doi:10.1016/S2095-7564(15)30279-8

Wellmann, F., and Caumon, G. (2018). "3-D Structural geological models: concepts, methods, and uncertainties," in *Advances in geophysics, 59* (Elsevier), 1–121. doi:10.1016/bs.agph.2018.09.001

Xie, J., Wang, G., Sha, Y., Liu, J., Wen, B., Nie, M., et al. (2017). GIS prospectivity mapping and 3D modeling validation for potential uranium deposit targets in Shangnan district, China. *J. Afr. Earth Sci.* 128, 161–175. doi:10.1016/j.jafrearsci.2016.12.001

frontiers

Supplementary Material

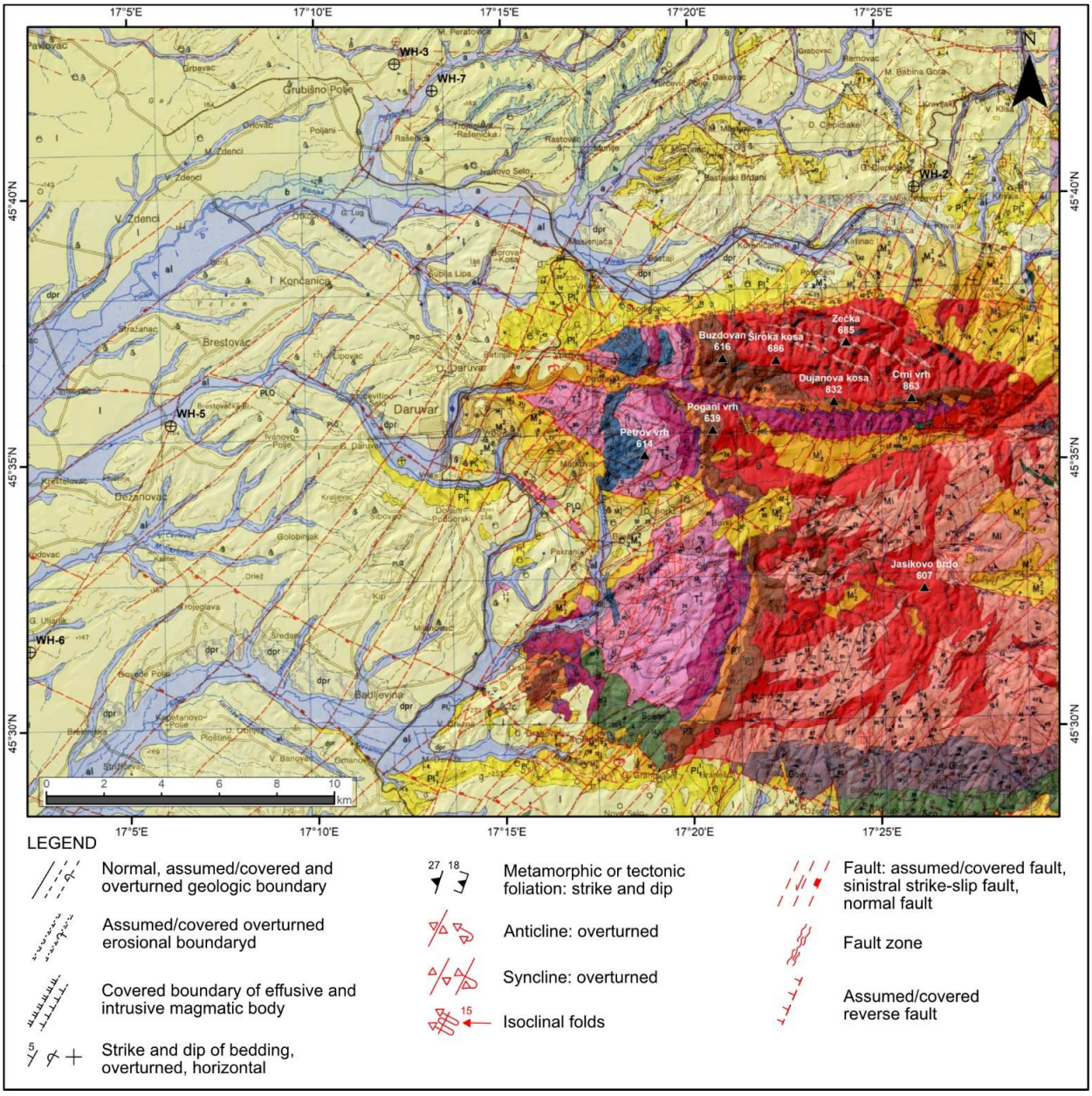

Supplementary Figure 1. Geological map of the study area (Jamičić et al., 1989). The lithological units are reported in Supplementary Figure 2. The extent corresponds to the extent of Figure 3 of the manuscript.

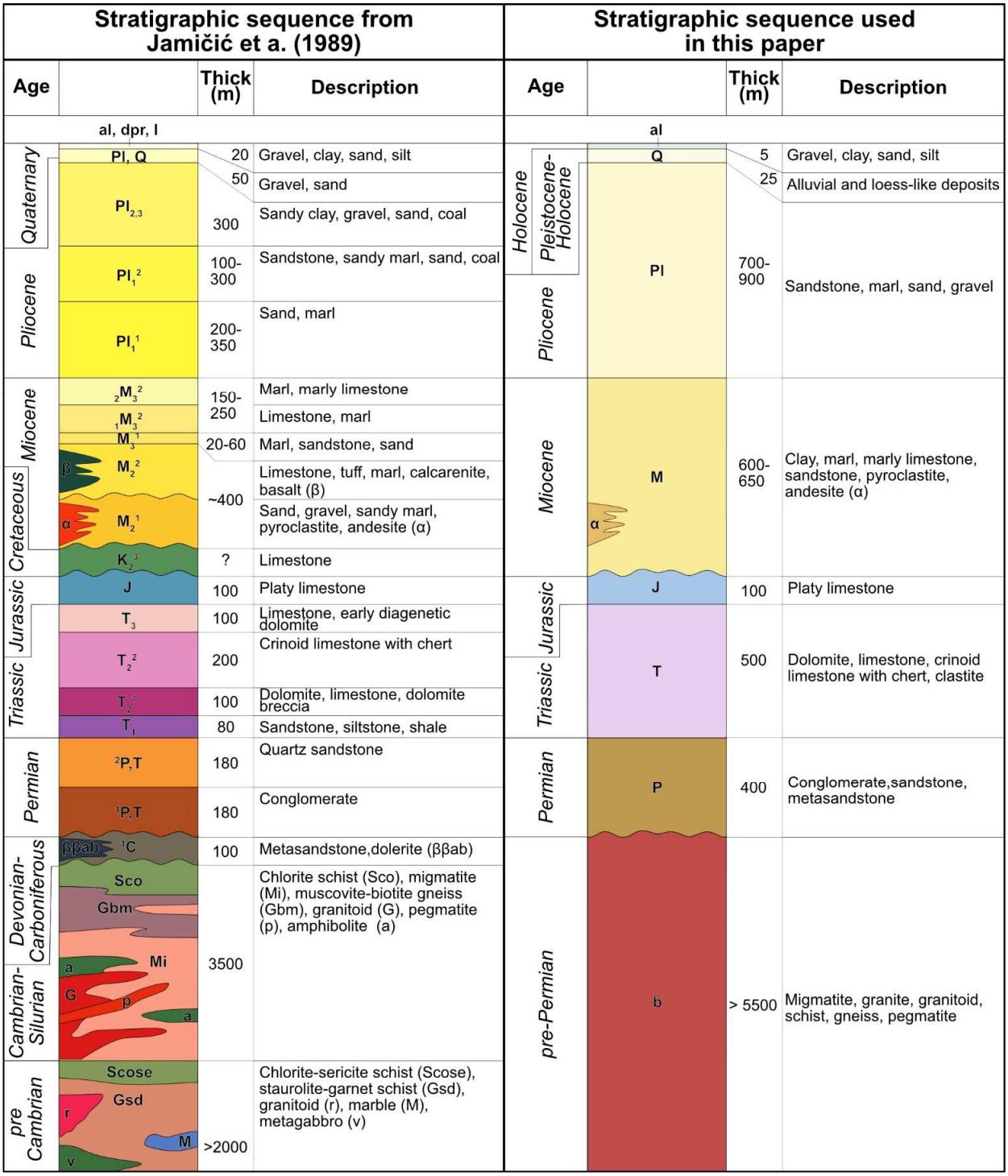

Supplementary Figure 2. Stratigraphic sequence from the geological map of the study area (Jamičić et al., 1989) and simplified stratigraphic sequence used in this work.

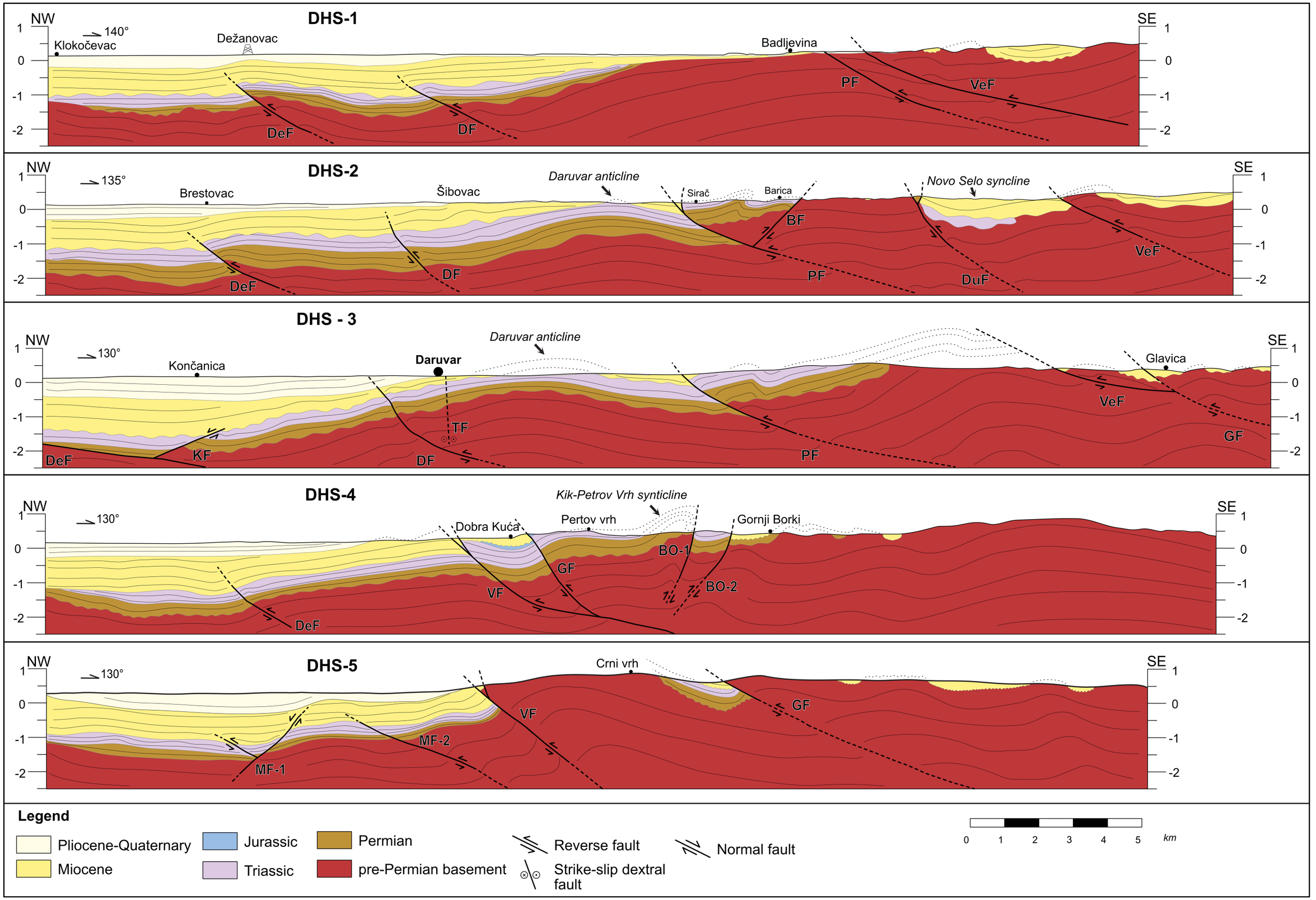

Supplementary Figure 3. Composite geological profiles investigating the Daruvar area at the margin between the Lonja-Ilova subdepression and the western part of Mount Papuk. Acronyms of the faults in the profiles: BF - Barica fault; BO - Borki fault;DF - Daruvar fault; DeF - Dežanovac fault; DuF - Dulj fault; GF - Gradina fault; MF - Munja fault ; KF - Končanica fault; PF - Pakrac fault; TF - Toplica fault; VF - Voćin fault; VeF - Velika fault.

5.2. # Paper 2: Reconstruction of Fault Architecture in the Natural Thermal Spring Area of Daruvar Hydrothermal System Using Surface Geophysical Investigations (Croatia)

By

Ivan Kosović, Maja Briški, Mirja Pavić, Božo Padovan, Ivica Pavičić, Bojan Matoš, Marco Pola and Staša Borović

sustainability

MDPI

Article

Reconstruction of Fault Architecture in the Natural Thermal Spring Area of Daruvar Hydrothermal System Using Surface Geophysical Investigations (Croatia)

Ivan Kosović [1], Maja Briški [1], Mirja Pavić [1,*], Božo Padovan [2], Ivica Pavičić [3], Bojan Matoš [3], Marco Pola [1] and Staša Borović [1]

[1] Croatian Geological Survey, Ulica Milana Sachsa 2, 10000 Zagreb, Croatia; ikosovic@hgi-cgs.hr (I.K.); mbriski@hgi-cgs.hr (M.B.); mpola@hgi-cgs.hr (M.P.); sborovic@hgi-cgs.hr (S.B.)
[2] Terra Compacta Ltd., Ulica Psunjska 3, 10000 Zagreb, Croatia; tc@terra-compacta.hr
[3] Faculty of Mining, Geology and Petroleum Engineering, University of Zagreb, Ulica Pierottijeva 6, 10000 Zagreb, Croatia; ivica.pavicic@rgn.unizg.hr (I.P.); bojan.matos@rgn.unizg.hr (B.M.)
* Correspondence: mpavic@hgi-cgs.hr

Abstract: The sustainable utilization of geothermal energy mostly depends on the characteristics of the geothermal resource from which it is extracted. Among others, detailed geological modeling is a key factor for estimating the potential of a geothermal resource. This research focuses on the modeling and reconstruction of the geological setting of the Daruvar thermal spring area using geophysical techniques. An integrated geophysical approach based on electrical resistivity tomography (ERT) and both active and passive seismic (MASW and HVSR) methods was used. Based on ERT results and the stratigraphic logs of the wells in Daruvar, three resistivity layers/geological units were identified. The deepest layer with resistivity < 150 Ωm is the Triassic carbonate that constitutes the thermal aquifer. Sharp lateral variations in the resistivity distributions within the bedrock were interpreted as fault damage zones saturated with thermal waters. Integrating the results of the seismic methods, the thickness of the first seismic layer that corresponds to the Quaternary cover was estimated from 5 to 20 m. Here, results of the geophysical investigations were combined into a 3D geological model highlighting the occurrence of subvertical N-S and E-W trending faults in the Daruvar spring area. The N-S-trending fault was interpreted as a fault plane parallel to the regionally mapped Daruvar fault. This fault juxtaposes the Triassic carbonate complex of the thermal aquifer with a Neogene sedimentary sequence of significantly lower permeability. Neogene–Quaternary tectonic activity further increased the fracturing and the permeability field in the Daruvar spring area, as proven by the smaller scale E-W faults and the well logs. This fracture network permits a quick upwelling of thermal fluids resulting in thermal springs with temperatures up to 50 °C. This work proves that the construction of a detailed geological model is crucial for assessing the reservoir and fault geometries in thermal systems hosted in fractured carbonate rocks.

Keywords: ERT; active and passive seismic; fault architecture; Triassic carbonate complex; 3D geological model; Croatia

Citation: Kosović, I.; Briški, M.; Pavić, M.; Padovan, B.; Pavičić, I.; Matoš, B.; Pola, M.; Borović, S. Reconstruction of Fault Architecture in the Natural Thermal Spring Area of Daruvar Hydrothermal System Using Surface Geophysical Investigations (Croatia). *Sustainability* **2023**, *15*, 12134. https://doi.org/10.3390/su151612134

Academic Editor: Xiaojun Feng

Received: 15 June 2023
Revised: 2 August 2023
Accepted: 4 August 2023
Published: 8 August 2023

1. Introduction

The European Union (EU) is promoting a clean energy transition through the increasing and sustainable utilization of renewable energy sources [1,2]. Geothermal energy is one of the renewable energy sources foreseen in the EU plans. Its sustainable utilization mostly depends on the characteristics of the geothermal resource from which it is extracted. The development of a profitable geothermal resource and its long-term sustainable exploitation are mainly controlled by the geological properties (e.g., lithologies, regional and local faults systems, water/rock interaction) of the connected geothermal system [3]. The geological setting controls the conduction and convection processes in the system driving the fluid

flow and heat transfer. Therefore, a detailed reconstruction of the subsurface is a key factor for estimating the potential of a geothermal resource.

Geological investigations in geothermal systems have been conducted at both regional and local scales, detailing the impact of the geological, structural, and hydrogeological settings on the fluid flow and temperature distribution [4–10]. Geothermal systems are dominantly controlled by systems of fault and fractures [11–14], since faults and their highly permeable damage zone are preferential pathways for the circulation of thermal fluids and their uprising [15–17]. Among the methods for geological reconstruction and subsurface modeling, geophysical methods can be used to measure the spatial and/or temporal variations in the physical properties of the subsurface, obtaining a quantitative model that completes the geological interpretation [18–20]. In particular, they represent the best approach for geological reconstruction where thick unconsolidated sediments cover the bedrock, limiting the possibility of direct measurements to a few stratigraphic logs.

Based on the research objectives and the geological and hydrogeological settings of the study area, different geophysical approaches can be applied. For the exploration of geothermal resources [21–26], they can be used to: (i) assess the distribution of lithologies, (ii) reconstruct the geometry of the aquifer, and (iii) reconstruct the geometry of faults and their damage zones. Among them, electrical resistivity tomography (ERT) and seismic methods can provide a detailed 3D local scale reconstruction of the subsurface. ERT is often used in groundwater investigations, revealing the aquifer geometry and the groundwater pathways [27–33]. Seismic methods can be used to map the morphology of the bedrock and to reconstruct the lithological sequence [34]. Active seismic techniques, such as refraction and reflection methods, can provide the best resolution, but they are expensive and time-consuming methods with several logistic limitations. Conversely, passive seismic methods are relatively fast and cheap, although they provide limited data. Among passive seismic approaches, the horizontal to vertical spectral ratio (HVSR) method is the most used to reconstruct the bedrock surface [35–39].

Croatia is particularly rich in geothermal resources due to favorable geological, hydrogeological, and thermal conditions resulting in numerous thermal and subthermal springs [40,41]. Most of these springs are situated in northern and eastern parts of the country, which are a part of the Pannonian Basin System (PBS). The PBS is characterized by polyphase tectonic evolution and the prevalence of a high geothermal gradient [42]. Tectonic activity resulted in a complex structural setting with the widespread occurrence of outcrops of highly fractured and permeable carbonate complexes that represent the recharge areas of local- to regional-scale geothermal systems.

The Daruvar hydrothermal system (DHS) is positioned in the NE part of the Republic of Croatia (Figure 1a). It is an intermediate scale hydrothermal system hosted in a carbonate complex manifesting in thermal springs with temperatures ranging from 38 to 50 °C. The occurrence of thermal waters in Daruvar has been known since the Roman age. The utilization of thermal resources increased in the 20th century. Exploration and exploitation wells had been drilled from the 1970s to the 2000s, allowing a preliminary geological reconstruction of the subsurface in the spring area [43]. Currently, the thermal waters are exploited from two springs and a thermal well providing a total yield of approximately 10 l/s. The exploited waters are used for therapeutic and balneological purposes in the nearby spa and pool complexes. Previous studies suggested that the occurrence of the Daruvar springs is affected by the local structural setting [44,45], but the architecture of these structures has never been detailed.

Here, geophysical investigations will be applied for the modeling and reconstruction of the geological and structural settings of the subsurface in the Daruvar thermal spring area. The research objective is to identify the impact of local faults system on the thermal water outflow. Results of ERT and HVSR investigations will be combined with the stratigraphic logs of thermal wells, obtaining a 3D geological reconstruction of the spring area.

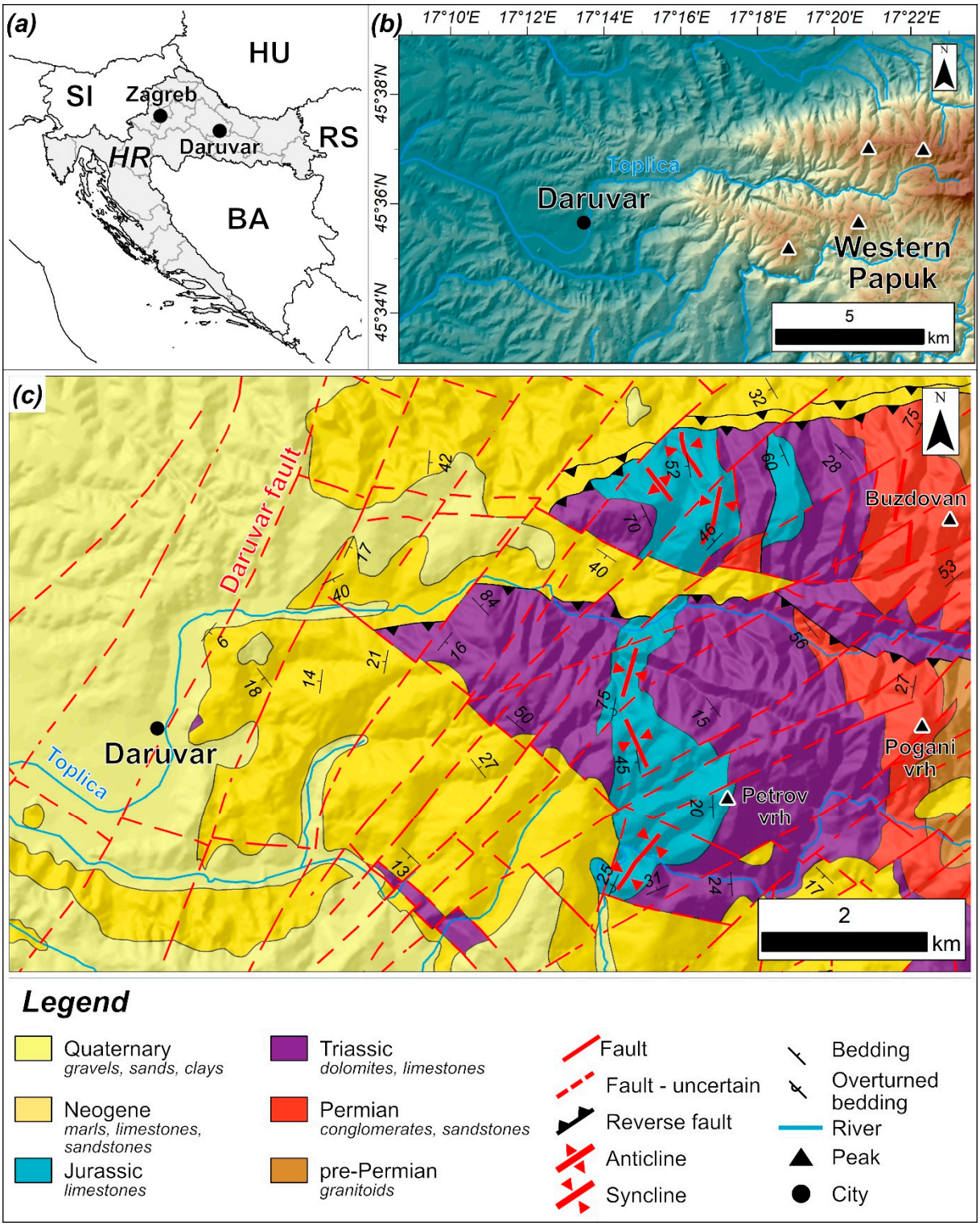

Figure 1. (**a**) Location of the study area in northeastern Croatia. Zagreb capital city and neighboring countries are shown (acronyms: BA: Bosnia-Herzegovina; HR: Croatia; HU: Hungary: RS: Serbia; SI: Slovenia). (**b**) Daruvar spring area and its surroundings on the western foothill of Papuk. The coordinates of the map are in GCS WGS 84 coordinate system using the WGS 84 datum. (**c**) Schematic geological map of the western Papuk Mt. (modified from [46]).

2. Materials and Methods

2.1. Geological and Hydrogeological Settings

The study area (western Papuk Mt.; Figure 1b) is located at the SW margin of the PBS. The PBS is a system of basins characterized by a complex polyphase deformation history that developed parallel with the Alpine–Dinarides–Carpathian orogen. The Croatian part of the PBS [47–50] was affected by an initial E-W extensional tectonic phase during the Early to Middle Miocene that formed systems of grabens and half-grabens, i.e., regional depressions (e.g., Drava and Sava depressions; [47]). The initial extension was followed by a Middle Miocene local scale compression and a Middle to Late Miocene deepening of the basin system due to crustal thermal subsidence. Tectonic inversion and structural reactivation commenced during the Pliocene–Quaternary, which enabled the regional compression/transpression of existing structures as a result of the continuous Adria–Europe plates collision and the general N-S compression [51]. The present-day structural setting of the Papuk area is mostly affected by the last Pliocene–Quaternary deformational phase characterized by compression/transpression [52]. The N-S compression caused the reactivation of two regional dextral faults, producing a conjugated fault set composed of NW-SE dextral and NE-SW sinistral faults in their interaction zone [52]. Progressive regional transpression was accommodated by folding and uplifting of the structures along the sinistral strike-slip faults. One of those sinistral faults is the Daruvar fault (Figure 1c), which affected the local geological and structural settings of the Daruvar spring area.

Lithostratigraphic units of western Papuk Mt. (Figure 1c) can be grouped into [46]: (i) pre-Permian granitoids, (ii) Permian units consisting of well-layered conglomerates and quartz sandstones, (iii) Triassic sedimentary rock complex composed of Lower Triassic quartz sandstones and laminated shales and Middle and Upper Triassic dolomites and limestones, (iv) Jurassic laminated limestones, (v) Neogene sedimentary complex consisting of marls, limestones, and sandstones, and (vi) Quaternary alluvial and colluvial unconsolidated sediments made of an alternation of clays, sands, and gravels.

The Daruvar spring area is located on the left bank of the Toplica river in the center of Daruvar town (Figure 1c). It consists of a few thermal springs (Antunovo vrelo, Blatna kupelj, Ivanovo vrelo, and Marijina vrela springs; Figure 2) with temperatures ranging from 38 to 50 °C [44]. In addition, 109 boreholes had been drilled from 1971 to 2009 [43,53]. The most important wells are D 1, Dar 1, DS 1, and HZ 1 (8.5, 190, 119, and 2.5 m deep, respectively; Figures 2 and 3) with temperatures from 22.7 to 43.5 °C [54]. Furthermore, the PD 2 exploration well (60 m deep; Figures 2 and 3) was drilled to the west of the spring area on the right bank of the Toplica river [55]. Among these objects, the D 1 well and the Antunovo vrelo and Ivanovo vrelo springs are exploited for supplying the Daruvar spa and pool complexes.

The Dar 1 well (Figure 3) shows the most comprehensive stratigraphic sequence in the spring area [56]. It is composed of: (i) Quaternary unconsolidated sediments mostly made of clays, sands, and gravels, (ii) a Miocene sedimentary complex, which is constituted by marls, lithotamnian limestones, and compact breccias locally marking the unconformity at the base of Badenian [57], and (iii) a Triassic carbonate complex with dolomites, limestones, and dolomitic breccias. The Neogene–Quaternary tectonic activity in the Daruvar area was proven by the occurrence of highly fractured intervals at depths of approximately 90, 135, 180, and 190 m. In the spring area (i.e., D 1 and DS 1 wells; Figure 3), the Triassic carbonate complex is in direct contact with the alluvial deposits.

The Triassic carbonate complex represents the main thermal aquifer, with high permeability (transmissivity of 1361 m^2/day; [58]) and secondary porosity resulting from the intense fracturing of the bedrock. Furthermore, thermal waters can be found in the gravel and sandy layers of the alluvial cover. The thermal water shows a predominant CaMg-HCO_3 hydrochemical facies, neutral pH ranging from 6.7 to 7.5, and an electrical conductivity of approximately 600 µS/cm [54]. The hydrochemical facies and the Mg^{2+}/Ca^{2+} versus Mg^{2+} ratio close to 0.5 [54] corroborate an interaction of the thermal waters with both

limestones and dolomites. Furthermore, stable isotope composition suggests a meteoric origin of the waters.

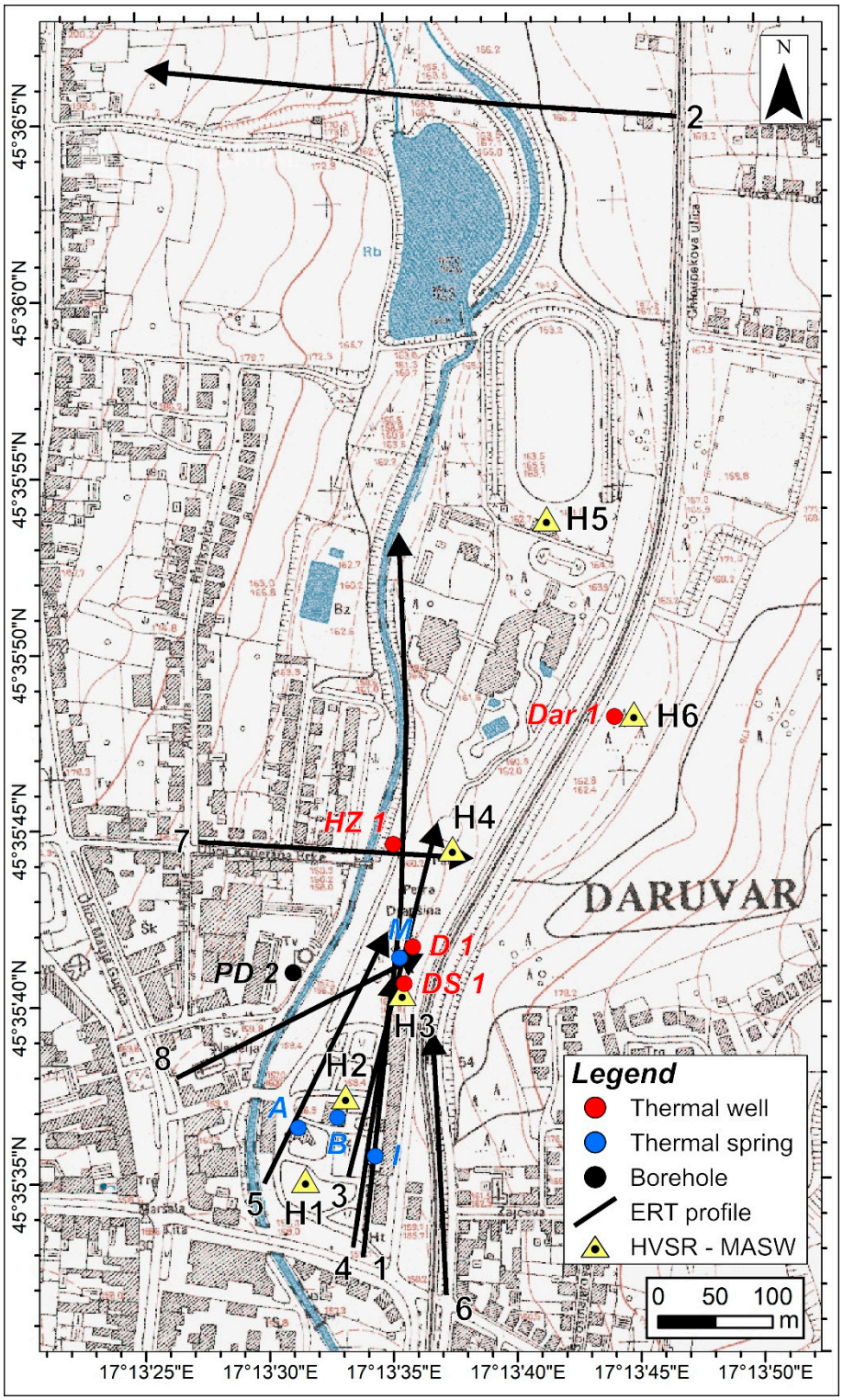

Figure 2. Topographic map showing: (i) the position of thermal wells and springs (Antunovo vrelo—A; Blatna kupelj—B; Ivanovo vrelo—I; Marijina vrela—M) in Daruvar, (ii) the traces of the electrical resistivity tomography sections (ERT), and (iii) the location of seismic investigations (HVSR, MASW). The coordinates of the map are in GCS WGS 84 coordinate system using the WGS 84 datum.

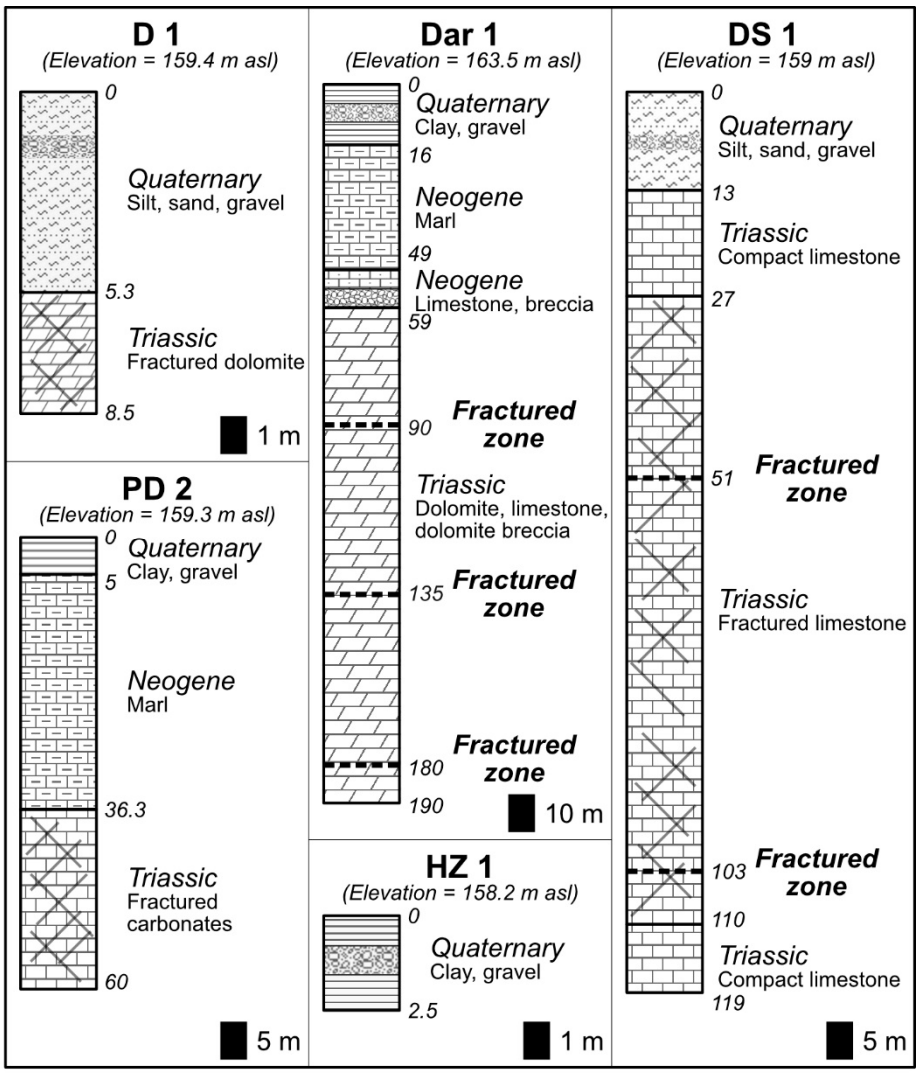

Figure 3. Stratigraphic logs of the wells and explorations boreholes in Daruvar. Their position is shown in Figure 2.

Ref. [44] proposed a conceptual model of the DHS. The recharge area is situated in the eastern hinterland of Daruvar (i.e., western slopes of Papuk Mt.), encompassing the Mesozoic carbonate complex (Figure 1c). Mesozoic carbonates are highly permeable, enabling the deep infiltration of meteoric water. The infiltrated water reaches a depth of approximately 1 km and warms due to the increased heat flow in this part of the PBS (i.e., 80 mW/m^2; [42]), resulting in a slightly high geothermal gradient. Permian clastic sedimentary units and pre-Permian crystalline rocks represent a barrier to deeper infiltration. In the area of Daruvar, the Mesozoic reservoir is tectonically brought in contact with younger Neogene rocks by the Daruvar fault. Due to the generally low permeability of the Neogene units, this contact is a lateral barrier for fluid circulation. The damage zone of the Daruvar fault increases the permeability field in the Daruvar spring area, being the main path for the rising and outflow of thermal waters. Despite its importance in the thermal water outflow, the architecture of the damage zone of the Daruvar fault is in general unknown.

2.2. Methods

2.2.1. Electrical Resistivity Tomography

Electrical resistivity tomography (ERT) is a geophysical method that is extensively applied to reconstruct the geometry of lithologies and structures in the subsurface [20,33,59].

ERT can be used to image the electrical resistivity distribution of the subsurface by injecting electrical currents and measuring electrical potentials along a profile. The resistivity generally depends on the mineralogical composition of the subsurface, its porosity, the water content, and the physical and chemical properties of the water [60]. ERT has been profitably applied in hydrogeological and structural investigations in many geothermal systems [22–24,61–63].

In this work, ERT was employed to delineate the structural and lithological properties of the Daruvar spring area. Eight profiles were acquired in 2021 and 2022 (Figure 2 and Table 1). Field measurements were conducted using the POLARES 2.0 electrical imaging system (PASI srl). This system was connected to stainless steel electrodes, which were laid out in a straight line with a constant spacing via a multi-core cable. Due to the complexity of the geological structures in the subsurface of the spring area, a Wenner–Schlumberger configuration was used since it resolves horizontal and vertical structures and has a greater depth of investigation [64]. Initially, profiles were measured at a frequency of 7.15 Hz and a maximum phase of 20° between the voltage signal and the current signal. Contact impedance value of the electrodes was checked since it can cause potential errors in the dataset [65]. The frequency was progressively lowered until the number of incorrect measurements was below 10% of the total.

Table 1. Geographic coordinates of the ERT profiles and their geometric features.

Profile	Coordinates		Azimuth	Number of Electrodes	Electrode Distance	Length of Profile
	Beginning	End	(°N)		(m)	(m)
ERT 1	17°13′33.7″ E; 45°35′32.86″ N	17°13′35.4″ E; 45°35′53.2″ N	3	64	10	630
ERT 2	17°13′46.78″ E; 45°36′5.14″ N	17°13′25.6″ E; 45°36′6.53″ N	275	48	10	470
ERT 3	17°13′33.14″ E; 45°35′35.14″ N	17°13′36.78″ E; 45°35′44.96″ N	14	48	5	235
ERT 4	17°13′33.3″ E; 45°35′33.14″ N	17°13′35.01″ E; 45°35′40.67″ N	9	48	5	235
ERT 5	17°13′29.74″ E; 45°35′34.98″ N	17°13′34.67″ E; 45°35′41.89″ N	26	64	5	315
ERT 6	17°13′37.05″ E; 45°35′31.77″ N	17°13′36.61″ E; 45°35′39.02″ N	357	48	5	235
ERT 7	17°13′27.18″ E; 45°35′44.67″ N	17°13′38″ E; 45°35′44.16″ N	93	48	5	235
ERT 8	17°13′26.23″ E; 45°35′37.99″ N	17°13′35.96″ E; 45°35′41.36″ N	63	48	5	235

The Res2DInv 4.9.3 software (https://www.aarhusgeosoftware.dk/res2dinv, accessed on 3 August 2023) was used to invert the field apparent resistivity data into 2D resistivity subsurface models using a Gauss–Newton method and a finite element solver [66,67]. The software has two different routines for creating 2D resistivity models based on the L_1-norm (or blocky, robust) and the L_2-norm (or smoothness-constrained least-squares) inversion methods [68]. For the collected dataset, the method based on L_2 norm was used because it gives optimal results where the subsurface resistivity changes in a gradual manner. This method minimizes the sum of squares of the spatial changes in the model resistivity and the data misfit [69]. In the Daruvar spring area, materials with both relatively high and low resistivity are expected. However, the occurrence of thermal water with high electrical conductivity and the high porosity of the sediments/rocks should decrease the bulk resistivities, resulting in smooth resistivity transitions between the different formations.

The inversion was terminated when the RMS was below 10%, except for profile ERT 4 for which it reached 12.4%.

2.2.2. Seismic Investigations

An integrated approach based on the passive horizontal to vertical spectral ratio (HVSR) and the active multichannel analysis of surface waves (MASW) methods was applied to map the thickness of the Quaternary cover in the Daruvar spring area. Similar methodological approaches have been used in thermal areas where recent sediments conceal the geometry of the bedrock [39,70–72].

The HVSR method is based on recording the vertical and horizontal components of the ambient seismic noise wavefield [73]. The seismic impedance contrast between the bedrock and the unconsolidated Quaternary sediments generates a peak in the H/V curve (i.e., ratio between the horizontal and vertical seismic ambient noise spectra) that can be used to assess the thickness of the alluvial cover. The thickness of the covering layer (h) can be calculated [73] as:

$$h = \frac{V_s}{4f_0} \quad (1)$$

with Vs being the shear-wave velocity of the sediments and f_0 the peak frequency of the H/V noise spectra.

The estimation of h depends on the subsurface Vs. This parameter can be assessed using the MASW approach in order to have a site-specific distribution of Vs. The Vs profile is reconstructed by measuring the propagation velocities of surface waves in the ground [74,75]. The dispersion curve of the surface waves is calculated resulting in the 1D model of Vs variation with depth.

In this study, ambient seismic noise was recorded at 6 stations (Figure 2 and Table 2). Stations H1 to H5 were selected to perform a N-S cross section parallel to the ERT 1 profile, while H3 and H6 were located in correspondence with the DS 1 and Dar 1 wells, respectively. The three orthogonal components (one vertical and two horizontals, i.e., N-S and E-W) of the signal were recorded using a 3D land geophone with an eigen-frequency of 2 Hz and 24-bit data acquisition board. The recording time for each station was 15 min with a sampling rate of 5 ms (sampling frequency of 200 Hz). At the same site, MASW investigations were conducted through seismic profiles composed of 24 geophones (4.5 Hz) at a distance of 2 m connected to a GEA-24 seismograph (PASI srl). As the source of the seismic wave, a hammer weighing 8 kg and a steel plate were used. The center of the seismic profile was located where the HVSR measurement was conducted.

Table 2. Coordinates of the HVSR and MASW investigations. The center of the MASW array corresponds to the location of the HVSR measurement.

HVSR/MASW	Coordinates	
	E	N
H1	17°13′31.40″	45°35′35.06″
H2	17°13′33.06″	45°35′37.42″
H3	17°13′35.37″	45°35′40.33″
H4	17°13′37.46″	45°35′44.42″
H5	17°13′41.38″	45°35′53.77″
H6	17°13′44.83″	45°35′48.19″

The data analysis consisted of (i) the computation of the H/V curve, (ii) the reconstruction of the Vs profile from MASW measurement, and (iii) the calculation of h at every site using Equation (1). Data processing of HVSR measurements was performed in the Geopsy 3.3.3 software (https://www.geopsy.org, accessed on 15 February 2023). For each measurement point, the Fourier amplitude spectrum of horizontal and vertical components of the ambient seismic noise was conducted. For calculating the Fourier spectrum, the Konno and Ohmachi smoothing method was used [76], then the frequency range within

which the spectra are calculated was defined. Finally, the H/V ratio was calculated. When calculating and displaying the H/V spectrum, the frequency range from 0.2 to 10 Hz was used.

Processing of the MASW measurement data was conducted in the ParkSEIS 3.0 program (https://www.parkseismic.com/parkseis/, accessed on 3 August 2023). The Fourier spectral analysis was performed for each individual recording in the time domain, obtaining the dispersion curve of the S-waves. By inversion of the dispersion curve, a 1D model of the change in S-wave velocity (*Vs*) was calculated [75]. In the performed inversions, an input model composed of 10 layers with a thickness of 2 m was used. The iteration was stopped when the error was lower than 5%. The input model was chosen after a preliminary analysis obtaining a good vertical resolution and reaching an observation depth that would be comparable with the presumed depth of the Quaternary cover in the Daruvar spring area.

3. Results

3.1. Electrical Resistivity Tomography (ERT)

The distribution of resistivity in the subsurface of the Daruvar area shows relatively low values, generally from 10 to 150 Ωm (Figures 4–6).

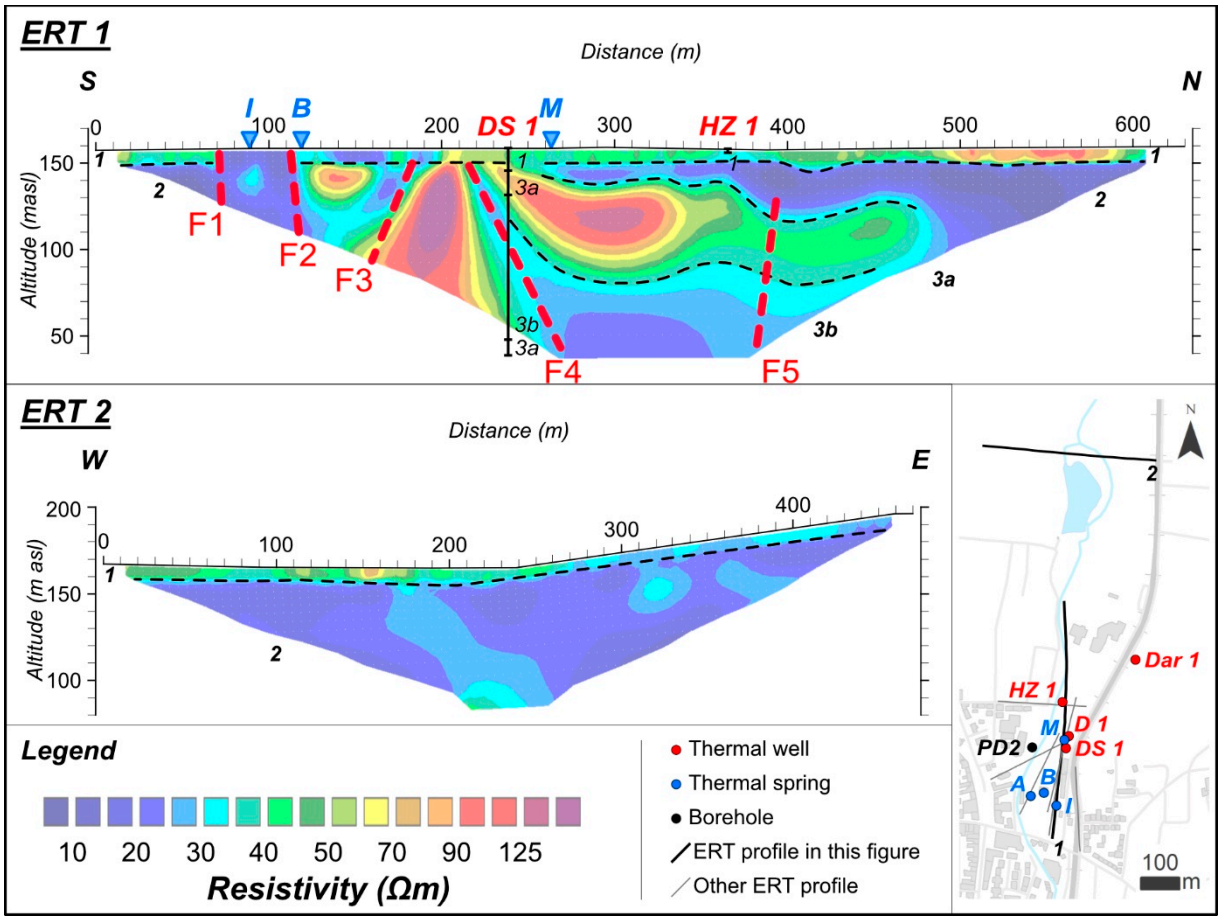

Figure 4. Inverse resistivity models of ERT profiles with 10 m spacing between electrodes. ERT 1 shows a general overview of the spring area, while ERT 2 investigated the northern part of the spring area. For acronyms of wells and springs and the location of profiles, see Figure 2.

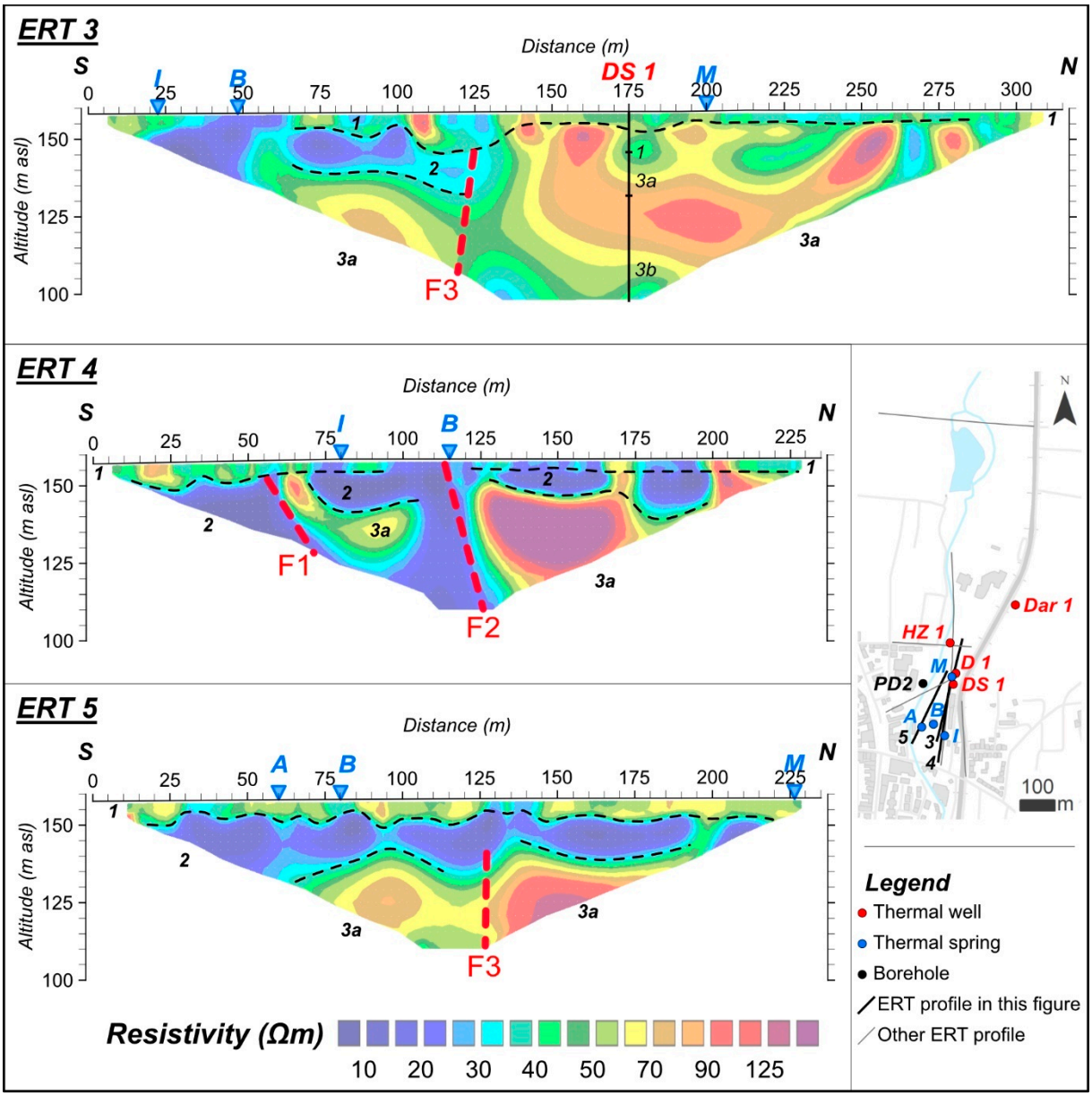

Figure 5. Inverse resistivity models of ERT profiles with 5 m spacing between electrodes within the Daruvar spring area. For acronyms of wells and springs and the location of profiles, see Figure 2.

Figure 4 shows the profiles with spacing between electrodes of 10 m providing a general overview of the spring area (i.e., ERT 1) and its surroundings (i.e., ERT 2). Data inversion resulted in an RMS error of 7% and 2.5% for ERT 1 and ERT 2, respectively.

The following layers were interpreted in ERT 1: (i) an upper domain (layer 1) with variable thickness of 5–10 m and resistivity of 30–50 Ωm, with localized anomalies of both low (<20 Ωm) and high (70–100 Ωm) resistivity, (ii) a second layer (2) with low resistivity (5–15 Ωm) showing a discontinuous geometry with a variable thickness of at least 20 m in the southern part, 5 m in the central part, and increasing up to 40 m in the northern part of the profile, (iii) a third layer (3a) with a thickness of approximately 50 m and resistivity generally ranging from 70 to 150 Ωm (and locally up to 224 Ωm) in the middle part of the profile and with a resistivity of 50–60 Ωm in the northern part, and (iv) a bottom layer (3b) characterized by resistivity values of 20–30 Ωm detected only in the central part of the profile. Additionally, several vertical low resistivity zones (10–30 Ωm) dividing the high resistivity bodies were observed (i.e., F1 to F5; Figure 4).

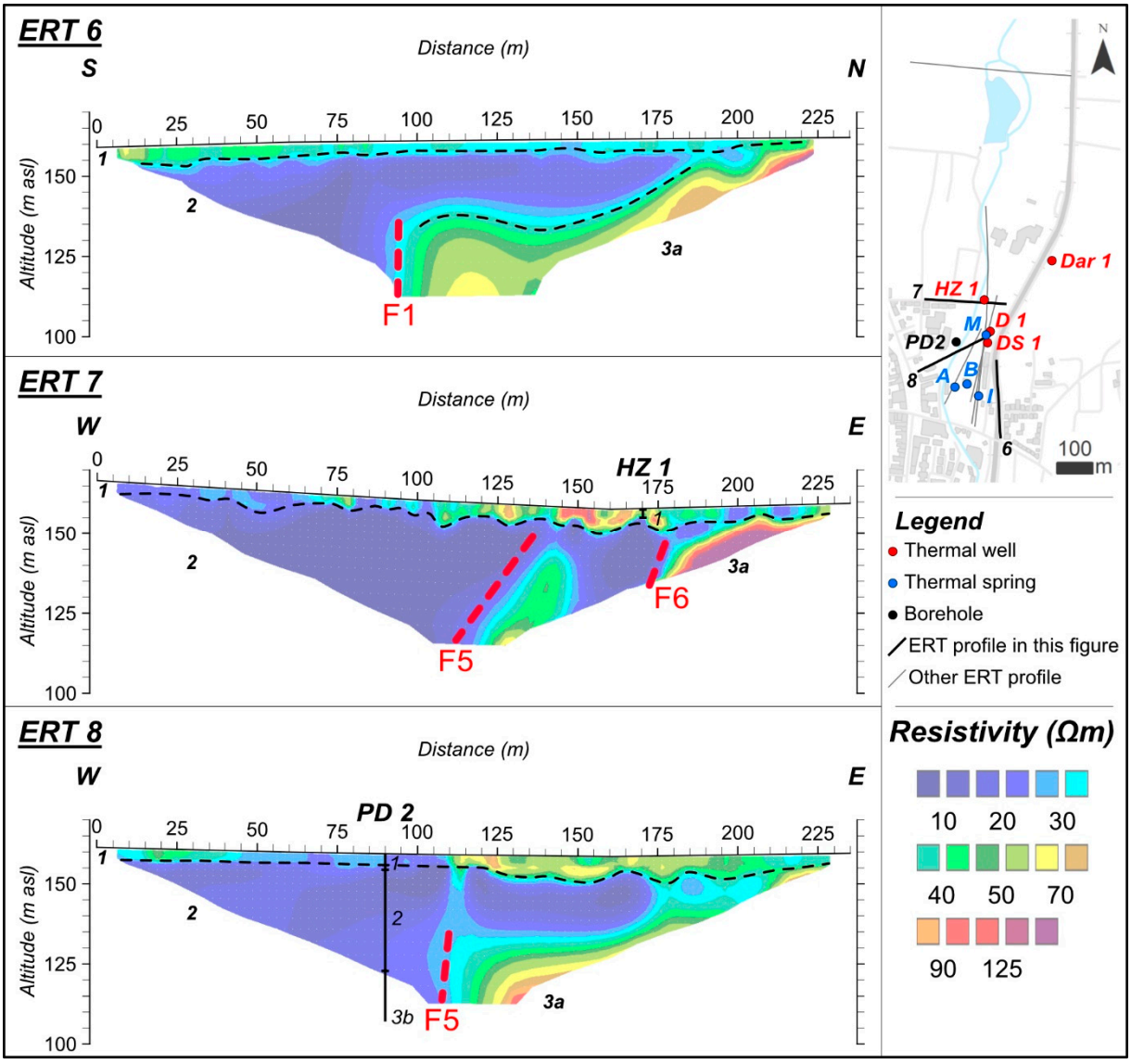

Figure 6. Inverse resistivity models of ERT profiles with 5 m spacing between electrodes. ERT 7 and ERT 8 investigate the north-western part of the Daruvar spring area, while ERT 6 investigates the south-eastern part. For acronyms of wells and springs and the location of profiles, see Figure 2.

The layers interpreted in ERT 2 were: (i) an upper domain (layer 1) with a thickness of 5–10 m and resistivity value decreasing from W to E (40 to 20 Ωm), and (ii) a second layer (2) showing resistivity of 20–30 Ωm and reaching a thickness of approximately 80 m in the middle part of the profile.

Figure 5 shows the profiles investigating the spring area conducted using a spacing between electrodes of 5 m. Data inversion resulted in an RMS error of 4.1%, 12.4%, and 5.6% for ERT 3, ERT 4, and ERT 5, respectively.

Three domains can be distinguished in the profile ERT 3: (i) an upper domain (layer 1) which has a variable thickness of 5–10 m and is characterized by resistivity values of 30–50 Ωm with small scale resistivity anomalies, (ii) a second domain (layer 2), visible only in the southern part of profile, with low resistivity of 10–30 Ωm, and (iii) a third domain (layer 3a) located at a depth higher than 20 m in the southern part of the profile and with resistivity values of 40–70 Ωm, and located at a depth higher than 5 m in the central and northern part of the profile having resistivity generally between 50 and 100 Ωm (locally up to 160 Ωm). Within layer 3a, a lateral decrease of resistivity is observed at the distance

between 125–135 m showing a prominent sub-vertical geometry and resistivity values of 30–40 Ωm (F3). Furthermore, a low resistivity area (10–20 Ωm) is depicted in the southern part of the profile in correspondence with the Ivanovo vrelo and Blatna kupelj springs.

In the profile ERT 4, the interpreted layers are: (i) an upper domain (layer 1) with a maximum thickness of 5 m and a variable resistivity of 20–40 Ωm, (ii) a second layer (2) with a resistivity of 10–20 Ωm and a thickness higher than 15 m in the southern part and from 5 to 15 m in the central and northern part of the profile, and (iii) a bottom domain (layer 3a) divided into two zones at 60 to 100 m and 125 to 175 m with resistivity values of 40–50 Ωm and >100 Ωm (maximum resistivity of 345 Ωm), respectively. These two zones are divided by a sharp lateral decrease of resistivity with values 10–20 Ωm (F2).

Three domains can be distinguished in the profile ERT 5: (i) an upper domain (layer 1) which has a thickness of approximately 5 m and resistivity values of 40–60 Ωm and small scale resistivity anomalies, (ii) a second domain (layer 2) showing good lateral continuity, a thickness of approximately 15 m, and resistivity of 10–20 Ωm, and (iii) a third domain (layer 3a) divided into two zones at 80 to 110 m and 130 to 180 m with resistivity values of approximately 70 and >90 Ωm (maximum resistivity of 150 Ωm), respectively. The two zones are divided by a vertical body with lower resistivity values of 50–60 Ωm (F3).

Figure 6 shows the profiles with spacing between electrodes of 5 m providing an overview of the north-western (i.e., ERT 7 and ERT 8) and south-eastern parts (i.e., ERT 6) of the spring area. Data inversion resulted in an RMS error of 3.5%, 6.5%, and 2.9% for ERT 6, ERT 7, and ERT 8, respectively.

The following layers are interpreted in ERT 6: (i) an upper domain (layer 1) with a thickness of 5 m and a resistivity of 30–40 Ωm, (ii) a second layer (2) with low resistivity (<20 Ωm) and a decreasing thickness from at least 30 m in the southern part to 5 m in the northern part of the profile, and (iii) a third layer (3a) with a thickness of at least 25 m in the middle part of the profile and resistivity generally ranging from 40 to 60 Ωm (locally up to 200 Ωm). A sharp lateral transition between layers 2 and 3a is observed (F1).

Three domains can be distinguished in the profile ERT 7: (i) an upper domain (layer 1), which has a thickness of 5 m and is characterized by resistivity of 20–40 Ωm, except for a high resistivity anomaly (90–110 Ωm) at 145–175 m, (ii) a second domain (layer 2) observed in the western and central part of the section with resistivity <10 Ωm and a thickness of at least 45 m, and (iii) a third domain (layer 3a) in the eastern part of the profile characterized by resistivity from 50 to 100 Ωm in the upper part and from 200 to 300 Ωm in the deeper part. The layer 3a shows a sharp transition to a very low resistivity body (<10 Ωm) towards the W (F6). Moving westward, the resistivity slightly increases (30–40 Ωm), followed by a sharp resistivity drop and the transition to layer 2 (F5).

Three layers based on the resistivity distribution are observed in ERT 8: (i) an upper domain (layer 1), which has a thickness of approximately 5 m and is characterized by low resistivity of 20–30 Ωm until 115 m, followed by slightly higher resistivity values (40–60 Ωm), (ii) a second domain (layer 2), which has a resistivity of 10–30 Ωm and a variable thickness of at least 45 m in the western part, approximately 25 m from 110 m to 170 m, and 10 m in the eastern part of the profile, and (iii) a third layer (3a) at a depth of 30 m in the central part of the profile with resistivity values of generally 40–70 Ωm and reaching values of approximately 100 Ωm in the deeper part of the layer. A sharp lateral transition between layers 2 and 3a is observed (F5).

3.2. Seismic Investigations

H/V spectral ratio method was applied to the six microtremor measurements (Figure 2 and Table 2) conducted in the Daruvar spring area. The results are shown in Figure 7. The interpreted H/V curves present f_0 peaks with variable shapes, from sharp to smooth, indicating a heterogenous seismic response in the subsurface. Generally, the measurements show sharp peaks in the H/V curve, except for H6 towards the east. The f_0 and amplitude of the peaks are reported in Table 3.

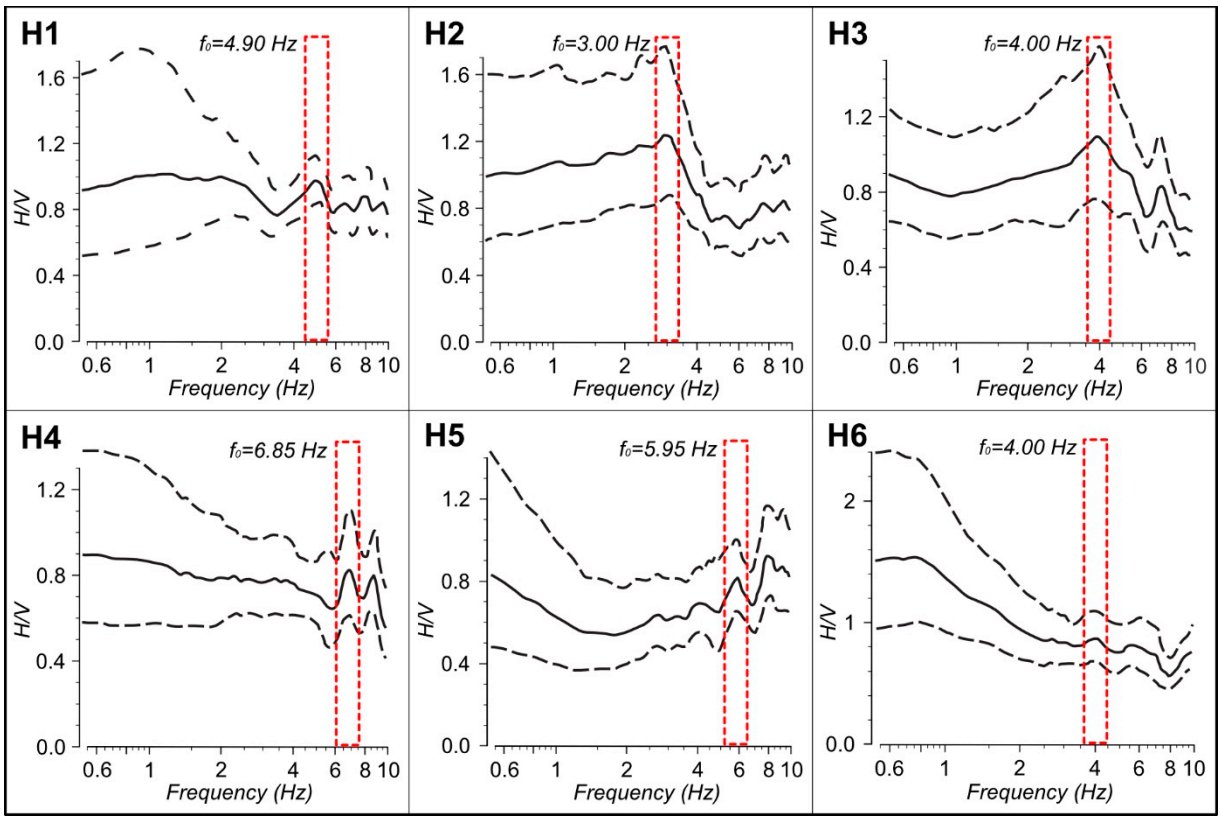

Figure 7. H/V spectral ratio measured at the stations H1 to H6. The black solid line represents the average of the H/V ratio, while the black dashed lines indicate the minimum and maximum values. The red dashed box highlights the first peak in the curve that was used to determine the thickness of first seismic layer. The locations are shown in Figure 2, while the coordinates are in Table 2.

Table 3. Calculation of the Quaternary cover thickness using the Nakamura method [73].

	f_0	Vs	h
	(Hz)	**(m/s)**	**(m)**
H1	4.90	229.5	11.71
H2	3.00	190.14	15.85
H3	4.00	232.06	14.5
H4	6.85	260.52	9.51
H5	5.95	356.49	14.98
H6	4.00	330.3	20.64

Furthermore, a reconstruction of the vertical variation in S-wave velocity (Vs) was conducted through the measurement of the ambient seismic noise using the MASW approach. The reached investigation depth was 20 m, and the *Vs* distributions at the different locations are shown in Figure 8. *Vs* values generally range from approximately 125 m/s to 690 m/s (black dots in Figure 8).

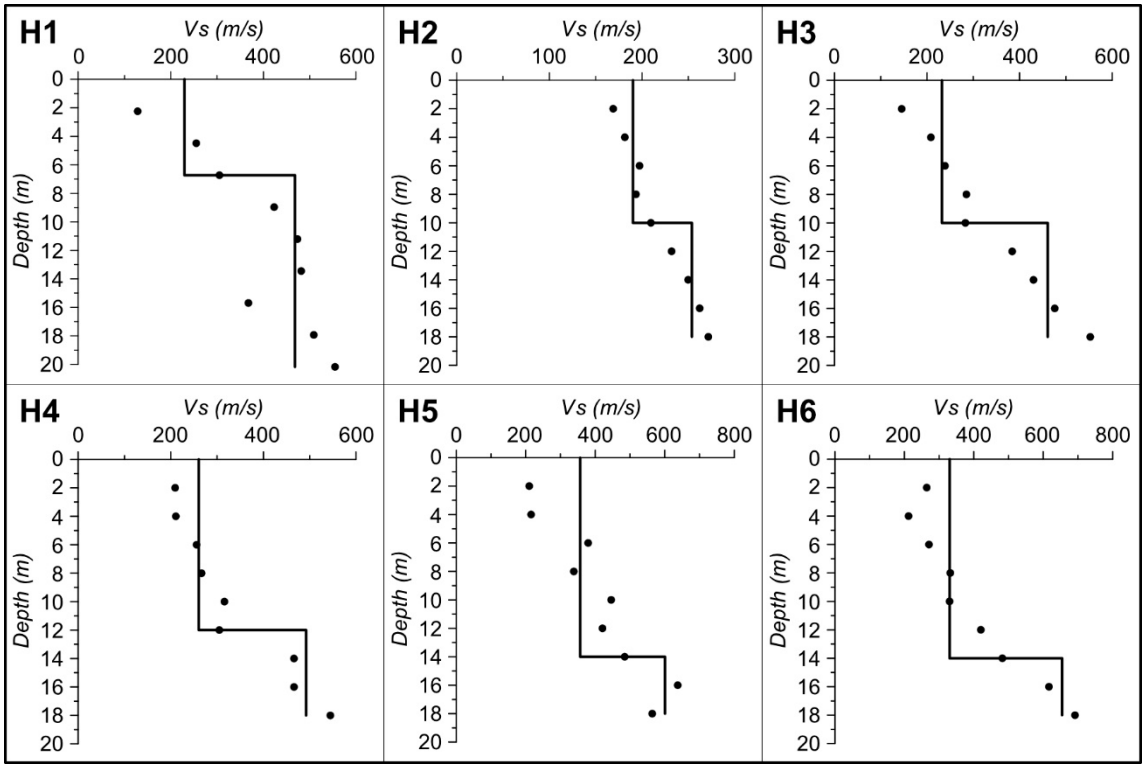

Figure 8. *Vs*-versus-depth profiles at H1 to H6 stations. Points represent the *Vs* values, while the solid line represents 1D profile obtained after the interpretation of the results.

The observed *Vs* were grouped based on the *Vs* values (black lines in Figure 8). Two seismic units can be distinguished. The thickness of the first seismic unit varies from 6 to 14 m, showing *Vs* from 190 to 356 m/s. *Vs* values in the second seismic unit range from 253 m/s to 654 m/s. It should be noted that H2 shows the lowest *Vs* values for both the first and the second seismic units.

The H/V frequency and the *Vs* of the first layer were used to estimate the thickness of the sedimentary cover, corresponding to the Quaternary alluvial cover, using Equation (1). The results are shown in Table 3.

4. Discussion

Reconstruction of the geological setting of a thermal system is one of the steps necessary for assessing the potential of a geothermal resource. Geophysical investigations have been profitably used to address this topic since their results can be used to indirectly reconstruct the geometry of the reservoir and of the fault systems driving the fluid circulation [19,22–24,39,61–63,71,72]. These methods are particularly applicable in areas where the geological data are limited to a few stratigraphic logs or where the alluvial cover conceals the subsurface structure.

In this work, an integrated geophysical approach based on electrical resistivity tomography (ERT) and both active and passive seismic (i.e., MASW and HVSR) methods was applied to construct a 3D model of the subsurface in the Daruvar spring area (Figure 2). The outflow of thermal waters in the study area is enhanced by the high permeability of the carbonate reservoir, resulting in thermal springs with water temperatures of 38–50 °C [44]. Although it was argued that the increased permeability field is connected with faults and their damage zones, their occurrence has never been proven.

The ERT profiles in the Daruvar area (Figure 2) showed heterogenous vertical and horizontal resistivity distributions (Figures 4–6). Four layers were recognized. A first, near-surface layer (layer 1) with resistivity values ranging from 30 to 50 Ωm was observed in all profiles (Figures 4–6). This domain contains zones with low (<20 Ωm) and high

(generally 70–100 Ωm) resistivity values, and its thickness varies from 5 to 10 m. The second layer (layer 2) showed discontinuous geometry with thickness variations from 20 to 40 m and a uniform resistivity ranging from 5 to 25 Ωm (Figures 4–6). The third layer (3a) had a maximum thickness of 50 m and resistivities ranging from 70 to 150 Ωm. A bottom layer (3b) was detected only in the central part of the longest profile (ERT 1; Figure 4) and it was characterized by resistivity values of 20–30 Ωm.

The lithologies of the observed layers were assessed considering the stratigraphic logs of the wells in the Daruvar thermal spring area (Figures 2 and 3).

Layer (1) was interpreted as the Quaternary alluvial cover composed of interchanging clays, sands, and gravels. Clay sediments generally show low resistivities (10–100 Ωm; [18]), while sands and gravels have higher resistivity (>200 Ωm; [60]). Considering the wide range of resistivity in granular materials, relatively low resistivity values were observed in layer 1. However, the occurrence of water in the pore spaces and its chemical composition and temperature could diminish the bulk electrical resistivity of the material. Reports of boreholes highlighted that the sandy layers of the alluvial cover host both fresh waters infiltrating from the Toplica river and thermal waters with moderate mineralization. Locally, the water content in the pore spaces could be lower, causing a local increase in the resistivity as shown by the ERT profiles.

Layer (2) was interpreted as the Neogene sedimentary complex of western Papuk mostly consisting of marls and locally bioclastic limestones in the lower part. Marls generally show resistivities in the range of 50–100 Ωm [34]. Similar to the Quaternary deposits, Neogene marls in the Daruvar area could be saturated with thermal or cold waters, causing the observed low resistivity values (5–25 Ωm).

Layer (3) was interpreted as the Triassic sedimentary rocks complex composed of dolomites and limestones. Based on the difference in the resistivity distribution, this layer was divided into a "more compact" and a "more fractured" part (i.e., layer 3a and 3b, respectively) with higher (70–150 Ωm) and lower (20–30 Ωm) resistivity values, respectively. The resistivity of carbonate rocks is generally higher than 800 Ωm [18]. On the other hand, the resistivities measured in layer 3 are much lower for both the compact and fractured parts. In order to estimate their bulk resistivity, the generalized version of the Archie's law [77–79] was used:

$$\rho = \frac{a}{\phi^m S^n} \rho_w \quad (2)$$

with ρ and ρ_w being the bulk and water resistivity, respectively, ϕ the porosity of the material, S the water saturation, and a, m, and n empirical parameters. Layer 3 was considered fully saturated (i.e., $S = 1$) by the Daruvar thermal waters. The ρ_w was calculated from the average electrical conductivity of the thermal water measured in the Antunovo vrelo spring (i.e., 578 µS/cm; [54]). The porosity was obtained from the well logging conducted in the Dar 1 well [56]. The average porosity value (7%) was considered representative of the compact carbonates since it permits the inclusion of small scale fractures that could not be highlighted during the well drilling but could contain thermal waters. The value at the 90th percentile of the porosity distribution (17%) was considered representative of the fractured portion since it permits the inclusion of both small- and large-scale fractures. The empirical parameters a and m were both set as equal to 1. These values are generally considered appropriate for a preliminary assessment of the resistivity in fractured carbonates [78–81]. The resulting ρ for the compact and the fractured parts of layer 3 (i.e., 3a and 3b, respectively) were 220 and 100 Ωm, respectively. These values are in the upper range of the observed values. However, it could be argued that the porosities measured through the well logging are representative of a rock volume smaller than the volume investigated with ERT. Increasing the representative elementary volume would increase the porosity [82], resulting in a decrease of the bulk resistivity.

Besides vertical variations in the resistivity distribution, lateral variations were observed (F1 to F5 in Figures 4–6). They were generally marked by low resistivity anomalies (up to 20 Ωm) within higher resistivity bodies (i.e., F4 in ERT 1; Figure 4) or by a sharp

transition in the resistivity distribution (i.e., F5 in ERT 6 and ERT 7; Figure 6). These lateral variations were interpreted as caused by the occurrence of faults/fractures and associated damage zones. The high secondary porosity of the fault damage zone and the occurrence of thermal waters decrease the bulk resistivity of the rock mass, resulting in the observed anomalies. Archie's law (Equation (2)) was used to assess the bulk resistivity of the fault damage zone. The highest porosity value measured during the Dar 1 well logging (41%) was considered representative since it could reflect a highly fractured rock mass with open fractures that is typical of a fault damage zone. Other parameters were kept constant. The resulting ρ was 40 Ωm, very similar to the observed values.

The results of ERT profiles were complemented by the results obtained from active and passive seismic methods. These methods were used to define the thickness of the Quaternary cover through the Nakamura approach [73] (Equation (1)). The reliability of the method was verified by comparing the results with the stratigraphic logs at the same locations. A thickness of 14.5 and 20.6 m was calculated at H3 and H6 (Table 3), respectively, roughly corresponding to the alluvial cover thickness in DS 1 and Dar 1 (Figure 3), respectively. In general, the estimated sedimentary thickness increased from a minimum value of 9.5 m in the central part of the study area (H4; Table 3 and Figure 2) to 11.7 m and 15 m towards south and north (i.e., H1 and H5, respectively; Table 3 and Figure 2). The results obtained by seismic investigations are comparable with the thickness of layer 1 in ERT 1 profile corroborating the results of the electrical resistivity tomography investigations.

Results of the integrated geophysical approach (i.e., ERT, MASW, and HVSR) and data from the stratigraphic logs of the wells were used to construct the 3D geological model of the thermal spring area in Daruvar. The Petroleum Experts Move 2019.1 (https://www.petex.com/products/move-suite/move/, accessed on 13 May 2023) software package was used since it allows integrating 1D and 2D data for a 3D visualization and analysis. Stratigraphic horizons, corresponding to the base of principal lithostratigraphic units/formations, were reconstructed as planes using the inverse distance weight algorithm based on the stratigraphic limits in the ERT profiles and the stratigraphic logs. Fault surfaces were constructed as planes with the spline curves algorithm based on the fault lines interpreted on the ERT sections.

The constructed 3D geological model (Figure 9) is oriented S-N, covering an area of approximately 400 $\times$ 600 m and reaching a depth of approximately 120 m, which corresponds to the maximum investigation depth of the ERT profiles. The ERT 2 profile was not used during the construction of the 3D model, since it is located far from other sections and it would result in significant uncertainty in the model.

Three stratigraphic units and four faults were modeled (Figure 9).

The first unit corresponds to the Quaternary alluvial cover with a variable thickness between 10 and 15 m. The second unit corresponds to the Neogene sedimentary complex. Its thickness is a few meters in the central part of the Daruvar spring area and increases toward the S and the N. It reaches a maximum of 40 and 30 m in the SW and SE corners, respectively, while it is up to 100 and 50 m in the NW and NE corners, respectively. It should be noted that the highest modeled thickness has a high uncertainty since data are not available in this part of the model. The third unit is composed of the Triassic carbonate complex that constitutes the main thermal reservoir. Its geometry has been partially reproduced since its bottom was arbitrarily placed at a depth of 120 m, corresponding to the maximum depth investigated with the ERT profiles. However, neither the profiles nor the wells reached the bottom of the reservoir unit, and its real thickness in the spring area is still debatable. In the central part of the study area, the Triassic complex is in direct contact with the Quaternary unit (i.e., ERT 1 and 3; Figures 4 and 5).

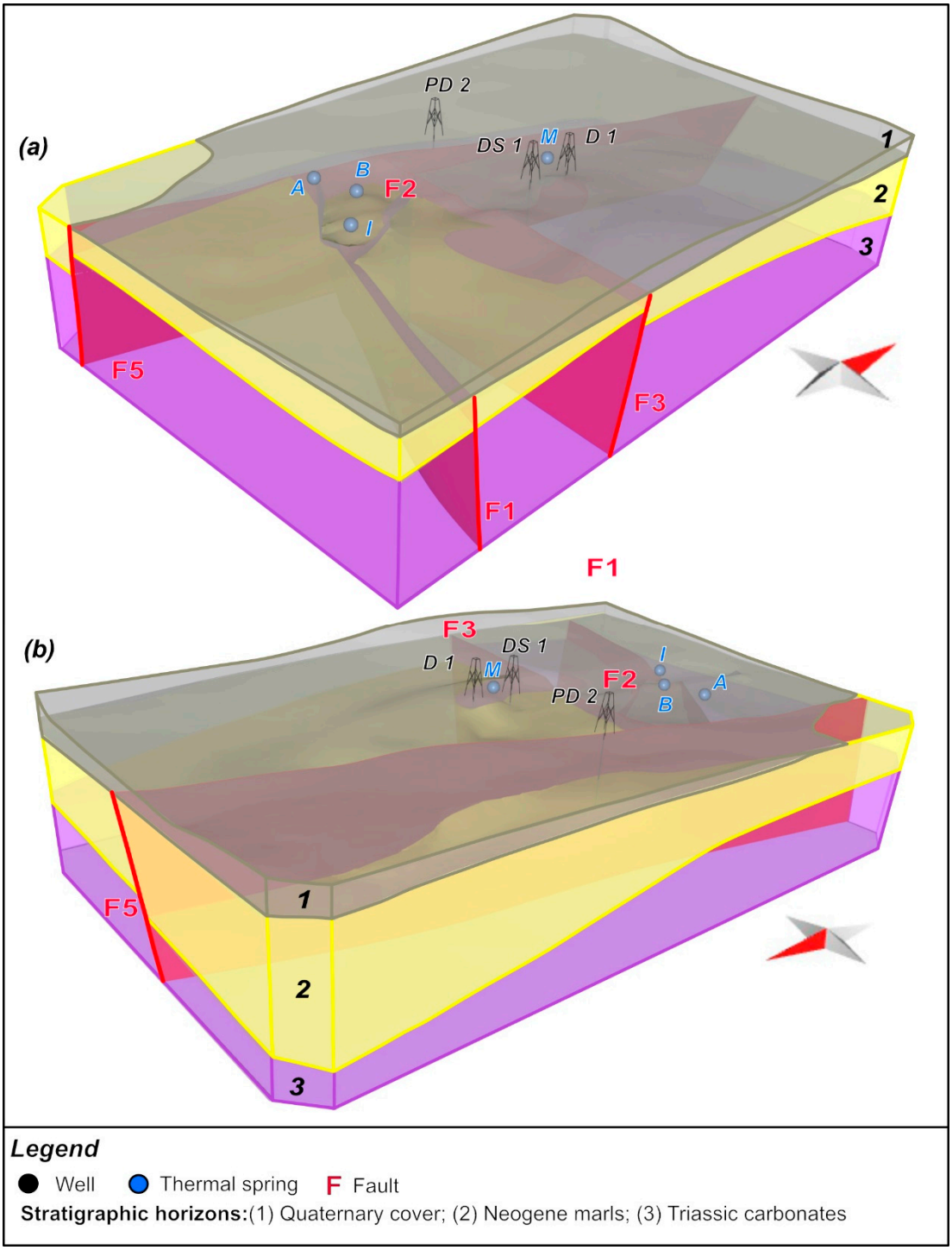

Figure 9. 3D geological model of the Daruvar thermal spring area (view from SE and NW in (**a**) and (**b**), respectively). Three stratigraphic units and four faults were identified. Acronyms of springs and wells are in Figure 2.

The modeled faults were F1, F2, F3, and F5 (Figure 9). The fault traces F4 (ERT 1; Figure 4) and F6 (ERT 7; Figure 6) were not modeled since they were depicted only in one profile. The fault F1 dips at a high angle toward NNE showing a length of 300 m in plain view. The dip direction varies from approximately 10°N in the eastern part to 40°N in the western part toward the contact with F5. Similarly, the dip decreases westward from subvertical to approximately 70° at the contact with F5. The fault F2 dips at high angle

(>80°) toward ENE (dip direction = 60–70°N) with a length of 130 m in plain view. The fault F3 dips at a high angle (80°) toward the S (dip direction = 180°N) with a length of 250 m in plain view. Fault F5 is the longest in the modeled area, extending within the whole modeling domain. The fault generally dips toward the W (dip direction = 280°N) at different angles. The dip varies from 85° in the southern part of the modeling domain to 65° toward the N.

The faults show a minor vertical throw, and only F5 shows a throw up to 15 m (ERT 8; Figure 6). Since shallow geophysical methods were employed in this work, the data on the vertical extent of the faults are limited and deeper data should be acquired in the future for a detailed kinematic analysis. Similarly, it is not possible to determine the horizontal movement.

F1 and F3 can be interpreted as E-W trending, high angle, antithetic faults, while F2 could represent a splay fault within their interaction zone. F5 borders westward the interaction zone and could be interpreted as a fault parallel to the regional, NE-SW trending, Daruvar fault, or it could correspond to its shallower part. Here, for a detailed interpretation addressing the relation between F5 and the Daruvar fault, a regional reconstruction should be performed.

The main outflow of the Daruvar thermal waters, represented by the Antunovo vrelo, Blatna kupelj, and Ivanovo vrelo springs (Figures 2 and 9), occurs within this interaction zone of the observed/mapped faults. The faults F1 and F5 border the interaction zone toward the S and the W, and accommodated the uplifting of the main thermal reservoir (i.e., Triassic carbonates) to shallow depths. Interaction zones between faults are preferential locations for the occurrence of thermal springs, and in general geothermal resources, since the kinematic transfer between the faults increases the rock fracturing and the permeability field [11,12]. This result improves the available conceptual model of the DHS, proving that the occurrence of an interaction zone between faults locally increases the permeability field of the aquifer, favoring the upwelling of the Daruvar thermal waters, and resulting in the observed thermal springs. A similar structure could occur at a larger scale, justifying the high transmissivity of the thermal aquifer calculated through the pumping test conducted in the Dar 1 well [56,58]. Furthermore, the faults F1 and F5 border westward and southward the Daruvar spring area, laterally juxtaposing the high permeable thermal aquifer with low permeable units (i.e., Neogene marls). The lateral contrast in the permeability could foster and localize the upwelling of the thermal waters.

5. Conclusions

The sustainable exploitation of a geothermal resource for its long-term utilization is related to both the water demand and the geological and hydrogeological characteristics of the geothermal field. Detailed geological modeling is a key factor for estimating the potential of a geothermal resource.

This research focused on the reconstruction of the geological and structural settings of the Daruvar thermal spring area using different geophysical methods. Their joint interpretation completed with the stratigraphic logs of exploitation wells and boreholes allowed the determination of the vertical and horizontal distributions of lithological units and proved the occurrence of faults deforming the bedrock in the Daruvar area. The data were used as the input for a 3D model that favored a better visualization and analysis of the results, improving the conceptual model of the Daruvar hydrothermal system. In particular, it was proved that an interaction zone between faults deforms the bedrock, increasing the fracturing and the permeability field. These conditions are favorable for the upwelling of thermal waters and for the formation of thermal springs as depicted in several geothermal fields worldwide.

This paper fosters the knowledge about thermal systems hosted in carbonate complexes that are typical of northern Croatia and the Pannonian basin in general. It proves that a cost-effective geophysical approach could be used to investigate shallow geothermal systems. Furthermore, 3D geological modeling could be profitably used to improve the

conceptual model of the system, providing insights on the connected geothermal resource and its sustainable utilization. In particular, the constructed 3D local model of the Daruvar spring area could be used in a regional- to local-scale reconstruction of the Daruvar hydrothermal system. Such multi-scale models are crucial for assessing the hydrogeological and thermal processes driving the development of a thermal system and can provide useful insights on the renewability of the geothermal resource and the sustainability of its utilization.

Author Contributions: Conceptualization and methodology, B.M., I.K., M.P. (Marco Pola), M.B. and S.B.; data collection by all authors; data curation, I.K. and M.P. (Marco Pola); software and formal analysis, I.K., I.P., M.P. (Marco Pola) and B.P.; writing—original draft preparation, M.P. (Marco Pola); writing—review and editing by all authors; visualization, I.K., B.M. and M.P. (Marco Pola); supervision, S.B.; research design and funding acquisition, S.B.; project administration, M.P. (Mirja Pavić) and S.B. All authors have read and agreed to the published version of the manuscript.

Funding: This research was funded by the HyTheC project of the Croatian Science Foundation (HRZZ), grant number UIP-2019-04-1218.

Institutional Review Board Statement: Not applicable.

Informed Consent Statement: Not applicable.

Data Availability Statement: Data available on request from the authors.

Acknowledgments: The authors would like to thank the colleagues H. Burić, T. Novosel, M. Mileusnić, N. Stanić, and M. Patekar for the support during the geophysical campaigns, and Daruvarske toplice–Special Hospital for Medical Rehabilitation and Pivovara Daruvar d.o.o. for logistic help on-site and sharing of existing materials.

Conflicts of Interest: The authors declare no conflict of interest.

References

1. EU CORDIS; European Climate Infrastructure and Environment Executive Agency (CINEA). *CORDIS Results Pack on Geothermal Energy—Supporting the Development of Europe's Geothermal Energy Sector*; Publications Office of the European Union: Luxembourg, 2022.
2. Fetting, C. *The European Green Deal*; ESDN Report; ESDN Office: Vienna, Austria, 2020.
3. Moeck, I.S. Catalog of Geothermal Play Types Based on Geologic Controls. *Renew. Sustain. Energy Rev.* **2014**, *37*, 867–882. [CrossRef]
4. Moeck, I.; Hinz, N.; Faulds, J.; Bell, J.; Kell-Hills, A.; Louie, J. 3D Geological Mapping as a New Method in Geothermal Exploration: A Case Study from Central Nevada. *GRC Trans.* **2010**, *34*, 807–812.
5. Pola, M.; Cacace, M.; Fabbri, P.; Piccinini, L.; Zampieri, D.; Torresan, F. Fault Control on a Thermal Anomaly: Conceptual and Numerical Modeling of a Low-Temperature Geothermal System in the Southern Alps Foreland Basin (NE Italy). *J. Geophys. Res. Solid Earth* **2020**, *125*, e2019JB017394. [CrossRef]
6. Siler, D.L.; Faulds, J.E.; Hinz, N.H.; Dering, G.M.; Edwards, J.H.; Mayhew, B. Three-Dimensional Geologic Mapping to Assess Geothermal Potential: Examples from Nevada and Oregon. *Geotherm. Energy* **2019**, *7*, 2. [CrossRef]
7. Torresan, F.; Piccinini, L.; Cacace, M.; Pola, M.; Zampieri, D.; Fabbri, P. Numerical Modeling as a Tool for Evaluating the Renewability of Geothermal Resources: The Case Study of the Euganean Geothermal System (NE Italy). *Environ. Geochem. Health* **2022**, *44*, 2135–2162. [CrossRef]
8. Maitra, A.; Singh, A.; Keesari, T.; Sharma, S.P.; Gupta, S. Elevated Equilibrium Geotherm in Stable Continental Shield: Evidence From Integrated Structural, Hydrological, and Electromagnetic Studies on Nonvolcanic Hot Springs in the Eastern Ghats Belt, India. *J. Geophys. Res. Solid Earth* **2020**, *125*, e2019JB017747. [CrossRef]
9. Fulignati, P.; Marianelli, P.; Sbrana, A.; Ciani, V. 3D Geothermal Modelling of the Mount Amiata Hydrothermal System in Italy. *Energies* **2014**, *7*, 7434–7453. [CrossRef]
10. Torresan, F.; Piccinini, L.; Pola, M.; Zampieri, D.; Fabbri, P. 3D Hydrogeological Reconstruction of the Fault-Controlled Euganean Geothermal System (NE Italy). *Eng. Geol.* **2020**, *274*, 105740. [CrossRef]
11. Faulds, J.E.; Hinz, N.H.; Dering, G.M.; Siler, D.L. The Hybrid Model—The Most Accommodating Structural Setting for Geothermal Power Generation in the Great Basin, Western USA. *Trans.-Geotherm. Resour. Counc.* **2013**, *37*, 3–10.
12. Curewitz, D.; Karson, J.A. Structural Settings of Hydrothermal Outflow: Fracture Permeability Maintained by Fault Propagation and Interaction. *J. Volcanol. Geotherm. Res.* **1997**, *79*, 149–168. [CrossRef]
13. Cacace, M.; Blöcher, G.; Watanabe, N.; Moeck, I.; Börsing, N.; Scheck-Wenderoth, M.; Kolditz, O.; Huenges, E. Modelling of Fractured Carbonate Reservoirs: Outline of a Novel Technique via a Case Study from the Molasse Basin, Southern Bavaria, Germany. *Environ. Earth Sci.* **2013**, *70*, 3585–3602. [CrossRef]

14. Pola, M.; Gandin, A.; Tuccimei, P.; Soligo, M.; Deiana, R.; Fabbri, P.; Zampieri, D. A Multidisciplinary Approach to Understanding Carbonate Deposition under Tectonically Controlled Hydrothermal Circulation: A Case Study from a Recent Travertine Mound in the Euganean Hydrothermal System, Northern Italy. *Sedimentology* **2014**, *61*, 172–199. [CrossRef]
15. Faulkner, D.R.; Jackson, C.A.L.; Lunn, R.J.; Schlische, R.W.; Shipton, Z.K.; Wibberley, C.A.J.; Withjack, M.O. A Review of Recent Developments Concerning the Structure, Mechanics and Fluid Flow Properties of Fault Zones. *J. Struct. Geol.* **2010**, *32*, 1557–1575. [CrossRef]
16. Caine, J.S.; Evans, J.P.; Forster, C.B. Fault Zone Architecture and Permeability Structure. *Geology* **1996**, *24*, 1025–1028. [CrossRef]
17. Bense, V.F.; Gleeson, T.; Loveless, S.E.; Bour, O.; Scibek, J. Fault Zone Hydrogeology. *Earth-Sci. Rev.* **2013**, *127*, 171–192. [CrossRef]
18. Bruhn, D.; Manzella, A.; Vuataz, F.; Faulds, J.; Moeck, I.; Erbas, K. Exploration Methods. In *Geothermal Energy Systems*; Wiley-VCH Verlag GmbH & Co. KGaA: Weinheim, Germany, 2010; pp. 37–112. ISBN 9783527408313.
19. Singh, A.; Sharma, S.P. Identification of Different Geologic Units Using Fuzzy Constrained Resistivity Tomography. *J. Appl. Geophys.* **2018**, *148*, 127–138. [CrossRef]
20. Chandra, P.C. *Groundwater Geophysics in Hard Rock*; CRC Press: Boca Raton, FL, USA, 2015; ISBN 9780429062605.
21. Yáñez, G.; Perez-Estay, N.; Araya-Vargas, J.; Sanhueza, J.; Figueroa, R.; Maringue, J.; Rojas, T. Shallow Anatomy of the San Ramón Fault (Chile) Constrained by Geophysical Methods: Implications for Its Role in the Andean Deformation. *Tectonics* **2020**, *39*, 2020TC006294. [CrossRef]
22. Lévy, L.; Maurya, P.K.; Byrdina, S.; Vandemeulebrouck, J.; Sigmundsson, F.; Árnason, K.; Ricci, T.; Deldicque, D.; Roger, M.; Gibert, B.; et al. Electrical Resistivity Tomography and Time-Domain Induced Polarization Field Investigations of Geothermal Areas at Krafla, Iceland: Comparison to Borehole and Laboratory Frequency-Domain Electrical Observations. *Geophys. J. Int.* **2019**, *218*, 1469–1489. [CrossRef]
23. Pérez-Estay, N.; Molina-Piernas, E.; Roquer, T.; Aravena, D.; Araya Vargas, J.; Morata, D.; Arancibia, G.; Valdenegro, P.; García, K.; Elizalde, D. Shallow Anatomy of Hydrothermal Systems Controlled by the Liquiñe-Ofqui Fault System and the Andean Transverse Faults: Geophysical Imaging of Fluid Pathways and Practical Implications for Geothermal Exploration. *Geothermics* **2022**, *104*, 102435. [CrossRef]
24. Richards, K.; Revil, A.; Jardani, A.; Henderson, F.; Batzle, M.; Haas, A. Pattern of Shallow Ground Water Flow at Mount Princeton Hot Springs, Colorado, Using Geoelectrical Methods. *J. Volcanol. Geotherm. Res.* **2010**, *198*, 217–232. [CrossRef]
25. Di Napoli, R.; Martorana, R.; Orsi, G.; Aiuppa, A.; Camarda, M.; De Gregorio, S.; Gagliano Candela, E.; Luzio, D.; Messina, N.; Pecoraino, G.; et al. The Structure of a Hydrothermal System from an Integrated Geochemical, Geophysical, and Geological Approach: The Ischia Island Case Study. *Geochem. Geophys. Geosyst.* **2011**, *12*, Q07017. [CrossRef]
26. Mandal, A.; Basantaray, A.K.; Chandroth, A.; Mishra, U. Integrated Geophysical Investigation to Map Shallow Surface Alteration/Fracture Zones of Atri and Tarabalo Hot Springs, Odisha, India. *Geothermics* **2019**, *77*, 24–33. [CrossRef]
27. Chalikakis, K.; Plagnes, V.; Guerin, R.; Valois, R.; Bosch, F.P. Contribution of Geophysical Methods to Karst-System Exploration: An Overview. *Hydrogeol. J.* **2011**, *19*, 1169–1180. [CrossRef]
28. Molli, G.; Doveri, M.; Manzella, A.; Bonini, L.; Botti, F.; Menichini, M.; Montanari, D.; Trumpy, E.; Ungari, A.; Vaselli, L. Surface-Subsurface Structural Architecture and Groundwater Flow of the Equi Terme Hydrothermal Area, Northern Tuscany Italy. *Ital. J. Geosci.* **2015**, *134*, 442–457. [CrossRef]
29. Rolia, E.; Sutjiningsih, D. Application of Geoelectric Method for Groundwater Exploration from Surface (A Literature Study). *AIP Conf. Proc.* **2018**, *1977*, 020018.
30. Sikah, J.N.; Aning, A.A.; Danuor, S.K.; Manu, E.; Okrah, C. Groundwater Exploration Using 1D and 2D Electrical Resistivity Methods. *J. Environ. Earth Sci.* **2016**, *6*, 55–63.
31. Briški, M.; Stroj, A.; Kosović, I.; Borović, S. Characterization of Aquifers in Metamorphic Rocks by Combined Use of Electrical Resistivity Tomography and Monitoring of Spring Hydrodynamics. *Geosciences* **2020**, *10*, 137. [CrossRef]
32. Mishra, U.; Mohapatra, A.K.; Mandal, A.; Singh, A. Identification of Potential Artificial Groundwater Recharge Sites in an Alluvial Setting: A Coupled Electrical Resistivity Tomography and Sediment Characterization Study. *Groundw. Sustain. Dev.* **2023**, *20*, 100875. [CrossRef]
33. Pradhan, R.M.; Singh, A.; Ojha, A.K.; Biswal, T.K. Structural Controls on Bedrock Weathering in Crystalline Basement Terranes and Its Implications on Groundwater Resources. *Sci. Rep.* **2022**, *12*, 11815. [CrossRef]
34. Reynolds, J.M. *An Introduction to Applied and Environmental Geophysics*; John Wiley & Sons: Hoboken, NJ, USA, 2011.
35. Yamanaka, H.; Takemura, M.; Ishida, H.; Niwa, M. Characteristics of Long-Period Microtremors and Their Applicability in Exploration of Deep Sedimentary Layers. *Bull.-Seismol. Soc. Am.* **1994**, *84*, 1831–1841. [CrossRef]
36. Mele, M.; Bersezio, R.; Bini, A.; Bruno, M.; Giudici, M.; Tantardini, D. Subsurface Profiling of Buried Valleys in Central Alps (Northern Italy) Using HVSR Single-Station Passive Seismic. *J. Appl. Geophys.* **2021**, *193*, 104407. [CrossRef]
37. EskIşar, T.; Özyalin, Ş.; Kuruoğlu, M.; Yilmaz, H.R. Microtremor Measurements in the Northern Coast of İzmir Bay, Turkey to Evaluate Site-Specific Characteristics and Fundamental Periods by H/V Spectral Ratio Method. *J. Earth Syst. Sci.* **2013**, *122*, 123–136. [CrossRef]
38. Giustini, F.; Brilli, M.; Carlucci, G.; Ciotoli, G.; Gaudiosi, I.; Mancini, M.; Simionato, M. Geophysical and Geochemical Multi-Method Investigations for Reconstructing Subsurfaces, Alluvial Sedimentology, and Structural Geology (Tiber Valley, Rome). *Int. J. Earth Sci.* **2023**, *112*, 197–216. [CrossRef]

39. Agostini, L.; Boaga, J.; Galgaro, A.; Ninfo, A. HVSR Technique in Near-Surface Thermal-Basin Characterization: The Example of the Caldiero District (North-East Italy). *Environ. Earth Sci.* **2015**, *74*, 1199–1210. [CrossRef]
40. Borović, S.; Marković, I. Utilization and Tourism Valorisation of Geothermal Waters in Croatia. *Renew. Sustain. Energy Rev.* **2015**, *44*, 52–63. [CrossRef]
41. Marković, T.; Borović, S.; Larva, O. Geochemical Characteristics of Thermal Waters of Hrvatsko Zagorje. *Geol. Croat.* **2015**, *68*, 67–77. [CrossRef]
42. Horváth, F.; Musitz, B.; Balázs, A.; Végh, A.; Uhrin, A.; Nádor, A.; Koroknai, B.; Pap, N.; Tóth, T.; Wórum, G. Evolution of the Pannonian Basin and Its Geothermal Resources. *Geothermics* **2015**, *53*, 328–352. [CrossRef]
43. Mraz, V. *Izvještaj o Hidrogeološkim Istražnim Radovima Na Području Daruvarskih Toplica II. Faza (Report on Conducted Hydrogeological Research in Daruvar Spa—Phase II)*; Geološki zavod Zagreb: Zagreb, Croatia, 1983.
44. Borović, S.; Pola, M.; Bačani, A.; Urumović, K. Constraining the Recharge Area of a Hydrothermal System in Fractured Carbonates by Numerical Modelling. *Geothermics* **2019**, *82*, 128–149. [CrossRef]
45. Šimunić, A. *Geotermalne i Mineralne Vode Republike Hrvatske*; Hrvatski Geološki Institut: Zagreb, Croatia, 2008; ISBN 978-953-6907-14.
46. Jamičić, D.; Vragović, M.; Matičec, D. *Osnovna Geološka Karta SFRJ 1:100,000. Tumač Za List Daruvar (Basic Geological Map of SFRJ 1:100,000. Explanatory Notes for Sheet Daruvar)*; Savezni geološki zavod Beograd; Geološki zavod Zagreb: Beograd, Serbia, 1989.
47. Prelogović, E.; Saftić, B.; Kuk, V.; Velić, J.; Dragaš, M.; Lučić, D. Tectonic Activity in the Croatian Part of the Pannonian Basin. *Tectonophysics* **1998**, *297*, 283–293. [CrossRef]
48. Saftić, B.; Velić, J.; Sztanó, O.; Juhász, G.; Ivković, Ž. Tertiary Subsurface Facies, Source Rocks and Hydrocarbon Reservoirs in the SW Part of the Pannonian Basin (Northern Croatia and South-Western Hungary). *Geol. Croat.* **2003**, *56*, 101–122. [CrossRef]
49. Tomljenović, B.; Csontos, L. Neogene-Quaternary Structures in the Border Zone between Alps, Dinarides and Pannonian Basin (Hrvatsko Zgorje and Karlovac Basins, Croatia). *Int. J. Earth Sci.* **2001**, *90*, 560–578. [CrossRef]
50. Lučić, D.; Saftić, B.; Krizmanić, K.; Prelogović, E.; Britvić, V.; Mesić, I.; Tadej, J. The Neogene Evolution and Hydrocarbon Potential of the Pannonian Basin in Croatia. *Mar. Pet. Geol.* **2001**, *18*, 133–147. [CrossRef]
51. Handy, M.R.; Ustaszewski, K.; Kissling, E. Reconstructing the Alps–Carpathians–Dinarides as a Key to Understanding Switches in Subduction Polarity, Slab Gaps and Surface Motion. *Int. J. Earth Sci.* **2015**, *104*, 1–26. [CrossRef]
52. Jamičić, D. The Role of Sinistral Strike-Slip Faults in the Formation of the Structural Fabric of the Slavonian Mts. (Eastern Croatia). *Geol. Croat.* **1995**, *48*, 155–160.
53. Babić, Ž.; Šikić, V.; Mraz, V. *Hidrogeološka Istraživanja Termomineralnih Vrela Kupališnog Lječilišta Daruvar (Hydrogeological Research of Thermomineral Springs at Daruvar Spa)*; Institut za Geološka Istraživanja Zagreb: Zagreb, Croatia, 1971.
54. Borović, S. Integrirani Hidrogeološko—Hidrogeokemijski Model Daruvarskog Geotermalnog Vodonosnika. Integrated Hydrogeological-Hydrogeochemical Model of Daruvar Geothermal Aquifer. Ph.D. Thesis, University of Zagreb, Zagreb, Croatia, 2015.
55. KARST, d.o.o. *Pivovara Daruvar—Izrada Istražne Bušotine Uz Spremnik Za Mazut (Pivovara Daruvar—Construction of an Exploratory Well next to a Tank)*; KARST d.o.o.: Zagreb, Croatia, 2021.
56. Ratkaj, I.; Kinjerovac, Z. *Završno Izvješće Vodoistražni Radovi Na Području Daruvara—Izrada Istražne Bušotine Dar-1 (Final Report on the Hydrogeological Investigations in the Area of Daruvar—Construction of the Exploration Well Dar-1)*; CROSCO, Naftni servisi d.o.o.: Zagreb, Croatia, 2009.
57. Brlek, M.; Iveša, L.; Brčić, V.; Santos, A.; Ćorić, S.; Milošević, M.; Avanić, R.; Devescovi, M.; Pezelj, Đ.; Mišur, I.; et al. Rocky-Shore Unconformities Marking the Base of Badenian (Middle Miocene) Transgressions on Mt. Medvednica Basement (North Croatian Basin, Central Paratethys). *Facies* **2018**, *64*, 25. [CrossRef]
58. Urumović, K.; Terzić, J.; Kopić, J.; Kosović, I. Identification of Aquifer and Pumped Well Parameters Using the Data Hidden in Non-Linear Losses. *Sustainability* **2023**, *15*, 11170. [CrossRef]
59. Loke, M.H.; Chambers, J.E.; Rucker, D.F.; Kuras, O.; Wilkinson, P.B. Recent Developments in the Direct-Current Geoelectrical Imaging Method. *J. Appl. Geophys.* **2013**, *95*, 135–156. [CrossRef]
60. Yoshino, T. Electrical Properties of Rocks. In *Encyclopedia of Solid Earth Geophysics*; Gupta, H.K., Ed.; Springer International Publishing: Cham, Switzerland, 2021; pp. 339–344. ISBN 978-3-030-58631-7.
61. Fikos, I.; Vargemezis, G.; Zlotnicki, J.; Puertollano, J.R.; Alanis, P.B.; Pigtain, R.C.; Villacorte, E.U.; Malipot, G.A.; Sasai, Y. Electrical Resistivity Tomography Study of Taal Volcano Hydrothermal System, Philippines. *Bull. Volcanol.* **2012**, *74*, 1821–1831. [CrossRef]
62. Chabaane, A.; Redhaounia, B.; Gabtni, H. Combined Application of Vertical Electrical Sounding and 2D Electrical Resistivity Imaging for Geothermal Groundwater Characterization: Hammam Sayala Hot Spring Case Study (NW Tunisia). *J. Afr. Earth Sci.* **2017**, *134*, 292–298. [CrossRef]
63. Pavić, M.; Kosović, I.; Pola, M.; Urumović, K.; Briški, M.; Borović, S. Multidisciplinary Research of Thermal Springs Area in Topusko (Croatia). *Sustainability* **2023**, *15*, 5498. [CrossRef]
64. Hermawan, O.R.; Eka Putra, D.P. The Effectiveness of Wenner-Schlumberger and Dipole-Dipole Array of 2D Geoelectrical Survey to Detect The Occurring of Groundwater in the Gunung Kidul Karst Aquifer System, Yogyakarta, Indonesia. *J. Appl. Geol.* **2016**, *1*, 71. [CrossRef]
65. Zhou, B.; Dahlin, T. Properties and Effects of Measurement Errors on 2D Resistivity Imaging Surveying. *Near Surf. Geophys.* **2003**, *1*, 105–117. [CrossRef]
66. Loke, M.H.; Barker, R.D. Rapid Least-Squares Inversion of Apparent Resistivity Pseudosections by a Quasi-Newton Method. *Geophys. Prospect.* **1996**, *44*, 131–152. [CrossRef]

67. Seaton, W.J.; Burbey, T.J. Evaluation of Two-Dimensional Resistivity Methods in a Fractured Crystalline-Rock Terrane. *J. Appl. Geophys.* **2002**, *51*, 21–41. [CrossRef]
68. Loke, M.H.; Petersen, K.D. *Rapid 2-D Resistivity & IP Inversion Using the Least-Squares Method (Res2DInv Manual)*; Seequent 2023, Ed.; Seequent: Arhus, Denmark, 2023.
69. Loke, M.H.; Acworth, I.; Dahlin, T. A Comparison of Smooth and Blocky Inversion Methods in 2D Electrical Imaging Surveys. *Explor. Geophys.* **2003**, *34*, 182–187. [CrossRef]
70. Galgaro, A.; Boaga, J.; Rocca, M. HVSR Technique as Tool for Thermal-Basin Characterization: A Field Example in N-E Italy. *Environ. Earth Sci.* **2014**, *71*, 4433–4446. [CrossRef]
71. Mitjanas, G.; Ledo, J.; Macau, A.; Alías, G.; Queralt, P.; Bellmunt, F.; Rivero, L.; Gabàs, A.; Marcuello, A.; Benjumea, B.; et al. Integrated Seismic Ambient Noise, Magnetotellurics and Gravity Data for the 2D Interpretation of the Vallès Basin Structure in the Geothermal System of La Garriga-Samalús (NE Spain). *Geothermics* **2021**, *93*, 102067. [CrossRef]
72. Cheng, F.; Xia, J.; Ajo-Franklin, J.B.; Behm, M.; Zhou, C.; Dai, T.; Xi, C.; Pang, J.; Zhou, C. High-Resolution Ambient Noise Imaging of Geothermal Reservoir Using 3C Dense Seismic Nodal Array and Ultra-Short Observation. *J. Geophys. Res. Solid Earth* **2021**, *126*, e2021JB021827. [CrossRef]
73. Nakamura, Y. What Is the Nakamura Method? *Seismol. Res. Lett.* **2019**, *90*, 1437–1443. [CrossRef]
74. Park, C.B.; Miller, R.D.; Xia, J. Multichannel Analysis of Surface Waves. *Geophysics* **1999**, *64*, 800–808. [CrossRef]
75. Xia, J.; Miller, R.D.; Park, C.B. Estimation of Near-Surface Shear-Wave Velocity by Inversion of Rayleigh Waves. *Geophysics* **1999**, *64*, 691–700. [CrossRef]
76. Konno, K.; Ohmachi, T. Ground-Motion Characteristics Estimated from Spectral Ratio between Horizontal and Vertical Components of Microtremor. *Bull. Seismol. Soc. Am.* **1998**, *88*, 228–241. [CrossRef]
77. Yue, W.Z.; Tao, G. A New Non-Archie Model for Pore Structure: Numerical Experiments Using Digital Rock Models. *Geophys. J. Int.* **2013**, *195*, 282–291. [CrossRef]
78. Glover, P.W.J. A Generalized Archie's Law for n Phases. *Geophysics* **2010**, *75*, E247–E265. [CrossRef]
79. Glover, P.W.J. Archie's Law—A Reappraisal. *Solid Earth* **2016**, *7*, 1157–1169. [CrossRef]
80. Asquith, G.; Krygowski, D.; Henderson, S.; Hurley, N. Basic Relationships of Well Log Interpretation. In *Basic Well Log Analysis*; American Association of Petroleum Geologists: Tulsa, OK, USA, 2019; pp. 1–20. [CrossRef]
81. Hamada, G.M.; Almajed, A.A.; Okasha, T.M.; Algathe, A.A. Uncertainty Analysis of Archie's Parameters Determination Techniques in Carbonate Reservoirs. *J. Pet. Explor. Prod. Technol.* **2013**, *3*, 1–10. [CrossRef]
82. Fetter, C.W. *Applied Hydrogeology*; Waveland Press: Long Grove, IL, USA, 2018.

5.3. # Paper 3: Hydrogeological parameterisation of the Daruvar thermal aquifer: Integration of fracture network analysis and well testing

By

Ivan Kosović, Bojan Matoš, Stefano Casiraghi, Gabriele Benedetti, Tihomir Frangen, Kosta Urumović, Ivica Pavičić, Andrea Bistacchi, Silvia Mittempergher, Marco Pola and Staša Borović

Geologia Croatica
Journal of the Croatian Geological Survey and the Croatian Geological Society
2024 | 77/2 | 99–125 | 12 Figs. | 1 Tab. | 4 Suppl. Figs. | 9 Suppl. Tabs. | www.geologia-croatica.hr

Hydrogeological parameterisation of the Daruvar thermal aquifer: integration of fracture network analysis and well testing

Ivan Kosović[1], Bojan Matoš[2,*], Stefano Casiraghi[3], Gabriele Benedetti[3], Tihomir Frangen[1], Kosta Urumović[1], Ivica Pavičić[2], Andrea Bistacchi[3], Silvia Mittempergher[3], Marco Pola[1] and Staša Borović[1]

[1] Croatian Geological Survey, Department of Hydrogeology and Engineering Geology, Sachsova 2, 10000 Zagreb, Croatia
[2] University of Zagreb, Faculty of Mining, Geology and Petroleum Engineering, Department of Geology and Geological Engineering, Pierottijeva 6, 10000 Zagreb, Croatia; (*corresponding author: bojan.matos@rgn.unizg.hr)
[3] Università degli Studi di Milano Bicocca, Dipartimento di Scienze dell'Ambiente e della Terra, Piazza della Scienza, 4, 20126 Milan, Italy

doi: 10.4154/gc.2024.11

Article history:
Manuscript recieved: May 8, 2024
Revised manuscript accepted: May 28, 2024
Available online: June 21, 2024

Abstract

Highly fractured Mesozoic carbonate rocks are the main reservoir of many geothermal resources in northern Croatia, being of environmental, cultural, and economic value for the local and regional communities. The Daruvar thermal springs (temperatures < 50°C) represent the outflow area of an intermediate scale, tectonically controlled, hydrothermal system hosted in Triassic carbonate rocks. Several investigations have been conducted in the Daruvar area detailing the architecture of regional and local fracture networks and quantifying the hydrogeological parameters of the thermal aquifer. In this work, an integrated approach based on structural and hydrogeological investigations was employed to model the network of fractures in the reservoir and quantify its impact on the hydraulic properties. Structural investigations were conducted in the Batinjska Rijeka quarry, considered as an outcrop analogue of the thermal aquifer, employing both a classical field approach and the virtual quantitative analysis of a 3D digital outcrop model. Structural analysis of the digital outcrop model allowed identification of two sub-vertical systems of discontinuities, dipping to the NW and the WSW respectively, in accordance with the data collected through direct field measurements. The main geometric features of the discontinuity network and their statistical distributions were employed to construct discrete fracture network models at both the outcrop scale (approximately 100 m) and the aquifer scale in Daruvar (approximately 700 m). Calibration of the input parameters allowed modelling of porosity and permeability values that reproduce the field values assessed through pumping tests, well tests, and well logging. This work highlights the importance of integrating geological and hydrogeological investigations to obtain a more reliable reconstruction and quantification of the processes driving the fluid flow in fractured aquifers and affecting the spatial distribution of their hydraulic properties.

Keywords: fracture network, carbonate aquifer, digital outcrop model, discrete fracture network modelling, northern Croatia

1. INTRODUCTION

Groundwater represents a strategic resource since it provides approximately half of the global volume of water withdrawn for domestic use and approximately one-fourth of the water for irrigation (UNITED NATIONS, 2022). Valuable groundwater resources are hosted in fractured bedrock aquifers (e.g., SINGHAL & GUPTA, 2010). It has been estimated that 10% of the world population relies on freshwater from carbonate aquifers (STEVANOVIĆ, 2019). This importance increases in the Mediterranean region where the karst groundwater-dependent ecosystems are extensively used, facing environmental threats (SIEGEL et al., 2023). Site-specific management plans considering both the principal flow paths and the hydraulic properties of the aquifer are crucial for a more efficient conservation of groundwater resources.

In rocks having low primary porosity and permeability, the bulk hydraulic properties are controlled by the network of fractures crosscutting the rock mass (SINGHAL & GUPTA, 2010). For fractures here we consider every kind of discontinuity including bedding discontinuities, schistosity, joints, shear fractures, veins, stylolites and other dissolution features, deformation and compaction bands, etc. (e.g., BISTACCHI et al., 2020; STORTI et al., 2022). The permeability field in the rock mass depends on the geometric features of the fractures (i.e., orientation, intensity, aperture, length, etc.) and the connectivity of the fracture network (e.g., FAYBISHENKO et al., 2000; DE DREUZY et al., 2001, 2002). Fault zones affect the groundwater circulation at both regional and local scales, primarily influencing the development of springs in hard rock terrains (e.g., KEEGAN-TRELOAR et al., 2022). The well-established conceptual model of fault zones generally includes a low permeable fault core surrounded by a highly fractured and permeable damage zone (e.g., CAINE et al., 1996; FAULKNER et al., 2010), although different hydraulic behaviours are documented (i.e., high permeability fault core; SMITH et al., 2013). The structural architecture of fault zones and the impact of fracture networks on the permeability field

have been extensively investigated using both structural and hydrogeological approaches. Still, the integration between these two disciplines is limited due to different methods and scales of investigation (e.g., BENSE et al., 2013). Outcrop geological and structural mapping supported by numerical modelling and pumping tests are the most common approaches to quantify the permeability of fractured aquifers in the field (SINGHAL & GUPTA, 2010; BENSE et al., 2013). Outcrop characterisation determines the main kinematic, chronological, and geometric features of the fracture network and the statistical distribution of fracture parameters. The classical field investigations can be supported by photogrammetric reconstruction of the outcrop. This technique can be used to investigate extensive outcrops, which may not even be accessible in field investigations, obtaining large datasets for a solid statistical analysis of the main discontinuity sets through the virtual structural analysis of the digital outcrop model (e.g., HODGETTS, 2013; BISTACCHI et al., 2015; MARTINELLI et al., 2020). These statistical distributions can be used to stochastically reconstruct the fracture network, employing the discrete fracture network (DFN) approach. Considering each fracture as a discrete object with peculiar hydraulic properties surrounded by an impermeable matrix, DFN models are profitably used to determine the permeability of fractured aquifers and rock masses (e.g., VOECKLER & ALLEN, 2012; LEI et al., 2017; MEDICI et al., 2020; CECCATO et al., 2021; SMERAGLIA et al., 2021; MAMMOLITI et al., 2023; MEDICI et al., 2023). However, calibrations and uncertainty analysis of parameters (particularly aperture) with permeability values from field investigations are generally lacking. Pumping tests consist of pumping groundwater from a well at different flow rates and measuring the drawdown in observation wells. The hydraulic properties (mostly transmissivity and hydraulic conductivity) of the aquifer are assessed by modelling the variations of the drawdown using analytical solutions (e.g., KRUSEMAN et al., 2000). Due to the heterogeneous structure of fractured aquifers, the identification of flow-bearing paths is crucial for assessing the most suitable modelling approach (e.g., CARRERA & MARTINEZ-LANDA, 2000; GUIHÉNEUF et al., 2021), as well as for understanding and managing the site. In contrast, hydrogeological investigations through pumping and well tests generally focus on assessing the hydrogeological properties of the aquifer and the efficiency of the tested well, but they generally lack insights into the fracture network architecture.

Among groundwater resources in fractured aquifers, geothermal resources are particularly important since they are potential renewable sources of raw materials and energy (e.g., FINSTER et al., 2015; SZANYI et al., 2023). Geothermal resources generally have a lower yield and higher management costs than groundwater resources. Therefore, assessing the hydraulic characteristics of the reservoir and the impact of regional and local fracture systems is crucial for the quantification of the renewable component of the system and the proposal of management plans for long-term sustainable exploitation (e.g., RYBACH & MONGILLO, 2006). Northern Croatia is rich in thermal springs that are mostly used for balneotherapy and tourism (BOROVIĆ & MARKOVIĆ, 2015). Here, connected geothermal resources have great potential since they share the favourable thermal features of the Pannonian area (HORVÁTH et al., 2015). The thermal spring area in Daruvar city (Figs. 1 and 2) is one of the most investigated thermal regions in Croatia (e.g., BOROVIĆ, 2015; BOROVIĆ et al., 2019; KOSOVIĆ et al., 2023; URUMOVIĆ et al., 2023; KOSOVIĆ et al., 2024).

Thermal springs in Daruvar (temperature up to 50°C; Fig. 3) have been documented since the Roman era, representing an economic and cultural value for the area. The Daruvar thermal field is the outflow area of an intermediate scale geothermal system hosted in a Mesozoic fractured carbonate reservoir. Previous studies investigated the hydraulic properties of the reservoir and the architecture of regional and local fracture systems (e.g., BOROVIĆ et al., 2019; KOSOVIĆ et al., 2024). In this work, an integrated approach combining structural data analysis and well testing is applied to detail the hydraulic properties of the Daruvar thermal aquifer. Structural investigations were conducted in the Batinjska Rijeka quarry (BRQ; Fig. 2) located 4 km NE of Daruvar. There, the Mesozoic carbonate rock complex is highly fractured representing an outcrop analogue of the aquifer. The discontinuities deforming the rock mass were investigated through both classical field investigations and the analysis of the digital outcrop model (DOM) of the quarry. A DFN model reproducing the observed network of discontinuities was constructed, and its capability of assessing the hydraulic properties of the aquifer was tested using data collected from several well tests and logs conducted in the Daruvar thermal field.

2. GEOLOGICAL AND HYDROGEOLOGICAL SETTINGS

2.1. Regional tectono-structural evolution

The study area is located along the western margin of Mount Papuk, which is part of the Slavonian Mts. (Fig. 1). The Slavonian Mts. are the best exposures of the Tisza continental block, i.e., a lithospheric fragment of the European foreland that formed beside the Adria microplate during the Middle Jurassic (Fig. 1; SCHMID et al., 2008). The polyphasic tectono-metamorphic evolution of the study area started with the Variscan and continued with the Alpine-Dinarides-Carpathian orogeny. The continuous convergence between the Tisza-Dacia mega block, the Adria microplate, and the European plate through the late Mesozoic-Cenozoic caused the stacking of the Mecsek, Bihor, and Codru nappe systems (BALEN et al., 2006; SCHMID et al., 2008). The Slavonian Mts. are part of the Bihor nappe system that also crops out in southern Hungary. Their structural architecture was significantly influenced by the proximity of the Sava suture zone (Fig. 1), which resembled the Cretaceous-Palaeogene regional suture zone between the Tisza block toward the NE and the Adria microplate block toward the SW (SCHMID et al., 2020). Furthermore, regional fault zones such as the Periadriatic lineament and the Mid-Hungarian fault line (Fig. 1) played important roles as tectonic boundaries between the main regional blocks accommodating the clockwise rotation of the Tisza-Dacia mega block, the counterclockwise rotation of the Adria plate, and the eastward lateral extrusion, at a scale of several hundreds of km (Fig. 1; PRELOGOVIĆ et

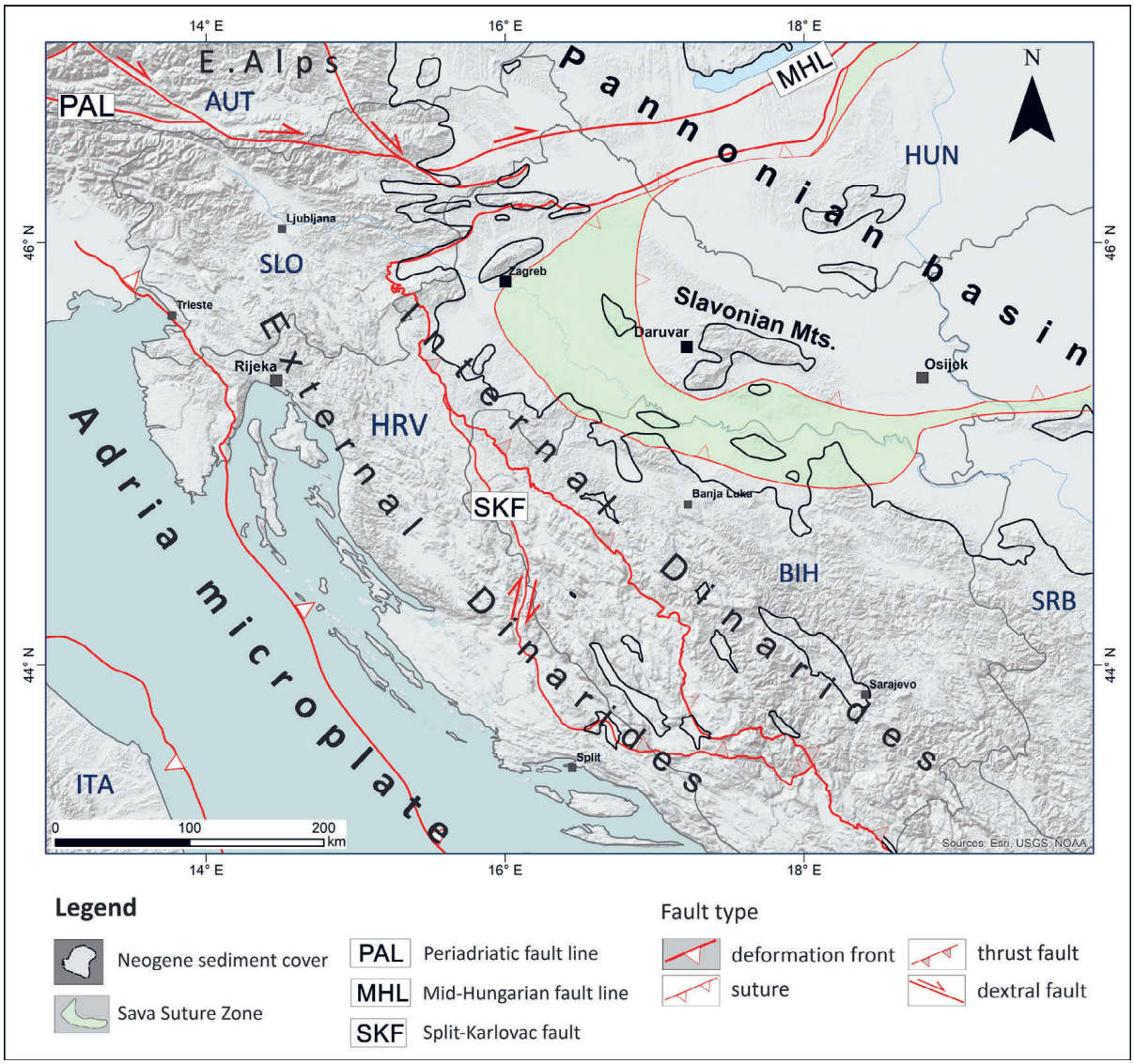

Figure 1. Regional tectonic map of the Alps, Dinarides, Tisza-Dacia mega block, and the European Foreland framework (after SCHMID et al., 2008, 2020). The map shows the principal regional faults and the outline of the Neogene basins (black line) including the Pannonian basin. The principal towns and the neighbouring states are depicted (acronyms: AUT – Austria, BiH – Bosnia and Herzegovina, HRV – Croatia, HUN – Hungary, ITA – Italy, SLO – Slovenia, SRB – Serbia).

al., 1998; TARI et al., 1999; CSONTOS & VÖRÖS, 2004; USTASZEWSKI et al., 2010)

After the climax of Cretaceous-Palaeogene tectonism, the opening of the Pannonian Basin System (PBS) between the Carpathians and the Dinarides occurred (BALEN et al., 2006). The tectonic evolution of the PBS was characterised by polyphase extension, compression, and tectonic inversion. Formed by Early-Middle Miocene NE-SW oriented back-arc type lithospheric extension, the PBS was characterised by systems of NW-SE striking normal faults that formed rift and wrench-type troughs filled with large amounts of syn-rift deposits (HORVÁTH et al., 2006; USTASZEWSKI et al., 2010). These basins and correlative structural highs were subjected to localised tectonic inversion during the Middle Miocene, but deepening and rapid thermal subsidence along existing NE-SW and NW-SE striking faults prevailed until the Early Pliocene (TOMLJENOVIĆ & CSONTOS, 2001; MALVIĆ & CVETKOVIĆ, 2013). Changes in the stress field due to the counterclockwise rotation of the Adria microplate and the consumption of the subducted European plate yielded a transition from extension to N-S compression/transpression, which resulted in regional tectonic inversion and fault reactivation (BADA et al., 2007; USTASZEWSKI et al., 2014). The Pliocene-Quaternary tectonic inversion accommodated regional folding and prevalent reverse and strike-slip faulting (JAROSINSKI et al., 2011). It yielded the uplift of the basement structural highs (e.g., Slavonian Mts.), the tectonic inversion of pre-existing basement structures and the formation of strike-slip fault-related positive flower structures (PRELOGOVIĆ et al., 1998; TOMLJENOVIĆ & CSONTOS, 2001).

2.2. Geological and structural setting of the study area

The geological setting of the NW part of the Slavonian Mts. was investigated by JAMIČIĆ et al. (1989). Due to its complexity, the lithological units of the study area (Fig. 2) were

reorganised by KOSOVIĆ et al. (2024) as follows: i) pre-Permian crystalline rocks, ii) Permian sedimentary units, iii) Triassic carbonate complex, iv) Jurassic limestones, v) Miocene sedimentary and magmatic rock complex, vi) Pliocene clastic sediments, vii) Pleistocene unconsolidated sediments, and viii) Holocene alluvial and colluvial unconsolidated sediments. The pre-Permian crystalline basement extends across a large surface area in western Papuk (Fig. 2), encompassing magmatic and metamorphic rock complexes that are partly transgressively covered by younger units (JAMIČIĆ et al., 1989; PAMIĆ et al., 2003). The onset of the Permian succession began with transgressive, well-layered conglomerates and quartz sandstones. Triassic and Jurassic formations constitute the Mesozoic carbonate rock complex that represents the main reservoir of the Daruvar thermal waters. The Triassic succession is characterised by Lower to Middle Triassic clastic deposits (e.g., sandstones, siltstones, and laminated shales) sedimented within a shallow-water environment (JAMIČIĆ et al., 1989; ŠIKIĆ, 1981). A gradual transition towards carbonates (e.g., dolomites, limestones, and crinoid limestones with chert) is observed in the Middle to Late Triassic, while the Late Triassic stratigraphic top is characterised by a pure dolomite-limestone succession (occasionally incorporating dolomite and limestone breccias and marly limestones; Fig. 2). In a sequence, Jurassic deposits are observed being represented by grey platy limestones with cherts. The Cretaceous collision between the Tisza block and the Adria and Europe plates caused emersion in the Slavonian Mts. Sedimentation was partly restored during the Middle Miocene E-W regional extension of the PBS. It continued through the Late Miocene-Pliocene and Quaternary (Fig. 2), characterised by a transition from coastal to freshwater depositional environments (SAFTIĆ et al., 2003). The youngest sediments are Quaternary unconsolidated sediments (from

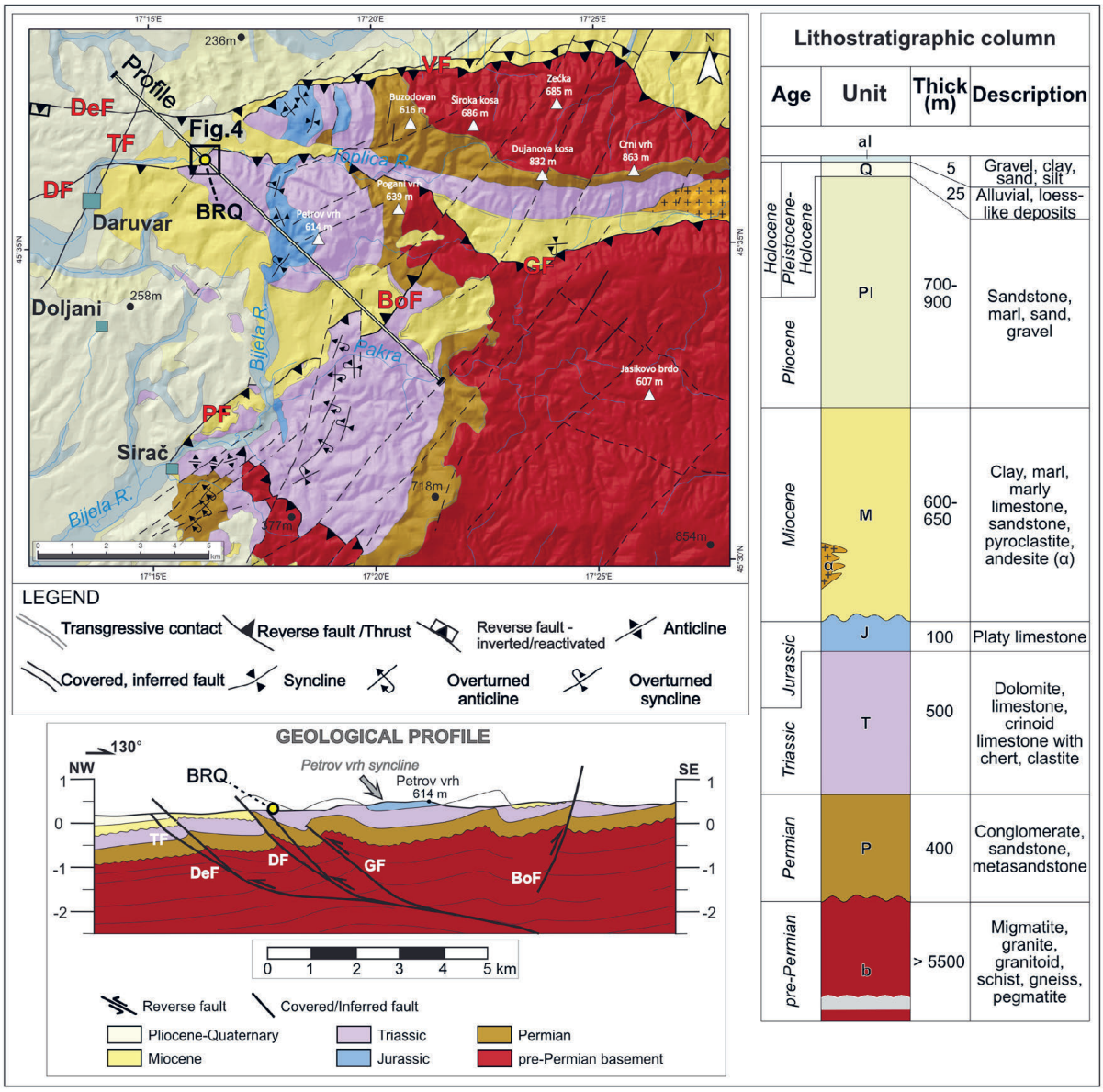

Figure 2. Simplified geological map of the Daruvar area and lithostratigraphic succession (modified from KOSOVIĆ et al., 2024). The black polygon represents the extent of Fig. 4A. Topographic peaks are denoted by white triangles, while the main towns are shown as teal polygons. The NW-SE striking geological profile (bottom) depicts the general structural relationships along the western margin of Mount Papuk, in the vicinity of the Batinjska Rijeka quarry (BRQ). Fault acronyms: BoF – Borki fault; DF – Daruvar fault; DeF – Dežanovac fault; GF – Gradina fault; PF – Pakrac fault; TF – Toplica fault.

sandy gravels to sandy clays), deposited by alluvial and gravitational processes (JAMIČIĆ et al., 1989).

The Cretaceous to Quaternary tectonic evolution of the study area is affected by the structural architecture of the Slavonian Mts. and the surrounding basins (KOSOVIĆ et al., 2024). The complex structural pattern of generally E-W striking thrust faults (i.e., Voćin fault, Gradina fault, Dežanovac fault, and Daruvar fault; Fig. 2) and multi-folded structures gently dipping towards both the NNW and SSE or ENE and WSW suggests a polyphase evolution, which began with regional Cretaceous-Palaeogene E-W contraction. This contraction formed an initial NW-SE striking fault and NNW and SSE dipping fold pattern, which rotated counterclockwise approximately 40° towards the NE during the Palaeogene (TOMLJENOVIĆ & CSONTOS, 2001; USTASZEWSKI et al., 2008). Counterclockwise regional rotation resulted in the final structural emplacement of the existing faults and folds, reoriented as E-W striking thrust faults and an ENE and WSW dipping fold system. Though the Neogene was characterized by regional E-W extension and the formation of predominantly normal faults, inherited faults/fold systems in the study area experienced only partial tectonic stretching and gravitational sliding. Contemporary, sediment deposition within pre-existing synclines occurred (Fig. 2; (JAMIČIĆ, 1995; TARI et al., 1999; TOMLJENOVIĆ & CSONTOS, 2001). The Pliocene-Quaternary regional N-S compression/transpression promoted continuous shortening and re-folding processes of the pre-existing structures coeval with the formation of dextral/sinistral faults (e.g., Toplica fault; TF in Fig. 2), which locally displaced existing E-W striking thrust faults.

2.3. Hydrogeological setting of the Daruvar thermal system

The lithostratigraphic sequence in the Daruvar thermal area (KOSOVIĆ et al., 2023) was assessed through boreholes and wells: i) Quaternary alluvial deposits, ii) Miocene or Pliocene marls, iii) Miocene bioclastic limestone, and iv) Triassic dolomites and limestones with an investigated thickness of 130 m. Core analyses and well logging evidenced that the Triassic carbonates are characterised by a uniform background fracture network and by localised corridors (total thickness of 24 m in the deepest well), showing a higher frequency of fractures. The thermal waters are hosted in fractured Triassic carbonate rocks, and subthermal waters can be found in the sandy layers of the alluvial cover and the Miocene biocalcarenites (BOROVIĆ et al., 2019). The aquifer transmissivity assessed through pumping and well tests ranges from 0.015 to 0.03 m^2/s (BOROVIĆ et al., 2019; URUMOVIĆ et al., 2023), while the average porosity measured through neutron borehole logging is 7.9%. Hydrochemical and isotope analyses of the thermal waters (BOROVIĆ, 2015) evidenced: i) a temperature from 18.2 to 49.8°C, nearly-neutral pH, and electrical conductivity of 550–700 µS/cm, ii) a calcium-bicarbonate hydrochemical facies indicating flow through a carbonate aquifer, iii) the meteoric origin of the water as depicted by O and H stable isotope ratios, iv) a reservoir equilibrium temperature of 80°C calculated using SiO_2 geothermometers, and v) a mean residence time between 11 and 15 ka assessed through ^{14}C activity.

These data, combined with the results of regional and local scale structural and geophysical investigations, were used to propose a conceptual model of the Daruvar hydrothermal system (BOROVIĆ et al., 2019; KOSOVIĆ et al., 2024). The recharge area of the system is located in the topographically higher Petrov vrh, approximately 8 km E of Daruvar (Fig. 2). Here, Mesozoic carbonate rocks extensively crop out and are deformed by N-S and E-W striking fractures that are potential paths for the infiltration of the meteoric waters (KOSOVIĆ et al., 2024). The general westward dip of the strata and E-W tensional open fractures favour the westward flow of the infiltrated waters in the Mesozoic reservoir. The waters are warmed to 80°C by the regional heat flow and convection processes in the aquifer. In the Daruvar area, they intercept an asymmetric anticline cogenetic to the Daruvar reverse fault (DF in Fig. 2). The fold is structurally reactivated by the regional polyphase tectonic evolution, increasing the fracturing of the bedrock. The thermal waters rise to shallow depths in the damage zone of the Daruvar fault and the fracture network in the hinge of the Daruvar anticline. The fold hinge could be affected by a local extensional regime increasing both the aperture of the fractures and the permeability field of the aquifer. The main outflow occurs within the interaction zone of local scale faults/fractures mapped through geophysical investigations (KOSOVIĆ et al., 2023). This structure further localises the flow of the thermal waters resulting in four thermal springs (Fig. 3) with temperatures between 38 and 50°C. Currently, the thermal waters are exploited from a well and two springs providing approximately 10 L/s.

3. METHODS

3.1. Structural-geological investigations and analysis

Geological field investigations were carried out from 2021 to 2023. Structural and geological data were collected NE of Daruvar in the Batinjska Rijeka quarry (BRQ) and the surrounding area (Fig. 2). This area was selected as it provides an extensive outcrop of the Mesozoic carbonate rock complex and it can be considered as an outcrop analogue of the Daruvar thermal aquifer. Data were collected at 59 locations and were spatially georeferenced using GIS software (Fig. 4A). Structural measurements included dip direction and dip angle of bedding, fractures, and faults. For faults, lineation and sense of slip, i.e. striations and slickenside orientations with their sense of movement, were also recorded. The resulting cumulative dataset incorporated 109, 284, and 50 measurements of bedding, fractures, and faults, respectively.

For the structural data analysis, the software Stereonet v.11 was used to plot bedding and fracture/joint data (ALLMENDINGER et al., 2011; CARDOZO & ALLMENDINGER, 2013). Determination of the most representative fracture sets was conducted by plotting the poles of fracture planes and constructing the contour plots of the poles' distribution using the 1% area contour method (ALLMENDINGER et al., 2011; CARDOZO & ALLMENDINGER, 2013). Fault planes and shear planes were used to determine the palaeostress field based on the geometric properties of the fault and its kinematics

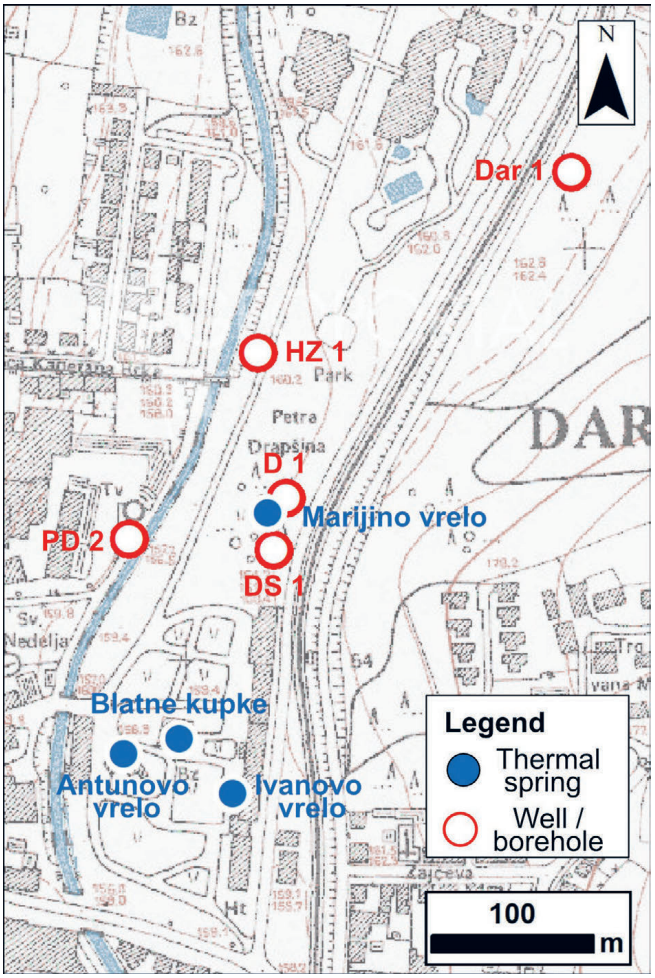

Figure 3. Map of the Daruvar thermal field area showing the thermal springs (blue dots) and the main wells and exploration boreholes (red circle).

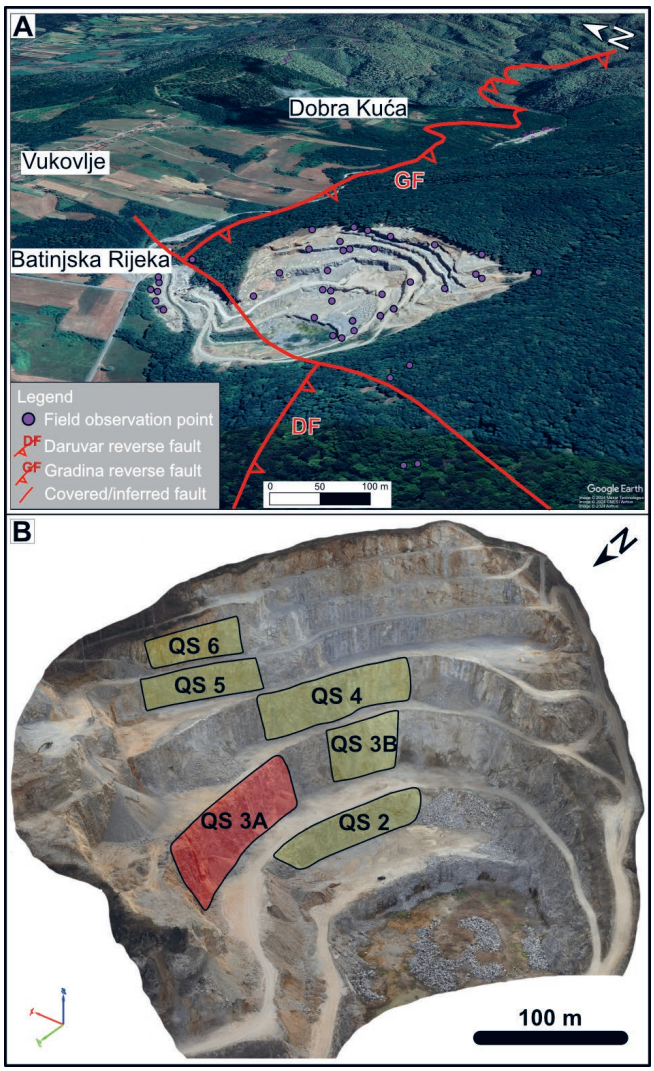

Figure 4. (A) Investigated area of the Batinjska Rijeka quarry (BRQ; image source: URL 1) with main faults (acronyms in Fig. 2). Observations (purple points) were conducted within the quarry area and its surroundings. (B) Digital outcrop model of the BRQ showing the sections (polygons) used for the digital structural analysis of the discontinuity systems. The section QS3A (red polygon) was chosen to detail the length of the main sets of discontinuities being the base for the DFN modelling.

(DOBLAS, 1998). Based on kinematic criteria, the fault data were analysed by the software Win-Tensor v. 5.9.2 and TectonicsFP v. 1.7.9 (ORTNER et al., 2002; DELVAUX & SPERNER, 2003). Fault data were separated into compatible fault groups, and theoretical maximum (σ1), mean (σ2), and minimum stress axes (σ3) were calculated using the P–T axis method (TURNER, 1953; MARRETT & ALLMENDINGER, 1990). The palaeostress field was analysed by constructing the synthetic focal mechanisms for each fault group using the Right Dihedra Method (ANGELIER & MECHLER, 1977).

3.2. Digital structural analysis and DFN modelling

The reconstruction of the network of discontinuities for quantifying the hydraulic parameters of the aquifer analogue was conducted through: i) imaging of the BRQ obtaining a 3D digital outcrop model (DOM) of the quarry, ii) digital structural analysis of the DOM reconstructing the main systems of discontinuities (i.e., both bedding and fractures), iii) statistical analysis of the main geometrical parameters of the systems, and iv) discrete fracture network (DFN) modelling of the discontinuity network for the hydraulic parameterisation.

The imaging of BRQ was performed in April 2023 using DJI Matrice 300 RTK unmanned aerial vehicle (UAV). The UAV was equipped with a Zenmuse P1 camera featuring a resolution of 45 megapixels, a full-frame size sensor, and a 35 mm focal length lens. The location of the UAV was determined with centimetre accuracy during the whole flight using the RTK (real-time kinematics) method and employing a supplementary GNSS device on a fixed position. Due to the complex quarry geometry, manual flying was used to control the UAV while capturing images resulting in a camera-wall distance of 15 to 65 m. 702 images were acquired with an image overlap up to of 90%. They were processed into a 3D DOM of the quarry (Fig. 4B) by means of "Structure from motion" algorithms using the photogrammetry software Pix4Dmapper v. 4.7.5 (URL 2). The resulting DOM was in sub-centimetre resolution (0.29-0.56 px/cm) covering a surface of 222,135 m^2.

The software CloudCompare v. 2.13.0 (URL 3) was employed for the digital structural analysis of the DOM. Sections of the walls (QS2-QS6; Fig. 4B), where discontinuity sets were more visible, were selected for analysis. Discontinuity

mapping was done employing the manual sampling technique "Trace tool" of the plugin Compass in the CloudCompare software (THIELE et al., 2017). This tool was used for the manual selection of the DOM's points that belong to a discontinuity surface and for the calculation of the 3D plane that best fits the points' selection. The dip direction and dip of the discontinuity were calculated from the fitted plane. The software Stereonet v.11 (ALLMENDINGER et al., 2011; CARDOZO & ALLMENDINGER, 2013) was used to determine the most representative sets of discontinuities in each section of the quarry following the methodology described in the field structural investigations. The analysis of the DOM showed that the rock mass in level 3 of the quarry was highly fractured. Therefore, the QS3A (Fig. 4B) was selected to detail the geometric analysis of the discontinuity sets, since it is the longest section in level 3 and has the greatest amount of data. The DomStudioOrientation script (URL 4) for clustering analysis and Fisher concentration parameter calculations were used to separate and assess the statistics of the main sets of discontinuities. The code was run using the software Matlab v. 9.11.0 (URL 5). A 2D front-view orthophotograph of the QS3A outcrop was performed and imported into the software QGIS v. 3.34.5 (URL 6) to manually vectorise the 2D traces of the discontinuities. The traces were used to: i) calculate the areal fracture intensity P21 (length of fractures over area) for each discontinuity set, and ii) assess the statistical distribution of the heights of the sets in the outcrop using the FracAbility package (URL 7), which allows fitting a statistical distribution to length data affected by censoring bias due to the finite size of the outcrops by applying survival analysis (BENEDETTI et al., 2024).

The data obtained from the structural analyses of the DOM and the QS3A section were used to build the DFN model of the investigated outcrop. The input parameters for each set of discontinuities were: mean dip, mean dip direction, Fisher K, mean length, standard deviation of length, length/height ratio, volumetric fracture density P32 (area of fractures over volume), and aperture. All parameters were determined from the previous analyses except for P32 and aperture, which were calibrated through the DFN modelling. P32 cannot be directly measured and needs to be estimated from P21. A linear relationship is expected between P21 and P32 for domains with similar properties (DERSHOWITZ & HERDA, 1992; MAULDON, 1994; WANG, 2005):

$$P32 = C21*P21 \quad (1)$$

Here, P32 was calibrated using the DFNworks Python package (HYMAN et al., 2015) with a procedure similar to that described in ANTONELLINI et al. (2014), KORNEVA et al. (2015) and ZAMBRANO et al. (2016). For each discontinuity set, it is necessary to target at least 3 different increasing P32 and run simulations for each target. The resulting DFN is sliced along the reference outcrop's mean plane to calculate the corresponding P21 value. The overall mean of the P21 values is the simulated value for the chosen target P32. At the end of each calibration procedure, it is possible to calculate the theoretical linear relationship of the P32/P21 ratio for each fracture set in a given homogeneous volume. This calibrated linear coefficient C21 can be then used to obtain the P32 value corresponding to the P21 measured on the DOM.

The calibration of the aperture and the calculation of the distributions of porosity (Φ) and permeability (k) were conducted employing the software Petroleum Experts Move v. 2019.1 (URL 8). This software has been profitably used to calculate the k field of fault zones in fractured carbonates (ANTONELLINI et al., 2014; KORNEVA et al., 2015; ZAMBRANO et al., 2016; GIUFFRIDA et al., 2019; ROMANO et al., 2020; SMERAGLIA et al., 2021; MAMMOLITI et al., 2023). Different approaches used by the software to assign the aperture to the discontinuity were tested. They consist of: i) a constant aperture, ii) an aperture proportional to the root length of the fracture, and iii) an aperture proportional to the length of the fracture. The proportionality constant in the second and third approaches is calculated by the software inputting the average aperture of the fracture set. The software discretises the modelling domain using a grid (i.e., geocellular volume), and then the Φ and the k tensor of the cell are computed. The Φ is obtained as the ratio between the total fracture volume in the cell and the cell volume, while the k tensor calculation is based on the geometric methodology described by ODA (1985).

3.3. Hydrogeological parameterisation

The hydrogeological parameterisation of the thermal aquifer was performed by analysing the results of a pumping test conducted on 27 February 2022 in Daruvar. The water was pumped from the well Dar 1 at different flow rates (Q). The water level variation was measured in the wells Dar 1, D 1, and DS 1 and in the spring Antunovo vrelo (Fig. 3) using a HOBO Water level data logger with a range of 9 m. The resolution of the water level measurement was 1 cm, while the temporal interval between the measurements was 60 s in Dar 1 and 10 s in the other objects. Manual measurements of the water level were conducted to constrain the measured data. The flow rate was measured at least three times during every single step. The results of this test are partially reported in URUMOVIĆ et al. (2023) where part of the dataset measured in Dar 1 was used to develop a new methodology for interpreting step-drawdown well tests. In this study, a double approach was used: i) the dataset was interpreted as a pumping test (i.e., exploitation and observation well), and ii) the data collected in Dar 1 were reinterpreted using the classical approach for interpreting step-drawdown well tests.

Since the Daruvar thermal aquifer is highly fractured, it can be considered as a quasi-homogenous porous medium at the investigated scale. The aquifer is confined because the water level is generally a few metres below the ground while the top of the aquifer is at least 5 m below the ground level. Therefore, the Theis-Hantush analytical solution (THEIS, 1935; HANTUSH, 1961a, b) for pumping tests in nonleaky confined aquifers was applied. The analysis of the collected data was performed using the software AQTESOLV v. 4.5 (DUFFIELD, 2007). It consisted of manually matching the Theis-type curve to the drawdown (Δ) plotted as a function of time on double logarithmic axes. Afterward, the software optimised the curve through a nonlinear weighted least-

squares parameter estimation, employing the Gauss-Newton linearisation method procedure. The estimated parameters were the transmissivity (T), the storativity (S), the hydraulic conductivity anisotropy ratio (Kz/Kr), and the saturated thickness (b).

Besides the pumping test analysis, the data collected in Dar 1 were further investigated as a step-drawdown well test. Details on the interpretations of well tests can be found in (KRUSEMAN et al., 2000). The collected data were used to determine the theoretical drawdown vs. flow rate curve of the well, the well efficiency (W), and its specific capacity (SC = Q/Δ). The specific capacity can be in turn used to determine the T of the aquifer using experimental relationships:

$$T\ (m^2/day) = 0.85*SC^{1.07} \quad (2)$$

$$T\ (m^2/s) = 2.39*SC^{1.07} \quad (3)$$

These equations were considered since they were developed, respectively, for a carbonate thermal aquifer in Italy (FABBRI, 1997) and dolomite aquifers in Slovenia (VERBOVŠEK, 2008). A similar methodological approach was profitably used to assess the transmissivity of a thermal aquifer in central Croatia (PAVIĆ et al., 2023).

4. RESULTS

4.1. Structural analysis of field data

The Batinjska Rijeka quarry (BRQ) is part of the Petrov vrh structural domain (KOSOVIĆ et al., 2024). Structurally, it is located at the intersection of the E-W striking Gradina fault to the NE and Daruvar fault to the SW (Fig. 4A). These two reverse faults are laterally displaced by a NE-SW striking fault (Fig. 4A) by approximately 570 m. Lithologically, the quarry is predominantly composed of a Middle Triassic dolomite and limestone succession (Fig. 2). At the southern face, interlayers of thin layered shale and siltstone/sandstone occur.

Strata orientation and fracture system

Measured bedding orientations indicate subvertical bedding within the dolomites and limestone strata (Fig. 5A) that are dipping either NE/SW (29 data) or SE/NW (39 data) at the dip angle >60° (Supplementary Tab. 1). The subvertical bedding in the quarry indicate at least two generations of isoclinal folds (Fig. 6A) that are characterised by fold axes dipping either towards the SE (138°) or the SW (228°) at dip angles of 42° and 16°, respectively (Fig. 6A). If the fold generations are considered as second-order structures, they can be interpreted as related to a first-order folded structure that generally dips towards the N at an angle of >65°.

The structural analysis encompassed 284 fractures (Fig. 6B). Three representative fracture systems were delineated (Supplementary Tab. 2 and Fig. 6B). The Fs1 fracture system (59 measurements) includes NNE-SSW striking subvertical fracture sets that dip to either the ESE or the WNW. The Fs2 fracture system counts 42 measured data. With a NNE-SSW strike similar to Fs1, this fracture system dips towards the ESE at an angle of 45°. The fracture system Fs3 (54 data), composed of two subsets, resembles two coupled subvertical fractures that dip either towards the NNE (22°) or the NNW (338°).

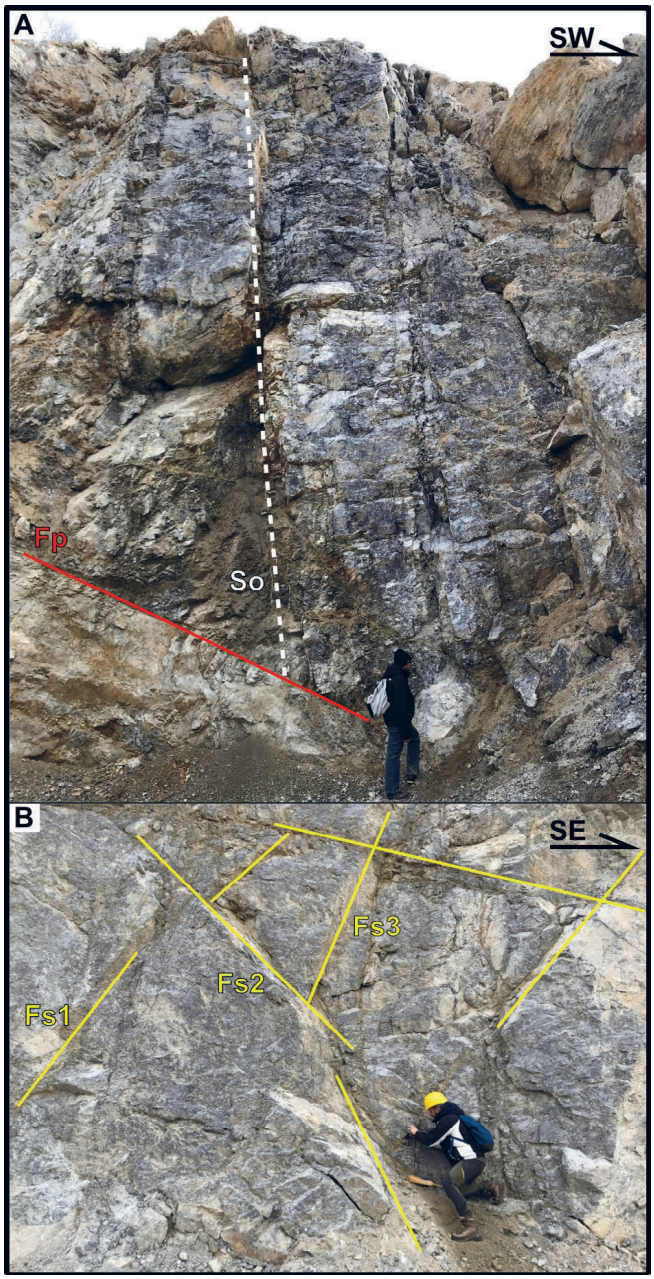

Figure 5. (A) Tectonised Triassic dolomites and dolomitised limestones in the BRQ at location 45.603°N, 17.272°E. Strata are steeply dipping towards the SW (So: 233/70) with a normal fault (198/60) at the base of carbonate beds. (B) Coupled fracture systems in the BRQ at location 45.606°N, 17.273°E. Measured fracture systems dip towards the ESE (Fs2: 100/45), NW (Fs3: 338/73), W (Fs1b: 288/82).

Faults and shear fracture analysis

Fault analysis focused on addressing the structural architecture and identification of the faults and shear fractures within the area. Due to heavily tectonised carbonate quarry faces and the active exploration of the quarry, 50 shear fractures/fault plane data were collected. Considering the stress field and kinematic criteria, three principal fault categories were identified and subdivided by fault groups and subsets (Fig. 6C and Supplementary Tab. 3).

Reverse fault planes (20 data; Figs. 6C and 7 and Supplementary Tab. 3) were separated into two fault sets (RFa and RFb). RFa subset shows an average SE dip direction (dip

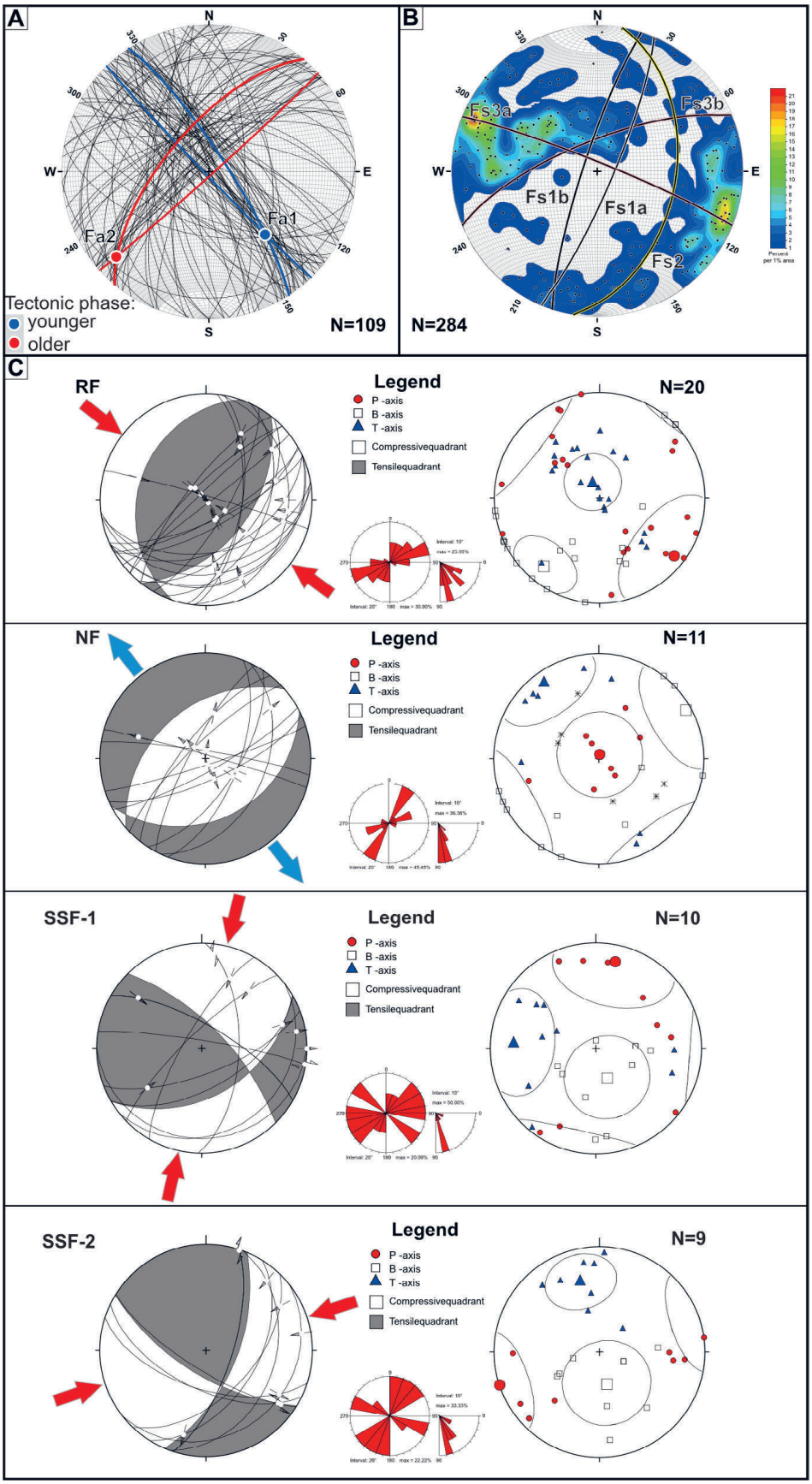

Figure 6. (A) Stereonets of the bedding orientations (small black circles) in the BRQ. Their interpretation highlights the occurrence of generally two generations of folds (fold limbs are shown as small blue and red circles) characterised by different fold hinges (blue and red points). (B) Structural diagrams of the main fracture systems (black small circles) in the study area. The orientations of the representative fracture systems (F_S) are reported in Supplementary Tab. 2. They are obtained from the distribution of the measured discontinuities represented here as poles (black points). (C) Structural diagrams for the interpreted fault systems (RF - reverse fault group; NF - normal fault group; SSF-1 and SSF-2 - strike-slip fault groups). In all plots, N indicates the number of measurements.

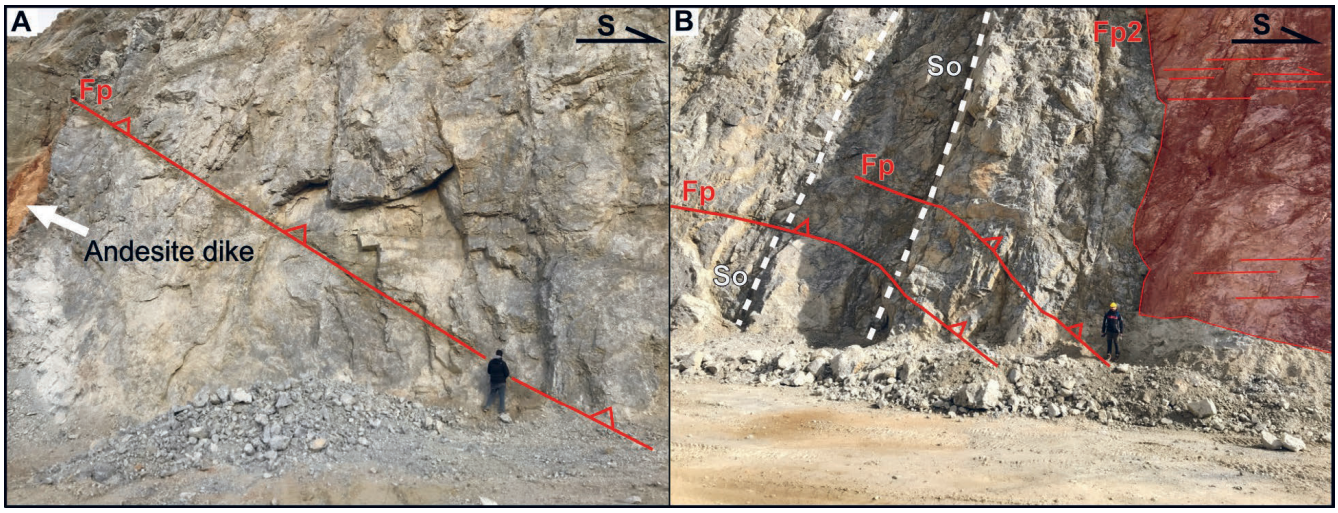

Figure 7. (A) Fault plane (167/45) observable across most of the BRQ faces, at location 45.606°N; 17.273°E. Fault plane shows reverse kinematics with indication of tectonic transport to the NW, while in the same time this fault plane experienced structural reactivation and tectonic inversion characterised by NW-SE oriented extension. (B) Reverse fault planes with average orientation 142/30 (Fp). Besides NW tectonic transport, we observed subvertical bedding with average strata orientation 318/75. In the right section, a subvertical bedding plane (Fp2) was structurally reactivated as a dextral fault.

angle of 56°), whereas the RFb fault subset dips towards the WNW at an angle of 36°. Structural analysis and computation of the representative palaeostress field using the P–T axes method and derived synthetic structural focal mechanism show that the palaeostress compressional field was associated with a NW-SE trending P-axis (the T-axis is subvertical, steeply dipping towards the NNW), hence NW-SE compression. This compressional palaeostress field may have resulted in the formation of the fold generation dipping towards SE (138°; Fig. 6A)

Normal fault planes (10 data; Supplementary Tab. 3 and Fig. 6C) showed orientations similar to the reverse faults. They were divided into two fault sets (NFa and NFb) characterised by NE–SW striking fault planes dipping towards either the SE or the NW, at angles of 41° and 50°, respectively. Kinematic and stress analysis indicates that observed normal faults were formed due to a subvertical P-axis steeply dipping towards the NNE (P-axis orientation is 14/87) and subhorizontal T-axis trending NW–SE. This stress field resulted in the NW–SE extension of the existing faulted structures.

Besides the reverse and normal faults, 19 strike-slip fault planes were measured (Supplementary Tab. 3; Figs. 6C and 7B). Measured data were separated based on geometry and kinematic compatibility into two fault systems (SSF-1 and SSF-2) and four group subsets. The SSF-1 group included 10 measured dextral/sinistral faults (dip angle between 53° and 73°) striking either NE–SW or NW–SE. The SSF-2 group incorporated conjugate fault pairs with NNE–SSW and SE-NW strike (dip angle between 66° and 71°). Mapped strike-slip fault planes often showed structural reactivation with both dextral/sinistral motions. Similar orientations of two NW-SE striking fault subsets (SSF-1b and SSF-2b) indicate fault structural reactivation and reorientation of the principal stress axes σ1 and σ3 within a relatively short timeframe. Both strike-slip fault groups were formed in two slightly different palaeostress fields. The SSF-1 fault group indicates a palaeostress field associated with the NNE–SSW trending P-axis, whereas SSF-2 fault group indicates a palaeostress field associated with an ENE-WSW trending P-axis. This implies that both strike-slip fault groups were tectonically active within a general NE-SW transpressional stress field.

4.2. Digital structural analysis of the DOM

The discontinuities digitalised in the selected sections of the DOM are shown in Fig. 8. The contour plots of the poles were used to identify the main sets of discontinuities in each section (Supplementary Tab. 4).

Quarry section 2 (length: 145 m, height: 17 m, representative dip direction and dip: 282/68) is located on the lowest level of the quarry. The DOM analysis reveals that three discontinuity systems crosscut the rock mass. The discontinuity system D1 is composed of two NE-SW striking subvertical discontinuities dipping at high angles (76° and 83°, respectively) toward the NW (D1a; 20 data) or ESE (D1b; 17 data). The D2 system is divided into D2a and D2b sets (23 and 15 data, respectively) and includes predominantly NNW-SSE striking discontinuities dipping towards the WSW or W with dip angles of 53° and 57°, respectively. The D3 system (21 data) is characterised by discontinuities that are steeply dipping at high angles (≥87°) towards the W.

Quarry face 3 is divided into sections A (length: 97 m, height: 30 m, representative dip direction and dip: 259/70) and B (length: 63 m, height: 31 m, representative dip direction and dip: 297/68). Analysis of the DOM in section 3A shows two discontinuity systems D1 and D2. The D1 system is characterised by two discontinuity sets (D1a and D1b; 132 and 43 measurements, respectively) dipping towards the WNW with dip angles of 68° and 83°. The D2 system comprises two sets dipping towards the WSW but at different dip angles. D2a (140 data) is steeply dipping towards the WSW at 75°, while set D2b (74 data) is gently dipping with a dip angle of 41°. The structural fabric of section 3B is similar to section 3A being deformed by two discontinuity systems (D1 and D2). The D1 system is characterised by NE-SW striking discontinuity sets.

Set D1a (124 data) dips towards the NNW (dip angle of 70°), whereas the D1b set (73 data) includes discontinuities that steeply dip towards the NW at a dip angle of 77°. The second discontinuity system (D2; 115 data) encompasses the NNW-SSE striking discontinuities that dip steeply towards the WSW at an angle of 72°.

Quarry face 4 (length: 108 m, height: 30 m, representative dip direction and dip: 290/66) is similar to quarry face 3 being deformed by two discontinuity systems D1 and D2. The D1 system is characterised by two sets (D1a and D1b; 103 and 86 data, respectively) steeply dipping towards the NNW or NW. The D2 system (89 measurements) includes predominantly NNW-SSE striking discontinuities steeply dipping towards the WSW (dip angle of 72°).

Quarry section 5 (length: 78 m, height: 18 m, representative dip direction and dip: 286/69) is deformed by two discontinuity systems (D1 and D2) that dip towards either the NW or W at angles of 71° and 72°, respectively.

Two discontinuity systems D1 and D2 were delineated in the highest face of the quarry (section 6; length: 53 m, height: 11 m, representative dip direction and dip: 298/65). The D1 system includes the D1a and D1b sets (16 and 9 data, respectively), characterised by discontinuities steeply dipping towards the NNW with a dip angle of approximately 70°. The D2 system encompasses NE-SW striking discontinuities that are steeply dipping towards the W at an angle of 60° (D2a set; 5 measurements) and 81° (D2b; 8 data), respectively.

Based on the structural analysis of the DOM, two subvertical systems (D1 and D2) of discontinuities can be distinguished. The D1 system generally dips toward the NW, while the D2 system shows a general NNW-SSE strike dipping towards the WSW. The section of the quarry QS3A (Fig. 4B) was selected for a detailed analysis of the discontinuity sets to derive the input parameters for the discrete fracture network (DFN) modelling. The high-resolution orthophotograph of the section was digitised in QGIS obtaining a shapefile of discontinuity traces, i.e. the intersections of the discontinuity planes with the quarry face (Fig. 9). Since the face dips 70° towards W, it intersects all the discontinuity systems identified in this sector of the quarry (Fig. 8). Sets D1a and D1b (subvertical in the orthophoto; red set in Fig. 9) differ by just 20° in strike and it was impossible to separate them based on their traces on the orthophotograph. They were merged into one set (named set V). The traces of systems D2a and D2b (at medium and low angle in the orthophoto; green set in Fig. 9) show a continuous range of plunges, without a clear cutoff angle between them. The medium to low angle traces were therefore considered as a merged system (named set H). The parameters calculated for the two merged sets visible in section QS3A are listed in Supplementary Tab. 5. The merged sets show a dispersed distribution of their spatial orientation, as evidenced by the relatively low values of the Fisher K (13.53 for set H and 18.83 for set V). Since section QS3A is subvertical, the length of the traces corresponds to fracture heights. The percentage of censored heights is 20% and 11.08% in sets V and H, respectively (Supplementary Tab. 5). A log-normal distribution best fits the distribution of the measured heights, accounting for censoring bias (Supplementary Fig. 1). The

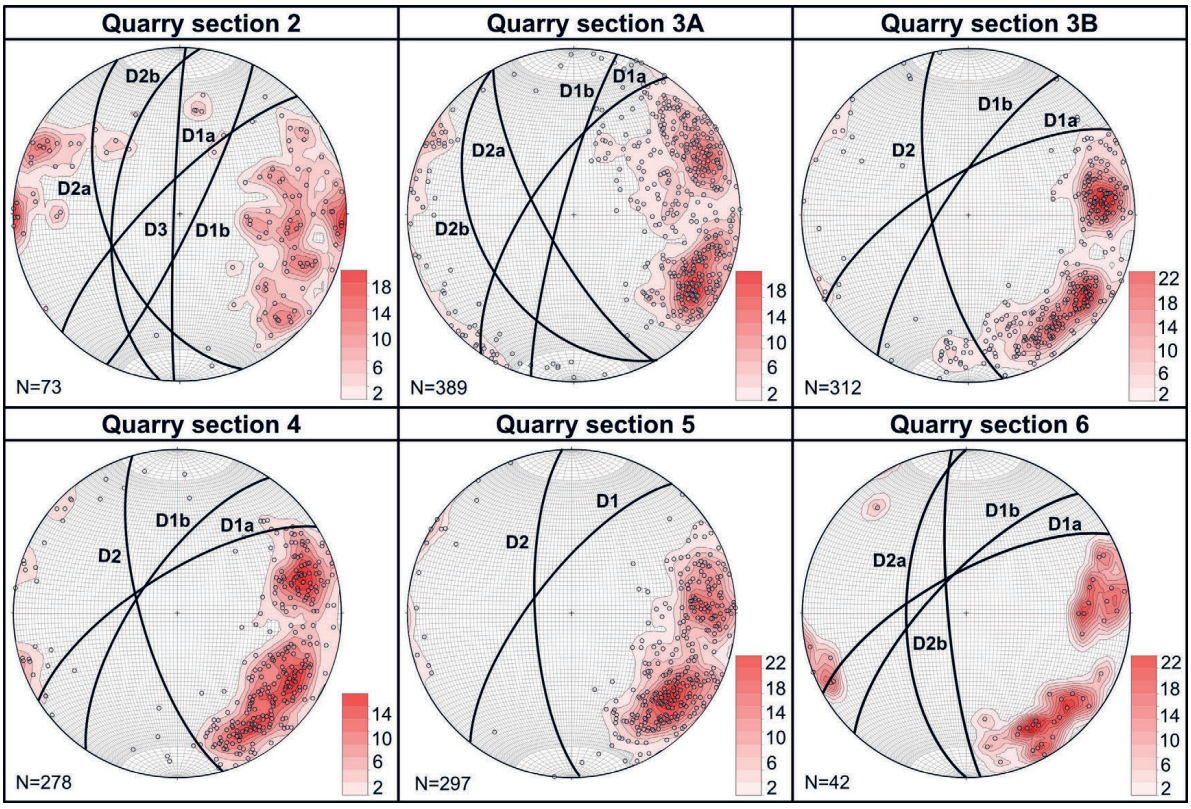

Figure 8. Structural diagrams of the main discontinuity systems in the different sections of the quarry (N: number of data). The orientations of the representative discontinuity systems are reported in Supplementary Tab. 4. They are obtained from the distribution of the measured discontinuities in the DOM of BRQ here represented as poles (black hollow points).

cumulative fracture lengths were used to calculate the areal fracture intensity P21 being 0.47 and 0.37 for set H and V, respectively.

4.3. DFN modelling of the aquifer outcrop analogue

The results obtained from the DOM and QS3A virtual structural analyses were used to build the DFN model of the outcrop. The model size was 100×100×30 m (XYZ; Fig. 10A) corresponding to the length and height of the QS3A section. The input parameters used for the construction of DFN models in both the software DFNworks and Move are reported in Supplementary Tab. 6 including the P32 and aperture values obtained after the calibration procedure.

The calibration of P32 was based on the iterative building of DFNs in the DFNworks software, pointing to a ratio C1 (Eq. 1) of 0.24 and 0.21 for set H and set V, respectively. These linear coefficients were used to calculate the P32 from the P21 obtained through the digitalisation of the fracture traces in the QS3A section resulting in P32 values of 1.98 and 1.18 m^2/m^3 for set H and set V, respectively.

The aperture was calibrated to fit the porosity (Φ) distribution in the DFN model with the Φ field measured during well logging of Dar 1 well. The analysis of the well log showed a large variation in the Φ ranging from 0.03 to 42% (average = 7.9%). The occurrence of outliers was indicated by the fact that the 10^{th} and 90^{th} percentiles of the distribution are 0.9 and 17%, respectively, suggesting a narrower Φ field. A closer inspection of the caliper well log showed a variation in the diameter of the borehole from 35 to 45 cm (nominal diameter of the drill bit was 31.1 cm), with the high Φ occurring in the well sections with larger diameters. These data suggest that the wall of the well locally collapsed (most probably in the more fractured part of the reservoir), affecting the measurement of the Φ. The section of the well with both a smaller and more homogeneous diameter was selected to obtain a more realistic assessment of the Φ. These conditions should point to a more compact wall of the well, resulting in Φ values that should better reflect the Φ field in the aquifer. The selected section was located at a depth of 100-130 m showing a homogenous diameter between 35 and 36 cm. The Φ within this interval is between 0.03 and 9.1% with an average value of 2.7%. The 10^{th} and 90^{th} percentiles of the distribution are 0.2 and 6.3%, respectively, suggesting a more homogeneous distribution around the average than the whole Φ dataset.

The Φ calibration was conducted testing values of the fracture aperture from 0.1 to 10 mm and combining them with the different approaches for assigning the aperture in the Move software. The modelling domain was discretised using a grid spacing of 0.5 m considering that the Φ in the Dar 1 well was calculated from the neutron log generally having a vertical resolution of 1 m and depth of investigation of 25 cm (LAI et al., 2024). The distributions of Φ and k obtained for the tested aperture values and employing the different methodological approaches are shown in Supplementary Figs. 2 and 3, respectively, while their statistical analyses are in Supplementary Tabs. 7 and 8. A general increase of both the Φ and k fields with the aperture was observed except for the minimum and 10^{th} percentile of the distributions, which were always 0. This value is the outcome of choosing a small grid size since the software assigns null Φ/k to those cells that are not cut by any structure. Considering the same aperture, the highest values were obtained with the method "aperture proportional to length", while the method "constant aperture" showed the lowest values. This discrepancy can be explained by the different methodological approaches for calculating the aperture. In the "aperture proportional to length" approach, long fractures have larger apertures than short fractures resulting in both higher Φ and k values. In the "constant aperture" approach, the same aperture is applied to all fractures diminishing the effect of long and potentially wider fractures on the hydraulic parameters. This effect is also visible by analysing the skewness and kurtosis values of the distributions. Skewness and kurtosis are higher than 0.9 and 3.8, respectively, suggesting right-skewed and leptokurtic distributions. These data suggest a clustering of the datasets toward low values with a long right tail toward high values. The highest skewness and kurtosis were observed in the "aperture proportional to length" approach enforcing the

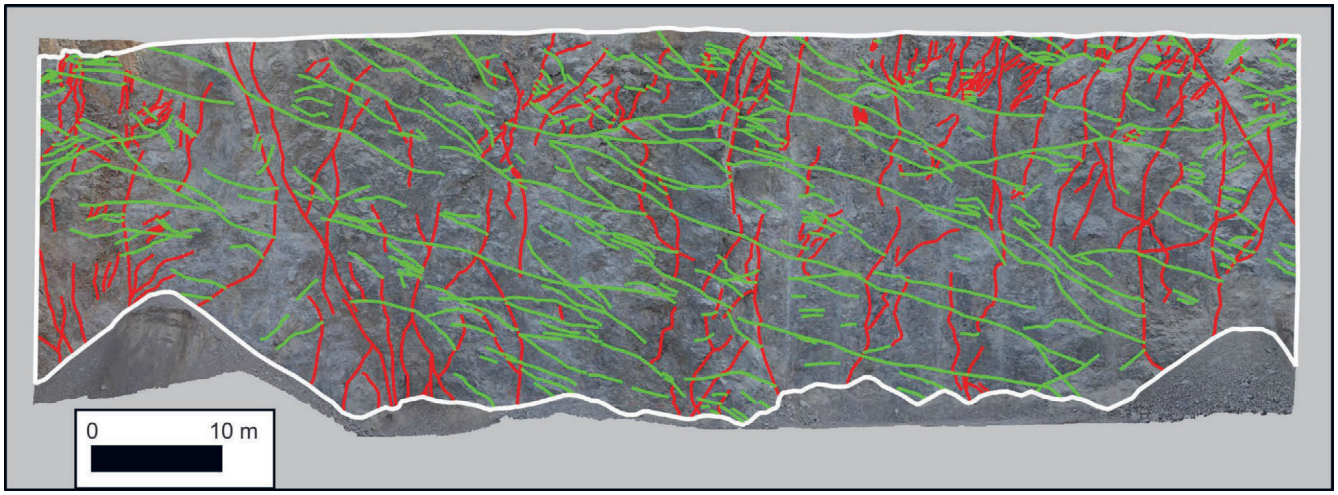

Figure 9. Orthophotograph of section QS3A digitised in QGIS to vectorise the traces of the discontinuity systems. Traces are divided into two discontinuity systems: subvertical (red; set V in Supplementary Tab. 5) and subhorizontal (green; set H in Supplementary Tab. 5).

occurrence of high Φ/k values associated with wider fractures. It should be noted that a similar asymmetric distribution was depicted in the experimental Φ of the Dar 1 well.

The statistical analysis of the Φ in the DFN models was further detailed to calibrate the aperture. A linear relationship (Fig. 10B) between the aperture and all statistical indexes is observed, except for the minimum and 10th percentile values. The slopes of the average values for the different methodological approaches were calculated to obtain the aperture fitting with the average Φ measured in Dar 1 well at a depth of 100–130 m. The resulting apertures were 8.9, 5.1, and 4.1 mm for the constant, root length, and length approaches, respectively. The aperture values obtained with the second and third approaches seem more realistic and applicable for a fractured aquifer, while wider apertures could be more representative of karst aquifers. The model was run with an aperture of 4.1 mm and employing the "aperture proportional to the fracture length" approach. The resulting Φ ranged from 0 to 22.7%, but the statistical analysis showed that the Φ distribution (red dots in Fig. 10C) fits the experimental values at the depth of 100–130 m (red lines in Fig. 10C) with only a minor discrepancy observed for the 75th percentile. The resulting k value ranged from 0 to 4.4×10^{6} D and an average value of 2.7×10^{5} D. The statistical distributions of both Φ and k are right-skewed and leptokurtic (skewness of 1.1 and 2.4, respectively, and kurtosis of 4.3 and 11.2, respectively) indicating a highly asymmetric distributions.

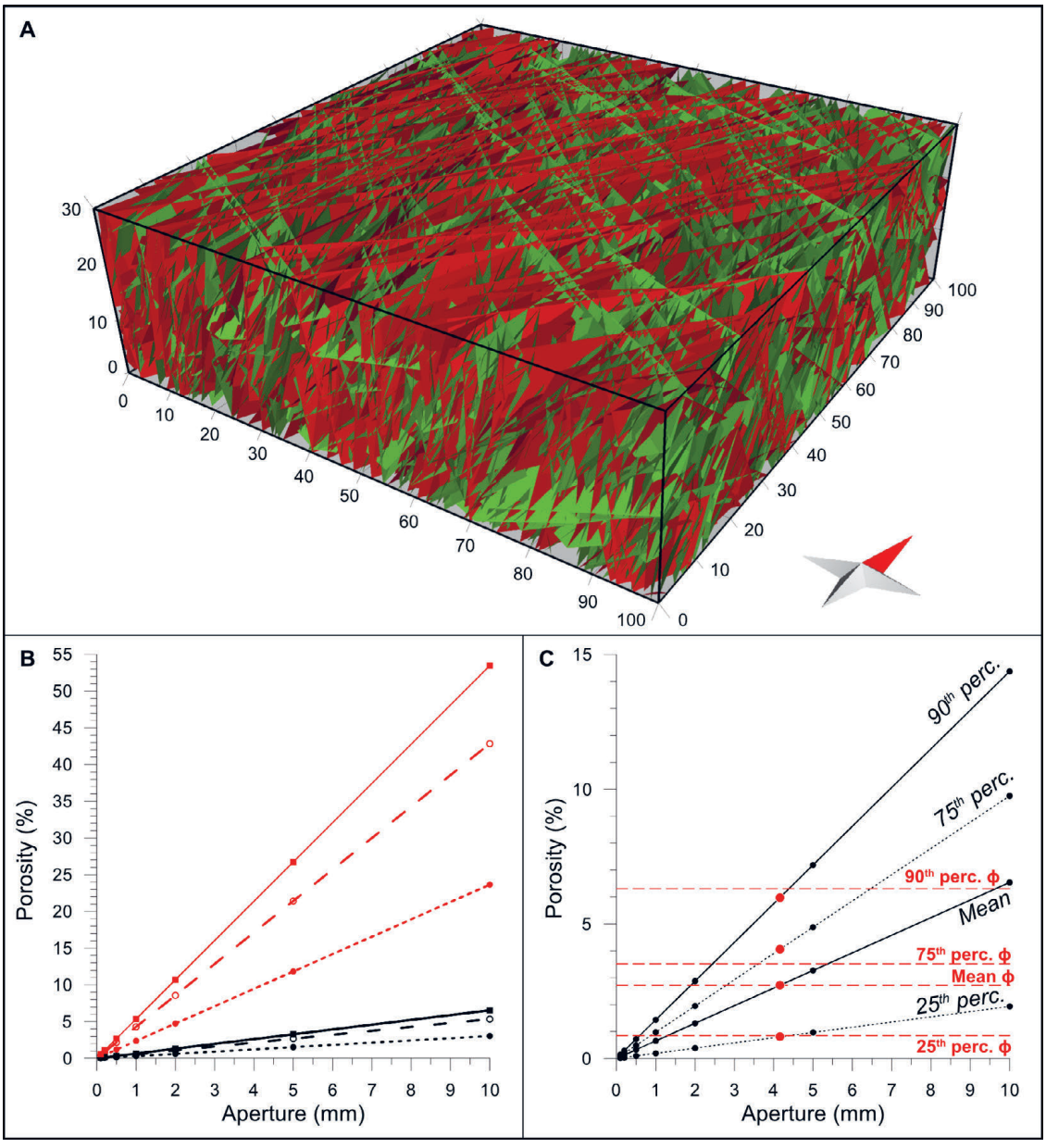

Figure 10. (A) DFN model obtained using the input parameters in Supplementary Tab. 5. The red and green discontinuities represent the vertical and horizontal discontinuity sets, respectively. (B) Mean (black lines) and maximum (red lines) porosity values obtained using different approaches for assigning the aperture to fractures in the DFN model (dotted lines: constant aperture; dashed lines: aperture proportional to the root of the length; full lines: aperture proportional to the length). (C) Porosity distribution (black lines) obtained using the "aperture proportional to length" approach. It was considered the best approach for fitting the experimental porosity distribution (dashed red lines) of the Dar 1 well at a depth of 100-130 m. The results obtained from the best model with aperture of 4.1 mm are shown as red dots suggesting a good fit with the experimental data.

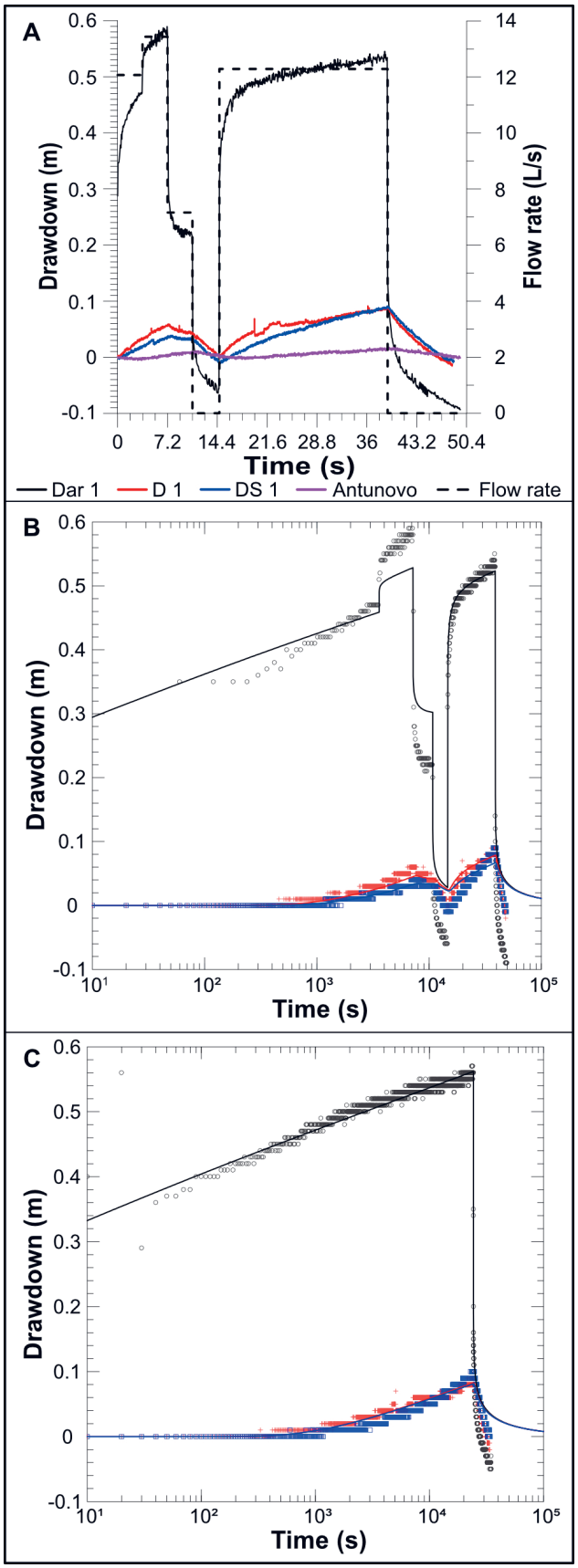

Figure 11. (A) Drawdown measured in the wells Dar 1, D 1, and DS 1 and the Antunovo vrelo spring during the pumping test conducted in 2022. The flow rate is shown as a step plot with a dashed line. (B-C) Drawdown data for Dar 1 (black circle), D 1 (red cross), and DS 1 (blue square) fitted with the theoretical Theis curves (black, red, and blue lines for Dar 1, D 1, and DS 1, respectively) for the whole pumping test (B) and the constant flow rate test (C).

4.4. Interpretation of pumping and well tests

The pumping test in the Daruvar thermal field lasted approximately 12 h. It was conducted performing 3 steps (i.e., step-drawdown test) with flow rates of 12.1, 13.4, and 7.2 L/s, respectively, lasting 1 h each (Fig. 11A). The pumping was stopped for 1 h measuring the recovery of the water level. Afterwards, a flow rate of 12.3 L/s was set for approximately 7 h (i.e., constant test). The subsequent recovery of the water level was measured for 1.5 h reaching the initial water level. A maximum drawdown (Δ) of 0.59 m was observed in the Dar 1 well at the end of the second pumping step, while the highest Δ in the observation wells D 1 and DS 1 was measured during the constant test reaching 0.09 m (Fig. 11A). The water level in the Antunovo vrelo spring was slightly affected by the pumping showing a Δ up to 0.01 m.

The Δ values measured in Dar 1, D1, and DS 1 were used for determining the hydrogeological parameters of the aquifer using both the Theis-Hantush analytical solution for pumping tests. The solution was calculated using the data from the whole pumping test (i.e., step-drawdown and constant tests; Fig. 11B) and only from the constant test (Fig. 11C). The obtained parameters are summarised in Supplementary Tab. 9. The results of the two methodological approaches are comparable. The transmissivity (T) is 3.82×10^{-2} m^2/s and 3.46×10^{-2} m^2/s, while the saturated thickness of the aquifer (b) is 61.5 and 68.4 m for the whole and constant tests, respectively. The saturated thickness value slightly corresponds to the length of the screened section of the Dar 1 well (53 m, and up to 59 m if a short part of casing between the two well screens is included).

Furthermore, the data measured in Dar 1 were used to assess the drawdown vs. flow rate curve of the well, the well efficiency (W), and the specific capacity (SC). The obtained results are summarised in Supplementary Fig. 4. The calculated drawdown vs. flow rate curve is:

$$\Delta = 14.6\ Q + 2186.6\ Q^2 \quad (4)$$

W is between 33% and 48% and decreases by increasing the flow rate. Although W is low showing a poor efficiency, it is acceptable considering that the Dar 1 well is relatively old and it has practically never been used. The SC was calculated considering both the experimental and theoretical Δ showing minor differences. The resulting T values are 3.8×10^{-2} m^2/s and 4.8×10^{-2} m^2/s for the equations 2 and 3, respectively. Considering that these values are obtained using experimental relationships developed in geological and hydrogeological settings different from the Daruvar thermal field, the slight discrepancy with the T calculated from the pumping test approach is acceptable.

5. DISCUSSION

5.1. Integrated interpretation of field and virtual structural data

Fractures are the main flow path in fractured aquifers (FAULKNER et al., 2010; BENSE et al., 2013). Reconstructing the geometric characteristics of the fracture network and the stress field deforming the rock mass can be useful in determining the preferential flow paths fostering the conceptual

model of the groundwater resource (SINGHAL & GUPTA, 2010). Integrated structural mapping based on field measurements and digital outcrop model (DOM) analysis was employed in this work to analyse the fracture network in the Batinjska Rijeka quarry (BRQ). The results of the field measurements indicate that the Mesozoic carbonate complex in the quarry is deformed by systems of folds and fractures being a representative outcrop analogue for the fractured carbonate reservoir of the Daruvar hydrothermal system. Folded structures in the BRQ are characterised by subvertical bedding (dipping either NE/SW or SE/NW; Fig. 6A) that have undergone extensive brittle deformation with the formation of three systems of fractures (Fs1 and Fs3 including fractures steeply dipping toward ESE or NNE, and Fs2 including low angle fractures dipping toward the ESE; Fig. 6B). The geometry, structural position, and subvertical orientation of these systems indicate a cogenetic relationship with the fold hinge zones that have an predominantly NE-SW and ESE-WNW strike. Structural observations of shear fractures/fault planes (Fig. 6C) corroborate the results of the bedding and fracture system analyses, suggesting that the present-day fracture pattern observed in the BRQ results from the multiphase regional tectonics (KOSOVIĆ et al., 2024). Cretaceous-Palaeogene E-W (or NE-SW) compression rotated by 40º counterclockwise is observed on NNE-striking reverse fault planes associated with a NW-SE oriented P-axis (Supplementary Tab. 3 and Fig. 6C). NE-striking normal faults indicate a NW-SE oriented extension and clockwise rotation of the existing NNE-striking reverse fault due to a tectonic inversion. The observed extension may be related to the collapse of the hanging wall structures of the Cretaceous-Palaeogene reverse faults due to either gravitational slip (e.g. TAVANI et al., 2012) or the initial extension of the PBS in the late Oligocene and Miocene (TOMLJENOVIĆ & CSONTOS, 2001). The N-S (NE-SW) compressional/transpressional phase from the Pliocene-Quaternary is observed on strike-slip fault planes (Supplementary Tab. 3), showing polyphase structural reactivation and repeated movements in both a dextral and sinistral sense. Considering the cross-cutting relationships between SSF-1 and SSF-2 fault systems and mapped reverse/normal faults, it indicates that the strike-slip fault planes are younger and probably associated with the most recent Pliocene-Quaternary tectonic phase in the study area (e.g., TOMLJENOVIĆ & CSONTOS, 2001; SCHMID et al., 2008). This NE-SW oriented stress field may also influence the bedding reorientation and the formation of a younger fold system that gently dips towards the SE (Fig. 6A).

Results of the DOM virtual structural analysis depicted two dominant subvertical systems (D1 and D2; Supplementary Tab. 4) of discontinuities. The D1 system generally dips toward the NW, while the D2 system dips towards the WSW. These results correspond well with the field observations (Supplementary Tabs. 1 and 2). The D1 system has the same orientation as the bedding So3 and the fracture set Fs3b. Discontinuity system D2 has a similar orientation to the bedding So2 and fracture set Fs1b. Other sets of bedding and fractures observed by field measurements don't clearly correspond with the discontinuity systems delineated in the DOM. Only the fracture set Fs1a (Supplementary Tabs. 1 and 2) could have an analogy with the discontinuity set D1b measured in quarry section 2 (Supplementary Tab. 4). However, this discontinuity set is depicted only in one section of the quarry and is obtained from a limited dataset, decreasing the reliability of its geometric characterisation in the DOM. The lack of correlation between field data and the DOM results could be associated with several factors. Fracture sampling in the DOM highly depends on the outcrop inclination and the fracture 3D spatial orientation (PRIEST, 1993; ZHANG & EINSTEIN, 1998; ZEEB et al., 2013). This difference significantly reduces the identification of potential fracture systems that are either parallel or steeply dipping in opposite directions to the quarry face during the DOM analysis. Furthermore, field investigations and virtual outcrop analysis have different resolution scales (TZIAVOU et al., 2018; MARTINELLI et al., 2020): discontinuities at the centimetre scale can be measured in the field, while they are impossible to digitalise in decametre scale DOMs. Bearing in mind the different resolutions of the methods, only metre scale discontinuities were measured during the field investigations in the BRQ. Still, a discrepancy between the results occurred highlighting the intrinsic difference between the two methodological approaches. However, the digital outcrop analysis of the BRQ covered a relatively large area favouring: i) reconstruction of the discontinuity network in remote or inaccessible portions of the outcrop, and ii) collection of a large dataset that was used for a detailed statistical analysis of the geometric features of the main discontinuity sets.

5.2. Hydrogeological parameterisation of the Daruvar thermal aquifer

Besides their primary role in the circulation of groundwater, networks of fractures can influence the distribution of the bulk permeability (k) and porosity (Φ) in fractured aquifers (e.g., FAYBISHENKO et al., 2000; SINGHAL & GUPTA, 2010; BENSE et al., 2013).

In this study, both classical hydrogeological investigations and discrete fracture network (DFN) modelling were conducted for the hydraulic parameterisation of the Daruvar carbonate thermal reservoir. Several pumping and well tests have been conducted in the Daruvar thermal field to assess the transmissivity (T) of the aquifer (BOROVIĆ, 2015; BOROVIĆ et al., 2019; URUMOVIĆ et al., 2023). In particular, BOROVIĆ (2015) critically revised and reanalysed the results from old pumping tests (1971, 1980, 1982, 2009), providing a solid estimation of T. Here, the results of a recent pumping test (2022) were analysed using several methodological approaches (THEIS, 1935; HANTUSH, 1961a, b; KRUSEMAN et al., 2000). The T values obtained in this work and from the literature range from 1.58×10^{-2} to 4.83×10^{-2} m^2/s showing a good concordance among the different methods (Tab. 1). The average T was used to calculate the aquifer k value considering: i) the lower density and viscosity of the thermal waters due to their temperature and salinity, and ii) both the thicknesses of the dolomite aquifer and the fracture corridors in the Dar 1 well (d and f, respectively; Tab. 1) and the saturated thicknesses calculated from the pumping test analysis (b; Tab. 1). The resulting average values of k (Tab. 1) are 16.4, 32.7, and 88.7 D considering d, b, and f as the aquifer thickness, respectively.

Table 1. Hydrogeological parameterisation of the Daruvar thermal aquifer obtained from: i) the interpretation of pumping and well tests in this study, ii) the well logging of Dar 1 well, and iii) the literature (BOROVIĆ et al., 2019; URUMOVIĆ et al., 2023).

		Average value	Minimum – Maximum	10^{th} – 90^{th} percentile
Investigated thickness of dolomite	*d (m)*	130	–	–
Saturated thickness	*b (m)*	65	61.5 – 68.4	–
Thickness of fracture corridors	*f (m)*	24		
Transmissivity	*T (m^2/s)*	3.5e-2	1.6e-2 – 4.8e-2	2.5e-2 – 4.3e-2
Storativity	*S (–)*	1.6e-3	1.1e-3 – 2e-3	–
Hydraulic conductivity anisotropy ratio	*Kz/Kr (–)*	1.3e-2	6.8e-3 – 2e-2	–
Permeability from d	*k d (D)*	16.4	7.4 – 22.7	11.8 – 20.3
Permeability from b	*k b (D)*	32.7	14.8 – 45.3	23.6 – 40.6
Permeability from f	*k f (D)*	88.7	40 – 122.8	63.8 – 109.9
Porosity	*Φ (%)*	7.9	0.03 – 42	0.9 – 17.4
Porosity at depth 100-130 m	*Φ* (%)*	2.7	0.03 – 9.1	0.2 – 6.3

These values show good consistency within the same order of magnitude and are within the range of k values for fractured and karst carbonate aquifers (FREEZE & CHERRY, 1979). The Φ of the aquifer was obtained through well logging of the Dar 1 well. Since the distribution of Φ values showed a large variability (Tab. 1), a section of the well with tight walls (depth of 100–130 m) was considered to obtain a narrower, more realistic, range of Φ. The average Φ for this section was 2.7% (Tab. 1) being within the range of Φ in carbonates (NG & SANTAMARINA, 2023).

The distribution of Φ at a depth of 100–130 m was used for the calibration of the DFN model of the BRQ outcrop analogue. The best fit of the model was obtained using an aperture of 4.1 mm resulting in an average Φ of 2.7% and an average k of 2.7×10^5 D. Although the Φ fits with the experimental values, the k value is 3-4 orders of magnitude higher than the measured k (Tab. 1). The reasons for this discrepancy could be that: i) the Φ used for the calibration corresponds to the total Φ, while effective Φ is relevant for the fluid flow, and ii) the size and the discretisation of the DFN model do not correspond to the area investigated by the pumping test and the hydrogeological representative elementary volume. In order to overcome these issues, a larger DFN model was conducted. The model size was increased to 700×700×150 m (XYZ; Fig. 12A) being more representative of the aquifer volume investigated by the pumping test. It was considered that the radius of influence of the pumping test was between the DS 1 and D 1 observation points and the Antunovo vrelo spring, because the experimental data showed variations of the water level in the observation wells (Figs. 3 and 11A). Therefore, the horizontal size of the model was calculated to be representative of twice the average distance between the exploitation well Dar 1 and the observation points (Dar 1 - D 1: 265 m, Dar 1 – Antunovo vrelo: 450 m; Fig. 3). The vertical size was chosen to be representative of the maximum investigated thickness of the dolomite in the Daruvar area (d in Tab. 1). The model was conducted using the software Move and it was discretised using: i) a geocellular volume with a cell size as the DFN model of the outcrop analogue for generating the fracture network, and ii) a single cell (i.e., the whole volume) for the hydraulic parameterisation. This "double-sized" geocellular volume permits: i) construction of the fractures using the input parameters of the outcrop DFN model (Supplementary Tab. 6), and ii) calculation of the hydraulic parameters over a volume that is representative of the investigated section of the aquifer. Through this approach, the fracture geometry at the aquifer scale DFN is constrained using the geometric parameters obtained from the DOM virtual structural analysis, and the bulk hydraulic parameters are calculated obtaining an estimation at the scale of the pumping test. The model was run using the "aperture proportional to the fracture length" approach since it seemed more reliable for fractured aquifers. Different aperture values were tested obtaining a linear and power correlation with Φ and k (Figs. 12B-C). The aperture of 4.1 mm (i.e., the best fit in the outcrop analogue DFN model) results in a Φ and k of 3.7% and 3.9×10^5 D, respectively. These values are slightly higher than the results of the outcrop scale DFN model, probably due to the different geocellular volume used for the calculations. The linear relationship between the aperture and Φ was used to recalibrate the aperture value fitting the average Φ at the depth of 100–130 m (Tab. 1). The resulting aperture of 3 mm was run in the model obtaining a k value of 1.5×10^5 D, which is 3–4 orders of magnitude higher than the experimental values. This result suggests once more that two different aperture values are needed for fitting the experimental Φ and k values. In particular, the hydraulic aperture of the fractures, which is smaller than the mechanical aperture (RENSHAW, 1995; POURASKARPARAST et al., 2024), should be used for reconstructing the k value in DFN models (e.g., SMERAGLIA et al., 2021). Furthermore, the effective Φ should be considered since fractured aquifers usually have dual porosity, with most of the storage volume being in the matrix and most of the flow being in the fracture network (WORTHINGTON et al., 2019). The Φ dataset used for the calibration of the DFN models was calculated from the neutron log and describes the total Φ of the Daruvar aquifer. Considering that effective Φ in carbonate rocks is at least one order of magnitude less than total Φ (WORTHINGTON et al., 2019), the fracture aperture for obtaining a Φ of 0.27% (i.e., one order of magnitude lower than the average Φ at the depth of 100-130 m; Tab. 1) was calculated and input to the model. The calculated fracture aperture was 0.3 mm resulting in a k value of 149.4 D, which is slightly higher than the experimental values. The effective Φ value was refined on the basis of the experimental Φ dataset, and the 10^{th} percentile of the Φ distribution was tested (Tab. 1). The corresponding fracture aperture (0.22 mm) was input to the model resulting in Φ and k values of 0.2% and 60.5 D, respectively. The k value fits with the experimental values being in the range of the k calculated from f and slightly higher than the values obtained from d and b (Tab. 1).

The results of the conducted numerical investigations highlight the importance of employing a "dual aperture" approach for fitting both experimental Φ and k values in DFN models. This approach is necessary since fractured aquifers are a dual continuum medium where the groundwater is

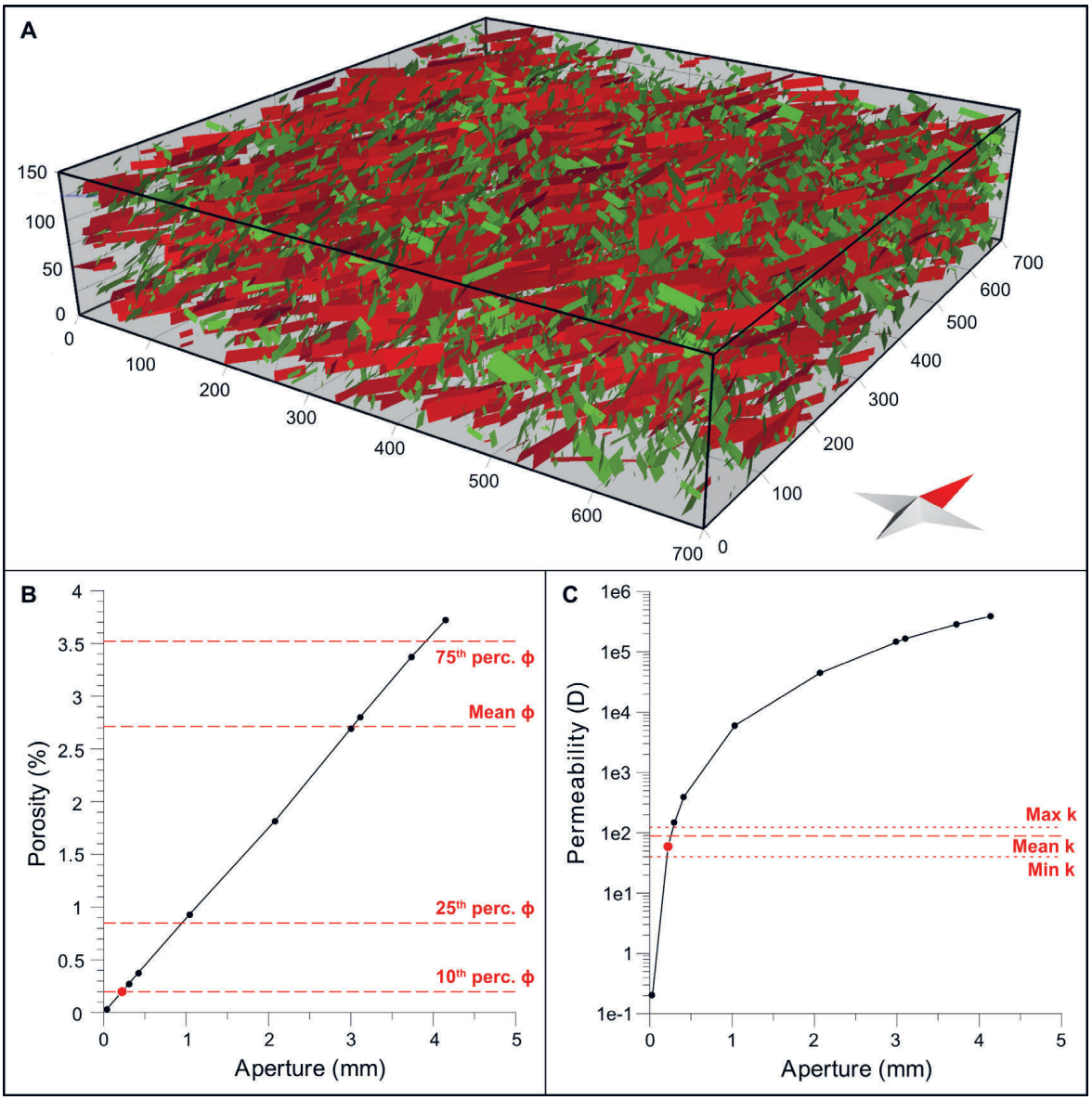

Figure 12. (A) Aquifer scale DFN model obtained using the input parameters in Supplementary Tab. 5. The red and green discontinuities (1% of the generated discontinuities is shown) represent the vertical and horizontal discontinuity set, respectively. (B-C) Porosity and permeability values (black dots) obtained from the aquifer scale DFN using different fracture apertures. The results of the best model (aperture of 0.22 mm) are shown as red dots pointing to a good fit with the experimental data (dashed lines).

mostly stored in the rock matrix, affecting the total porosity of the aquifer, while the fluid flow occurs in the fractures, being influenced by their hydraulic aperture and the effective porosity of the aquifer. This difference should also be considered for the analytical interpretation of pumping tests. Here, a generally well accepted analytical method reproducing the aquifer as an equivalent porous medium was used (SINGHAL & GUPTA, 2010), but it provides only a rough estimation of the k value. The estimation of k in dual porosity media requires more sophisticated field investigations (i.e., flowmeter and quantitative visual logging, tracer tests) and analytical methods for modelling the pumping test results (i.e., MOENCH, 1984).

6. CONCLUSIONS

This paper describes the results of an integrated approach for reconstructing the network of fractures and quantifying the hydraulic parameters in fractured aquifers. Structural and hydrogeological investigations were conducted in the Daruvar thermal area and its hinterland detailing the structural architecture and the hydraulic parameterisation of the carbonate thermal aquifer. The results obtained through field and virtual structural analyses were used as input parameters to construct discrete fracture network models at different scales to estimate the aquifer properties. The modelling results were compared with the results of hydrogeological field investigations obtaining a good correlation. These results permit the quantification of the impact of the fracture network on the permeability field of the Daruvar thermal aquifer as observed in fractured aquifers.

The results obtained in the investigation of the Daruvar thermal area demonstrate that an integrated approach is invaluable in investigating and modelling fractured media. The utilisation of such an integrated approach permits a

quantitative structural and hydrogeological reconstruction of the aquifer and the network of fractures favouring the fluid flow accounting for the advantages of both techniques. Field analysis can be used to determine the geological relationship among structures and the stress field developing the discontinuities. Remote sensing photogrammetry allows the construction of a 3D digital model of the outcrop favouring the collection of large datasets for a detailed quantitative description and statistical analysis of geological objects' geometry and their spatial relationships (HODGETTS, 2013; BISTACCHI et al., 2015; MARTINELLI et al., 2020). Field research can add a conceptual link to the results of the data analysis in the DOM obtaining a more comprehensive geological interpretation. Furthermore, the obtained results highlight the importance of correlating the results from structural and hydrogeological investigations. Structural data can be used to construct discrete fracture network models of the fractured aquifer that need to be calibrated using the data from hydrogeological investigations. Depending on the available experimental dataset of hydrogeological properties, the model calibration needs to account for the dual porosity of fractured aquifers and the difference between the mechanical and hydraulic aperture of the fractures.

ACKNOWLEDGMENT

The authors would like to thank the editorial team for the support during the preparation and the revision of the manuscript, the two anonymous reviewers for their useful comments, the Daruvarske toplice–Special Hospital for Medical Rehabilitation and Pivovara Daruvar d.o.o. for logistic help on-site and sharing of existing materials and Matej MANJARIĆ and INTER-PROMET d.o.o. for allowing the access to the Batinjska Rijeka quarry and the logistic support during the investigations. This research was funded by the HyTheC project of the Croatian Science Foundation (HRZZ), grant number UIP-2019-04-1218.

REFERENCES

ALLMENDINGER, R.W., CARDOZO, N. & FISHER, D.M. (2011): Structural geology algorithms: Vectors and tensors.– Cambridge University Press, 289 p. doi: 10.1017/CBO9780511920202

ANGELIER, J. & MECHLER, P. (1977): Sur une methode graphique de recherche des contraintes principales egalement utilisables en tectonique et en seismologie: la methode des diedres droits.– Bulletin de la Société Géologique de France, S7-XIX(6), 1309–1318. doi: 10.2113/gssgfbull.S7-XIX.6.1309

ANTONELLINI, M., CILONA, A., TONDI, E., ZAMBRANO, M. & AGOSTA, F. (2014): Fluid flow numerical experiments of faulted porous carbonates, Northwest Sicily (Italy).– Marine and Petroleum Geology, 55, 186–201. doi: 10.1016/j.marpetgeo.2013.12.003.

BADA, G., HORVÁTH, F., DÖVÉNYI, P., SZAFIÁN, P., WINDHOFFER, G. & CLOETINGH, S. (2007): Present-day stress field and tectonic inversion in the Pannonian basin.– Global and Planetary Change, 58/1–4, 165–180. doi: 10.1016/j.gloplacha.2007.01.007

BALEN, D., HORVÁTH, P., TOMLJENOVIĆ, B., FINGER, F., HUMER, B., PAMIĆ, J. & ÁRKAI, P. (2006): A record of pre-Variscan Barrovian regional metamorphism in the eastern part of the Slavonian Mountains (NE Croatia).– Mineralogy and Petrology, 87/1–2, 143–162. doi: 10.1007/s00710-006-0120-1

BENSE, V. F., GLEESON, T., LOVELESS, S. E., BOUR, O. & SCIBEK, J. (2013): Fault zone hydrogeology.– Earth-Science Reviews, 127, 171–192. doi: 10.1016/j.earscirev.2013.09.008

BENEDETTI, G., CASIRAGHI, S., BISTACCHI, A., & BERTACCHI, D. (2024): FracAbility: A python toolbox for survival analysis in fractured rock systems.– In: EGU General Assembly, Vienna, Austria, 14–19 Apr 2024. EGU24-22156. doi: 10.5194/egusphere-egu24-22156, 2024.

BISTACCHI, A., BALSAMO, F., STORTI, F., MOZAFARI, M., SWENNEN, R., SOLUM, J., TUECKMANTEL, C. & TABERNER, C. (2015): Photogrammetric digital outcrop reconstruction, visualization with textured surfaces, and three-dimensional structural analysis and modeling: Innovative methodologies applied to fault-related dolomitization (Vajont Limestone, Southern Alps, Italy).– Geosphere, 11/6, 2031–2048. doi: 10.1130/GES01005.1

BISTACCHI, A., MITTEMPERGHER, S., MARTINELLI, M. & STORTI, F. (2020): On a new robust workflow for the statistical and spatial analysis of fracture data collected with scanlines (or the importance of stationarity).– Solid Earth. doi: 10.5194/se-2020-83

BOROVIĆ, S. (2015): Integrirani hidrogeološko - hidrogeokemijski model Daruvarskog geotermalnog vodonosnika [*Integrated hydrogeological-hydrogeochemical model of Daruvar geothermal aquifer* – in Croatian].– Unpubl. PhD Thesis, Faculty of Mining, Geology and Petroleum Engineering, University of Zagreb, 228 p.

BOROVIĆ, S. & MARKOVIĆ, I. (2015): Utilization and tourism valorisation of geothermal waters in Croatia.– Renewable and Sustainable Energy Reviews, 44, 52–63. doi: 10.1016/j.rser.2014.12.022

BOROVIĆ, S., POLA, M., BAČANI, A. & URUMOVIĆ, K. (2019): Constraining the recharge area of a hydrothermal system in fractured carbonates by numerical modelling.– Geothermics, 82, 128–149. doi: 10.1016/j.geothermics.2019.05.017

CAINE, J. S., EVANS, J. P. & FORSTER, C. B. (1996): Fault zone architecture and permeability structure.– Geology, 24/11, 1025–1028. doi: 10.1130/0091-7613(1996)024<1025:FZAAPS>2.3.CO

CARDOZO, N. & ALLMENDINGER, R. W. (2013): Spherical projections with OSXStereonet.– Computers and Geosciences, 51, 193–205. doi: 10.1016/j.cageo.2012.07.021.

CARRERA, J. & MARTINEZ-LANDA, L. (2000): Mixed discrete-continuum models: A summary of experiences in test interpretation and model prediction.– In: FAYBISHENKO, B., WITHERSPOON, P.A. & BENSON, S.M. (eds.): Dynamics of Fluid in Fractured Rock, 251–265. doi: 10.1029/GM122p0251

CSONTOS, L. & VÖRÖS, A. (2004): Mesozoic plate tectonic reconstruction of the Carpathian region.– Palaeogeography, Palaeoclimatology, Palaeoecology, 210/1, 1–56. doi: 10.1016/j.palaeo.2004.02.033

CECCATO, A., VIOLA, G., ANTONELLINI, M., TARTAGLIA, G. & RYAN, E.J. (2021): Constraints upon fault zone properties by combined structural analysis of virtual outcrop models and discrete fracture network modelling.– Journal of Structural Geology, 152, 104444. doi: 10.1016/j.jsg.2021.104444

DELVAUX, D. & SPERNER, B. (2003): New aspects of tectonic stress inversion with reference to the TENSOR program.– Geological Society, London, Special Publications, 212/1, 75–100. doi: 10.1144/GSL.SP.2003.212.01.06

DERSHOWITZ, W.S. & HERDA, H.H. (1992): Interpretation of fracture spacing and intensity.– All Days, ARMA-92-0757.

DOBLAS, M. (1998): Slickenside kinematic indicators.– Tectonophysics, 295/1–2, 187–197. doi: 10.1016/S0040-1951(98)00120-6

DE DREUZY, J.-R., DAVY, P. & BOUR, O. (2002): Hydraulic properties of two-dimensional random fracture networks following power law distributions of length and aperture.– Water Resources Research, 38/12, 1276. doi: 10.1029/2001WR001009

DE DREUZY, J., DAVY, P. & BOUR, O. (2001): Hydraulic properties of two-dimensional random fracture networks following a power law length distribution: 2. Permeability of networks based on lognormal distribution of apertures.– Water Resources Research, 37/8, 2079–2095. doi: 10.1029/2001WR900010

DUFFIELD, G.M. (2007): AQTESOLV for Windows Version 4.5 User's Guide.– HydroSOLVE, Inc., Reston, VA.

FABBRI, P. (1997): Transmissivity in the Geothermal Euganean Basin: A Geostatistical Analysis.– Ground Water, 355, 881–887. doi: 10.1111/j.1745-6584.1997.tb00156.x

FAULKNER, D.R., JACKSON, C.A.L., LUNN, R.J., SCHLISCHE, R.W., SHIPTON, Z.K., WIBBERLEY, C.A.J. & WITHJACK, M.O. (2010): A review of recent developments concerning the structure, mechanics and fluid flow properties of fault zones.– Journal of Structural Geology, 32/11, 1557–1575. doi: 10.1016/j.jsg.2010.06.009

FAYBISHENKO, B., WITHERSPOON, P.A. & BENSON, S.M. (2000): Dynamics of Fluids in Fractured Rock. Geophysical Monograph Series. Vol. 122. – American Geophysical Union, Washington, D. C. doi:10.1029/GM122

FREEZE, R.A. & CHERRY, J.A. (1979): Groundwater.– Englewood Cliffs, NJ: Prentice-Hall, 604 p.

FINSTER, M., CLARK, C., SCHROEDER, J. & MARTINO, L. (2015): Geothermal produced fluids: Characteristics, treatment technologies, and management options.– Renewable and Sustainable Energy Reviews, 50, 952–966. doi: 10.1016/j.rser.2015.05.059

GIUFFRIDA, A., LA BRUNA, V., CASTELLUCCIO, P., PANZA, E., RUSTICHELLI, A., TONDI, E., GIORGIONI, M. & AGOSTA, F. (2019): Fracture simulation parameters of fractured reservoirs: Analogy with outcropping carbonates of the Inner Apulian Platform, southern Italy.– Journal of Structural Geology, 123, 18–41. doi: 10.1016/j.jsg.2019.02.007

GUIHÉNEUF, N., DAUSSE, A., DE DREUZY, J.R. & PARKER, B.L. (2021): Flow-bearing structures of fractured rocks: Insights from hydraulic property scalings revealed by a pumping test.– Journal of Hydrology, 598. doi: 10.1016/j.jhydrol.2020.125715

HANTUSH, M.S. (1961a): Aquifer Tests on Partially Penetrating Wells.– Journal of the Hydraulics Division, 87/5, 171–195. doi: 10.1061/JYCEAJ.0000639

HANTUSH, M. S. (1961b): Drawdown Around a Partially Penetrating Well.– Journal of the Hydraulics Division, 87/4, 83–98. doi: 10.1061/JYCEAJ.0000633

HODGETTS, D. (2013): Laser scanning and digital outcrop geology in the petroleum industry: A review.– Marine and Petroleum Geology, 46, 335–354. doi: 10.1016/j.marpetgeo.2013.02.014

HORVÁTH, F., MUSITZ, B., BALÁZS, A., VÉGH, A., UHRIN, A., NÁDOR, A., KOROKNAI, B., PAP, N., TÓTH, T. & WÓRUM, G. (2015): Evolution of the Pannonian basin and its geothermal resources.– Geothermics, 53, 328–352. doi: 10.1016/j.geothermics.2014.07.009

HORVÁTH, F., BADA, G., SZAFIÁN, P., TARI, G., ÁDÁM, A. & CLOETINGH, S. (2006): Formation and deformation of the Pannonian Basin: Constraints from observational data.– Geological Society Memoir, 32, 191–206. doi: 10.1144/GSL.MEM.2006.032.01.11

HYMAN, J.D., KARRA, S., MAKEDONSKA, N., GABLE, C.W., PAINTER, S.L. & VISWANATHAN, H.S. (2015): dfnWorks: A discrete fracture network framework for modeling subsurface flow and transport.– Computers & Geosciences, 84, 10–19. doi: 10.1016/j.cageo.2015.08.001

JAMIČIĆ, D. (1995): The role of sinistral strike-slip faults in the formation of the structural fabric of the Slavonian Mts. (eastern Croatia).– Geologia Croatica, 48/2, 155–160.

JAMIČIĆ, D., VRAGOVIĆ, M. & MATIČEC, D. (1989): Osnovna geološka karta SFRJ 1:100 000. Tumač za list Daruvar (Basic geological map of SFRJ 1:100 000. Explanatory notes for sheet Daruvar). – Geol. zavod, Zagreb, Sav. geol. zavod Beograd, Beograd, 55 p.

JAROSINSKI, M., BEEKMAN, F., MATENCO, L. & CLOETINGH, S. (2011): Mechanics of basin inversion: Finite element modelling of the Pannonian Basin System.– Tectonophysics, 502/1–2, 121–145. doi: 10.1016/j.tecto.2009.09.015

NG, K. & SANTAMARINA, J. C. (2023): Mechanical and hydraulic properties of carbonate rock: The critical role of porosity.– Journal of Rock Mechanics and Geotechnical Engineering, 15/4, 814–825. doi: 10.1016/j.jrmge.2022.07.017

KEEGAN-TRELOAR, R., IRVINE, D.J., SOLÓRZANO-RIVAS, S.C., WERNER, A.D., BANKS, E.W. & CURRELL, M.J. (2022): Fault-controlled springs: A review.– Earth-Science Reviews, 230, 104058. doi: 10.1016/j.earscirev.2022.104058

KORNEVA, I., CILONA, A., TONDI, E., AGOSTA, F. & GIORGIONI, M. (2015): Characterisation of the permeability anisotropy of Cretaceous platform carbonates by using 3D fracture modeling: the case study of Agri Valley fault zones (southern Italy).– Italian Journal of Geosciences, 134/3, 396–408. doi: 10.3301/IJG.2014.26

KOSOVIĆ, I., BRIŠKI, M., PAVIĆ, M., PADOVAN, B., PAVIČIĆ, I., MATOŠ, B., POLA, M. & BOROVIĆ, S. (2023): Reconstruction of Fault Architecture in the Natural Thermal Spring Area of Daruvar Hydrothermal System Using Surface Geophysical Investigations (Croatia).– Sustainability, 15/16, 12134. doi: 10.3390/su151612134

KOSOVIĆ, I., MATOŠ, B., PAVIČIĆ, I., POLA, M., MILEUSNIĆ, M., PAVIĆ, M. & BOROVIĆ, S. (2024): Geological modeling of a tectonically controlled hydrothermal system in the southwestern part of the Pannonian basin (Croatia).– Frontiers in Earth Science. 12:1401935. doi: 10.3389/feart.2024.1401935

KRUSEMAN, G.P., DE RIDDER, N.A. & VERWEIJ, J.M. (2000): Analysis and evaluation of pumping test data.Vol. 47.– International institute for land reclamation and improvement, Wageningen, 378 p.

LAI, J., SU, Y., XIAO, L., ZHAO, F., BAI, T., LI, Y., LI, H., HUANG, Y., WANG, G. & QIN, Z. (2024): Application of geophysical well logs in solving geologic issues: Past, present and future prospect.– Geoscience Frontiers, 15/3, 101779. doi: 10.1016/j.gsf.2024.101779

LEI, Q., LATHAM, J.-P. & TSANG, C.-F. (2017): The use of discrete fracture networks for modelling coupled geomechanical and hydrological behaviour of fractured rocks.– Computers and Geotechnics, 85, 151–176. doi: 10.1016/j.compgeo.2016.12.024

MAMMOLITI, E., PEPI, A., FRONZI, D., MORELLI, S., VOLATILI, T., TAZIOLI, A. & FRANCIONI, M. (2023): 3D Discrete Fracture Network Modelling from UAV Imagery Coupled with Tracer Tests to Assess Fracture Conductivity in an Unstable Rock Slope: Implications for Rockfall Phenomena.– Remote Sensing, 15/5, 1222. doi: 10.3390/rs15051222

MALVIĆ, T. & CVETKOVIĆ, M. (2013): Lithostratigraphic units in the Drava Depression (Croatian and Hungarian parts) – a correlation.– Nafta, 64/1, 27–33.

MARRETT, R. & ALLMENDINGER, R.W. (1990): Kinematic analysis of fault-slip data.– Journal of Structural Geology, 12/8, 973–986. doi: 10.1016/0191-8141(90)90093-E

MARTINELLI, M., BISTACCHI, A., MITTEMPERGHER, S., BONNEAU, F., BALSAMO, F., CAUMON, G. & MEDA, M. (2020): Damage zone characterization combining scan-line and scan-area analysis on a km-scale Digital Outcrop Model: The Qala Fault (Gozo).– Journal of Structural Geology, 140, 104144. doi: 10.1016/j.jsg.2020.104144

MAULDON, M. (1994): Intersection probabilities of impersistent joints.– International Journal of Rock Mechanics and Mining Sciences & Geomechanics Abstracts, 31/2, 107–115. doi: 10.1016/0148-9062(94)92800-2

MEDICI, G., LING, F. & SHANG, J. (2023): Review of discrete fracture network characterization for geothermal energy extraction.– Frontiers in Earth Science, 11, 1–17. doi: 10.3389/feart.2023.1328397

MEDICI, G., SMERAGLIA, L., TORABI, A. & BOTTER, C. (2020): Review of Modeling Approaches to Groundwater Flow in Deformed Carbonate Aquifers.– Groundwater, 593, 334–351. doi: 10.1111/gwat.13069

MOENCH, A.F. (1984): Double-porosity models for a fissured groundwater reservoir with fracture skin.– Water Resources Research, 207, 831–846. doi: 10.1029/WR020i007p00831

ODA, M. (1985): Permeability tensor for discontinuous rock masses.– Géotechnique, 35/4, 483–495. doi: 10.1680/geot.1985.35.4.483

ORTNER, H., REITER, F. & ACS, P. (2002): Easy handling of tectonic data: the programs TectonicVB for Mac and TectonicsFP for Windows™.– Computers & Geosciences, 28/10, 1193–1200. doi: 10.1016/S0098-3004(02)00038-9

PAMIĆ, J., RADONIĆ, G. & PAVIĆ, G. (2003): Geološki vodič kroz Park prirode Papuk (Geological guide through the Papuk nature park).– Park prirode Papuk, Požega, 66 p.

PAVIĆ, M., KOSOVIĆ, I., POLA, M., URUMOVIĆ, K., BRIŠKI, M. & BOROVIĆ, S. (2023): Multidisciplinary Research of Thermal Springs Area in Topusko (Croatia).– Sustainability, 15/6, 5498. doi: 10.3390/su15065498

POURASKARPARAST, Z., AGHAEI, H., COLOMBERA, L., MASOERO, E. & GHAEDI, M. (2024): Fracture aperture: A review on fundamental concepts, estimation methods, applications, and research gaps.– Marine and Petroleum Geology, 164, 106818. doi: 10.1016/j.marpetgeo.2024.106818

PRELOGOVIĆ, E., SAFTIĆ, B., KUK, V., VELIĆ, J., DRAGAŠ, M. & LUČIĆ, D. (1998): Tectonic activity in the Croatian part of the Pannonian basin.– Tectonophysics, 297/1–4, 283–293. doi: 10.1016/S0040-1951(98)00173-5

PRIEST, S.D. (1993): Discontinuity Analysis for Rock Engineering. Vol. 30. – Springer Netherlands, Dordrecht, 323–324 p. doi:10.1007/978-94-011-1498-1

RENSHAW, C.E. (1995): On the relationship between mechanical and hydraulic apertures in rough-walled fractures.– Journal of Geophysical Research: Solid Earth, 100/B12, 24629–24636. doi: 10.1029/95JB02159

ROMANO, V., BIGI, S., CARNEVALE, F., DE'HAVEN HYMAN, J., KARRA, S., VALOCCHI, A.J., TARTARELLO, M.C. & BATTAGLIA, M. (2020): Hydraulic characterization of a fault zone from fracture distribution.– Journal of Structural Geology, 135, 104036. doi: 10.1016/j.jsg.2020.104036

RYBACH, L. & MONGILLO, M. (2006): Geothermal Sustainability-A Review with Identified Research Needs.– GRC Transactions, 30, 1083–1090.

SAFTIĆ, B., VELIĆ, J., SZTANO, O., JUHASZ, G. & IVKOVIĆ, Ž. (2003): Tertiary Subsurface Facies, Source Rocks and Hydrocarbon Reservoirs in the SW Part of the Pannonian Basin (Northern Croatia and South-Western Hungary).– Geologia Croatica, 56/1, 101–122. doi: 10.4154/232

SCHMID, S.M., FÜGENSCHUH, B., KOUNOV, A., MAȚENCO, L., NIEVERGELT, P., OBERHÄNSLI, R., PLEUGER, J., SCHEFER, S., SCHUSTER, R., TOMLJENOVIĆ, B., USTASZEWSKI, K. & VAN HINSBERGEN, D.J.J. (2020): Tectonic units of the Alpine collision zone between Eastern Alps and western Turkey.– Gondwana Research, 78, 308–374. doi: 10.1016/j.gr.2019.07.005

SCHMID, S.M., BERNOULLI, D., FÜGENSCHUH, B., MATENCO, L., SCHEFER, S., SCHUSTER, R., TISCHLER, M. & USTASZEWSKI, K. (2008): The Alpine-Carpathian-Dinaridic orogenic system: correlation and evolution of tectonic units.– Swiss Journal of Geosciences, 101/1, 139–183. doi: 10.1007/s00015-008-1247-3

SIEGEL, L., GOLDSCHEIDER, N., PETITTA, M., XANKE, J., ANDREO, B., et al. (2023): Distribution, threats and protection of selected karst groundwater-dependent ecosystems in the Mediterranean region.– Hydrogeology Journal, 31/8, 2231–2249. doi: 10.1007/s10040-023-02711-9

SINGHAL, B.B.S. & GUPTA, R.P. (2010): Applied Hydrogeology of Fractured Rocks. – Springer Netherlands, Dordrecht. doi: 10.1007/978-90-481-8799-7

SMERAGLIA, L., MERCURI, M., TAVANI, S., PIGNALOSA, A., KETTERMANN, M., BILLI, A. & CARMINATI, E. (2021): 3D Discrete Fracture Network (DFN) models of damage zone fluid corridors within a reservoir-scale normal fault in carbonates: Multiscale approach using field data and UAV imagery.– Marine and Petroleum Geology, 126, 104902. doi: 10.1016/j.marpetgeo.2021.104902

SMITH, S.A.F., BISTACCHI, A., MITCHELL, T.M., MITTEMPERGHER, S. & DI TORO, G. (2013). The structure of an exhumed intraplate seismogenic fault in crystalline basement.– Tectonophysics, 599, 29–44. doi: 10.1016/j.tecto.2013.03.031

STEVANOVIĆ, Z. (2019): Karst waters in potable water supply: a global scale overview.– Environmental Earth Sciences, 78/23, 662. doi: 10.1007/s12665-019-8670-9

STORTI, F., BISTACCHI, A., BORSANI, A., BALSAMO, F., FETTER, M., OGATA, K. (2022). Spatial and spacing distribution of joints at (over-) saturation in the turbidite sandstones of the Marnoso-Arenacea Fm. (Northern Apennines, Italy).– Journal of Structural Geology, 156, 104551. doi: 10.1016/j.jsg.2022.104551

SZANYI, J., RYBACH, L. & ABDULHAQ, H.A. (2023): Geothermal Energy and Its Potential for Critical Metal Extraction – A Review.– Energies, 16/20, 1–28. doi: 10.3390/en16207168

ŠIKIĆ, K. (1981): Facijesi mezozoika Papuckog gorja [Facies of the Mesozoic of Mount Papuk – in Croatian]. – Unpubl. PhD Thesis, Faculty of Science, University of Zagreb.

TARI, G., DÖVÉNYI, P., DUNKL, I., HORVÁTH, F., LENKEY, L., STEFANESCU, M., SZAFIÁN, P. & TÓTH, T. (1999): Lithospheric structure of the Pannonian basin derived from seismic, gravity and geothermal data.– Geological Society, London, Special Publications, 156/1, 215–250. doi: 10.1144/GSL.SP.1999.156.01.12

TAVANI, S., STORTI, F., BAUSÀ, J. & MUÑOZ, J. A. (2012): Late thrusting extensional collapse at the mountain front of the northern Apennines (Italy).– Tectonics, 31/4. doi: 10.1029/2011TC003059

THEIS, C.V. (1935): The relation between the lowering of the Piezometric surface and the rate and duration of discharge of a well using groundwater storage.– Eos, Transactions American Geophysical Union, 16/2, 519–524. doi: 10.1029/TR016i002p00519

THIELE, S.T., GROSE, L., SAMSU, A., MICKLETHWAITE, S., VOLLGGER, S.A. & CRUDEN, A.R. (2017): Rapid, semi-automatic fracture and contact mapping for point clouds, images and geophysical data.– Solid Earth, 8/6, 1241–1253. doi: 10.5194/se-8-1241-2017

TOMLJENOVIĆ, B. & CSONTOS, L. (2001): Neogene-quaternary structures in the border zone between Alps, Dinarides and Pannonian Basin (Hrvatsko zgorje and Karlovac basins, Croatia).– International Journal of Earth Sciences, 90/3, 560–578. doi: 10.1007/s005310000176

TURNER, F.J. (1953): Nature and dynamic interpretation of deformation lamellae in calcite of three marbles.– American Journal of Science, 251/4, 276–298. doi: 10.2475/ajs.251.4.276

TZIAVOU, O., PYTHAROULI, S. & SOUTER, J. (2018): Unmanned Aerial Vehicle (UAV) based mapping in engineering geological surveys: Considerations for optimum results.– Eng. Geol., 232, 12–21. doi: 10.1016/j.enggeo.2017.11.004

UNITED NATIONS (2022): The United Nations World Water Development Report 2022: Groundwater: Making the invisible visible. UNESCO, Paris, 225 p.

URUMOVIĆ, K., TERZIĆ, J., KOPIĆ, J. & KOSOVIĆ, I. (2023): Identification of Aquifer and Pumped Well Parameters Using the Data Hidden in Non-Linear Losses.– Sustainability (Switzerland), 15/14, 11170. doi: 10.3390/su151411170

USTASZEWSKI, K., HERAK, M., TOMLJENOVIĆ, B., HERAK, D. & MATEJ, S. (2014): Neotectonics of the Dinarides-Pannonian Basin transition and possible earthquake sources in the Banja Luka epicentral area.– Journal of Geodynamics, 82, 52–68. doi: 10.1016/j.jog.2014.04.006

USTASZEWSKI, K., SCHMID, S. M., FÜGENSCHUH, B., TISCHLER, M., KISSLING, E. & SPAKMAN, W. (2008): A map-view restoration of the Alpine-Carpathian-Dinaridic system for the Early Miocene.– Swiss Journal of Geosciences, 101/SUPPL. 1. doi: 10.1007/s00015-008-1288-7

USTASZEWSKI, K., KOUNOV, A., SCHMID, S. M., SCHALTEGGER, U., KRENN, E., FRANK, W. & FÜGENSCHUH, B. (2010): Evolution of the Adria-Europe plate boundary in the northern Dinarides: From continent-continent collision to back-arc extension.– Tectonics, 29/6, TC6017. doi: 10.1029/2010TC002668

VERBOVŠEK, T. (2008): Estimation of Transmissivity and Hydraulic Conductivity from Specific Capacity and Specific Capacity Index in Dolomite Aquifers.– Journal of Hydrologic Engineering, 13/9, 817–823. doi: 10.1061/(ASCE)1084-0699(2008)13:9(817)

VOECKLER, H. & ALLEN, D. M. (2012): Estimating regional-scale fractured bedrock hydraulic conductivity using discrete fracture network (DFN) modeling.– Hydrogeology Journal, 20/6, 1081–1100. doi: 10.1007/s10040-012-0858-y

WANG, X. (2005): Stereological interpretation of rock fracture traces on borehole walls and other cylindrical surfaces.– Virginia Techp.

WORTHINGTON, S.R.H., FOLEY, A.E. & SOLEY, R.W.N. (2019): Transient characteristics of effective porosity and specific yield in bedrock

aquifers.– Journal of Hydrology, 578, 124129. doi: 10.1016/j.jhydrol.2019.124129

ZAMBRANO, M., TONDI, E., KORNEVA, I., PANZA, E., AGOSTA, F., JANISECK, J.M. & GIORGIONI, M. (2016): Fracture properties analysis and discrete fracture network modelling of faulted tight limestones, Murge Plateau, Italy.– Italian Journal of Geosciences, 135/1, 55–67. doi: 10.3301/IJG.2014.42

ZEEB, C., GOMEZ-RIVAS, E., BONS, P. D. & BLUM, P. (2013): Evaluation of sampling methods for fracture network characterization using outcrops.– AAPG Bulletin, 97/9, 1545–1566. doi: 10.1306/02131312042

ZHANG, L. & EINSTEIN, H. H. (1998): Estimating the Mean Trace Length of Rock Discontinuities.– Rock Mechanics and Rock Engineering, 31/4, 217–235. doi: 10.1007/s006030050022

URL 1: https://earth.google.com/web/@45.53570123,17.29653113,232.31602905a,6291.71769557d,35y,-12.560923h,2.44982084t,0r/data=OgMKATA (visited April 2024)

URL 2: https://www.pix4d.com/product/pix4dmapper-photogrammetry-software/ (visited April 2024)

URL 3: https://www.cloudcompare.org/ (visited April 2024)

URL 4: https://doi.org/10.5281/zenodo.7890077 (visited April 2024)

URL 5: https://www.mathworks.com/ (visited April 2024)

URL 6: http://qgis.org (visited April 2024)

URL 7: https://doi.org/10.5281/zenodo.11032168 (visited April 2024)

URL 8: https://www.petex.com/products/move-suite/move/ (visited April 2024)

Supplementary Table 1. Average orientations of the measured carbonate beds with computed fold axes.

Strata orientation	Data	Dip direction (°)	Dip angle (°)	Strike	Fold axis orientation	
					Dip direction (°)	Dip angle (°)
So1	29	57	80	147-327	138	42
So2		226	88	136-316		
So3	39	310	66	40-220	228	16
So4		138	88	48-228		

Supplementary Table 2. Average orientation of the three fracture sets in BRQ.

Fracture system	Data	Dip direction (°)	Dip angle (°)	Strike
Fs1a	31	113	81	23-203
Fs1b	28	288	82	18-198
Fs2	42	100	45	10-190
Fs3a	32	22	85	112-292
Fs3b	22	338	73	68-248

Supplementary Table 3. Mean geometrical properties of the observed fault planes with calculated kinematic indicators and parameters. Fault planes (Fault types: R – reverse; N – normal; SSF – strike-slip were grouped following their geometrical properties. Orientations of the P- and T-axes are based on constructed synthetic structural beach-ball diagrams (Fig. 6).

Fault group	Subset	Data	Dip direction (°)	Dip angle (°)	Pitch (°)	Striation		P-axis		T-axis	
						Trend (°)	Plunge (°)	Trend (°)	Plunge (°)	Trend (°)	Plunge (°)
RF	RFa	20	128	56	72	115	43	128	12	336	76
	RFb		289	36	76	261	66				
NF	NFa	11	153	41	81	126	65	14	87	325	11
	NFb		319	50	79	211	68				
SSF-1	SSF-1a	10	150	52	24	78	20	13	17	275	23
	SSF-1b		45	73	17	308	16				
SSF-2	SSF-2a	9	113	66	18	67	11	252	1	345	30
	SSF-2b		211	71	19	124	17				

Supplementary Table 4. Average orientations of the main discontinuity sets in the quarry sections (QS2-QS6) and amount of data constituting the sets.

Quarry section	Set	Data	Dip direction (°)	Dip angle (°)	Strike
QS2	D1a	20	315	76	45-225
	D1b	17	116	83	26-206
	D2a	23	248	53	158-338
	D2b	15	277	57	137-317
	D3	21	272	87	2-182
QS 3A	D1a	132	304	68	34-214
	D1b	43	285	83	15-195
	D2a	140	241	75	151-331
	D2b	74	240	41	150-330
QS 3B	D1a	124	329	70	59-239
	D1b	73	303	77	33-213
	D2	115	258	72	168-348
QS 4	D1a	103	328	70	58-238
	D1b	86	304	69	34-214
	D2	89	254	72	164-344
QS 5	D1	182	308	71	38-218
	D2	115	267	72	177-357
QS 6	D1a	16	331	70	61-241
	D1b	9	313	72	43-223
	D2a	5	270	60	0-180
	D2b	8	265	81	175-355

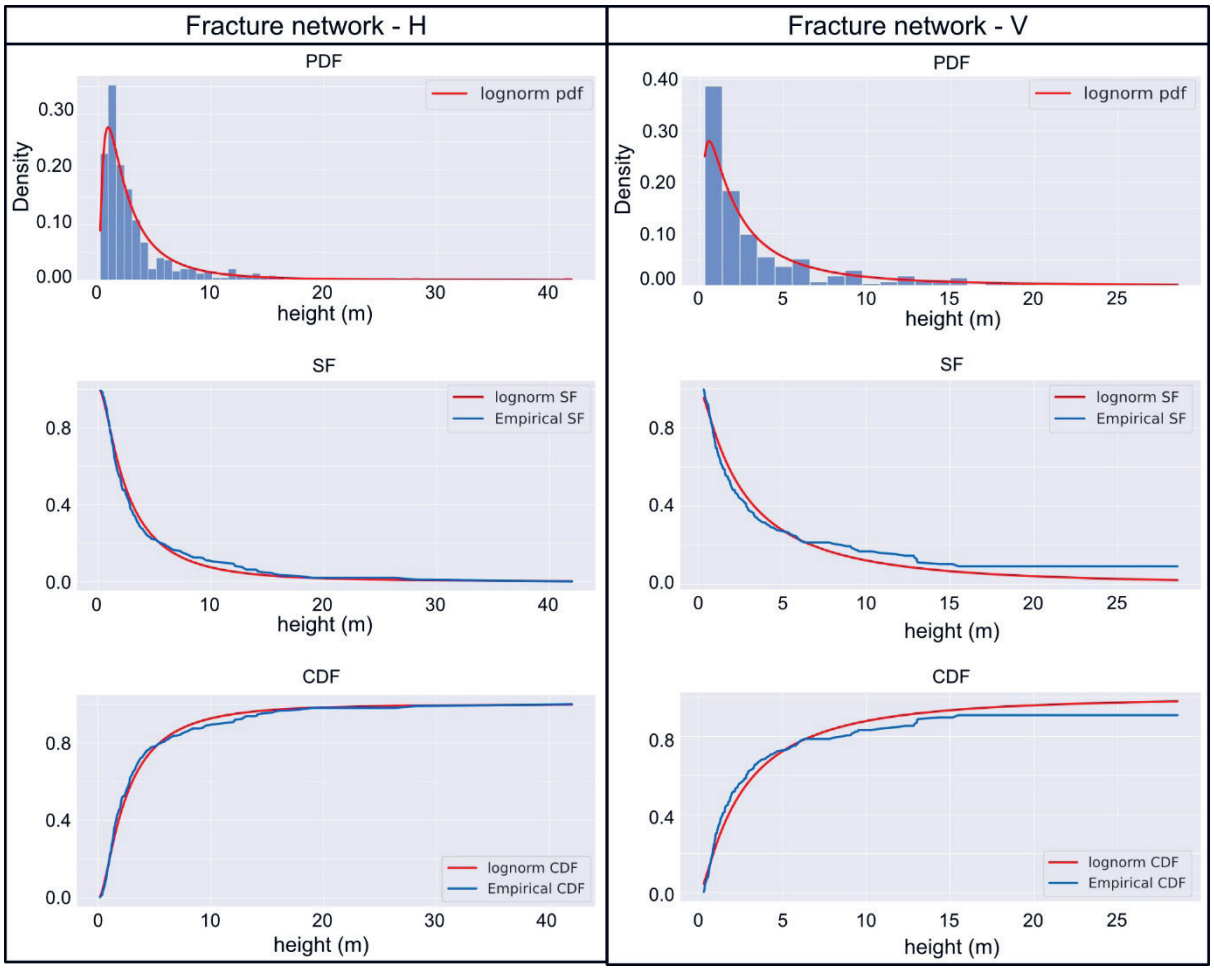

Supplementary Figure 1. Statistical distribution of the heights of the horizontal (H) and vertical (V) fracture network (Quarry Section - 3A). Statistical analysis of the main geometrical parameter (height) was performed by using FracAbility.

Supplementary Table 5. Results of statistical analysis for the horizontal (H) and vertical (V) discontinuity network.

	Discontinuity set - H		Fracture network - V	
Total number of fractures	352		260	
% censored	11.08		20	
	Data	Fit	Data	Fit
Mean	3.5306	3.8836	3.6673	5.0660
Median	2.0381	2.3812	1.8787	2.4461
Mode	0.2029	0.8952	0.3225	0.5703
B5	0.5387	0.4680	0.4375	0.3361
B95	12.4790	12.1160	13.1371	17.8025
Std	4.5250	5.0036	4.5258	9.1879
Var	20.4755	25.0358	20.4825	84.4173

Supplementary Table 6. Input parameters used for the construction of the DFN model of the QS3A section. The measurement units of the parameters are reported in brackets. The obtained model is shown in Fig. 10.

Parameter	Set - H	Set - V
Dip direction	240.86	295.86
Dip	64.92	74.79
Fisher K	13.53	18.83
Height – mean *(m)*	3.88	5.06
Height – STD *(m)*	5.00	9.18
Length/Height ratio	0.25	0.25
Sum of fractures heights *(m)*	1244.96	961.19
P21 *(m/m^2)*	0.47	0.37
P32 *(m^2/m^3)*	1.98	1.18
Aperture *(mm)*	4.15	4.15

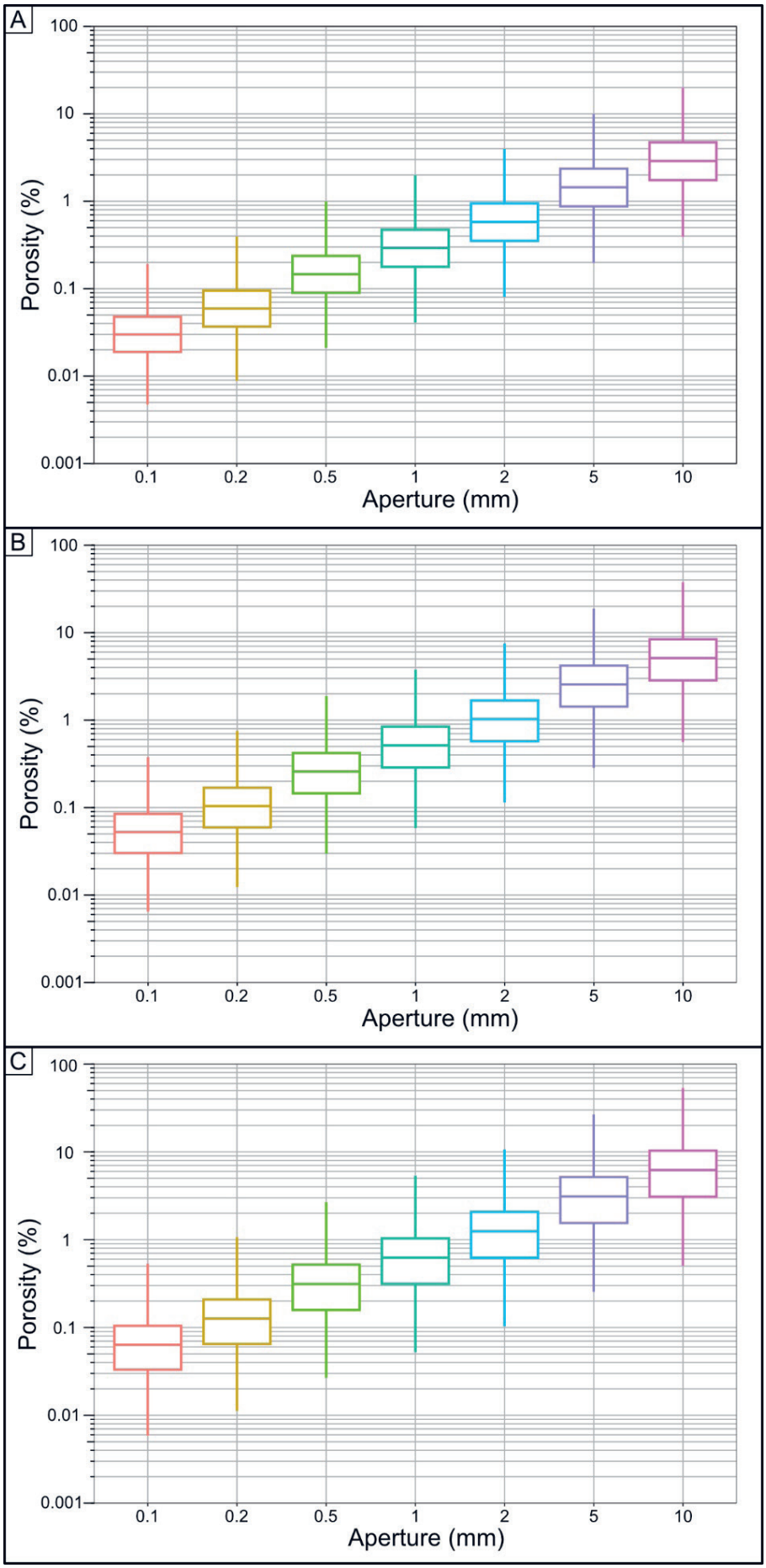

Supplementary Figure 2. Distributions of porosity (Φ) obtained for the tested aperture values and employing the different methodological approaches.

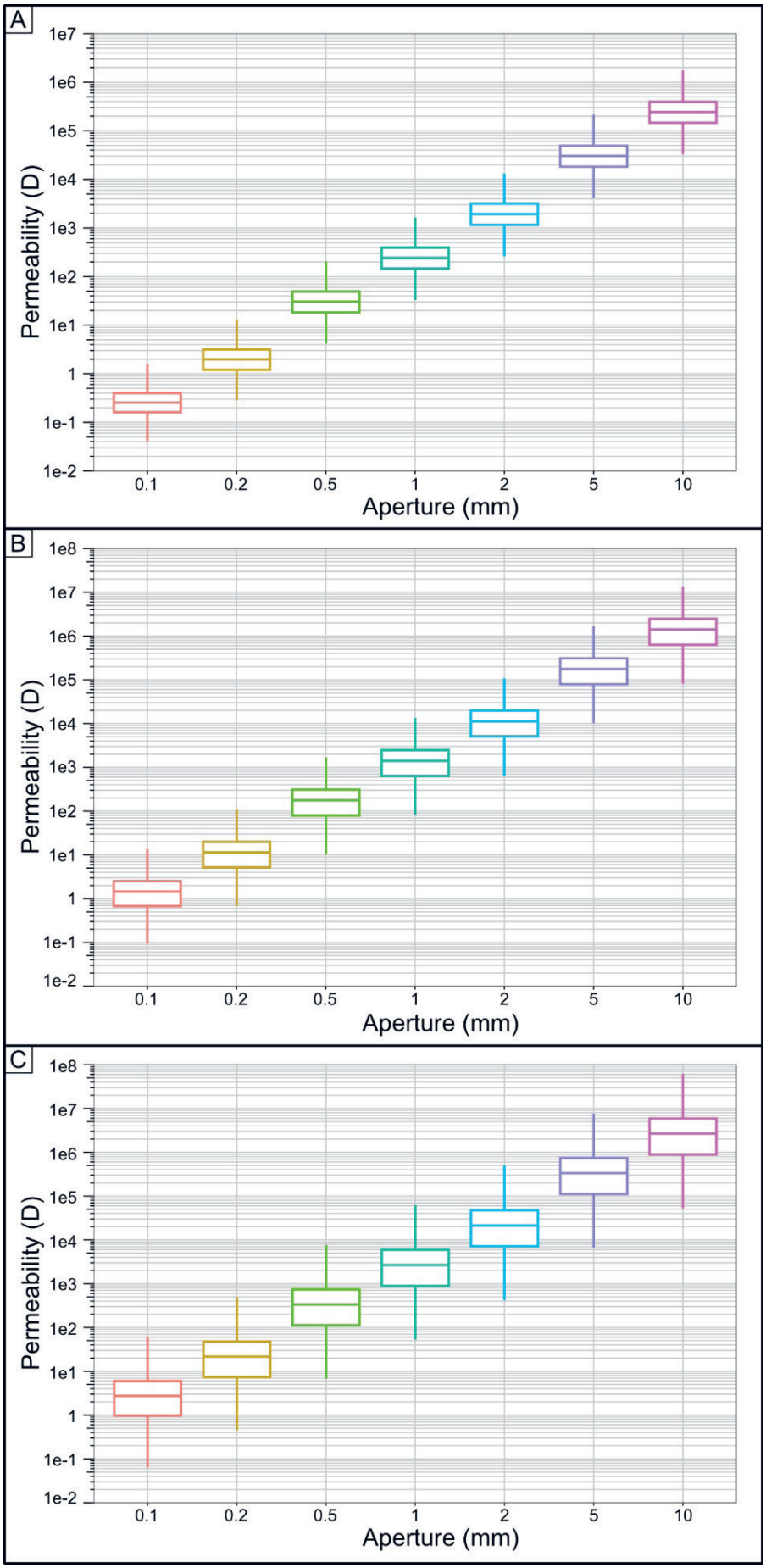

Supplementary Figure 3. Distributions of permeability (k) obtained for the tested aperture values and employing the different methodological approaches.

Supplementary Table 7. Statistical distributions of the porosity (Φ) in the DFN models conducted considering different methodological approaches for assigning the fracture aperture and using different aperture values.

Aperture (mm)		Porosity – Φ (%)											
		Mean	Median	Standard deviation	Min	Max	Skewness	Kurtosis	10th perc.	25th perc.	50th perc.	75th perc.	90th perc.
Constant	0.1	0.03	0.03	0.02	0.00	0.24	0.91	3.85	0.00	0.01	0.03	0.05	0.06
	0.2	0.06	0.05	0.05	0.00	0.47	0.91	3.85	0.00	0.02	0.05	0.09	0.13
	0.5	0.15	0.13	0.12	0.00	1.18	0.91	3.85	0.00	0.05	0.13	0.23	0.32
	1	0.30	0.26	0.25	0.00	2.37	0.91	3.85	0.00	0.11	0.26	0.45	0.64
	2	0.61	0.51	0.49	0.00	4.73	0.91	3.85	0.00	0.22	0.51	0.90	1.29
	5	1.52	1.28	1.23	0.00	11.83	0.91	3.85	0.00	0.55	1.28	2.25	3.21
	10	3.04	2.56	2.46	0.00	23.65	0.91	3.85	0.00	1.10	2.56	4.50	6.43
Root square length	0.1	0.05	0.05	0.04	0.00	0.43	0.97	4.00	0.00	0.02	0.05	0.08	0.11
	0.2	0.11	0.09	0.09	0.00	0.86	0.97	4.00	0.00	0.04	0.09	0.16	0.23
	0.5	0.27	0.23	0.22	0.00	2.14	0.97	4.00	0.00	0.09	0.23	0.40	0.57
	1	0.53	0.46	0.44	0.00	4.28	0.97	4.00	0.00	0.18	0.46	0.79	1.14
	2	1.07	0.91	0.88	0.00	8.57	0.97	4.00	0.00	0.36	0.91	1.59	2.28
	5	2.67	2.29	2.21	0.00	21.42	0.97	4.00	0.00	0.91	2.29	3.97	5.70
	10	5.34	4.57	4.42	0.00	42.84	0.97	4.00	0.00	1.81	4.57	7.94	11.41
Length	0.1	0.07	0.05	0.06	0.00	0.53	1.09	4.34	0.00	0.02	0.05	0.10	0.14
	0.2	0.13	0.11	0.11	0.00	1.07	1.09	4.34	0.00	0.04	0.11	0.20	0.29
	0.5	0.33	0.27	0.28	0.00	2.67	1.09	4.34	0.00	0.10	0.27	0.49	0.72
	1	0.65	0.55	0.57	0.00	5.35	1.09	4.34	0.00	0.19	0.55	0.98	1.44
	2	1.31	1.09	1.14	0.00	10.69	1.09	4.34	0.00	0.39	1.09	1.95	2.88
	5	3.27	2.73	2.85	0.00	26.73	1.09	4.34	0.00	0.97	2.73	4.88	7.19
	10	6.54	5.47	5.70	0.00	53.46	1.09	4.34	0.00	1.93	5.47	9.75	14.38

Supplementary Table 8. Statistical distribution of the permeability (k) in the DFN models conducted considering different methodological approaches for assigning the fracture aperture and using different aperture values.

Aperture (mm)		Permeability – k (D)											
		Mean	Median	Standard deviation	Min	Max	Skewness	Kurtosis	10th perc.	25th perc.	50th perc.	75th perc.	90th perc.
Constant	0.1	2.5e-1	2.2e-1	2.e-1	0.00	1.9	0.85	3.69	0.00	9.3e-2	2.2e-1	3.8e-1	5.3e-1
	0.2	2	1.7	1.6	0.00	1.5e1	0.85	3.69	0.00	7.4e-1	1.7	3	4.3
	0.5	3.2e1	2.7e1	2.5e1	0.00	2.3e2	0.85	3.69	0.00	1.2e1	2.7e1	4.7e1	6.6e1
	1	2.5e2	2.2e2	2.e2	0.00	1.9e3	0.85	3.69	0.00	9.3e1	2.2e2	3.8e2	5.3e2
	2	2.e3	1.7e3	1.6e3	0.00	1.5e4	0.85	3.69	0.00	7.4e2	1.7e3	3.e3	4.3e3
	5	3.2e4	2.7e4	2.5e4	0.00	2.3e5	0.85	3.69	0.00	1.2e4	2.7e4	4.7e4	6.6e4
	10	2.5e5	2.2e5	2.e5	0.00	1.9e6	0.85	3.69	0.00	9.3e4	2.2e5	3.8e5	5.3e5
Root square length	0.1	1.6	1.2	1.5	0.00	1.4e1	1.28	4.99	0.00	3.8e-1	1.2	2.3	3.6
	0.2	1.2e1	9.8e	1.2e1	0.00	1.1e2	1.28	4.99	0.00	3.1	9.8	1.9e1	2.9e1
	0.5	2.e2	1.5e2	1.8e2	0.00	1.7e3	1.28	4.99	0.00	4.8e1	1.5e2	2.9e2	4.5e2
	1	1.6e3	1.2e3	1.5e3	0.00	1.4e4	1.28	4.99	0.00	3.8e2	1.2e3	2.3e3	3.6e3
	2	1.2e4	9.8e3	1.2e4	0.00	1.1e5	1.28	4.99	0.00	3.1e3	9.8e3	1.9e4	2.9e4
	5	2.e5	1.5e5	1.8e5	0.00	1.7e6	1.28	4.99	0.00	4.8e4	1.5e5	2.9e5	4.5e5
	10	1.6e6	1.2e6	1.5e6	0.00	1.4e7	1.28	4.99	0.00	3.8e5	1.2e6	2.3e6	3.6e6
Length	0.1	3.8	2.2	4.8	0.00	6.1e1	2.40	11.22	0.00	4.7e-1	2.2	5.4	9.7
	0.2	3.1e1	1.7e1	3.8e1	0.00	4.9e2	2.40	11.22	0.00	3.8	1.7e1	4.3e1	7.8e1
	0.5	4.8e2	2.7e2	6.e2	0.00	7.7e3	2.40	11.22	0.00	5.9e1	2.7e2	6.7e2	1.2e3
	1	3.8e3	2.2e3	4.8e3	0.00	6.1e4	2.40	11.22	0.00	4.7e2	2.2e3	5.4e3	9.7e3
	2	3.1e4	1.7e4	3.8e4	0.00	4.9e5	2.40	11.22	0.00	3.8e3	1.7e4	4.3e4	7.8e4
	5	4.8e5	2.7e5	6.e5	0.00	7.7e6	2.40	11.22	0.00	5.9e4	2.7e5	6.7e5	1.2e6
	10	3.8e6	2.2e6	4.8e6	0.00	6.1e7	2.40	11.22	0.00	4.7e5	2.2e6	5.4e6	9.7e6

Supplementary Table 9. Hydrogeological parameters obtained from the interpretation of the pumping test using Dar 1 as exploitation well and D 1 and DS 1 as observation wells. The estimated parameters are: transmissivity (T), storativity (S), hydraulic conductivity anisotropy ratio (Kz/Kr), and saturated thickness (b).

Parameter	Whole test	Constant test
T (m^2/s)	3.82e-2	3.46e-2
S (-)	2.05e-3	1.14e-3
Kz/Kr (-)	6.81e-3	1.98e-2
b (m)	61.53	68.42

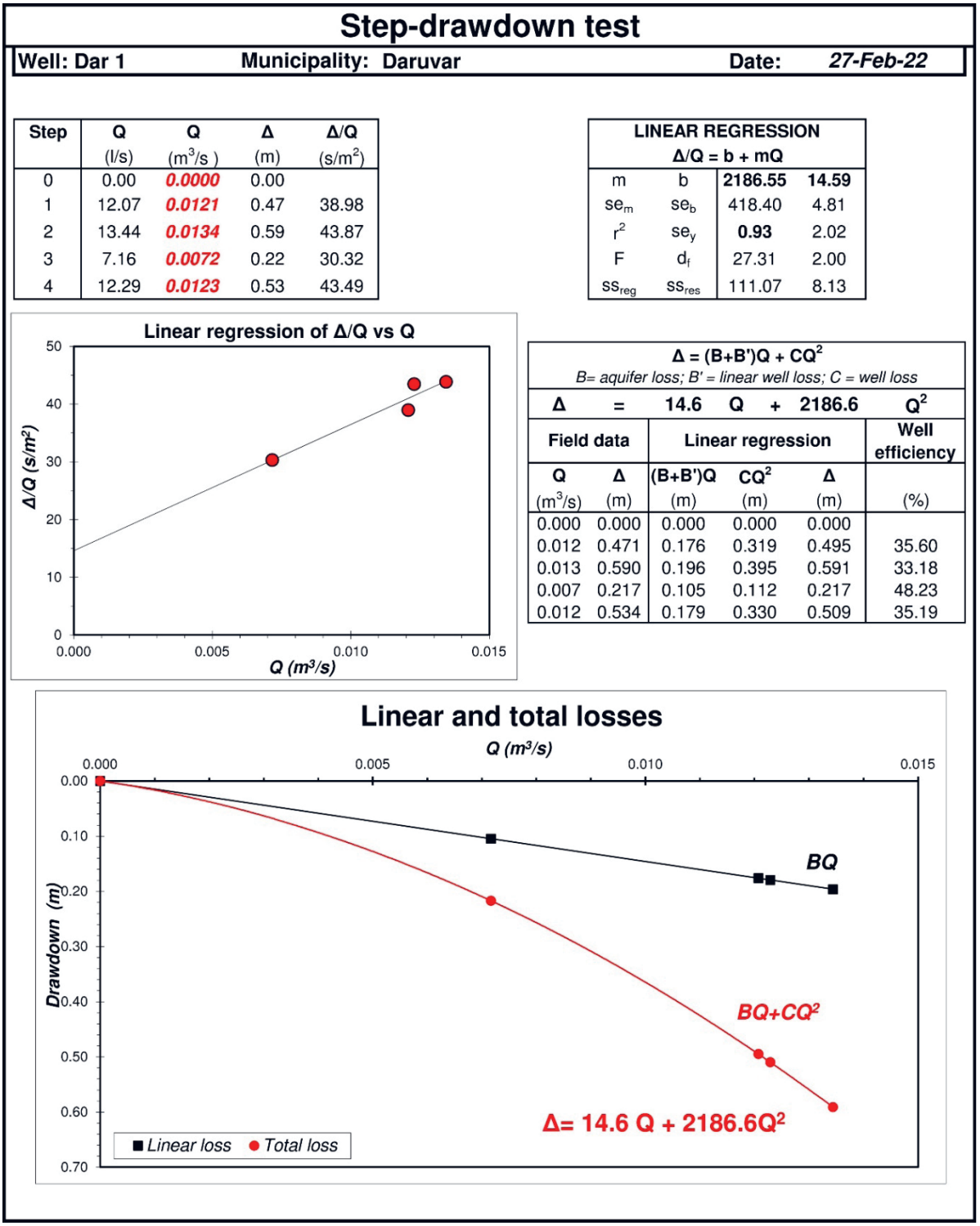

Supplementary Figure 4. Interpretation of the step-drawdown test results conducted in the Dar 1 well.

6. DISCUSSION

To achieve the objectives of the research, four hypotheses were tested using the described multidisciplinary methodology. According to the set hypotheses, the synthesis of the results is presented and discussed below.

Hypothesis #1: Regional and local geological and structural-geological influence on the development of DHS.

Detailed reconstruction of the geological and tectonic settings is crucial to determine the processes favoring the circulation of thermal waters and influencing the renewability of the geothermal resource and the sustainability of its exploitation (MAGRI et al., 2010; FAULDS et al., 2013; SCHECK-WENDEROTH et al., 2014; BREHME et al., 2016; POLA et al., 2020; TORRESAN et al., 2021). The geo-tectonic reconstruction of a certain area is generally conducted by integration of field investigations and geophysical data, at regional and local scales. While field investigations enable the reconstruction of the surficial geometry of geological formations and fractures and the assessment of the kinematics of the principal faults, geophysical data can add crucial subsurface constraints to the surficial geological reconstruction. Geological and geophysical datasets can be integrated to construct a 3D geological model of the subsurface (e.g., PAVIČIĆ et al., 2018; OLIEROOK, 2020; JIA et al., 2021; PANZERA et al., 2022). As a result, 3D modeling in geological and hydrogeological applications provides a useful tool for interpreting and visualizing the impact of geological structures on the development of hydrothermal systems.

The study area (Figure 1) is located along the western margin of Mount Papuk, which is part of the Slavonian Mountains. Its structural architecture was significantly influenced by the proximity of the Sava suture zone, which was the Cretaceous-Paleogene regional suture zone between the Tisza block toward NE and the Adria microplate block toward SW (e.g., SCHMID et al., 2020), and the development of the Pannonian basin system (PBS), which was affected by a Miocene-Quaternary polyphase extension, compression, and tectonic inversion (e.g., BALEN et al., 2006). The complex structural pattern of generally E-W striking thrust faults (i.e., Voćin fault, Gradina fault, Dežanovac fault, and Daruvar fault) and multi-folded structures gently dipping towards both NNW and SSE or ENE and WSW suggests a polyphase evolution of the study area which onset with the regional Cretaceous-Paleogene E-W contraction (KOSOVIĆ et al., 2024a). This contraction formed an initial pattern of NW-SE striking faults and NNW and SSE dipping folds (Figure 7A). A counterclockwise regional rotation of approximately 40°

towards NE occurred during the Paleogene (TOMLJENOVIĆ & CSONTOS, 2001; USTASZEWSKI et al., 2008) resulting in the final structural emplacement of existing faults and folds, reoriented as E-W striking thrust faults and ENE and WSW dipping fold system. The Neogene was characterized by a regional E-W extension with the formation of dominantly normal faults, but inherited faults/fold systems experienced only partial tectonic stretching and gravitational sliding in the study area. The Pliocene-Quaternary regional N-S compression/transpression promoted continuous shortening and re-folding processes of existing structures coeval with the formation of dextral/sinistral faults (e.g., Toplica fault), which locally displaced existing E-W striking thrust faults (Figure 7A). The final structural architecture of the study area and its evolution, assessed through the results of field geological investigations, are in line with the regional polyphase tectonic history of the Croatian part of the PBS (e.g., JAMIČIĆ, 1995; PRELOGOVIĆ et al., 1998; LUČIĆ et al., 2001; TOMLJENOVIĆ & CSONTOS, 2001; SAFTIĆ et al., 2003).

Geological relationships at the surface and subsurface of the study area were described in detail using constructed composite geological profiles reaching an investigation depth of approximately 2.5 km (KOSOVIĆ et al., 2024a). Here, the DHS-3 geological profile from KOSOVIĆ et al. (2024a) is used as an example to describe the geological units, tectonic styles, and structures since it is located in the central part of the study area (Figure 7B).

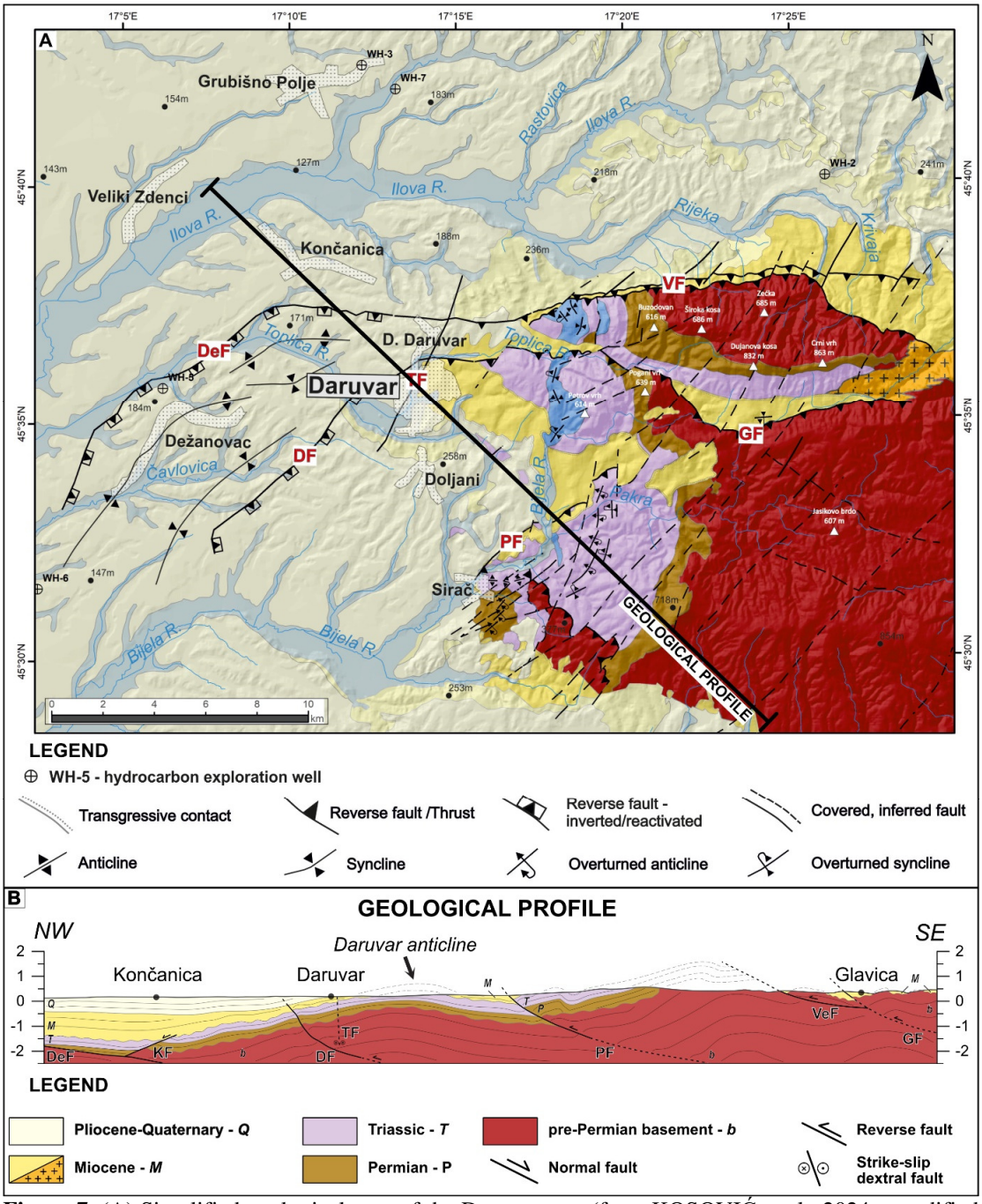

Figure 7. (A) Simplified geological map of the Daruvar area (from KOSOVIĆ et al., 2024a; modified from JAMIČIĆ et al., 1989; ŠOLAJA, 2010). Fault acronyms: DF, Daruvar fault; DeF, Dežanovac fault; GF, Gradina fault; PF, Pakrac fault; TF, Toplica fault; VF, Voćin fault. Topographic peaks are denoted by white triangles. White polygons indicate larger settlements and towns. The black line in the figure represents the trace of the geological profile. (B) Composite geological profile investigating the central part of the study area (modified from KOSOVIĆ et al., 2024a). It shows the Daruvar anticline deforming the subsurface in the vicinity of Daruvar. The horizontal and vertical scale is 1:1.

Structurally, two domains can be distinguished (Figure 7B). The NW domain covers the area of the Lonja-Ilova subdepression, filled by Neogene-Quaternary sediments that are up to 1.5 km thick, while the pre-Neogene basement is composed of Permian-Triassic sedimentary units and pre-Permian crystalline rocks (MALVIĆ & VELIĆ, 2011). The Permian-Triassic sedimentary complex is generally following the pre-Permian basement paleorelief. From NW towards SE, the Permian-Triassic complex is shallowing reaching the surface in the vicinity of the Daruvar city. N-S striking normal faults (e.g., Munije 1 and Munije 2) pinpoint the Neogene extension in the PBS and the opening of accommodation space (Figure 7B). Furthermore, differential thicknesses of the Neogene deposits in the fault's hangingwall/footwall suggest structural reactivation and tectonic inversion (e.g., Dežanovac fault). The pre-Neogene complex of the Lonja-Ilova subdepression crops out forming the western slopes of Mount Papuk. Here, the contact between the Neogene-Quaternary sediments and the pre-Neogene rock complex is mainly transgressive, but dozens of mapped tectonic contacts indicate NW-SE contraction. Reverse faults are generally associated with cogenetic asymmetric folds characterized by gently inclined NW limbs and steeper and shorter SE limbs. This peculiar geometry suggests structure tectonic transport towards N-NW. Daruvar anticline is an example of a gentle asymmetric anticline associated with the Daruvar-Gradina reverse faults. It generally resembles a remobilized pre-Permian structural high that was transgressively covered by Permian-Triassic sediments and faulted afterward. In this context, the subvertical Toplica fault could be interpreted as a tensional fracture system developed in the hinge zone of the Daruvar anticline that was probably later reactivated as a dextral strike-slip fault zone (KOSOVIĆ et al., 2023, 2024a).

The SE parts of the constructed profile reflect the structural architecture of the western margin of the Slavonian mountains (Figure 7B). Here, the tectonic uplift of the crystalline basement resulted in overall exposure of pre-Permian basement due to the erosion of the Permian-Mesozoic cover, while at the local scale, we could find patches of transgressively deposited Neogene sediments. The structural architecture of this area is cogenetic with two principal reverse low angle faults, i.e., NNE striking Voćin and Gradina faults which accommodated regional N-S compression.

Following the principal structural discontinuities, the structural framework of the Daruvar hinterland can be divided into three structural domains separated by regional E-W or NE-SW striking reverse faults: i) Dujanova kosa, ii) Petrov vrh, and iii) Sirač. Mesozoic carbonates (i.e., the main thermal aquifer) extensively crop out in all these domains representing potential recharge areas of the DHS. Due to their peculiar architecture, these domains can be considered

as separated hydrogeological compartments. The Sirač and Dujanova kosa domains were excluded as potential recharge areas due to their morphological, geological, and hydrogeological settings affecting the lateral continuity of the aquifer or reducing the potential pressure drive for the fluid flow. In the conceptual model of DHS proposed during this research (KOSOVIĆ et al., 2024a), the recharge area of the system is located in the Petrov vrh domain in accordance with the conceptual model proposed by BOROVIĆ et al. (2019). The geological and structural architecture of Petrov vrh is characterized by the regional NNE-SSW striking Daruvar asymmetric anticline formed in the hangingwall of the SE dipping Daruvar reverse fault and the connected E-W striking Gradina thrust fault (Figure 7B). This structure favors both the extensive outcropping of the Mesozoic carbonate rock complex in the recharge area and the fracturing of the bedrock. The elevation of the Petrov vrh recharge area (average value of 400 m a.s.l.; maximum value of 613 m a.s.l.) is higher than the elevation in the Daruvar outflow area (value of approximately 160 m a.s.l.) promoting the development of a topographically driven groundwater flow system (FOSTER & SMITH, 1998). Furthermore, it should be pointed out that the elevation in Petrov vrh is higher than the elevation in both Dujanova kosa and Sirač domains (average value of 397 and 349 m a.s.l. in Dujanova kosa and Sirač, respectively; maximum value of 570 and 552 m a.s.l. in Dujanova kosa and Sirač, respectively). This promotes a higher hydraulic drive provided to the DHS by the Petrov vrh recharge area than other potential recharge areas. Since the distance between the recharge and the outflow areas is from 4 to 8 km, the DHS can be considered as an intermediate groundwater system following the seminal work of TOTH (1963).

Hypothesis #2: Fracture networks are preferential flow paths in the DHS.

Fracture networks and fault damage zones represent preferred flow paths in fractured aquifers due to their higher permeability and porosity fields than the surrounding host rock with low permeability and porosity (e.g., CAINE et al., 1996; BENSE et al., 2013). The spatial distribution of deformation structures and stress orientation of the youngest tectonic events are often conditioned by pre-existing discontinuities that represent weakened zones in the subsurface. The constant deformation keeps the fracture open, prevents the sealing of the fracture by deposition of minerals, and can lead to the widening of the existing damage zone and the secondary sets of fractures and folds. The combination of these processes promotes the permeability/porosity of the fracture locally increasing the permeability/porosity of the aquifer and acting as a preferential flow path for the fluid flow (FAULKNER et al., 2010).

Structural data analysis of strata orientation, fracture systems, and fault systems presented in this study corroborates the complexity of the tectonic evolution in the Daruvar area (KOSOVIĆ et al., 2024a). Cogenetically with the formation of folded and refolded structures, the Mesozoic carbonate complex experienced extensive brittle deformation. Measured fractures resembled N-S (locally NNE-SW, NNW-SSE) and subordinately E-W striking subvertical tensional fractures that were subparallel with the observed fold hinge zones. N-S striking fracture systems show shear reactivation features (e.g., slickenside overgrowths) characterized by dextral/sinistral motions. This reactivation is connected to the Pliocene-Quaternary N-S oriented P-axis (HERAK et al., 2009). On the other hand, E-W striking discontinuities are less frequent and generally without indications of structural reactivation suggesting that E-W striking folded structures are less affected by ongoing tectonic deformation due to their structural position and the low regional strain rates (<1–2 mm/y; GRENERCZY et al., 2005; HERAK et al., 2009).

The influence of fault and fracture systems on the fluid flow in DHS was highlighted in the hydrogeological conceptual model proposed during this research (KOSOVIĆ et al., 2024a). Structural analysis conducted in the recharge area of Petrov vrh (Figure 8) revealed two sets of steeply dipping fractures that generally strike E-W (NE-SW) and N-S (NW-SE). Due to the recent N-S oriented stress field, the N-S discontinuities could have a wider and highly deformed damage zone connected to their reactivation. The E-W discontinuities are less frequent, but they may be affected by a local transtensional regime in the hinge zone of the currently deformed E-W oriented folds. These observed structural relations in the Petrov vrh area are favorable for the high permeability of the bedrock resulting in a high effective infiltration in the recharge area. The low permeability pre-Permian crystalline rocks and the Permian sedimentary units act as aquitards beneath the Mesozoic aquifer, both preventing the deeper infiltration of the waters and channeling the fluid flow (e.g., DOMENICO & SCHWARTZ, 1998). Dissolution processes in the Mesozoic carbonates could add to the fracturing enhancing their permeability field (e.g., GOLDSCHEIDER et al., 2010). This permeability contrast prevents a deep infiltration of the meteoric waters that are more prone to flow in the carbonate aquifer. In addition, the dipping of the aquitard units toward W channels the fluid flow favoring the westward circulation of the infiltrated waters. Finally, the E-W fractures could act as preferential regional flow paths.

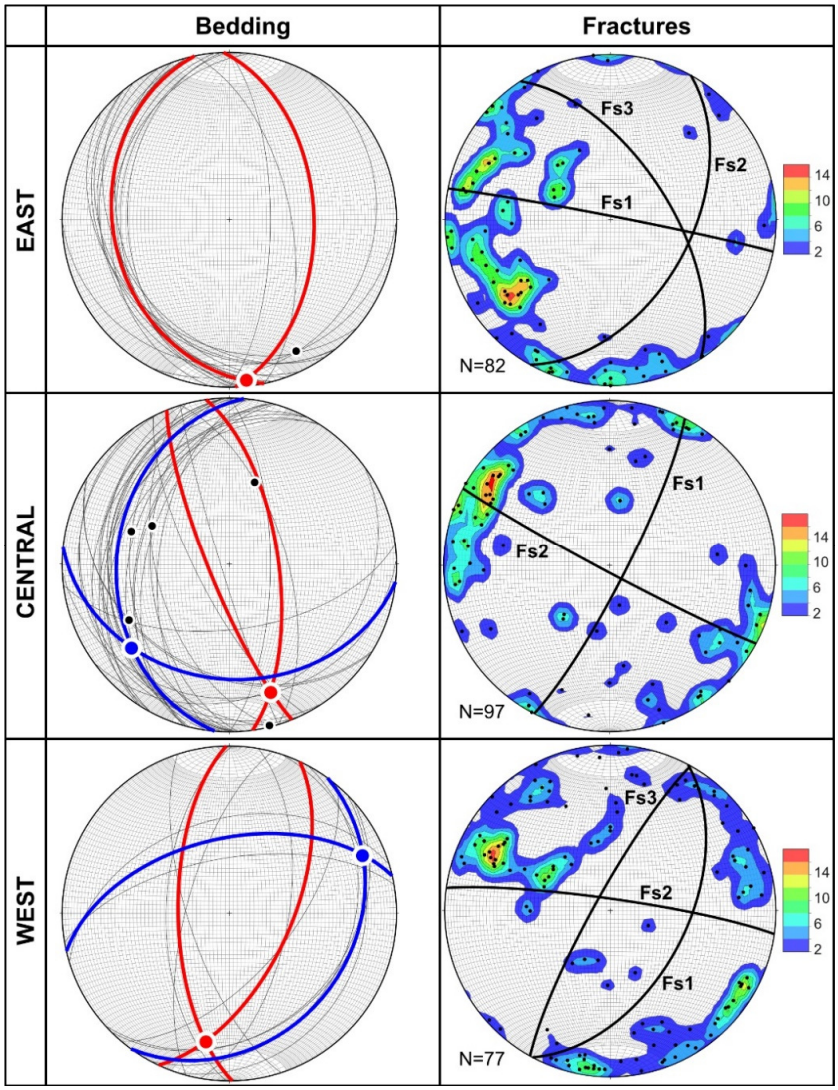

Figure 8. Stereonets of the bedding and fracture orientations in the eastern, central, and western sections of Petrov vrh (modified from KOSOVIĆ et al., 2024a). Interpretation of bedding highlights the occurrence of two generations of folds (thick blue and red circles) with different fold axes (blue and red points) corroborating a polyphase tectonic evolution with processes of refolding. The orientations of the representative fracture systems (Fs) in the Petrov vrh domain are obtained from the distribution of the measured discontinuities (contour plot using a rainbow color ramp) represented here as poles (black points; N: amount of data). The fracture sets are compatible with the observed folding and its reactivation.

Hypothesis #3: Extensive tectonized fault zones in the Daruvar area allow the rising of thermal waters.

The thermal waters flow in the Mesozoic aquifer and reach the town of Daruvar where natural thermal springs occur (Antunovo vrelo, Blatna kupelj, and Ivanovo vrelo springs; Figure 4). The subsurface architecture is affected by the NNE-SSW striking Daruvar asymmetric fold

cogenetically formed in the hangingwall of the SE dipping Daruvar reverse fault (Figure 9A; KOSOVIĆ et al., 2024a). The polyphase tectonic evolution of the Daruvar anticline considerably affected the structural framework of the area which favored continuous Paleogene-Quaternary fracturing of the bedrock. Considering well-established conceptual models of the stress regime in fault-related folds (FREHNER, 2011; LI et al., 2018; NABAVI & FOSSEN, 2021), a localized extensional regime is expected in the topmost section of the fold hinge zone increasing the fracture aperture and the permeability field (KOSOVIĆ et al., 2024a,b). Field observations and core samples from the thermal wells showed that the Mesozoic aquifer is characterized by a uniform background fracture network with localized corridors showing a higher frequency of fractures. The thermal waters rise to shallow depths in the damage zone of the Daruvar fault and cogenetic fractures that are deforming the hinge of the Daruvar anticline. In this context, the subvertical N-E striking dextral Toplica fault, which is a structurally reactivated and tectonically inverted tensional fracture system, could act as a preferential flow path for the quick rise of the thermal waters with a minor loss of temperature from the deeper part of the aquifer (Figure 9A; KOSOVIĆ et al., 2023, 2024a). The Toplica fault could be the fault F5 in the local scale model of the Daruvar spring area obtained through shallow geophysical investigations (Figure 9B; KOSOVIĆ et al., 2023). This fault borders the Daruvar thermal field westwardly, and together with an E-W striking fault to the S (F1 in Figure 9B) accommodated the uplift of the Mesozoic thermal aquifer to shallower depths. The geophysical investigations furthermore highlighted that the main outflow of the Daruvar thermal waters occurs within the interaction zone of local scale faults/fractures resulting in four thermal springs with temperatures between 38 and 50 °C. Interaction zones between faults and fracture systems are preferential locations for the occurrence of thermal springs since the kinematic transfer between the faults increases the rock fracturing and enhances the permeability field (CUREWITZ et al., 1997; FAULDS et al., 2013).

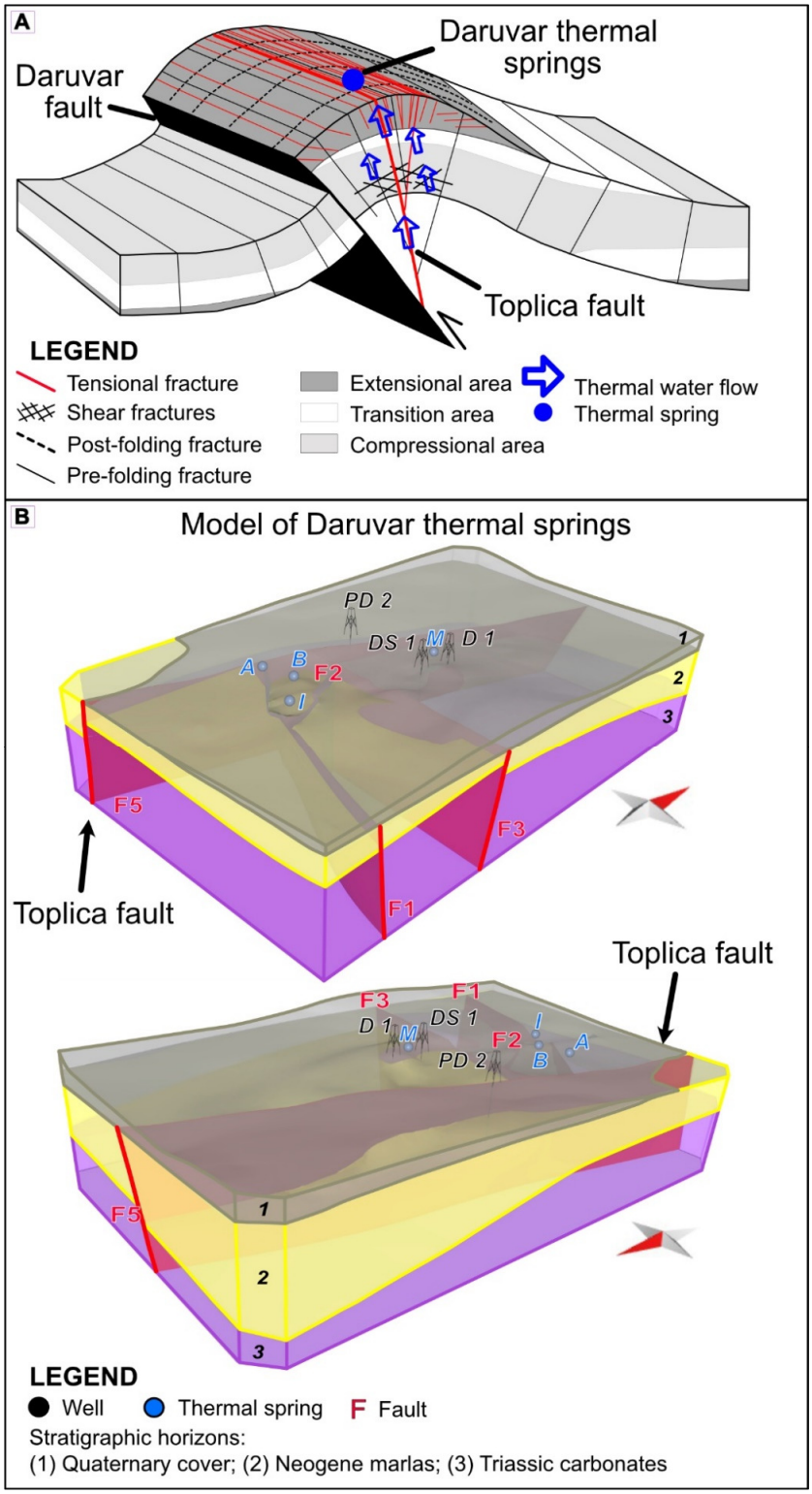

Figure 9. (A) Schematic conceptual model of the structural assemblage in the subsurface of the Daruvar area (from KOSOVIĆ et al., 2024a, modified from FREHNER, 2011 and LI et al., 2018) affecting the upwelling of the Daruvar thermal waters. The NNE-SSW striking Daruvar anticline structurally forms in the hangingwall of the Daruvar reverse fault. In the hinge zone, cogenetic tensional fractures were structurally reactivated during the Pliocene-Quaternary and tectonically inverted as a strike-slip fault

zone (i.e., Toplica fault). The localized extensional regime in the topmost part of the hinge zone and its polyphase deformation increase the fracturing of the bedrock and the permeability field favoring the outflow of the thermal waters in the Daruvar spring area. (B) Fi Three stratigraphic units and four faults were identified.

Hypothesis #4: Hydrogeological parameters in dolomite aquifers can be determined through numerical modeling of fracture systems

The assessment of the hydrogeological properties of fractured aquifers is generally conducted through discrete fracture network (DFN) numerical modeling or well testing and logging. Remote sensing photogrammetry allows the construction of a 3D digital model of the outcrop favoring the collection of large datasets for a detailed quantitative description and statistical analysis of geological object's geometry and their spatial relationships (HODGETTS, 2013; BISTACCHI et al., 2015; MARTINELLI et al., 2020). Through the constraining of the digital outcrop model (DOM) with field measurements of the geometrical features of the fracture network, the results can be used as input parameters of DFN modeling for the hydrogeological parametrization of the rock mass. DFN models reproduce each fracture as a discrete object with peculiar hydraulic properties surrounded by an impermeable matrix (LEI et al., 2017; MEDICI et al., 2023), and they are profitably used to determine the permeability of fractured carbonates (e.g., ANTONELLINI et al., 2014; KORNEVA et al., 2015; ZAMBRANO et al., 2016; GIUFFRIDA et al., 2019; ROMANO et al., 2020; SMERAGLIA et al., 2021). The distribution of the hydrogeological parameters obtained from the DFN modeling can be constrained using the results of field hydrogeological and geophysical investigations like pumping tests and well logging. In pumping tests, the hydraulic properties (mostly transmissivity and hydraulic conductivity) of the aquifer are assessed by modeling the variations of the drawdown in observation wells due to the extraction of groundwater using analytical solutions (e.g., KRUSEMAN et al., 2000). Well logging is used to image the distribution of lithologies and fractures in the well and to quantitatively assess the distribution of several petrophysical parameters in the subsurface (LAI et al., 2024).

In this research, both structural and hydrogeological investigations were conducted in the Daruvar thermal area and its immediate hinterland and combined to assess the porosity (Φ) and permeability (k) of the carbonate thermal aquifer (KOSOVIĆ et al., 2024b). Structural measurements and photogrammetric imagining were conducted in the Batinjska Rijeka quarry (BRQ), which provides an extensive outcrop of the Mesozoic carbonate rock complex and can be considered as an outcrop analog of the Daruvar thermal aquifer. The results of the DOM

virtual structural analysis depicted two dominant subvertical systems (D1 and D2) of discontinuities that reflect bedding and fracture systems from field investigations. A section of the quarry (QS3A in KOSOVIĆ et al., 2024b) was selected for a detailed analysis of the geometrical features of the discontinuity sets (set V and H corresponding to D1 and D2, respectively) deriving the input parameters for the DFN modeling (Table 1). The geometrical features of these systems (i.e., dip direction, dip angle, Fisher K, mean height, height standard deviation, total height, length/height ratio, P21, Table 1) obtained from the DOM were used as input parameters used for the construction of DFN models. DFN models were constructed at different scales resembling: i) the outcrop investigated with the virtual structural analysis (XYZ: 100×100×30 m), and ii) the thermal aquifer in Daruvar investigated through the pumping test of Dar 1 well (XYZ: 700×700×150 m; Figure 10A). The parameters P32 and aperture of the fractures were required by the software to complete the DFN models and were estimated after a calibration procedure. The calibration of the P32 (volumetric intensity) was conducted using the outcrop scale DFN starting from the P21 (areal intensity) obtained from the DOM analysis, while the calibration of the aperture was conducted iteratively to fit the Φ and k values from hydrogeological investigations using both DFN models.

Parameter	Set - H	Set - V
Dip direction	240.86	295.86
Dip	64.92	74.79
Fisher K	13.53	18.83
Height – mean *(m)*	3.88	5.06
Height – STD *(m)*	5.00	9.18
Length/Height ratio	0.25	0.25
Total height *(m)*	1244.96	961.19
P21 *(m/m^2)*	0.47	0.37
P32 *(m^2/m^3)*	1.98	1.18
Aperture for Φ *(mm)* – outcrop scale DFN	4.15	4.15
Aperture for Φ *(mm)* – aquifer scale DFN	3	3
Aperture for k *(mm)* – aquifer scale DFN	0.22	0.22

Table 1. Input parameters used for the construction of the DFN models conducted at the outcrop and aquifer scale (modified from KOSOVIĆ et al., 2024b). The measurement units of the parameters are reported in brackets. The values of P32 and aperture were obtained after a calibration. In particular, a "dual aperture" approach was used for the calibration of the fracture aperture with experimental porosity (Φ) and permeability (k) values. The obtained model for the aquifer scale DFN is shown in Figure 10.

Hydrogeological investigations in the Daruvar area have been conducted since the 1970s consisting in well loggings and pumping and well tests to assess the transmissivity (T) of the

aquifer (BOROVIĆ, 2015; BOROVIĆ et al., 2019; URUMOVIĆ et al., 2023). Within this research, the results of the pumping test conducted exploiting the Dar 1 well in 2022 were analyzed (KOSOVIĆ et al., 2024b). The dataset of T from the different sources was used to calculate the aquifer k resulting in values from 7.4 to 122.8 D considering different thicknesses of the aquifer obtained from the stratigraphic log of Dar 1 well (Table 2). The Φ of the aquifer was obtained through a neutron log conducted in Dar 1. Since the distribution of Φ values showed a large variability due to local collapses of the walls in the well, a section with tight walls (depth of 100–130 m) was considered to obtain a more realistic Φ. The average Φ for this section was 2.7% (Table 2) being within the range of Φ in carbonates (NG & SANTAMARINA, 2023).

Different values of fracture aperture were tested in the DFN models obtaining a linear and power correlation with Φ and k, respectively (Figures 10B and 10C, respectively). Considering the Φ at a depth of 100-130 m, the calibrated aperture values were 4.1 and 3 mm for the outcrop and aquifer scale DFN, respectively. These values are slightly different due to the different grid sizes used for the discretization of the modeled volumes. The resulting average k values were 2.7×10^5 and 1.5×10^5 D for the outcrop and aquifer scale DFNs, respectively, being 3-4 orders of magnitude higher than the measured k (Table 2). This discrepancy was interpreted as connected to the fact that the fracture aperture was calibrated using the distribution of Φ obtained from the neutron log of the Dar 1 well, which determines the total Φ of the aquifer. However, fractured aquifers usually have a dual porosity with most of the storage volume being in the matrix and most of the flow being in the fracture network (SINGHAL & GUPTA, 2010). Therefore, the fluid flow is influenced by the effective Φ that can be at least one order of magnitude less than total Φ in fractured carbonate aquifers (WORTHINGTON et al., 2019). The difference between total and effective Φ was accounted in the conducted DFN models using a “dual aperture” approach and was tested in the aquifer scale DFN. Using the linear relation between the aperture and Φ, the fracture aperture for obtaining a Φ of 0.27% (i.e., one order of magnitude lower than the average Φ at the depth of 100-130 m; Table 2) was calculated and input to the model. The calculated fracture aperture was 0.3 mm resulting in a k value of 149.4 D, which is slightly higher than the experimental values. The effective Φ value was refined on the basis of the experimental Φ dataset, and the 10^{th} percentile of the Φ distribution was tested (Table 2). The corresponding fracture aperture (0.22 mm) was input to the model resulting in k value of 0.2% and 60.5 D, respectively. The k value fits with the experimental values being in the range of the k calculated from f (total thickness of fracture corridors in Dar

1 well) and slightly higher than the values obtained from d and b (saturated thickness from pumping test and investigated thickness of dolomites in Dar 1, respectively; Table 2).

		Average value	Minimum - Maximum	10^{th} - 90^{th} percentile
Investigated thickness of dolomite	*d (m)*	130	-	-
Saturated thickness	*b (m)*	65	61.5 – 68.4	-
Thickness of fracture corridors	*f (m)*	24		
Transmissivity	*T* (m^2/s)	3.5e-2	1.6e-2 - 4.8e-2	2.5e-2 - 4.3e-2
Storativity	*S (-)*	1.6e-3	1.1e-3 – 2e-3	-
Hydraulic conductivity anisotropy ratio	*Kz/Kr (-)*	1.3e-2	6.8e-3 – 2e-2	-
Permeability from d	*k d (D)*	16.4	7.4 - 22.7	11.8 - 20.3
Permeability from b	*k b (D)*	32.7	14.8 - 45.3	23.6 - 40.6
Permeability from f	*k f (D)*	88.7	40 - 122.8	63.8 - 109.9
Porosity	*Φ (%)*	7.9	0.03 - 42	0.9 - 17.4
Porosity at depth 100-130 m	*Φ* (%)*	2.7	0.03 - 9.1	0.2 - 6.3

Table 2. Hydrogeological parameterization of the Daruvar thermal aquifer obtained from: i) the interpretation of pumping and well tests in this study, ii) the well logging of Dar 1 well, and iii) the literature (BOROVIĆ et al., 2019; URUMOVIĆ et al., 2023).

The obtained results highlight the importance of employing both structural and hydrogeological approaches in the investigation of fractured aquifers. Still, the integration between these two disciplines is limited due to different methods and investigation scales (e.g., BENSE et al., 2013). However, structural data can be used to determine the architecture of the network of fractures and discontinuities in the rock mass, while hydrogeological investigations supported by numerical modeling calibrated from structural results can provide a solid hydrogeological parametrization of the aquifer (e.g., SINGHAL & GUPTA, 2010; MEDICI et al., 2023).

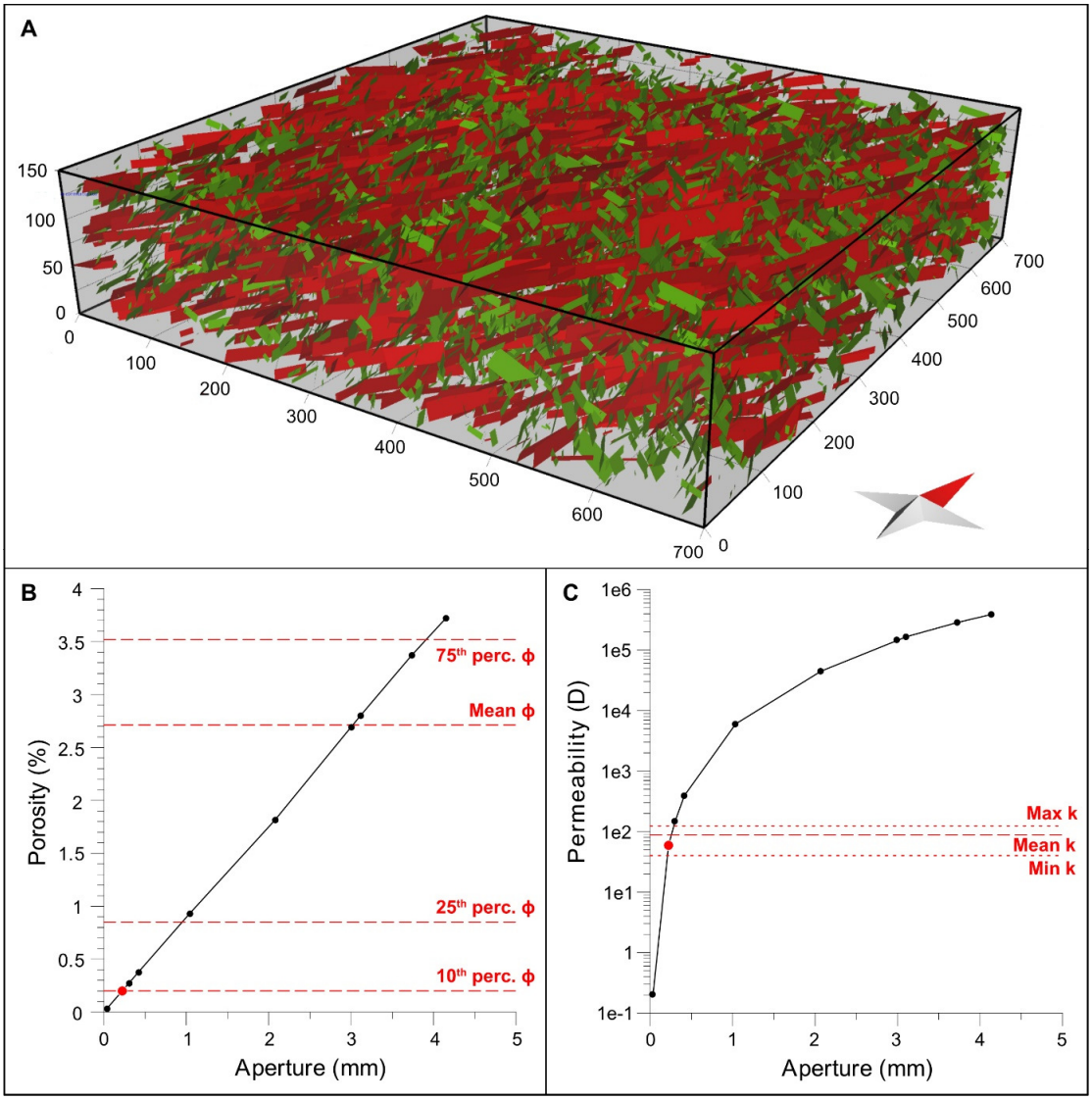

Figure 10. (A) The aquifer scale DFN model was obtained using the input parameters in Table 1. The red and green discontinuities (1% of the generated discontinuities is shown) represent the V and H discontinuity sets, respectively. (B-C) Porosity and permeability values (black dots) were obtained from the aquifer scale DFN using different fracture apertures. The results of the best model (aperture of 0.22 mm) are shown as red dots pointing to a good fit with the experimental data (dashed lines).

7. CONCLUSION

The sustainable exploitation of a geothermal resource for its long-term utilization is related to both the water demand and the geological and hydrogeological characteristics of the geothermal field. Detailed geological modeling is a key factor for estimating the potential of a geothermal resource. Highly fractured Mesozoic carbonate rocks form the main reservoir for many geothermal resources in northern Croatia. One of the most significant thermal manifestations in this region is the thermal springs area in the Daruvar city with water temperatures ranging from 38 to 50°C. These springs are part of the Daruvar hydrothermal system (DHS), an intermediate scale, tectonically controlled, system hosted within a Mesozoic carbonate rock complex.

This research focused on the reconstruction of the geological framework and the tectonic evolution of western Papuk and the geological impact on the development of the Daruvar hydrothermal system (DHS) and its geothermal resource. The objectives were to: i) assess the influence of the regional and local structural-geological setting on the development of DHS, ii) determine the main preferential flow paths in the DHS, iii) quantify the impact of tectonized fault zones on the rising of thermal waters in the Daruvar area, and iv) obtain a solid hydrogeological parametrization of the fractured carbonate aquifer.

Here, the reconstruction of the geological assemblage allowed: i) the detailing of the geometries of the reservoir and the regional and local scale fault and fold systems, and ii) the assessment of geological impact on the fluid flow and the water/rock interaction in the DHS. The field investigations dataset was integrated with geological and geophysical data to develop composite geological profiles and a 3D geological model of the study area. Results display a pattern of generally N-S and E-W striking folds and cogenetic fracture systems with orientations parallel to the fold axes, where E-W striking fracture systems are regional flow paths that enable infiltration of meteoric water to 1 km depth and the heating by the local geothermal gradient.

In the Daruvar area, anticline and fault/fracture systems accommodated the uplift of the carbonate reservoir to shallow depths, promoting the bedrock fracturing and increase of the permeability field. The polyphase tectonic evolution affecting the study area suggests Pliocene-Quaternary structural reactivation of the Daruvar anticline favoring the continuous fracturing of the bedrock. A localized extensional regime was identified in the topmost section of the fold hinge zone which increases the fracture aperture and the permeability field of the Daruvar thermal spring area. Accordingly, the thermal waters rose to shallow depths in the damage zone

of the Daruvar and Toplica faults and their cogenetic fractures that deformed the hinge of the Daruvar anticline. In this context, the subvertical N-E striking dextral Toplica fault, which is a structurally reactivated and tectonically inverted tensional fracture system, could act as a preferential flow path for the quick rise of the thermal waters with a minor loss of temperature from the deeper part of the carbonate reservoir. The results of the geophysical investigations combined into a 3D geological model highlighted that the main outflow of the Daruvar thermal waters occurs within the interaction zone of local scale subvertical N-S and E-W trending faults/fractures.

Besides the geological and structural investigations of the regional and local geological assemblage, hydrogeological investigations were conducted in the Daruvar thermal area and combined with the results of detailed local scale structural investigations to detail the hydrogeological setting of the Daruvar thermal aquifer and its hydrogeological parametrization. Structural investigations were conducted in an outcrop analog of the thermal aquifer (i.e., Batinjska Rijeka quarry), employing both a classical field approach and the virtual quantitative structural analysis of the discontinuity network through a 3D digital outcrop model. The assessment of the hydrogeological properties of fractured aquifers was conducted through discrete fracture network numerical modeling or well testing and logging. The main geometric features of the discontinuity network and their statistical distributions were employed to construct discrete fracture network models at both the outcrop scale (approximately 100 m) and the aquifer scale in Daruvar (approximately 700 m). Calibration of the input parameters allowed the modeling of porosity and permeability values that reproduce the field values assessed through pumping tests, well tests, and well logging.

A multidisciplinary and multiscale methodological approach was used in this research for the geological reconstruction of the study area, the proposal of a new hydrogeological conceptual model of the DHS, and the hydrogeological parametrization of the fractured carbonate reservoir. This approach combined structural, geophysical, and hydrogeological investigations conducted at regional and local scales. The results of this research demonstrate the applicability of integrating different methodologies in the hydrogeological characterization of fractured carbonate aquifers. Beside classical hydrogeological investigations, structural investigations can provide insights into the reservoir geometry and the main discontinuity systems that are preferential paths for the fluid flow. In the context of the exploration of geothermal systems, the regional geological setting, the architecture of the aquifer, and the main flow paths influence the thermal and hydrochemical features of the connected geothermal resource. The integration of multidisciplinary investigations can provide a comprehensive

overview of the impact of geological processes favoring the development of detailed plans for the sustainable exploitation of the resource. The approach used in this research can be applied to similar geothermal systems in carbonate rocks that represent one of the main thermal aquifers in northern Croatia and the Pannonian basin area. This aquifer hosts several local scale hydrothermal systems that flow out in thermal springs but are not explored by wells. The proposed approach can provide a first insight into the hydrogeological properties of the aquifer, which can be used for planning the exploration of the geothermal resource. Furthermore, the used approach can be extended to the hydrogeological investigations of carbonate aquifers that are valuable groundwater resources in the whole Mediterranean area.

8. REFERENCES

ANGELIER, J. & MECHLER, P. (1977): Sur une methode graphique de recherche des contraintes principales egalement utilisables en tectonique et en seismologie : la methode des diedres droits.– Bulletin de la Société Géologique de France, S7-XIX(6), 1309–1318. doi: 10.2113/gssgfbull.S7-XIX.6.1309.

AXELSSON, G. (2010). Sustainable geothermal utilization - case histories; definitions; research issues and modelling.– Geothermics 39, 283–291. doi:10.1016/j.geothermics.2010.08.001.

BABIĆ, Ž., ŠIKIĆ, V., MRAZ, V. (1971): Hidrogeološka Istraživanja Termomineralnih Vrela Kupališnog Lječilišta Daruvar (Hydrogeological Research of Thermomineral Springs at Daruvar Spa); Institut za Geološka Istraživanja Zagreb: Zagreb, Croatia.

BALEN, D., HORVÁTH, P., TOMLJENOVIĆ, B., FINGER, F., HUMER, B., PAMIĆ, J. & ÁRKAI, P. (2006): A record of pre-Variscan Barrovian regional metamorphism in the eastern part of the Slavonian Mountains (NE Croatia).– Mineralogy and Petrology, 87(1–2), 143–162. doi: 10.1007/s00710-006-0120-1.

BENSE, V. F., GLEESON, T., LOVELESS, S.E., BOUR, O. & SCIBEK, J. (2013): Fault zone hydrogeology.– Earth-Science Reviews, 127, 171–192. doi: 10.1016/j.earscirev.2013.09.008.

BENEDETTI, G., CASIRAGHI, S., BISTACCHI, A., & BERTACCHI, D. (2024): FracAbility: A python toolbox for survival analysis in fractured rock systems.– EGU General Assembly 2024, Vienna, Austria, 14–19 Apr 2024, EGU24-22156. https://doi.org/10.5194/egusphere-egu24-22156, 2024.

BOROVIĆ, S. & MARKOVIĆ, I. (2015): Utilization and tourism valorisation of geothermal waters in Croatia.– Renewable and Sustainable Energy Reviews, 44, 52–63. doi: 10.1016/j.rser.2014.12.022.

BOROVIĆ, S., POLA, M., BAČANI, A. & URUMOVIĆ, K. (2019): Constraining the recharge area of a hydrothermal system in fractured carbonates by numerical modelling.– Geothermics, 82, 128–149. doi: 10.1016/j.geothermics.2019.05.017.

BUNDSCHUH, J. & CÉSAR SUÁREZ, A. M. (2010): Introduction to the numerical modeling of groundwater and geothermal systems. London: CRC Press. doi:10.1201/b10499.

CHENG, F., XIA, J., AJO-FRANKLIN, J.B., BEHM, M., ZHOU, C., DAI, T., XI, C., PANG, J., ZHOU, C. (2021): High-Resolution Ambient Noise Imaging of Geothermal

Reservoir Using 3C Dense Seismic Nodal Array and Ultra-Short Observation.– Journal of Geophysical Research: Solid Earth, 126, e2021JB021827.

CUREWITZ, D. & KARSON, J. A. (1997): Structural settings of hydrothermal outflow: fracture permeability maintained by fault propagation and interaction.– Journal of Volcanology and Geothermal Research, 79, 149–168. doi:10.1016/S0377-0273(97)00027-9

DOBLAS, M. (1998): Slickenside kinematic indicators.– Tectonophysics, 295(1–2), 187–197.

DOMENICO, P. A. & SCHWARTZ, F. W. (1998): Physical and chemical hydrogeology. New York: Wiley.

FAYBISHENKO, B., WITHERSPOON, P. A. & BENSON, S. M. (2000): Dynamics of Fluids in Fractured Rock.Geophysical Monograph Series. Vol. 122.– American Geophysical Union, Washington, D. C. doi:10.1029/GM122.

FAULDS, J. E., HINZ, N. H., DERING, G. M. & SILER, D. L. (2013): The hybrid model — the most accommodating structural setting for geothermal power generation in the great basin, western USA.– Geothermal Resource Council Transactions, 37, 4–10.

FINSTER, M., CLARK, C., SCHROEDER, J. & MARTINO, L. (2015): Geothermal produced fluids: Characteristics, treatment technologies, and management options.– Renewable and Sustainable Energy Reviews, 50, 952–966. doi: 10.1016/j.rser.2015.05.059.

FORSTER, C. & SMITH, L. (1988): Groundwater flow systems in mountainous terrain: 1. Numerical modeling technique.– Water Resources Research, 24(7), 999.

FREHNER, M. (2011): The neutral lines in buckle folds.– Journal of Structural Geology, 33, 1501–1508. doi:10.1016/j.jsg.2011.07.005

GOLDSCHEIDER, N., MÁDL-SZŐNYI, J., ERŐSS, A. & SCHILL, E. (2010): Revisión: Recursosde aguas termales en acuíferos de rocas carbonáticas.– Hydrogeology Journal, 18, 1303–1318. doi:10.1007/s10040-010-0611-3

GRENERCZY, G., SELLA, G., STEIN, S. & KENYERES, A. (2005): Tectonic implications of the GPS velocity field in the northern Adriatic region.– Geophysical Research Letters, 32, 1–4. doi:10.1029/2005GL022947.

GWD (2006): Groundwater Directive 2006/118/CE, Directive of the European Parliament and of the Council on the protection of groundwater against pollution and deterioration, OJ L372, 27/12/ 2006.

HANDY, M.R., USTASZEWSKI, K., KISSLING, E. (2015): Reconstructing the Alps–Carpathians–Dinarides as a Key to Understanding Switches in Subduction Polarity, Slab

Gaps and Surface Motion.– Internal Journal of Earth Science, 104, 1–26. doi:10.1007/s00531-014-1060-3.

HANTUSH, M.S. (1961a): Aquifer Tests on Partially Penetrating Wells.– Journal of the Hydraulics Division, 87(5), 171–195. doi: 10.1061/JYCEAJ.0000639.

HERAK, D., HERAK, M. & TOMLJENOVIĆ, B. (2009): Seismicity and earthquake focal mechanisms in North-Western Croatia.– Tectonophysics 465, 212–220.

HORVÁTH, F., MUSITZ, B., BALÁZS, A., VÉGH, A., UHRIN, A., NÁDOR, A., KOROKNAI, B., PAP, N., TÓTH, T. & WÓRUM, G. (2015): Evolution of the Pannonian basin and its geothermal resources.– Geothermics, 53(January 2015), 328–352. doi: 10.1016/j.geothermics.2014.07.009.

HYMAN, J.D., KARRA, S., MAKEDONSKA, N., GABLE, C.W., PAINTER, S.L. & VISWANATHAN, H. S. (2015): dfnWorks: A discrete fracture network framework for modeling subsurface flow and transport.– Computers & Geosciences, 84, 10–19. doi: 10.1016/j.cageo.2015.08.001.

JAMIČIĆ, D. (1995): The role of sinistral strike-slip faults in the formation of the structural fabric of the Slavonian Mts. (eastern Croatia).– Geologia Croatica, 48(2), 155–160.

JAMIČIĆ, D., VRAGOVIĆ, M. & MATIČEC, D. (1989): Osnovna geološka karta SFRJ 1:100 000. Tumač za list Daruvar (Basic geological map of SFRJ 1:100 000. Explanatory notes for sheet Daruvar). – Geol. zavod, Zagreb, Sav. geol. zavod Beograd, Beograd, 55 p.

KOSOVIĆ, I., BRIŠKI, M., PAVIĆ, M., PADOVAN, B., PAVIČIĆ, I., MATOŠ, B., POLA, M. & BOROVIĆ, S. (2023): Reconstruction of Fault Architecture in the Natural Thermal Spring Area of Daruvar Hydrothermal System Using Surface Geophysical Investigations (Croatia).– Sustainability, 15(16), 12134. doi: 10.3390/su151612134.

KOSOVIĆ, I., MATOŠ, B., PAVIČIĆ, I., POLA, M., MILEUSNIĆ, M., PAVIĆ, M. & BOROVIĆ, S. (2024a): Geological modeling of a tectonically controlled hydrothermal system in the southwestern part of the Pannonian basin (Croatia).– Frontiers in Earth Science, 1401935. doi: 10.3389/feart.2024.1401935.

KOSOVIĆ, I., MATOŠ, B., CASIRAGHI, S., BENEDETTI, G., FRANGEN, T., URUMOVIĆ, K., PAVIČIĆ, I., BISTACCHI, A., MITTEMPERGHER, S., POLA, M. & BOROVIĆ, S. (2024b): Hydrogeological parameterisation of the Daruvar thermal aquifer: Integration of fracture network analysis and well testing.– Geologia Croatica, 77(2), 99-125. doi: 10.4154/gc.2024.11.

KRUSEMAN, G. P., DE RIDDER, N. A. & VERWEIJ, J. M. (2000): Analysis and evaluation of pumping test data.Vol. 47. – International institute for land reclamation and improvement, Wageningen, 378 p.

LAI, J., SU, Y., XIAO, L., ZHAO, F., BAI, T., LI, Y., LI, H., HUANG, Y., WANG, G. & QIN, Z. (2024): Application of geophysical well logs in solving geologic issues: Past, present and future prospect.Geoscience Frontiers, 15/3, 101779. doi:10.1016/j.gsf.2024.101779

LARVA, O. & MRAZ, V. (2008): Daruvarske toplice - elaborat utvrđivanja eksploatacijske izdašnosti Ivanovog vrela i objekta Š-3 (Daruvar thermal field – determination of the exploitation yield of the Ivano vrelo spring and the Š-3 well). Zagreb.

LI, Y., HOU, G., HARI, K. R., NENG, Y., LEI, G., TANG, Y. et al. (2018). The model of fracture development in the faulted folds: the role of folding and faulting.– Marine Petroleum Geology, 89, 243–251. doi:10.1016/j.marpetgeo.2017.05.025.

LÉVY, L., MAURYA, P.K., BYRDINA, S., VANDEMEULEBROUCK, J., SIGMUNDSSON, F., et al. (2019): Electrical Resistivity Tomography and Time-Domain Induced Polarization Field Investigations of Geothermal Areas at Krafla, Iceland: Comparison to Borehole and Laboratory Frequency-Domain Electrical Observations.– Geophysical Journal International, 218, 1469–1489. doi.org/10.1093/gji/ggz240.

LOKE, M.H., CHAMBERS, J.E., RUCKER, D.F., KURAS, O., WILKINSON, P.B. (2013): Recent Developments in the Direct-Current Geoelectrical Imaging Method.– Journal of Applied Geophysics, 2013, 95, 135–156. doi.org/10.1016/j.jappgeo.2013.02.017.

LUČIĆ, D., SAFTIĆ, B., KRIZMANIĆ, K., PRELOGOVIĆ, E., BRITVIĆ, V., MESIĆ, I., TADEJ, J. (2001): The Neogene Evolution and Hydrocarbon Potential of the Pannonian Basin in Croatia.– Marine Petroleum Geology, 18, 133–147.

LUND, J. W. & TOTH, A. N. (2021): Direct utilization of geothermal energy 2020 worldwide review.– Geothermics, 90, 101915. doi: 10.1016/j.geothermics.2020.101915.

MARGAT, J. & DER GUN, J. (2013): Groundwater around the world: a geographic synopsis. – Crc Press, Boca Raton, 341 p.

MEDICI, G., LING, F. & SHANG, J. (2023): Review of discrete fracture network characterization for geothermal energy extraction.– Frontiers in Earth Science, 11(December), 1–17. doi: 10.3389/feart.2023.1328397.

MOECK, I. S. (2014): Catalog of geothermal play types based on geologic controls.– Renewable and Sustainable Energy Reviews, 37, 867–882. doi:10.1016/ j.rser.2014.05.032

MRAZ, V. (1983): Izvještaj o Hidrogeološkim istražnim radovima na području Daruvarskih Toplica II. Faza (Report on Conducted Hydrogeological Research in Daruvar Spa—Phase II); Geološki zavod Zagreb: Zagreb, Croatia.

NABAVI, S. T. & FOSSEN, H. (2021): Fold geometry and folding – a review.– Earth-Science Review, 222, 103812. doi:10.1016/j.earscirev.2021.103812

OFTERDINGER, U., MACDONALD, A.M., COMTE, J.C. & YOUNG, M.E. (2019): Groundwater in fractured bedrock environments: managing catchment and subsurface resources – an introduction.– Geological Society, London, Special Publications, 479(1), 1–9. doi: 10.1144/SP479-2018-170.

PAVIĆ, M., KOSOVIĆ, I., POLA, M., URUMOVIĆ, K., BRIŠKI, M. & BOROVIĆ, S. (2023): Multidisciplinary Research of Thermal Springs Area in Topusko (Croatia).– Sustainability, 15(6), 5498. doi: 10.3390/su15065498.

PRELOGOVIĆ, E., SAFTIĆ, B., KUK, V., VELIĆ, J., DRAGAŠ, M. & LUČIĆ, D. (1998): Tectonic activity in the Croatian part of the Pannonian basin.– Tectonophysics, 297(1–4), 283–293. doi: 10.1016/S0040-1951(98)00173-5.

RYBACH, L. & MONGILLO, M. (2006): Geothermal Sustainability-A Review with Identified Research Needs.– Geothermal Resource Council Transactions, 30, 1083–1090.

SAFTIĆ, B., VELIĆ, J., SZTANO, O., JUHASZ, G. & IVKOVIĆ, Ž. (2003): Tertiary Subsurface Facies, Source Rocks and Hydrocarbon Reservoirs in the SW Part of the Pannonian Basin (Northern Croatia and South-Western Hungary).– Geologia Croatica, 56(1), 101–122. doi: 10.4154/232.

SCHMID, S. M., FÜGENSCHUH, B., KOUNOV, A., MAŢENCO, L., NIEVERGELT, P., et al. (2020): Tectonic units of the Alpine collision zone between Eastern Alps and western Turkey.– Gondwana Research, 78(July 2019), 308–374. doi: 10.1016/j.gr.2019.07.005.

SCHMID, S.M., BERNOULLI, D., FÜGENSCHUH, B., MATENCO, L., SCHEFER, S., SCHUSTER, R., TISCHLER, M. & USTASZEWSKI, K. (2008): The Alpine-Carpathian-Dinaridic orogenic system: correlation and evolution of tectonic units.– Swiss Journal of Geosciences, 101(1), 139–183. doi: 10.1007/s00015-008-1247-3.

SIEGEL, L., GOLDSCHEIDER, N., PETITTA, M., XANKE, J., ANDREO, B., et al. (2023): Distribution, threats and protection of selected karst groundwater-dependent ecosystems in the Mediterranean region.– Hydrogeology Journal, 31(8), 2231–2249. doi: 10.1007/s10040-023-02711-9.

SINGHAL, B. B. S. & GUPTA, R. P. (2010): Applied Hydrogeology of Fractured Rocks. – Springer Netherlands, Dordrecht. doi:10.1007/978-90-481-8799-7.

STEVANOVIĆ, Z. (2019): Karst waters in potable water supply: a global scale overview.– Environmental Earth Sciences, 78(23), 662. doi: 10.1007/s12665-019-8670-9.

SZANYI, J., RYBACH, L. & ABDULHAQ, H. A. (2023): Geothermal Energy and Its Potential for Critical Metal Extraction—A Review.– Energies, 16(20), 1–28. doi: 10.3390/en16207168.

ŠIKIĆ, K. (1981): Facijesi mezozoika Papuckog gorja (Facies of the Mesozoic of Mount Papuk– in Croatian). – Unpubl. PhD Thesis, Faculty of Science, University of Zagreb.

THEIS, C.V. (1935): The relation between the lowering of the Piezometric surface and the rate and duration of discharge of a well using ground-water storage.– Eos, Transactions American Geophysical Union, 16(2), 519–524. doi: 10.1029/TR016i002p00519.

THIELE, S. T., GROSE, L., SAMSU, A., MICKLETHWAITE, S., VOLLGGER, S.A. & CRUDEN, A. R. (2017): Rapid, semi-automatic fracture and contact mapping for point clouds, images and geophysical data.– Solid Earth, 8(6), 1241–1253.

TOMLJENOVIĆ, B. & CSONTOS, L. (2001): Neogene-quaternary structures in the border zone between Alps, Dinarides and Pannonian Basin (Hrvatsko zgorje and Karlovac basins, Croatia).– International Journal of Earth Sciences, 90(3), 560–578.

TORRESAN, F., PICCININI, L., CACACE, M., POLA, M., ZAMPIERI, D. & FABBRI, P. (2021). Numerical modeling as a tool for evaluating the renewability of geothermal resources: the case study of the Euganean Geothermal System (NE Italy).– Environ. Geochem. Health 4, 2135–2162. doi:10.1007/s10653-021-01028-4.

TOTH, J. (1963): A Theoretical Analysis of Groundwater Flow in Small Drainage Basins.– Journal of Geophysical Research, 68(15), 4795–4812.

UNITED NATIONS (2022): The United Nations World Water Development Report 2022: Groundwater: Making the invisible visible. UNESCO, Paris, 225p.

URUMOVIĆ, K., TERZIĆ, J., KOPIĆ, J. & KOSOVIĆ, I. (2023): Identification of Aquifer and Pumped Well Parameters Using the Data Hidden in Non-Linear Losses.– Sustainability (Switzerland), 15(14), 11170. doi: 10.3390/su151411170.

WORTHINGTON, S.R.H., FOLEY, A.E. & SOLEY, R.W.N. (2019): Transient characteristics of effective porosity and specific yield in bedrock aquifers.– Journal of Hydrology, 578, 124129. doi: 10.1016/j.jhydrol.2019.124129.

9. BIOGRAPHY OF THE AUTHOR

Ivan Kosović was born on May 17, 1983 in Makarska. After graduating from high school, he enrolled in the Study of Geology at the Faculty of Science at the University of Zagreb and graduated in the academic year 2007/2008. In the period from 2010 to 2015, he was employed in the construction company Viadukt d.d. at the workplace of an engineering geologist. He worked on the tasks of engineering-geological supervision during the construction of tunnels, foundations of bridges, viaducts, and cuts. During that period, he authored a large number of engineering geological reports and studies. From 2015 until today, he has been employed at the Department of Hydrogeology and Engineering Geology of the Croatian Geological Survey (CGS). At the CGS, he works as an engineering geologist and works on the development of surface and deep geophysical research. In surface research, he specializes in the field of seismic (refraction and reflection) and geoelectrical methods, and deep geophysical research in the field of magnetotelluric measurements. He is a collaborator on national competitive projects financed by the Croatian Science Foundation, and projects financed by EU funds. In 2020, he was elected to the title of lecturer at the Faculty of Civil Engineering of the University of Zagreb, where he participates in the teaching of the courses Applied Geology and Hydrogeology and Engineering Geology. He is a member of the Croatian Geological Society, Croatian Geotechnical Society, and international society IAEG, ISRM, and ISSMGE. As an author, he published 11 scientific papers.

List of published papers (July 2024)

Kosović, Ivan; Matoš, Bojan; Casiraghi, Stefano; Benedetti, Gabriele; Frangen, Tihomir; Urumović, Kosta; Pavičić, Ivica; Bistacchi, Andrea; Mittempergher, Silvia; Pola, Marco, Staša Borović. Hydrogeological parameterisation of the Daruvar thermal aquifer: integration of fracture network analysis and well testing // Geologia Croatica, 77 (2024), 2; 99-125. doi: 10.4154/gc.2024.11.

Kosović, Ivan; Matoš, Bojan; Pavičić, Ivica; Pola, Marco; Mileusnić, Morena; Pavić, Mirja; Borović, Staša. Geological modeling of a tectonically controlled hydrothermal system in the southwestern part of the Pannonian basin (Croatia) // Frontiers in earth science (Lausanne), 12 (2024), 1401935, 24. doi: 10.3389/feart.2024.1401935.

Kosović, Ivan; Briški, Maja; Pavić, Mirja; Padovan, Božo; Pavičić, Ivica; Matoš, Bojan; Pola, Marco; Borović, Staša. Reconstruction of Fault Architecture in the Natural Thermal Spring Area of Daruvar Hydrothermal System Using Surface Geophysical Investigations (Croatia) // Sustainability, 2023 (2023), 15; 12134, 22. doi: 10.3390/su151612134.

Podolszki, Laszlo; Miklin, Luka; Kosović, Ivan; Gulam, Vlatko. Multi-Level Data Analyses in the Gajevo Landslide Research, Croatia // Remote sensing, 15 (2023), 200; rs15010200, 19. doi: 10.3390/rs15010200.

Urumović, Kosta; Terzić, Josip; Kopić, Jasna; Kosović, Ivan. Identification of Aquifer and Pumped Well Parameters Using the Data Hidden in Non-Linear Losses // Sustainability, 2023 (2023), 15; 11170, 14. doi: 10.3390/su151411170.

Pavić, Mirja; Kosović, Ivan; Pola, Marco; Urumović, Kosta; Briški, Maja; Borović, Staša. Multidisciplinary Research of Thermal Springs Area in Topusko (Croatia) // Sustainability, 15 (2023), 6; doi: 10.3390/su15065498.

Patekar, Matko; Bašić, Mihaela; Pola, Marco; Kosović, Ivan; Terzić, Josip; Lucca, Alessio; Mittempergher, Silvia; Berio, Luigi Riccardo; Borović, Staša. Multidisciplinary investigations of a karst reservoir for managed aquifer recharge applications on the island of Vis (Croatia) // Acque sotterranee, Italian journal of groundwater, 11 (2022), 1; 37-48. doi: 10.7343/as-2022-557.

Podolszki, Laszlo; Kosović, Ivan; Novosel, Tomislav; Kurečić, Tomislav. Multi-Level Sensing Technologies in Landslide Research — Hrvatska Kostajnica Case Study, Croatia // Sensors, 22 (2022), 1; 177, 21. doi: 10.3390/s22010177.

Pollak, Davor; Gulam, Vlatko; Novosel, Tomislav; Avanić, Radovan; Tomljenović, Bruno; Hećej, Nina; Terzić, Josip; Stipčević, Josip; Bačić, Mario; Kurečić, Tomislav; Dolić, Mario; Bostjančić, Iris; Wacha, Lara; Kosović, Ivan; Budić, Marko; Vukovski, Matija; Belić, Nikola; Špelić, Marko; Brčić, Vlatko; Barbača, Josip; Kordić, Branko; Palenik, Damir; Filjak, Radovan; Frangen, Tihomir; Pavić, Mirja; Urumović, Kosta; Sečanj, Marin; Matoš, Bojan; Govorčin, Marin; Kovačević, Meho Saša; Librić, Lovorka. The preliminary inventory of coseismic ground failures related to December 2020 – January 2021 Petrinja earthquake series // Geologia Croatica, 74 (2021), 2; 189-208. doi: 10.4154/gc.2021.08

Pola, Marco; Pavičić, Ivica; Rubinić, Vedran; Kosović, Ivan; Galović, Lidija; Borović, Staša; Wacha, Lara; Urumović, Kosta. First results of multidisciplinary investigations for the hydrogeological conceptual modelling of loess deposits in eastern Croatia // Acque sotterranee, Italian journal of groundwater, 9 (2020), 1; 43-49. doi: 10.7343/as-2020-432.

Briški, Maja; Stroj, Andrej; Kosović, Ivan; Borović, Staša. Characterization of Aquifers in Metamorphic Rocks by Combined Use of Electrical Resistivity Tomography and Monitoring of Spring Hydrodynamics // Geosciences, 10 (2020), 4; 137, 18. doi: 10.3390/geosciences10040137.